

https://dspace.org/

Influence of two-directional ingress of corrosion agents on the initiation and propagation of steel corrosion in concrete

Zakka, Ze Gyang

2020
https://hdl.handle.net/10539/31202

Downloaded from a DSpace repository. https://dspace.org/

Influence of two-directional ingress of corrosion agents on the initiation and propagation of steel corrosion in concrete

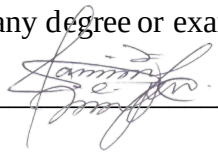
Ze Gyang Zakka

A thesis submitted to the Faculty of Engineering and the Built Environment, University of the Witwatersrand, Johannesburg in fulfillment of the requirements for the degree of Doctor of Philosophy in Engineering.

Johannesburg, 2020

DECLARATION

I, Ze Gyang, Zakka hereby declare that this thesis is my own unaided work. It is being submitted for the degree of Doctor of Philosophy in Engineering to the University of the Witwatersrand, Johannesburg. It has not been submitted before for any degree or examination to any University.



(Signature of Candidate)

08 day of October year 2020

ABSTRACT

Most research in steel reinforced concrete corrosion over the past 40 years has predominantly focused on corrosion due to uni-directional (1D) chloride ingress. This thesis presents results of measurements that are related to steel corrosion in cracked and uncracked concretes that are exposed to 1D chloride ingress and bi-directional (2D) chloride ingress. The concrete exposed to 1D chloride ingress typifies reinforcement within elements such as walls and slabs while the 2D chloride ingress is assessed in reinforcement bars that are located at orthogonal edges of concrete elements such as square edged beams and columns.

72 beam specimens of dimension 150 × 150 × 625 mm were used in this study. Two equal number of beams were cast using a binder blend of plain Portland cement (PC) with fly ash (FA) (70%PC:30%FA) and ground granulated blast furnace slag (SL) (50%PC:50%SL) with water-to-binder ratio = 0.40. The beams were reinforced with 10 mm diameter high yield reinforcement bars embedded 20 mm from the exposed face(s) of the beam. Three reinforcement arrangements were used: a single isolated reinforcement bar placed at an orthogonal edge, in the middle of the specimen, or at an orthogonal edge and electrically connected to a stainless-steel rod near the other face of the concrete. After casting, the specimens were cured by immersion in potable water for 28 days after which the chloride ingress direction was modified (1D or 2D) using an epoxy paint. A single mechanical crack of width 0.16 mm to 0.40 mm was induced in one-half of each specimen set using the 3-point bending technique. A sustained flexural load was imposed on the cracked specimens by clamping them in pairs (back-to-back) in a 3-point bending technique. All the specimens were exposed to a 2-week wetting-drying in 5% NaCl solution then air-drying in an ambient laboratory conditions (temperature of 20 ± 5^{o}C and relative humidity of 40 ± 10%) for the total experimental duration of 110 weeks. The corrosion potential, corrosion rate, and concrete resistivity were measured 24 hours after the wetting cycle and 24 hours before the end of the drying cycle.

In general, corrosion initiation occurred earlier in the cracked and uncracked PC/SL specimens that were exposed to 2D chloride ingress while there was no significant difference in the time-to-corrosion initiation in the PC/FA specimens. After corrosion initiation, the corrosion rate of specimens with reinforcement bars at the

orthogonal edges proceeded at a rate that was higher than that of specimens with reinforcement bars in the middle of the concrete beam. This trend was more significant in the cracked specimens as they attained a mean corrosion rate that was more than 2 times that of the uncracked specimens.

The cracked PC/FA and PC/SL concrete specimens exposed to 2D chloride ingress attained a corrosion rate of 11.0 $\mu A/cm^2$ and 4.3 $\mu A/cm^2$ while the specimens exposed to 1D chloride ingress attained 4.8 $\mu A/cm^2$ and 3.9 $\mu A/cm^2$ respectively. On the other hand, the uncracked PC/FA and PC/SL concrete specimens exposed to 2D chloride ingress attained corrosion rates of 5.0 $\mu A/cm^2$ and 1.5 $\mu A/cm^2$ while the specimens exposed to 1D chloride ingress attained corrosion rates of 2.2 $\mu A/cm^2$ and 1.6 $\mu A/cm^2$ respectively. The cracked and uncracked specimens with stainless-steel rods had lower corrosion rates. The lower corrosion rate can be explained by the limiting of the corrosion rate by the cathodic reaction. The concrete resistivity of concrete exposed to 2D chloride exposure signified a high risk of corrosion (<10 kΩ.cm) while that of specimens exposed to 1D chloride ingress signified lower corrosion risk (>10 kΩ.cm). In line with the corrosion rate of the specimens, the corrosion-induced damage in the concrete, corrosion pit factors, and steel mass loss in the concrete with steel bars at orthogonal edges and exposed to 2D chloride ingress were significantly higher than that of concrete with reinforcement bars that are away from the concrete edge.

The results of this study show that reinforcement bars which are placed at orthogonal edges of cracked and uncracked concrete elements and exposed to 2D ingress of corrosion agents are prone to corrode faster than those which are farther away from the concrete edges. The higher corrosion rate also results in longer and wider corrosion-induced cracks. In order to improve the corrosion free life of steel bars at orthogonal edges, the minimum recommended cover should be adopted. The corrosion of the edge reinforcement bars can also be limited by using cathodic protection, surface treatments to limit ingress of aggressive agents of corrosion, galvanized or stainless-steel bars should be provided at the edges of concrete elements that are severely exposed.

ACKNOWLEDGEMENTS

I wish to thank my supervisor, Dr. Mike Benjamin Otieno who was of immense assistance during my research. I wish to also extend my gratitude to the Head of School (Prof. Taigbenu) and other staff members of the School of Civil and Environmental Engineering; Prof. Yunus Ballim, Prof. Sunny Nwaubani, Dr. Luis Torres, Mr. Ryan Bradley, Ms. Janina Kanjee, Ms. Elizabeth Simelane, Mr. Edward Pretorius, Mr. Wayne Costopoulos, Mr. Banele Qumba, Mr. Stephen Ndlovu, Mr. Samuel Mabote, Mr. Henrique Licotso, Mr. Eric Rood, Mr. Williams Mainganye, Ms Lubica Korac and Ms Pinkie Steyn for their contribution during the execution of this research project. To my colleagues; Mr. Kudzai Mushunje, Mr. Owolabi Abideen, Mr Nura Shanono, Ms. Moshadi Mogodi, Mr. Arif Muhammad, Mr. Williams Dunu, I say thank you for your contributions.

My family members, Kim, Simi, Weng and my adorable wife, Subenisemeni, I acknowledge your forbearance with me, especially when you needed me, but I had to be in the laboratory or over in school to work through the day and night. Many thanks to my siblings and their families and to my brethren in Christ, Pastors Bonney and Mimi Cheyip, Pastor Sama and family, Pastor Uche Ahaiwe and family and the members of Faith Bible Church, South Africa.

I acknowledge AfriSam, Pretoria Portland Cement (PPC) Company, Galva-glow (Pty), ABE (Pty), Sika South Africa, South African National Research Foundation (NRF), and The Concrete Institute, South Africa (TCI). We appreciate you for funding the experimental work and services rendered.

TABLE OF CONTENTS

DECLARATION ii

ABSTRACT iii

ACKNOWLEDGEMENTS v

TABLE OF CONTENTS vi

LIST OF FIGURES xii

LIST OF TABLES xix

NOMENCLATURE xx

1 CHAPTER 1: INTRODUCTION 1

1.1 Background of the study 1

1.2 Problem statement 2

1.3 Motivation of the study 4

1.4 Research questions 5

1.5 Research aim 5

1.6 Research objectives 6

1.7 Chapter summary 6

2 CHAPTER 2: LITERATURE REVIEW 8

2.1 Introduction 8

2.2 Fundamentals of RC corrosion 8

2.3 Types of steel reinforced concrete corrosion 10

2.3.1 Carbonation-induced corrosion 10

2.3.2 Chloride-induced corrosion 10

2.4 Macrocell and microcell corrosion 11

2.5 Transport mechanisms in concrete 12

2.5.1 Convection 13

2.5.2 Diffusion 13

2.5.3 Permeation 14
2.5.4 Migration 14
2.6 Free and bound chlorides in concrete 16
2.6.1 Bound chlorides 16
2.6.2 Free chlorides 16
2.6.3 Total chlorides 17
2.7 Fundamentals of steel corrosion in concrete 17
2.7.1 Corrosion initiation phase 18
2.7.2 Corrosion propagation phase 18
2.8 Chloride ingress in concrete 19
2.8.1 1D chloride ingress 20
2.8.2 2D chloride ingress 21
2.9 Chloride penetration in cracked concrete 35
2.10 Chloride threshold 36
2.11 Corrosion assessment techniques 38
2.11.1 Visual inspection 38
2.11.2 Half-cell potential measurement 39
2.11.3 Concrete resistivity measurement 41
2.11.4 Corrosion rate measurement techniques 45
2.11.5 Gravimetric method 51
2.12 Factors influencing corrosion assessment measurements 53
2.12.1 Factors influencing concrete electrical resistivity measurements 54
2.12.2 Factors influencing corrosion rate measurements 62
2.13 Literature review summary 73
3 CHAPTER 3: EXPERIMENTAL METHODS 76
3.1 Introduction 76

3.2 Concrete materials for specimen production....76
3.2.1 Binders....76
3.2.2 Coarse and fine aggregates....77
3.3 Concrete mix and compressive strength....78
3.4 Steel reinforcement type and preparation....79
3.5 Concrete cover....80
3.6 Reinforcement details....80
3.7 Beam specimen production....82
3.8 Specimen curing....83
3.9 RC beam epoxy coating....84
3.10 Cracked and uncracked beam specimens....84
3.10.1 Crack width measurement....85
3.10.2 Mechanically induced crack width of specimens....86
3.11 Concrete durability index tests....87
3.11.1 Oxygen permeability test....88
3.11.2 Water sorptivity index test....91
3.11.3 Chloride conductivity index test....93
3.12 Chloride ponding; wetting and drying cycles....95
3.13 Steel corrosion measurement and assessment....95
3.13.1 Steel corrosion potential measurement....96
3.13.2 Concrete resistivity measurement....97
3.13.3 Corrosion rate measurement....98
3.13.4 Visual observation....99
3.13.5 Reinforcement bar mass and corrosion pit depth measurement....100
3.14 Chloride penetration profile measurement....101
3.14.1 Determination of acid-soluble chloride concentration in concrete 102

3.15 Summary of experimental methods.....103
4 CHAPTER 4: RESULTS AND DISCUSSION.....105
4.1 Introduction.....105
4.2 Concrete cover quality.....106
4.3 Corrosion potential of reinforcement bars.....107
4.3.1 Corrosion potential in uncracked reinforced concrete.....109
4.3.2 Corrosion potential of the cracked concrete.....111
4.4 Corrosion rate of PC/FA and PC/SL concrete.....113
4.4.1 Corrosion rate of the uncracked concretes.....113
4.4.2 Corrosion rate in cracked concrete.....115
4.4.3 Summary of corrosion rate results.....117
4.4.4 Relationship between corrosion rate and corrosion potential.....123
4.5 Concrete resistivity results.....125
4.5.1 Corrosion rate and concrete resistivity.....129
4.6 Chloride penetration profile in cracked and uncracked concrete.....131
4.6.1 Corrosion rate and chloride concentration.....133
4.7 Corrosion-induced cracks.....134
4.7.1 Characterization of corrosion-induced cracks.....134
4.8 Reinforcement mass loss and pitting depths.....135
4.8.1 Corrosion pits.....137
4.8.2 Corrosion pit factors.....145
4.9 Closing remarks.....145
5 CHAPTER 5: CONCLUSIONS AND RECOMMENDATIONS.....147
5.1 Introduction.....147
5.2 Conclusions.....148
5.2.1 Corrosion initiation and propagation phases.....148

5.2.2 Factors influencing the corrosion rate 148
5.2.3 Corrosion-induced cracks.....150
5.2.4 Pitting corrosion depths and reinforcement mass loss 150
5.3 Limitations of the research 150
5.4 Practical implications of the research findings 152
5.5 Recommendations for further work 153
REFERENCES.....155
Appendix A: Data analysis.....173
Appendix A. 1: Introduction 173
Appendix A. 2: Outlier identification 173
Appendix A. 3: Data collation and analysis 174
Appendix A. 3. 1: Half-cell potential data analysis 174
Appendix A. 3. 2: Resistivity data analysis 174
Appendix A. 3. 3: Corrosion rate data analysis.....175
Appendix A. 4: Data smoothing.....175
Appendix A. 4. 1: Moving average 176
Appendix A. 5: Error bars 176
Appendix B: Corrosion measurement results.....177
Appendix B. 1: Half-cell potential measurement plots 177
Appendix B. 2: Corrosion rate measurement plots 179
Appendix B. 3: Concrete resistivity plots 183
Appendix C: Visual assessment – Corrosion-induced cracks.....185
Appendix C. 1: Visual assessment - Crack-factors 185
Appendix C. 2: Corrosion-induced crack patterns.....187
Appendix C. 3: Summary of visual defects in the RC beam specimens 191
Appendix D: Atmospheric temperature variation during test period 193

Appendix E: Photographs of corroded bars in concrete.....194

Appendix F: t-test results of durability parameters.....199

Appendix G: t-test results of concrete resistivity.....200

Appendix H: Cross section of OPI and CCI apparatus.....201

LIST OF FIGURES

Figure 1.1: Schematic illustration of 1D, 2D and 3D chloride ingress 3
Figure 1.2: Schematic of exposure to corrosion agents and reinforcement positions in concrete element.....7
Figure 2.1: Typical RC corrosion cell (Bioubakhsh, 2011) 9
Figure 2.2: (a) Macrocell corrosion (b) Amplified section - A (Ji *et al.*, 2016).....12
Figure 2.3: RC corrosion phases (Tuutti, 1982).....17
Figure 2.4: Typical measured and predicted chloride diffusion in concrete within the splash zone (Hunkeler *et al.*, 2005)**.** 21
Figure 2.5: Physical model of 2D chloride diffusion (Kang and Shim, 2011) 22
Figure 2.6: Typical 2D chloride ingress profile at a RC orthogonal corner.....22
Figure 2.7: Comparison of 1D and 2D chloride diffusion in stressed and unstressed concrete (Zhang, Sun, Chen, *et al.*, 2011; Zhang, Sun, Liu, *et al.*, 2011).....24
Figure 2.8: Corrosion distribution along length of reinforcement bar in the beam (a) Tensile face and (b) compressive face of the beam (Zhang, Castel and François, 2010).....26
Figure 2.9: Distribution of mass loss ratio of segmented reinforcement bar along the longitudinal direction of corroded reinforcement bar in RC beams accelerated by galvanic method (Ye *et al.*, 2018). 30
Figure 2.10**:** Mass loss ratio distribution along length of corroded steel in RC beams subjected to artificial climate exposure method (a) specimens without sustained loads (b) specimens with 30% sustained loads (c) specimens with 60% sustained loads (Ye *et al.*, 2018). 29
Figure 2.11**:** Chloride ion concentration profile along a concrete edge after 30 years of exposure, 50 mm from the surface with sides of: (a) 100 × 100 mm and (b) 400 × 400 mm cross sections (Frier and Sørensen, 2007). 31
Figure 2.12: Probability distributions for the time-to-corrosion initiation of corner reinforcement bar using random variable, random field and finite element methods (Frier and Sørensen, 2007)**.** 33
Figure 2.13**:** Numerically determined and measured chloride profile from concrete bridge pier (Kang and Shim, 2011)**.** 33

Figure 2.14: Non-uniform corrosion in corner and middle reinforcement bars (Muthulingam and Rao, 2015) 34
Figure 2.15: Chloride ingress through faces of unsealed cracks 36
Figure 2.16: Half-cell potential experimental set-up. 40
Figure 2.17: 4 point (Wenner probe) concrete resistivity meter (Polder, 2001) 43
Figure 2.18: One electrode-disc measurement set for concrete resistivity measurement (Azarsa and Gupta, 2017). 45
Figure 2.19: Linear Polarization resistance method setup (Gepraegs and Hansson, 2005) 46
Figure 2.20: Typical LPR curve acquired from a specimen (Pillai *et al.*, 2015) 47
Figure 2.21: A typical Tafel plot showing anodic (β_a) and cathodic (β_c) slopes (Gold standard corrosion science group, 2018) 48
Figure 2.22: A typical coulostatic perturbation and response (Hassanein, Glass and Buenfeld, 1998) 49
Figure 2.23: Potential transient (a) high corrosion rate and (b) low corrosion rate 50
Figure 2.24: Residual reinforcement bar in uniform and pitting corrosion (Cao and Cheung, 2014) 51
Figure 2.25**:** Concrete resistivity at various moisture contents (a) partially absorbed water; (b) absorbed water (saturated surface-dry); and (c) absorbed + free surface water using different methods (Kim, Zi and Lange, 2017) 57
Figure 2.26**:** Effect of pore saturation on mortar resistivity (Lopez and Gonzalez, 1993) 57
Figure 2.27: Relationship between measured resistivity and temperature (Gowers and Millard, 1999) 58
Figure 2.28: Schematic summary of concrete resistivity measurement recommendations (Gowers and Millard, 1999) 60
Figure 2.29: Positioning of Wenner probes (a) transverse and (b) away from reinforcement mesh to reduce resistivity measurement error (Polder, 2001; Lataste *et al.*, 2003) 62
Figure 2.30: Average corrosion rates of 26 – 31 week specimens showing influence of crack width, cover depth and concrete quality on corrosion rate (Otieno, 2010) 65

Figure 2.31: Dependence of the solubility of oxygen in water and water vapor tension on the ambient temperature (Zivica, 2002) 71
Figure 2.32: Corrosion rate as a function of external RH in case of corrosion initiation due to chlorides for high and low density concretes (Tuutti, 1982) 72
Figure 3.1**:** Particle size distribution curve of fine aggregate 78
Figure 3.2: Longitudinal and transverse section through concrete mould 80
Figure 3.3: Cross section of beam specimens showing chloride exposure, reinforcement details, and specimen labeling key. 81
Figure 3.4: RC beam specimen production 83
Figure 3.5: Cast beam specimens 83
Figure 3.6: Typical cracked RC beam loading rig 85
Figure 3.7: Crack microscope 86
Figure 3.8: Durability index test disc extraction from 100 mm concrete cube (extracted discs shown photo were sourced from SANS 3001-CO3-1: 2015). 88
Figure 3.9: OPI test (a) Laboratory equipment (b) Cross-section of OPI cell (SANS 3001-CO3-2:, 2015). 88
Figure 3.10: Water sorptivity durability index test setup 91
Figure 3.11: Arrangement of CCI test set up (SANS 3001-CO3-3, 2015) 94
Figure 3.12: $Cu/CuSO_4$ half-cell meter 96
Figure 3.13: Corrosion rate measurement setup – coulostat method 99
Figure 3.14: Outside caliper dividers and Vernier calipers 100
Figure 3.15: Cross section of 1D and 2D chloride profile sampling 101
Figure 3.16: Change in color during acid-soluble chloride test (a) PC/FA sample after adding indicator (b) PC/SL sample after adding indicator and H_2O_2 (c) after titration 103
Figure 3.17: Flowchart of experimental program 104
Figure 4.1: 3-point moving average for corrosion potential of uncracked PC/FA specimens exposed to 1D and 2D chloride ingress 108
Figure 4.2: 3-point moving average for corrosion potential of uncracked PC/SL specimens exposed to 1D and 2D chloride ingress 108
Figure 4.3: 3-point moving average for corrosion potential of cracked PC/FA specimens exposed to 1D and 2D chloride ingress 108

Figure 4.4: 3-point moving average for corrosion potential of cracked PC/SL specimens exposed to 1D and 2D chloride ingress 109
Figure 4.5: Mean corrosion potential of reinforcement bars in concrete (week 54 – week 110) 110
Figure 4.6: 3- point moving average corrosion rates of uncracked PC/FA specimens 113
Figure 4.7: 3- point moving average corrosion rates of uncracked PC/SL specimens 114
Figure 4.8: Rust stains on uncracked RC beam specimens (a) G1D-UC-M3 (b) F2D-UC-M3, and (c) F2D-UC-ES1 (circles indicate rust stain locations) 115
Figure 4.9: 3- point moving average corrosion rates of cracked PC/FA specimens 116
Figure 4.10: 3- point moving average corrosion rates of cracked PC/SL specimens 116
Figure 4.11: Corrosion rate of (a) uncracked and (b) cracked PC/SL concrete exposed to 1D and 2D chloride ingress 117
Figure 4.12: Corrosion rate of cracked and uncracked specimens exposed to (a & b) 1D and (c & d) 2D chloride ingress 119
Figure 4.13: Corrosion rate of the concrete specimens (after last wetting cycle - 28) 120
Figure 4.14: Corrosion rate vs corrosion potential in uncracked (a) PC/FA, and (b) PC/SL concrete specimens 123
Figure 4.15: Corrosion rate vs corrosion potential in cracked (a) PC/FA, and (b) PC/SL concrete specimens 124
Figure 4.16: 3-point moving average for concrete resistivity of uncracked PC/FA concrete specimens 125
Figure 4.17: 3-point moving average for concrete resistivity of uncracked PC/SL concrete specimens 126
Figure 4.18: 3-point moving average for concrete resistivity of cracked PC/FA concrete specimens 126
Figure 4.19: 3-point moving average for concrete resistivity of cracked PC/SL concrete specimens 126

Figure 4.20: Concrete resistivity of (a) uncracked and (b) cracked PC/FA specimens exposed to 1D and 2D chloride ingress 128
Figure 4.21: Concrete resistivity of (a) uncracked and (b) cracked PC/SL specimens exposed to 1D and 2D chloride ingress 128
Figure 4.22: Mean concrete resistivity (week 24 - 110) of cracked and uncracked PC/FA and PC/SL RC beams exposed to 1D and 2D chloride ingress 129
Figure 4.23: Corrosion rate vs concrete resistivity of uncracked (a) PC/FA and (b) PC/SL concrete specimens 130
Figure 4.24: Corrosion rate vs concrete resistivity of cracked (a) PC/FA and (b) PC/SL concrete specimens 130
Figure 4.25: Total chloride profiles for (a) PC/FA and, (b) PC/SL concrete.....132
Figure 4.26: Corrosion rate vs chloride concentration at depth of reinforcement bar 133
Figure 4.27: Corrosion-induced cracks of concrete with reinforcement at (a & b) edge (-E), and (c & d) middle of beam (-M). 134
Figure 4.28: Average crack-factor of PC/FA and PC/SL cracked RC beam specimens 135
Figure 4.29: Mass loss of reinforcement bars 136
Figure 4.30**:** Corrosion pits on reinforcement bars of uncracked beam specimens (a) F2D-UC-M3, and (b) G2D-UC-M1 (Sketch shows section of rod shown in the picture) 137
Figure 4.31: Photograph of corroded reinforcement bars from cracked PC/FA concrete specimens 138
Figure 4.32: Photographs of corroded reinforcement bars from cracked PC/SL concrete specimens 139
Figure 4.33: Pitting depths along reinforcement bar length PC/FA concrete exposed to 1D ingress of corrosion agents 141
Figure 4.34: Pitting depths along reinforcement bar length of PC/FA concrete exposed to 2D ingress of corrosion agents. 142
Figure 4.35: Pitting depths along reinforcement bar length PC/SL concrete exposed to 1D ingress of corrosion agents 143
Figure 4.36: Pitting depths along reinforcement bar length PC/SL concrete exposed to 2D ingress of corrosion agent 144

Figure B. 1**:** Half-cell potentials of uncracked PC/FA and PC/SL RC beam specimens exposed to 1D chloride ingress**.**.....177
Figure B. 2: Half-cell potentials of uncracked PC/FA and PC/SL RC beam specimens exposed to 2D chloride ingress.....177
Figure B. 3: Half-cell potentials of cracked PC/FA and PC/SL RC beam specimens exposed to 1D chloride ingress. 178
Figure B. 4: Half-cell potentials of cracked PC/FA and PC/SL RC beam specimens exposed to 2D chloride ingress. 178
Figure B. 5**:** Corrosion rate of uncracked PC/FA and PC/SL RC beam specimens exposed to 1D chloride ingress. 179
Figure B. 6**:** Corrosion rate of uncracked PC/FA and PC/SL RC beam specimens exposed to 2D chloride ingress. 179
Figure B. 7: Corrosion rate of cracked PC/FA and PC/SL RC beam specimens exposed to 1D chloride ingress. 179
Figure B. 8: Corrosion rate of cracked PC/FA and PC/SL RC beam specimens exposed to 2D chloride ingress. 180
Figure B. 9: Corrosion rate of (a) uncracked and cracked (b) PC/SL concrete exposed to 1D and 2D chloride ingress.....180
Figure B. 10: Corrosion rate of (a) uncracked and (b) cracked PC/FA concrete exposed to 1D and 2D chloride ingress.....181
Figure B. 11: Corrosion rate of RC beam specimens exposed to 1D and 2D chloride ingress.....182
Figure B. 12: Concrete resistivity of uncracked PC/FA and PC/SL RC beam specimens exposed to 1D chloride ingress.....183
Figure B. 13: Concrete resistivity of uncracked PC/FA and PC/SL RC beam specimens exposed to 2D chloride ingress.....183
Figure B. 14**:** Concrete resistivity of cracked PC/FA and PC/SL RC beam specimens exposed to 1D chloride ingress.....184
Figure B. 15: Concrete resistivity of cracked PC/FA and PC/SL RC beam specimens exposed to 2D chloride ingress.....184

Figure C. 1**:** Visual defects in cracked (PC/FA) RC beams exposed to 1D chloride ingress.....187
Figure C. 2**:** Visual defects in cracked (PC/FA) RC beams exposed to 2D chloride ingress.....188
Figure C. 3: Visual defects in cracked (PC/SL) RC beams exposed to 1D chloride ingress.....189
Figure C. 4**:** Visual defects in cracked (PC/SL) RC beams exposed to 2D chloride ingress.....190
Figure C. 5: Summary of visual defects on PC/FA specimens exposed to 1D chloride ingress 191
Figure C. 6: Summary of visual defects on PC/SL specimens exposed to 1D chloride ingress.....191
Figure C. 7**:** Summary of corrosion-induced defects on PC/FA specimens exposed to 2D chloride ingress 192
Figure C. 8: Summary of corrosion-induced defects on PC/SL specimens exposed to 2D chloride ingress 192
Figure D. 1: Mean temperature variation during the test period.....193
Figure E. 1**:** Photographs of corroded reinforcement bars in uncracked concrete (contd.).....194
Figure E. 2**:** Photographs of corroded reinforcement bars in cracked PC/FA concrete (contd.).....195
Figure E. 3**:** Photographs of corroded reinforcement bars in cracked PC/FA concrete (contd.).....196
Figure E. 4**:** Photographs of corroded reinforcement bars in cracked PC/SL concrete (contd.).....197
Figure E. 5**:** Photographs of corroded reinforcement bars in cracked PC/SL concrete. 198
Figure H. 1: Cross section of oxygen permeability index test apparatus…...…..200
Figure H. 2: Cross section of chloride conductivity index test apparatus……200

LIST OF TABLES

Table 2.1: British Standard and American Concrete Institute steel reinforced concrete chloride limits. 37
Table 2.2: Electrochemical and non-electrochemical methods of corrosion assessment (Bjegovic, Mikulic and Sekulic, 2007).....38
Table 2.3: Interpretation of corrosion potential results (ASTM C876, 2009).....40
Table 2.4: Typical HCP ranges for concrete in certain conditions (Gulikers, Polder and Raupach, 2003).....54
Table 3.1: Chemical composition of the binders for concrete production.....77
Table 3.2: Aggregate physical properties.....78
Table 3.3: Concrete mix materials 78
Table 3.4: Mean 28 and 90-day concrete compressive strength 79
Table 3.5: Mechanical-induced crack widths for PC/FA and PC/SL specimens...86
Table 4.1: Durability Index test results 106
Table 4.2: Independent t-test result summary of DI parameters 107
Table 4.3: Corrosion rate of specimens exposed to 1D and 2D chloride ingress 121
Table 4.4: Reinforcement bar pitting factors 145
Table A. 1: Number of corrosion rate data recorded per specimen set.....175
Table C. 1: Crack width and length of PC/FA specimens exposed to 1D chloride ingress.....185
Table C. 2: Crack width and length of PC/SL specimens exposed to 1D chloride ingress.....185
Table C. 3: Crack width and length of PC/FA specimens exposed to 2D chloride ingress.....186
Table C. 4: Crack width and length of PC/SL specimens exposed to 2D chloride ingress.....186

NOMENCLATURE

1D	Uni-directional
2D	Bi-directional
3D	Three-directional
C	Cracked concrete
C_{bound}	Bound chloride concentration
C_{free}	Free chloride concentration or water-soluble chlorides
C_{total}	Total chloride concentration or acid-soluble chlorides
CCI	Chloride conductivity index
FA	Fly ash
M_i	Initial mass of steel reinforcement bar
M_{sv}	Vacuum saturated mass of concrete
M_f	Final mass of steel reinforcement bar
MTK	Metakaolin
n_{cl}	Concrete porosity to sodium chloride solution
n_w	Concrete porosity to water
OPI	Oxygen permeability index
PC	Plain Portland cement/ Ordinary Portland cement/ Unblended cement
RC	Steel reinforced concrete
SCMs	Supplementary cementitious materials
SL	Ground granulated blast furnace slag
SF	Silica fume
t_{init}	Time-to-corrosion initiation
t_{prop}	Corrosion propagation phase
UC	Uncracked concrete
w/b	Water-to-binder ratio
WSI	Water sorptivity index

1.1 Background of the study

Corrosion of steel embedded in concrete has been identified as the major cause of durability failure and reduced service life of steel reinforced concrete (RC) structures (Fang et al. 2006; Isgor and Razaqpur 2006). The alkalinity of the concrete (pH > 12) in newly constructed RC structures prevents the steel reinforcement from corroding due to the formation of a passive protective oxide layer on its surface. This protective layer can however be destroyed by carbonation of the concrete to the depth of the steel reinforcement bar (known as carbonation-induced corrosion) or by the buildup of chlorides to a critical concentration on the steel surface in a process known as chloride-induced corrosion (Broomfield, 2007; Torres-Luque, Bastidas-Arteaga, Schoefs, Sánchez-Silva, & Osma, 2014).

Carbonation-induced corrosion is normally occasioned by a reduction in the concrete pH due to the formation of carbonic acid ($CaCO_3$) in the concrete pore solution. This type of corrosion is prevalent in RC structures that are located farther away from coastal regions. Chloride-induced corrosion on the other hand does not always result in a change in the concrete pH since the chlorides are derived from salts such as calcium chloride (CaCl) and sodium chloride (NaCl) (E. Poulsen & Mejlbro, 2006; Shi, Xie, Fortune, & Gong, 2012). The chloride ions can reach the steel surface by penetration from the external environment or when the concrete mix materials are contaminated by chlorides. In general, chloride-induced corrosion has been reported to be the most prevalent concrete deterioration mechanism and it affects structures which are in marine environments and where chloride based salts (e.g. deicing salts) are used (Broomfield, 2007).

The use of RC as a major construction material has been due on its versatility and the compatibility of steel reinforcement and concrete (Ballim & Graham, 2009; Cairns, 1996). In addition to the load resistance provided by the concrete, it is also required to enhance the durability of RC structures by protecting the reinforcement bars from fire and the environment. The corrosion of the reinforcement bar thus results in a reduction in the load carrying capacity of the structure due to loss of its cross-sectional area and bond with the surrounding concrete due to rust formation

on the steel surface. Corroded steel reinforcement bars also lose ductility which is an important parameter in load bearing structures. Thus, the corrosion of embedded reinforcement bars in concrete negatively influences the structural integrity and service life of RC structures. This raises the need for an understanding of concrete deterioration mechanisms and durability design of RC structures in environments which have a high risk of corrosion (Alexander, Ballim, & Stanish, 2008; Allen, 1998; Gjorv, 2013; Litzner & Becker, 1998).

Several codes of practice for RC structures have adopted specifications which aim to improve the durability of RC structures in corrosion prone environments. Some of these specifications include; providing minimum cover to reinforcement, minimum binder content, limiting crack widths, and mix water to binder ratio (Edvardsenl & Mohr 2000; EN1992-1-1 2004; SABS 0100-1 2000). It is reasonably assumed by designers that adherence to these specifications will provide some measure of confidence that the time-to-corrosion initiation will be delayed. Despite these specifications, it is opined that the long-term performance of a RC structure will depend on the severity of its exposure, aggressiveness of its environment, and resistance of the concrete to the penetration of corrosion causing agents.

1.2 Problem statement

Zhang et al. (2011) noted that in over 40 years of corrosion studies, many valuable results of chloride-induced corrosion have been obtained and successfully applied in the service life prediction of field structures. However, the scope of most of the laboratory studies have been limited to uni-directional (1D) ingress of corrosion agents into the concrete (e.g. where only one face of a RC specimen is exposed to chlorides) (Michel et al. 2013; Otieno, 2008; Richard et al. 2010; Scott, 2004; Suryavanshi and Swamy, 1996). While 1D ingress of corrosion agents simulates elements such as walls and slabs (see Figure 1.1a), it has been shown by some researchers that the diffusion rate of chloride ions at orthogonal edges (herein referred to as bi-directional (2D) ingress) of concrete elements is higher than that which occurs on a concrete which is exposed to 1D ingress since the chlorides penetrate from two mutually perpendicular faces of the concrete. It can thus be reasonably assumed that the ingress of other corrosion-causing agents such as moisture and oxygen are also higher at orthogonal edges and will lead to a reduction

in the corrosion-free life of reinforcement bars that are close to these locations within concrete elements (Jin et al. 2015a; Kang and Shim, 2011; Val and Trapper, 2006, 2008; Zhang et al. 2011). In contrast to the 1D ingress of corrosion agents (e.g. walls and slabs), the 2D chloride ingress simulates the in-service condition of rectangular RC beams and columns which are subjected to multi-facial chloride ingress with its severity depending on the RC exposure condition. Although it can be observed that the terminal end of RC columns, beams, and corbels may be subjected to three-directional (3D) ingress by corrosion agents, 2D chloride ingress is deemed to be more critical as it affects the entire length of the reinforcing rod (Figure 1.1b), which will in turn influence the load bearing capacity of the RC member. 3D chloride ingress on the other hand mainly causes deterioration at the terminal end of reinforcement bars (Figure 1.1c (*i*)). Although a combination of 2D and 3D chloride ingress at the terminal end of steel reinforced concrete elements (e.g. beams, columns, and corbels) may also be critical, this study will only focus on the effect of 2D ingress of corrosion agents in reinforced concrete.

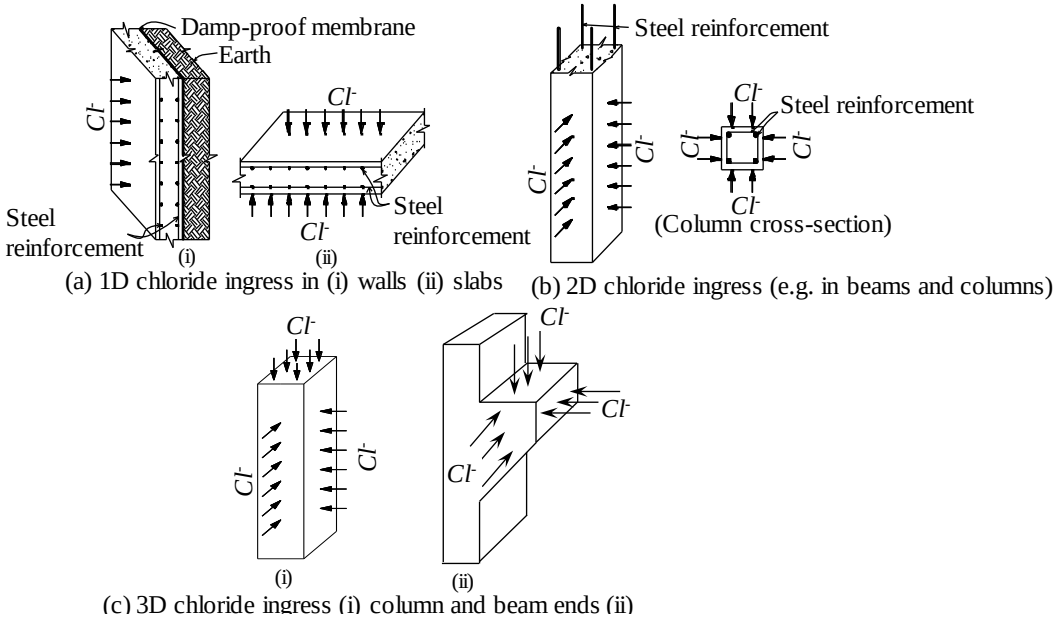


Figure 1.1: Schematic illustration of 1D, 2D and 3D chloride ingress

Apart from the ingress direction of corrosion agents into concrete, the ability of concrete to provide an effective barrier which will delay corrosion initiation of embedded steel reinforcement bars has been identified to be impaired when the concrete cover is cracked (Otieno et al. 2010). In this case, the cover cracks provide an easy ingress path for corrosion agents to penetrate the concrete thereby

shortening the time-to-corrosion initiation of the embedded steel reinforcement bars. The presence of cover cracks in RC elements that are subjected to multi-directional chloride ingress may result in early deterioration of reinforcement bars that are located near the edge of concrete elements. This study assumes that there will be early deterioration of reinforcement bars that are located near orthogonal edges of concrete elements as a result of higher diffusion rate of chlorides and other corrosion-causing agents (at the edges due to multi-directional ingress) as compared to that of RC elements which are subjected to uni-directional (1D) ingress of the corrosion agents.

1.3 Motivation of the study

Considering the Fick's second law by Crank (1975), Morga and Marano (2015) mentioned that its general solution depends on the geometry of the element where the diffusion occurs as well as the shape of its source. Hence, it can be implied that there is a relationship between a RC element geometry, penetration of corrosion-causing agents into concrete, and time-to-corrosion initiation of steel reinforcement bars embedded in concrete. This has led some scholars to propose solutions to Fick's second law for chloride ingress using 2D models in rectangular beams and columns as against 1D models (Frier and Sørensen 2007; Val and Trapper 2008; Martín-Pérez et al. 2001).

Results of a study conducted by Val and Trapper (2008) on the time-to-corrosion initiation of steel reinforcement in a RC wall (exposed to 1D chloride penetration) and RC column with orthogonal edges (exposed to 2D chloride penetration) in a marine environment showed that for the same concrete cover thickness to reinforcement, the probability of corrosion initiation was higher in reinforcement bars that were located near the edge of the concrete elements (e.g. rectangular beams and columns edges exposed to 2D chloride penetration) compared to reinforcement bars in the middle of an RC wall (that is exposed to 1D chloride penetration). These results along with that of other researchers such as Jin et al. 2015a; Kang and Shim, 2011; Val and Trapper, 2006; Zhang et al. 2011, demonstrate the importance of determining the effect of 2D chloride penetration on corrosion initiation and propagation of reinforcement bars placed at various locations within concrete elements.

Other studies on the time-to-corrosion initiation and corrosion-induced cracking of uncracked RC specimens subjected to 2D chloride ingress have been undertaken by Sørensen and Frier (2004), Val and Trapper (2006, 2008), Frier and Sørensen (2007), Kang and Shim (2011), Zhang, Sun, Chen, *et al.* (2011), Zhang, Sun, Liu, *et al.* (2011), Jin *et al.* (2015), however, there is no published literature on corrosion initiation and propagation studies in cracked concrete subject to 2D chloride penetration. Since the presence of cover cracks influences the transport mechanisms of corrosion agents into concrete and the corrosion of embedded steel reinforcement bars, this study focuses on the influence of 2D chloride ingress in cracked concrete. After corrosion of the steel reinforcement bar has been initiated, the sustenance of the corrosion process depends on the availability of oxygen and moisture at the steel surface, hence, though the term 2D chloride ingress is used in this study, it is worth noting that the term is not restricted to chloride ingress alone, it also refers to the ingress of corrosion-causing agents into the concrete.

1.4 Research questions

1. To what extent does 2D ingress of corrosion agents affect the corrosion of reinforcement bars placed at orthogonal edges of cracked RC as compared to 1D ingress of corrosion agents?
2. To what extent does the binder type affect corrosion propagation of steel reinforcement bars placed at orthogonal edges of concrete specimens subjected to 1D and 2D ingress of corrosion agents?
3. What influence does a larger cathodic area have on the corrosion rate of reinforcement bars that are located near the edge of an RC element that is subjected to 1D and 2D ingress of corrosion agents?
4. Is there a relationship between the concrete resistivity and corrosion rate of steel placed at orthogonal edges of concrete specimens subjected to 1D and 2D ingress of corrosion agents?

1.5 Research aim

This study aims to assess the influence of cracks on corrosion initiation and propagation of embedded steel in concrete which is subjected to 2D ingress of corrosion causing agents.

1.6 Research objectives

The objectives of this study are;

1. To determine the time-to-corrosion initiation of embedded steel in cracked and uncracked concrete subject to 1D and 2D ingress of corrosion agents
2. To determine the influence of 1D and 2D ingress of corrosion agents on the corrosion rate of reinforcement bars placed at orthogonal edges of cracked and uncracked RC elements
3. To assess the influence of cover cracks on steel reinforcement bar corrosion
4. To determine the effect of a change in the cathodic area on the corrosion rate of RC beams subject to 1D and 2D ingress of corrosion agents
5. To assess the effect of binder type on concrete resistivity and steel corrosion rate
6. To assess the mass loss of the steel reinforcement due to its corrosion
7. To determine the 2D chloride penetration profile in the concrete and chloride concentration at steel level at the end of the experiment.

1.7 Chapter summary

Chloride-induced corrosion was identified as the dominant cause of reinforced concrete deterioration in marine regions and areas where chloride based deicing salts are used. Although much research has provided an understanding of the corrosion process, most of the research methodology design simulates uni-directional (1D) ingress of corrosion agents. In real structures, the penetration of corrosion agents may occur in 1D (e.g. in walls and slabs), 2D (bi-directional; e.g. at the edge of rectangular columns and beams), or in 3D (three-directions: e.g. the terminal end of columns, beams, and in corbels). This study focuses on 2D ingress of corrosion agents.

The influence of the ingress directions of corrosion agents on the corrosion of reinforcement bars that are placed at various locations in concrete specimens made of PC(70)/FA(30) and PC(50)/SL(50) were assessed. A schematic (transverse) section of the concrete exposure and reinforcement positions of the specimens used in this study is shown in Figure 1.2 (note: this diagram illustrates all 6 specimens used in this study, the specimen details is provided in Figure 3.4).

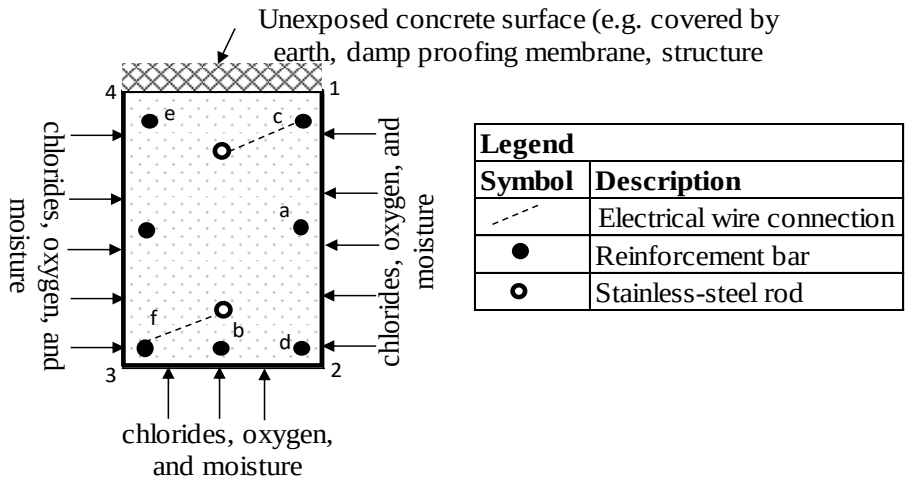


Figure 1.2: Schematic of exposure to corrosion agents and reinforcement positions in concrete element.

The concrete element in Figure 1.2 has of 4 edges which are exposed to 1D or 2D ingress of corrosion agents. The position of the reinforcement bars in relation to the concrete edges therefore determines if it is predominantly exposed to 1D or 2D ingress of corrosion agents. One may then ask the question; will the corrosion free life and corrosion characteristics of the reinforcement bars be the same with respect to their location within the concrete element and exposure to corrosion agents in cracked and uncracked concrete. This question will be answered by assessing the 28-day concrete durability index parameters and corrosion measurements (corrosion potential, concrete resistivity, corrosion rate) of concrete that is exposed to chlorides in a laboratory-based experiment.

After the termination of the wetting and drying cycles, the deterioration of the reinforcement bars (pitting depths and mass loss) and chloride concentration at various depths within the concrete (on surfaces exposed to 1D and edges exposed to 2D ingress of corrosion agents) was determined and conclusions were drawn from the results.

2.1 Introduction

The durability performance and service life of RC structures are governed by several parameters such as concrete quality, cover depth to reinforcement, and most significantly its exposure conditions (Verma et al. 2014). BS 8110-1, (1997) states that most concrete deterioration processes occur in the presence of moisture with thin sections subjected to hydrostatic pressure from only one side, partly immersed sections, corners and edges more vulnerable to effects of chemical or climatic deterioration.

The influence of environmental deterioration on the service life of RC structures has been reported to be most pronounced in chloride laden environments such as marine environments and where chloride-based salts (e.g. de-icing salts) are used. The penetration of chlorides into concrete in these environments and its buildup to a sufficient concentration at the surface of embedded steel reinforcement bars initiates its corrosion.

This chapter presents an overview of literature relating to fundamental principles of corrosion of steel embedded in concrete, causes of steel corrosion in concrete, transport mechanisms in concrete, free and bound chlorides, corrosion phases of steel in concrete, chloride concentration and corrosion initiation due to 1D and 2D chloride ingress, methods of steel corrosion assessment and factors influencing steel corrosion in concrete.

2.2 Fundamentals of RC corrosion

Corrosion is generally defined as an electrochemical process which could either include or exclude the input of an impressed current (Caré & Raharinaivo, 2007). The corroding material deteriorates as it reacts with its environment. In most instances, corrosion is progressive and may necessitate periodic repair, replacement or result in complete failure of a structure.

The corrosion of steel in concrete occurs by the formation of electrochemical cells (Figure 2.1), however, unlike conventional electrochemical cells which have distinct anodes and cathodes, the anode and cathode of a RC corrosion cell are located on the same reinforcement bar where the corroding region on the

reinforcement bar is the anode while the non-corroding region is the cathode. The concrete pore solution serves as an electrolyte which provides the ionic connection between the anode and cathode sites and lastly, the steel reinforcement provides electrical connectivity between the anode and cathode sites (Adiyastuti, 2005; Gowers & Millard, 1999; PCA, 2002; R. B. Polder, Peelen, Stoop, & Neeft, 2011; Raupach, 2006).

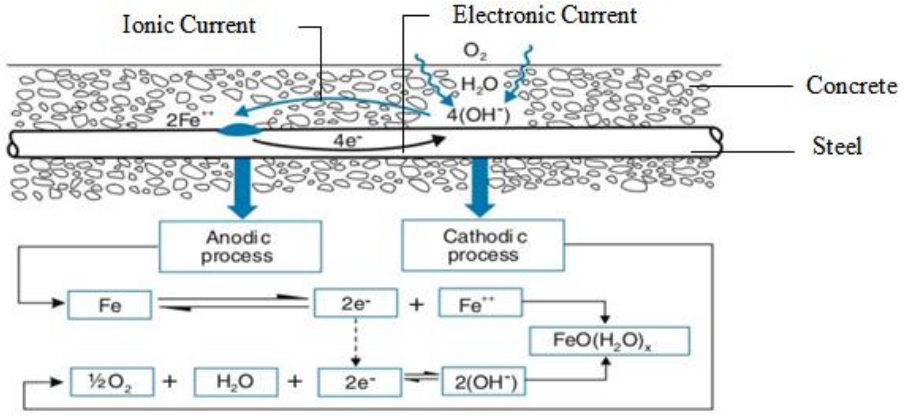


Figure 2.1: Typical RC corrosion cell (Bioubakhsh, 2011)

The possible chemical reactions (Eqn. 2.1 – 2.6) that may occur in a RC corrosion cell were stated by Ahmad (2003) as follows;

Anodic process: Oxidation reactions;

$$Fe \rightarrow Fe^{2+} + 2e^- \quad (2.1)$$

$$3Fe + 4H_2O \rightarrow Fe_3O_4 + 8H^+ + 8e^- \quad (2.2)$$

$$2Fe + 3H_2O \rightarrow Fe_2O_3 + 6H^+ + 6e^- \quad (2.3)$$

$$Fe + 2H_2O \rightarrow HFeO_2^- + 3H^+ + 2e^- \quad (2.4)$$

Cathodic process: Reduction reactions;

$$2H_2O + O_2 + 4e^- \rightarrow 4OH^- \quad (2.5)$$

or

$$2H^+ + 2e^- \rightarrow H_2 \quad (2.6)$$

The main problem with corrosion is the formation and accumulation of oxides, hydroxides, and complexes of iron at the anode (Eqn. 2.1 - 2.4). The products of corrosion are normally porous and have higher specific volumes (about 2 – 10 times) compared to the parent steel thereby yielding expansive forces which can

cause defects such as cracks, spalling, or delamination in the concrete (Cabrera, 1996; Isgor & Razaqpur, 2006; Tracy Dawn Marcotte, 2001; Němeček, Kruis, Koudelka, & Krejčí, 2018). Concrete defects (e.g. cracks, connected pores etc.) allow easy penetration of corrosion agents into the concrete. While the accumulation of the corrosion products in the steel-concrete interface has been reported to sometimes slow the corrosion rate due to the stifling of oxygen supply to the corroding steel, the development of corrosion-induced cracks, spalls, and delamination has also been shown to allow transportation of the corrosion products away from the steel surface. This causes the steel to be further exposed to the corrosion-causing agents thereby resulting in its rapid deterioration.

2.3 Types of steel reinforced concrete corrosion

The corrosion of steel embedded in concrete is mostly initiated by a breakdown of the steel oxide protective layer due to either concrete carbonation (carbonation-induced corrosion) or chlorides (chloride-induced corrosion). The mechanism of these types of corrosion is herein briefly discussed.

2.3.1 Carbonation-induced corrosion

Concrete carbonation occurs when atmospheric carbon-dioxide dissolves in concrete pore solution thereby depleting the calcium hydroxide and precipitating calcium carbonate in the concrete pores. This process reduces the concrete pH from above 12.5 to less than 9, thereby making the steel reinforcement susceptible to corrosion once the carbonation front reaches the steel surface. A rising incidence in this type of corrosion is anticipated due to climate change as a result of rise in atmospheric CO_2 concentration, temperature, and humidity (Broomfield, 2007; Peng & Stewart, 2015).

Though this study is not focused on carbonation-induced corrosion, it is important to note that structures that are prone to chloride-induced corrosion can be affected by concrete carbonation. The effect of carbonation in chloride-induced corrosion can result in the release of bound chlorides to take part in the corrosion process. This is further discussed in Section 2.6.1.

2.3.2 Chloride-induced corrosion

Chlorides can contaminate both fresh and hardened concrete. In fresh concrete, chloride contamination can occur through materials (such as mix water, aggregates, chloride laden groundwater and admixtures) used in its production (Broomfield, 2007; Florea & Brouwers, 2012). The presence of chlorides beyond prescribed limits in fresh concrete can also result in early and rapid corrosion of steel reinforcement as a result of poor alkalinity development of the pore solution; an alkaline pore solution with a high pH (> 12) protects the steel reinforcement from corrosion (ACI Committee 222R-01). Binders can also be a source of chloride contamination in concrete, though the percentage chemical composition of chlorides prescribed (≤ 0.10 percent by weight of cement) in various cement standards is below the limit which can cause steel corrosion (SANS 50197-1: 2013). In cases where fresh concrete has been contaminated by chlorides, further penetration of chlorides into the concrete from the environment may result in increased risk of RC corrosion (Broomfield, 2007).

The major means of chloride contamination in hardened concrete is by penetration from its environment (e.g. in marine environments and where chloride-based deicing salts are used). The chlorides penetrate the concrete through its finished surface or defects (e.g. cracks, concrete cold joint, bleeding holes). A buildup of sufficient concentration of chloride ions on the steel reinforcement surface results in its depassivation and subsequent corrosion.

Apart from initiating the corrosion of the steel reinforcement bar, chloride ions also improve the ionic conductivity of the concrete pore solution thereby easing the movement of ions between the anodic and cathodic sites of the corrosion cell.

It is worth noting that though carbonation-induced corrosion is occasioned by a reduction in pH of the concrete, chloride-induced corrosion seldom results in a reduction of the concrete pH (Neville, 1995).

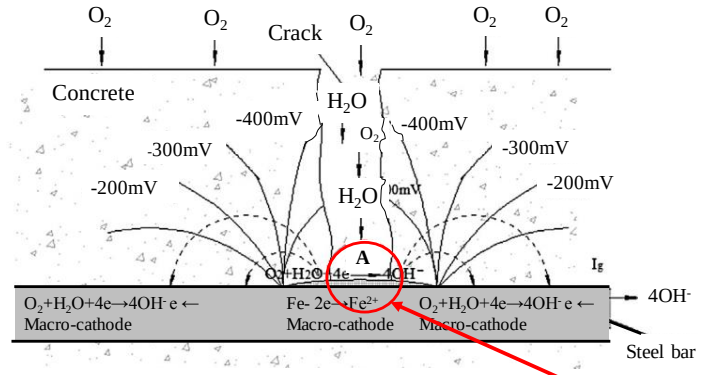
This study will focus on chloride contamination of concrete by penetration from its environment.

2.4 Macrocell and microcell corrosion

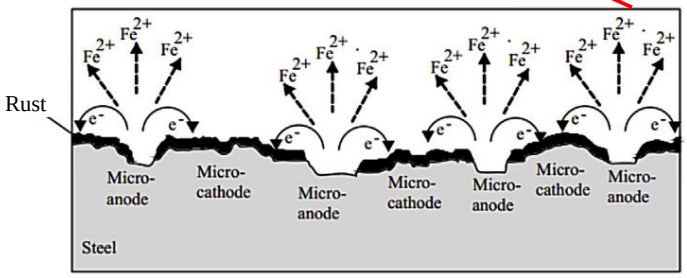
Macrocell corrosion (Figure 2.2) is widely associated with chloride-induced corrosion. It is associated with the formation of distinct anodes and cathodes (also

known as corrosion pits) on the steel surface. In most instances, the anode is small while the cathode is large. The pitting points mostly coincide with positions on the reinforcement bar where transverse or longitudinal concrete cracks have developed.

Microcell corrosion (also known as uniform corrosion) on the other hand is mostly associated with carbonation-induced corrosion. Unlike macrocell corrosion which has distinct anode and cathode sites, the anode and cathode sites are adjacent to each other. The uniform penetration and spread of chloride ions on the surface of a reinforcement bar can also result in uniform corrosion; this has been observed as the chloride profile approaches the rear side of the reinforcement bar (Cao & Cheung, 2014; R. Zhang, Castel, & François, 2010).



(a) Macrocell corrosion at location of flexural crack



(b) Amplified section A

Figure 2.2: (a) Macrocell corrosion (b) Amplified section - A (Ji, Hu, Zhang, & Bao, 2016)

2.5 Transport mechanisms in concrete

The initiation and propagation of the RC corrosion depend on the sustained penetration of chloride ions, moisture and oxygen from the environment onto the steel surface. The transportation of these corrosion causing and sustaining agents to the steel level can occur by one or more of the following mechanisms (Branko, 2014; Hunkeler et al., 2005; J. F. Pacheco, 2015; E. Poulsen & Mejlbro, 2006).

2.5.1 Convection

This is the flow of moisture from a region of higher moisture content to that with lesser moisture content. The moisture serves to convey the chloride ions into the concrete through the concrete pores. The moisture flux due to capillary suction and moisture diffusion (J_θ) is given by Eqn. 2.7 (Oh & Jang, 2007);

$$J_\theta = -D_\theta \frac{\partial \theta}{\partial x} \quad 2.7$$

where D_θ is the moisture diffusion coefficient,

θ is the moisture content per unit weight of concrete

x is the depth from the concrete surface

The convection transport mechanism is dominant within the first few millimeters (0 – 10 mm) from the concrete surface which is subjected to wetting and drying cycles. The concentration of chlorides in this zone is not well defined as the chlorides penetrate the concrete when it is wet and move out when the concrete dries out. The ingress of chloride ions into concrete has been simulated as a convection-diffusion model by some researchers (Němeček et al., 2018; Oh & Jang, 2007), however, at depths greater than 10 mm, diffusion has been shown to be the dominant mode of chloride penetration in concrete (Hunkeler et al., 2005). The presence of cracks in concrete may increase the concrete area that is exposed to wetting and drying and increase the chloride concentration around the crack opening. The cracks may result in easy penetration of corrosion agents into concrete, thus reducing the time-to-corrosion initiation of the reinforcement bars.

2.5.2 Diffusion

This occurs as a result of a concentration gradient between regions in contact wherein the chlorides move from a region of higher concentration to that of lower concentration. Ionic diffusion in concrete can be determined using Fick's first law of diffusion (Eqn. 2.8) (Bioubakhsh, 2011);

$$J = -D \frac{dc}{dx} \quad 2.8$$

where J is the rate of mass transfer in a unit area,

D is the diffusion coefficient

c is the concentration of the fluid over a distance x

This transport mechanism has been widely agreed by researchers to be dominant at depths that are beyond the convection zone (greater than 10 mm from the concrete surface) (Branko, 2014; Hunkeler et al., 2005; E. Poulsen & Mejlbro, 2006). In cracked concrete, the combined effect of convection and diffusion may significantly influence the penetration of chlorides into the concrete due to an increase in the area exposed to the chlorides.

2.5.3 Permeation

This occurs when the flow of ions is driven by a difference in hydraulic pressure between two zones which are in contact. This transport mechanism is influenced by the ability of the concrete pores to allow transfer of fluids through it due to the influence of external pressure. The concrete pore structure can be influenced by the concrete binder type, the curing method and its duration, compaction, aggregate size, and w/b ratio. Darcy's law is used to compute the permeability of a fluid through a porous medium. The law states that the steady-state rate of flow is directly proportional to the hydraulic gradient (Eqn. 2.9);

$$\vartheta = -\frac{k}{\mu}.\frac{dP}{dL} \qquad 2.9$$

where ϑ is the apparent velocity of flow,

k is the intrinsic permeability of the porous medium

μ is the viscosity of the fluid,

dP is the pressure loss over the flow path dL

This mode of transport mechanism in concrete is prevalent in hydraulic structures where only one or both sides of the structure are subjected to different pressures. In general, concrete permeability is an important factor in the corrosion of reinforced concrete since it also governs the penetration of chloride ions into the concrete.

2.5.4 Migration

This is the flow of ions caused by a difference in electrical potential, e.g. where chloride ions move to regions of positive potential under the influence of an electric field. The transportation of chlorides under the influence of an electric field is known as flux action, this method is widely used in assessing chloride penetration

into concrete. The Nernst-Planck equation (Eqn. 2.10) is used to compute the flow of ions through a porous medium;

$$J_i = D_i \frac{\partial c_i}{\partial x} + \frac{z_i F}{RT} D_i c_i \frac{\partial E}{\partial x} \qquad 2.10$$

where J_i is the flux of specie i

D_i is the diffusion coefficient of specie i

c_i is the ionic concentration of specie i in the pore fluid

x is the distance

z_i is the electrical charge of species i

F Faraday constant

E is the charge potential

$\frac{\partial E}{\partial x}$ is the electric field

R is the universal gas constant, and

T is the absolute temperature

Eqn. 2.10 indicates the flux due to chloride diffusion and migration. The general Nernst-Planck equation includes diffusion, migration and convection (C. Andrade, 1993).

Concrete durability index parameters measure the water sorptivity, oxygen permeability and chloride ion conductivity of concrete. The durability index tests (discussed in Section 3.11) are used to determine the penetrability of concrete to fluids, gases, and ions. Concrete elements may be subject to more than one transport mechanism, however, the dominance of a transport mechanism in a concrete will depend on its exposure condition, mix composition, stress condition, and presence or absence of defects (e.g. cracks).

There is a consensus among researchers of concrete durability that convection is the dominant means of chloride transportation in the first few millimeters from the concrete surface (since chlorides easily move in and out of the concrete due to cyclic wetting and drying) while at greater depths (> 10 mm), diffusion dominates (Hunkeler et al., 2005; C. H. Lu, Gao, & Liu, 2014; E. Poulsen & Mejlbro, 2006).

2.6 Free and bound chlorides in concrete

Chlorides in concrete exist in the form of either free or bound chlorides;

2.6.1 Bound chlorides

These chlorides are either chemically bound by reacting with the cement paste, physically absorbed by the cement gel or trapped in the cement gel or capillary pores in a process known as chloride binding (Castellote et al. 1999; Hope et al. 1985; Kong et al. 2002; Poulsen and Mejlbro 2006). Chloride binding occurs when the aluminates (C_3A and C_4AF) in cement remove free chloride from the pore solution of the cement gel thereby decreasing the risk of steel corrosion (in concrete) by forming a solid phase known as Friedel's salt (Alonso et al. 2001; Dhir et al. 1996; Suryavanshi and Swamy 1996). Chloride binding is a complicated process (see Eqn. 2.11 and 2.12) that can be affected by many factors such as the chloride concentration, binder composition, hydroxyl concentration in the pore solution, cation of the chloride salt, temperature, supplementary cementitious materials, carbonation, presence of sulfate ions and an electric field (Yuan, Shi, De Schutter, Audenaert, & Deng, 2009).

$$Ca(OH)_2 + 2NaCl \leftrightarrow CaCl_2 + 2Na^+ + 2OH^- \quad 2.11$$

$$C_3A + CaCl_2 + 10H_2O \rightarrow Ca_3Al_2O_6.CaCl_2.10H_2O \quad 2.12$$

2.6.2 Free chlorides

These are chloride ions which diffuse into the concrete pore solution; they are also referred to as water-soluble chlorides. Early studies by Hope et al. (1985) concluded that only the free chloride content in concrete was responsible for the corrosion of steel in concrete, while bound chlorides did not contribute to the steel corrosion. This conclusion has however been disputed as the release of bound chlorides to participate in the corrosion process has been reported in several laboratory and field inspection tests where the solubility of bound chlorides (Friedel's salt) has been found to increase with the degree of carbonation and leaching, thereby allowing both free and bound chlorides to participate in the corrosion process (Broomfield 2007; Glass and Buenfeld 2000; Poulsen and Mejlbro 2006; Suryavanshi and Swamy 1996). Despite the proposal that bound chlorides are also released to participate in the corrosion process, it has been widely agreed that the percentage

of free chloride concentration in concrete gives an indication of how easily the steel reinforcement will corrode in the chloride contaminated concrete.

2.6.3 Total chlorides

The summation of the free and bound chlorides in concrete is referred to as the total chloride content (Eqn. 2.13)(Y. Lu, Garboczi, Bentz, & Davis, 2012).

$$C_{total} = C_{free} + C_{bound} \quad 2.13$$

where C_{total} = the total chloride concentration (acid-soluble chlorides),

C_{free} = (water-soluble chlorides) is the free chloride concentration and

C_{bound} = is the bound chloride concentration.

The total chloride is also referred to as acid soluble chlorides. Binder blends of PC with FA, SL or silica fume (SF) have been found to have more capacity to bind chloride ions, improve the concrete pore structure, reduce diffusion and flow of chloride ions which in turn delays in the corrosion process in these concretes when compared to plain PC concrete (Arya and Xu 1995; Dhir et al. 1996; Otieno 2010; Scott 2004).

2.7 Fundamentals of steel corrosion in concrete

Tuutti (1982) proposed that the corrosion of steel in concrete occurs in two main phases; an initiation (t_{init}) and propagation phase (t_{prop}). The two phases are schematically represented in Figure 2.3;

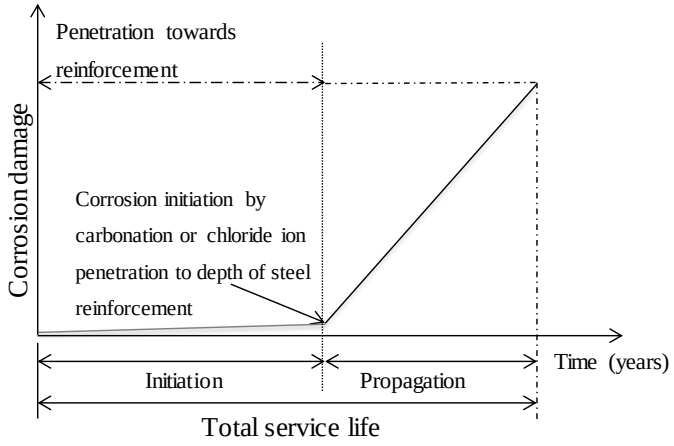


Figure 2.3: RC corrosion phases (Tuutti, 1982)

2.7.1 Corrosion initiation phase

The time-to-corrosion initiation phase refers to the time it takes for either the carbonation front or sufficient concentration of chlorides to reach the steel reinforcement and breakdown the protective oxide layer at the steel surface. In this corrosion phase, no visible damage to the concrete (in form of corrosion-induced cracks) is noticeable (Hunkeler et al., 2005; Morga & Marano, 2015; D. V. Val & Trapper, 2006).

In uncracked concrete, the time-to-corrosion initiation could take a long time depending on the concrete cover quality and exposure conditions while in cracked concrete, the time-to-corrosion initiation is almost none existent except in cases where the cracks seal up due to ettringite formation or accumulation of mineral deposits and prevent the penetration of the corrosion causing agents (i.e. chloride ions, oxygen, and moisture) (Bertolini, Elsener, Pedeferri, & Polder, 2004; Jang, Kim, & Oh, 2011).

2.7.2 Corrosion propagation phase

After the steel has been depassivated (i.e. at corrosion initiation), the sustained presence of both oxygen and moisture within the vicinity of the reinforcement bar aids corrosion propagation. The reinforcement damage in the corrosion propagation phase mainly depends on the continual supply of moisture, oxygen to the corrosion site, and to an extent further chloride ingress. Depending on the corrosion rate, the propagation phase may result in the gradual or rapid damage and subsequent shortening the service life of the RC structure (Broomfield 2007). In this phase, there is a reduction in the cross-sectional area of the reinforcement bar as it dissolves thereby causing a buildup of corrosion products at the concrete–steel interface (T. D. Marcotte & Hansson, 2007). The accumulation of the corrosion products exerts pressure on the concrete and causes it to crack, spall, and in some instances, delaminate. Rust stains may also be evident when the products of corrosion reach the concrete surface via openings such as cracks or via the concrete pores. The load carrying capacity of severely corroded RC structures is reduced, deflection may become more pronounced and the structure may collapse if not repaired immediately.

2.8 Chloride ingress in concrete

Chloride ingress into concrete is a complex process which depends on concrete penetrability, surface concentration of chlorides, environmental factors (temperature, average relative humidity, wetting and drying cycles) and mechanical interactions such as stress conditions caused by loading which can result in surface cracks (Bastidas-Arteaga, Chateauneuf, Sánchez-Silva, Bressolette, & Schoefs, 2010; Martín-Pérez et al., 2001; D. V. Val & Trapper, 2006). The correlation between chloride penetration and corrosion initiation has led to the development of models by researchers based on the modes of chloride penetration, hence, chloride penetration into concrete has been modeled as either a pure diffusion process using Fick's second law or as a combination of diffusion, convection, and migration. However, chloride diffusion has been widely agreed to be the dominant means of chloride transport in uncracked concrete.

The Fick's second law formulated in 1855 defines the change in chloride ion concentration at a certain depth from the concrete surface with respect to time. For a constant diffusion coefficient, Fick's second law for a three-dimensional rectangular shaped object can be stated in Eqn. 2.14 (Crank, 1975);

$$\frac{\partial C}{\partial t} = D\left(\frac{\partial^2 C}{\partial x^2} + \frac{\partial^2 C}{\partial y^2} + \frac{\partial^2 C}{\partial z^2}\right) \qquad 2.14$$

Where C = concentration of the diffusing substance

x, y and z = space coordinates,

D = the diffusion coefficient and,

t = time

From Eqn. 2.14, it can be deduced that the external faces of a RC element can be subject to chloride ingress in 1D, 2D or three-dimensions (3-D) depending on its shape and exposure to chlorides (Figure 1.1). When 1D (x - linear) chloride penetration is dominant (e.g. in walls and slabs), Eqn. 2.15 is reduced to a 1D chloride flow into the concrete (Figure 1.1a) (Bastidas-Arteaga et al. 2010). In contrast to walls and slabs, rectangular columns and beams are subject to either 2D

(*x* and *y*) (Figure 1.1b) or 3-D (*x*, *y*, and *z*) chloride ingress at their orthogonal corners (Figure 1.1c).

While the 3D chloride ingress only affects the end of a concrete element, 1D and 2D chloride ingress affect the entire length of the reinforcement bar on the exposed concrete face. Considering this chloride ingress dimensions, 1D and 2D chloride ingress can be adjudged to have the most detrimental effect on RC structures when compared to 3D chloride ingress. The next subsections cover 1D and 2D chloride ingress.

2.8.1 1D chloride ingress

Most chloride-induced RC deterioration research has focused on 1D chloride ingress. As stated in Section 1.2, this type of chloride ingress best simulates exposure of reinforcement bars that are located in the faces walls and slabs (Figure 1.1a). The chloride diffusion into the concrete can be determined by using a 1D term of the Fick's second law given in Eqn. 2.14. This equation can be restated for a 1D case (see Eqn. 2.15);

$$\frac{\partial C}{\partial t} = D\left(\frac{\partial^2 C}{\partial x^2}\right) \qquad 2.15$$

Crank (1975) presented an analytical solution to Eqn. 2.15 (see Eqn. 2.16) which has been used to predict chloride concentration at various depths from the concrete surface at any given time. Certain assumptions used in this solution are; not considering the effect of chloride binding, the absence of chlorides in the concrete at the beginning of the diffusion process, and the diffusion occurs in a semi-infinite media with a constant diffusion coefficient *D*. This analytical solution can be utilized to estimate the chloride ion concentration as a function of depth from the concrete surface (*x*) and time (*t*) respect to chloride concentration at the concrete surface (C_s);

$$C_{x,t} = C_s\left[1 - erf\left(\frac{x}{2\sqrt{D_a t}}\right)\right] \qquad 2.16$$

where C_s = chloride ion concentration at the surface of the concrete in contact with the chlorides (g/m^3),

$C_{x,t}$ = chloride concentration at depth x at a given time, $t > 0$; g/m^3),

x = chloride penetration depth from the concrete surface (m),

erf = mathematical error function and,

t = time of exposure (s)

D_a = apparent chloride diffusion coefficient (m^2/s).

Though Eqn. 2.16 may estimate the time it takes for a certain concentration of chlorides (C) to reach a depth (x), and initiate corrosion, the time (t) it takes for an unacceptable level of RC damage will depend on the corrosion rate.

Figure 2.4 illustrates a plot of the solution to Fick's second law analytic solution for a 1D chloride ingress case with measured data at depths beyond the convection zone (a depth slightly greater than 5 mm from the concrete surface).

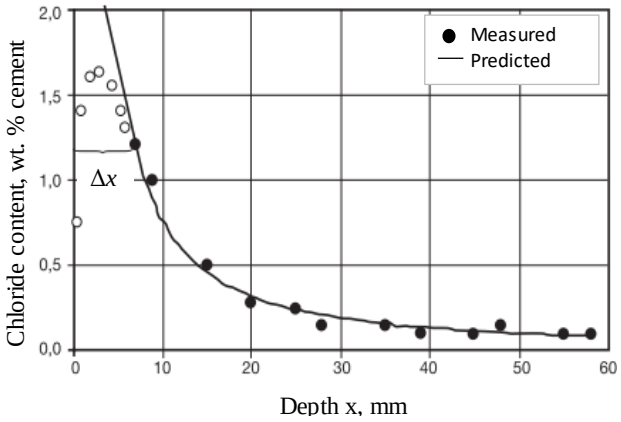


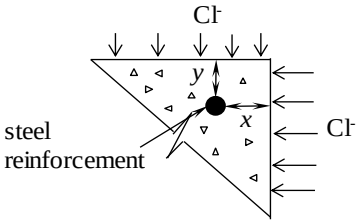
Figure 2.4: Typical measured and predicted chloride diffusion in concrete within the splash zone (Hunkeler et al., 2005).

This diffusion profile (Figure 2.4) represents uncracked concrete. This chloride diffusion profile can be used to predict the time-to-corrosion initiation due to 1D chloride penetration, however when a concrete element is subjected to 2D chloride ingress (e.g. at orthogonal corners), the chlorides will penetrate the concrete at a higher rate thereby reducing the time-to-corrosion initiation of the reinforcement bars which are located at orthogonal corners.

In cracked concrete, it can be assumed that the chloride penetration profile will not have the same pattern as that of uncracked concrete. The influence of cover cracks on chloride penetration into concrete will be discussed in Section 2.9.

2.8.2 2D chloride ingress

Various studies conducted on the corrosion of reinforcement bars placed at orthogonal corners and subjected to 2D chloride ingress have shown that the time-to-corrosion initiation was overestimated when predicted using the 1D chloride diffusion model (Kang & Shim, 2011; D. V. Val & Trapper, 2006; Dimitri V. Val & Trapper, 2008; Y. Zhang, Sun, Chen, et al., 2011; Y. Zhang, Sun, Liu, et al., 2011). Though this overestimation is based on the time-to-corrosion initiation, it can be inferred that if the same influence is noticed in the corrosion propagation phase, then the steel deterioration may proceed at a higher rate when compared to that of steel reinforced elements exposed to 1D chloride ingress. A sketch of an exposure to 2D chloride ingress at an orthogonal corner of a reinforced concrete element is shown in Figure 2.5.



x and *y* are concrete cover to reinforcement from the vertical and horizontal concrete surfaces

Figure 2.5: Physical model of 2D chloride diffusion (Kang & Shim, 2011)

The proceeding sub-sections will review factors which have been identified to accelerate 2D chloride diffusion in concrete.

2.8.2.1 2D chloride ingress diffusion profile

In 2D chloride ingress, there is a simultaneous penetration of chlorides from adjacent faces of the concrete which results in higher chloride penetration due to an interaction of the penetrating chlorides; these results in a curved profile instead of an orthogonal one (see Figure 2.6).

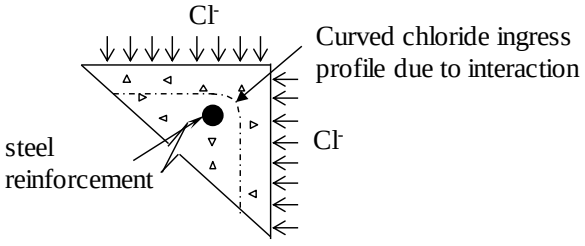


Figure 2.6: Typical 2D chloride ingress profile at a RC orthogonal corner

The curve at the concrete edge indicates the interaction of the chloride ions penetration profile from the adjacent faces of the concrete. Zhang, Sun, Chen, *et al.* (2011) quantified the effect of diffusion interaction at orthogonal corners of the PC and PC/FA concretes based on 2D and 3D chloride ingress and proposed an interaction coefficient (K_{nD}), defined as the acceleration rate exceeding 1D chloride ingress(Eqn. 2.17). The theoretical chloride diffusion coefficient (D_T) was computed based on the assumption that there is no interaction where the chloride diffusion profiles meet. Hence, D_T for the 2D and 3D chloride ingress were respectively computed as √2 and √3 of 1D chloride concentration.

$$K_{nD} = \frac{D_E}{D_T} \qquad 2.17$$

Where n = chloride ingress directions (n= 2 or 3),

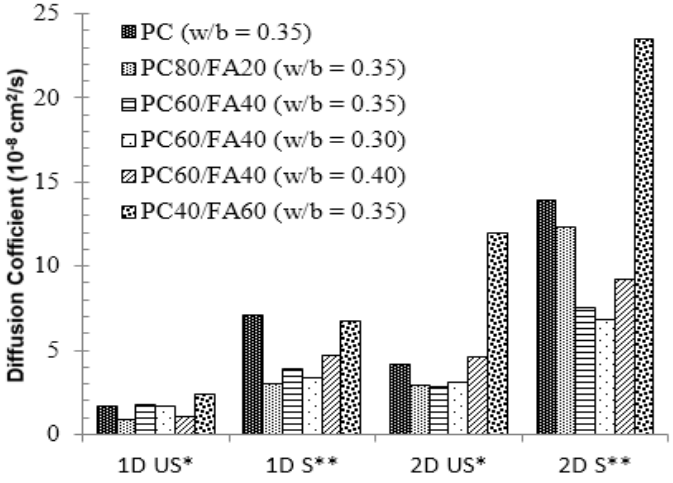
D_E and D_T = experimental and theoretical diffusion coefficients respectively.

Using a regression plot, they determined the chloride interaction coefficient (K_{nD}) in relation to exposure age to chlorides (t = 12 months). The results of their experiment showed that 2D and 3D chloride penetration at orthogonal corners was about twice the 1D rate (K_{2D}= 2.01) and K_{3D}= 2.27 respectively. Hence, chloride ingress is twice as higher at corners subjected to 2D chloride ingress compared to concrete elements which are exposed to 1D chloride ingress. The result of this experiment was based on concrete which was not subjected to stress; however, most in-service structures are subjected to some form of stress. The next section will consider the influence of stress on 2D chloride diffusion in concrete.

2.8.2.2 Influence of stress on 2D chloride diffusion coefficients

Results of further studies by Zhang, Sun, Chen, *et al.* (2011) and Zhang, Sun, Liu, *et al.* (2011) on rectangular concrete beams showed that the chloride diffusion coefficient is influenced by the concrete exposure as well as its stress condition (Figure 2.7). They investigated 2 sets of specimens; stressed and unstressed specimens which were immersed in 3.5% chloride solution. A flexural load, equivalent to 35% of the beams total stress resistance was imposed on the stressed specimens while the unstressed specimens were not loaded. The flexural stress used

in this experiment did not cause visible cracks on the concrete surface, this may not be the case in in-service structures where the flexural stresses are likely to create cracks which widen or close depending on the imposed load on the structure.



US*Effective chloride diffusion in unstressed concrete determined after 6 months immersion

S**Apparent chloride diffusion coefficient in stressed concrete determined after 12 months immersion

Figure 2.7: Comparison of 1D and 2D chloride diffusion in stressed and unstressed concrete (Y. Zhang, Sun, Chen, et al., 2011; Y. Zhang, Sun, Liu, et al., 2011).

The results obtained in relation to the chloride ingress directions (for both stressed and unstressed specimens) show that the specimens exposed to 2D chloride ingress had higher effective and apparent chloride diffusion coefficients than specimens exposed to 1D chloride ingress. The stressed specimens had markedly higher chloride diffusion coefficients compared to the unstressed specimens, irrespective of their chloride ingress dimensions

They proposed a stress acceleration factor ($K_{\delta s}$) for the chloride penetration in concrete as a ratio of chloride diffusion coefficient in the stressed state ($D_{\delta s}$) at flexural stress (δs) and chloride diffusion coefficient (D_o) in the unloaded state (Eqn. 2.18);

$$K_{\delta s} = \frac{D_{\delta s}}{D_o} \qquad 2.18$$

An estimate of the stress acceleration factor of concrete in stressed condition provides an understanding of the effect of stress on chloride diffusion at orthogonal corners of RC elements. Even though the specimen cross-sectional dimensions was

not considered in their study (it has been reported that diffusion is higher in small cross sections than large cross-sections (Frier and Sørensen 2007)), the results of their study further indicate that chloride diffusion is higher in concrete which is stressed than one which is unstressed. The results of their study did not give an insight into the likely effects of the increased chloride diffusion coefficients on the corrosion of embedded steel reinforcement, however, it can be reasonably assumed that the high diffusion rate of chlorides into the concrete will decrease the time-to-corrosion initiation of reinforcement bars that are located at orthogonal corners of concrete elements.

The interaction of the chloride diffusion profiles, and stress acceleration factor can be used to transform 1D chloride diffusion rates to equivalent 2D or 3D diffusion rates. However, to adapt to changing scenarios, the concrete material characteristics (concrete quality, binder type and composition, w/b ratio, concrete age) and other external factors (such as temperature, relative humidity and stress) which may influence chloride penetration into concrete may need to be factored into the equation for these parameters (i.e. Eqn. 2.17 and 2.18).

An insight into the effect of stress on the corrosion of embedded steel reinforcement was provided in a study by Zhang, Castel and François (2010). They applied a flexural load (using the 3-point bending technique) to their specimens (150 × 280 × 3000 mm RC beams). In contrast to the study carried out by Zhang, Sun, Chen, et al. 2011; Zhang, Sun, Liu, et al. 2011 where the stress applied to their specimens did not result in noticeable flexural cracks, the specimens used by Zhang et al. 2010 were loaded until flexural cracks were induced in the beams. The results presented (see Figure 2.8) are for specimens exposed to a 3.5% NaCl fog spray (with all 4 surfaces of the beam exposed) over a period of 23 years.

They found out that the highest loss in cross sectional area in both the tensile and compression reinforcement bars occurred at the mid-span (between 1 m – 1.8 m) of the beam. In other parts of the reinforcement bar that are away from the beams mid-span (i.e. towards its ends), minimal cross-sectional area loss was observed (Figure 2.8). While the loss in cross-sectional area of reinforcement bars (at mid-span) in the tensile face was between 17 – 35 mm^2 (Figure 2.8a), the loss observed in the compressive face was between 3 – 15 mm^2 (Figure 2.8b), hence, the beam

reinforcement bars that were subject to tensile stresses corroded more than the those subjected to compressive stresses. Even though both faces of the concrete are subjected to stresses, the higher cross-sectional area loss of the steel bar in the tension face of the beam indicates that the penetration of corrosion-causing agents is most critical on the concrete face which is subjected to tension compared to that which is in compression. Cracks which provide a preferred zone for the penetration of chlorides, air and moisture which give rise to early corrosion initiation and sustain its propagation are likely to be formed at the mid-span of the beams tensile face (Bentz et al., 2013). Hence, corrosion initiation is likely to be earlier and propagate on faces that are subjected to tensile stresses.

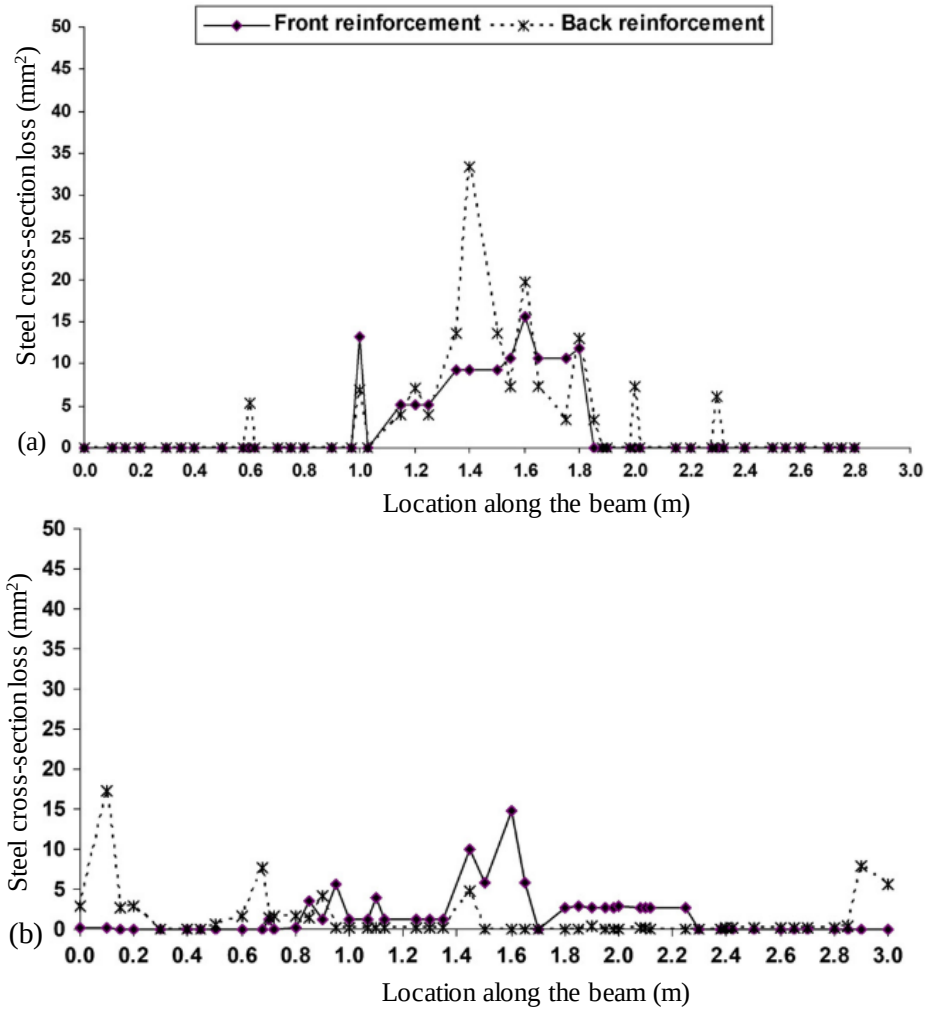


Figure 2.8: Corrosion distribution along length of reinforcement bar in the beam (a) Tensile face and (b) compressive face of the beam (R. Zhang et al., 2010).

It is noticed that the back side of the reinforcement bar (surface that is away from the concrete surface) corroded more than its front face for the bars in the tensile region, this may have been due to defects (e.g. bleeding and settlement of fresh concrete) at the steel-concrete interface (SCI) when the concrete was cast (Tarek Uddin Mohammed, Otsuki, Hamada, & Yamaji, 2002; Söylev & François, 2005). These defects may have created reservoirs for the chloride solution. The contact of these chloride reservoirs with the steel reinforcement may result in the formation of large anodes. The voids also provide space for the products of corrosion to fill.

The steel mass loss can also be used in relation to the cross-sectional area loss (Eqn. 2.19). Hence, an acceptable cross-sectional dimension loss in the steel bar can be determined in relation to the mass loss. This relationship is useful in estimating load bearing capacity of structures and their remaining service life.

$$\Delta A_s = \frac{\Delta m}{m} . A_s \qquad 2.19$$

where ΔA_s is the average steel cross-section area loss (mm^2),

Δm is change in mass of steel per unit of length (g),

m is the initial mass of the steel reinforcement bar per unit of length (g), A_s is the cross-sectional of the non-corroded steel (mm^2).

Ye et al. (2018a) also conducted a similar study to that which was undertaken by Zhang et al. (2010), however their study sought to investigate the performance of reinforced concrete beams which have corroded under various levels of sustained flexural loads and corrosion acceleration techniques (galvanic method and artificial climate exposure technique). 3 sets of steel RC beams with the dimensions 100 × 160 × 1400 mm were used in this experiment. The first specimen set were subjected to 0% flexural loads, while the other 2 specimen sets were subjected to 30% and 60% of their ultimate flexural loads using the 4-point bending technique. To accelerate the corrosion process, an impressed galvanic current kept at 0.1A and a NaCl ponding solution of 3.5% was used for the first set of specimens while the other specimens which were kept in an artificial exposure climate condition (40 ± 0.5°C and 90% relative humidity) had an admixture of 3.5% NaCl by mass of binder added to the concrete mix.

Longitudinal (corrosion-induced) cracks along the length of the steel reinforcement bars were noticed 60 days after the start of the experiment in both specimens exposed to galvanic and the artificial exposure environment. The corrosion induced crack widths were monitored until they reached approximate values of 0.3 mm, 0.5 mm, 0.8 mm and 1.0 mm after which the reinforcement bars were removed from the RC beams specimens. The beams with 0% flexural loads showed a similar mass loss along the length of the corroded reinforcement bar (Figure 2.9a) while the specimens that had a flexural imposed load of 30% and 60% had a higher loss in steel at the middle of the reinforcement bar compared to its ends (see Figure 2.9b and Figure 2.9c respectively). The specimen with the 60% flexural stress had the highest steel mass loss, then those with 30% flexural load while those without any flexural load had the least mass loss. The location where there is the highest mass loss in the steel bars of the specimens with the sustained flexural load coincides with locations where the flexural stress is most dominant (at the mid-span of the specimen). The corrosion-causing agents easily penetrate concrete sections that are subjected to tension stresses.

Contrary to their findings in the artificial climate exposure, the beams subjected to galvanic corrosion did not show much variance in steel mass loss along the length of the reinforcement bar (Figure2.10), hence, they concluded that the mass loss ratio in the specimens exposed to the artificial climate depicted service conditions thereby making them most suited for the study of RC beams under sustained flexural loads. The presence of admixed chlorides in this concrete mix may have influenced the results of the study since the steel reinforcement bars are in direct contact with the chlorides thereby causing it to readily depassivate; the supply of chlorides in the galvanic corrosion process on the other hand rely on it penetrating into the concrete In the galvanic method, the chloride penetration is not only influenced by the stress imposed on the concrete but it is also affected by the impressed current which is applied along the entire length of the reinforcement bar. This current causes chloride ingress along the reinforcement bar length through migration of the ions. The key below can be used to identify the specimens in the graphs presented in figure 2.10 and Figure 2.9.

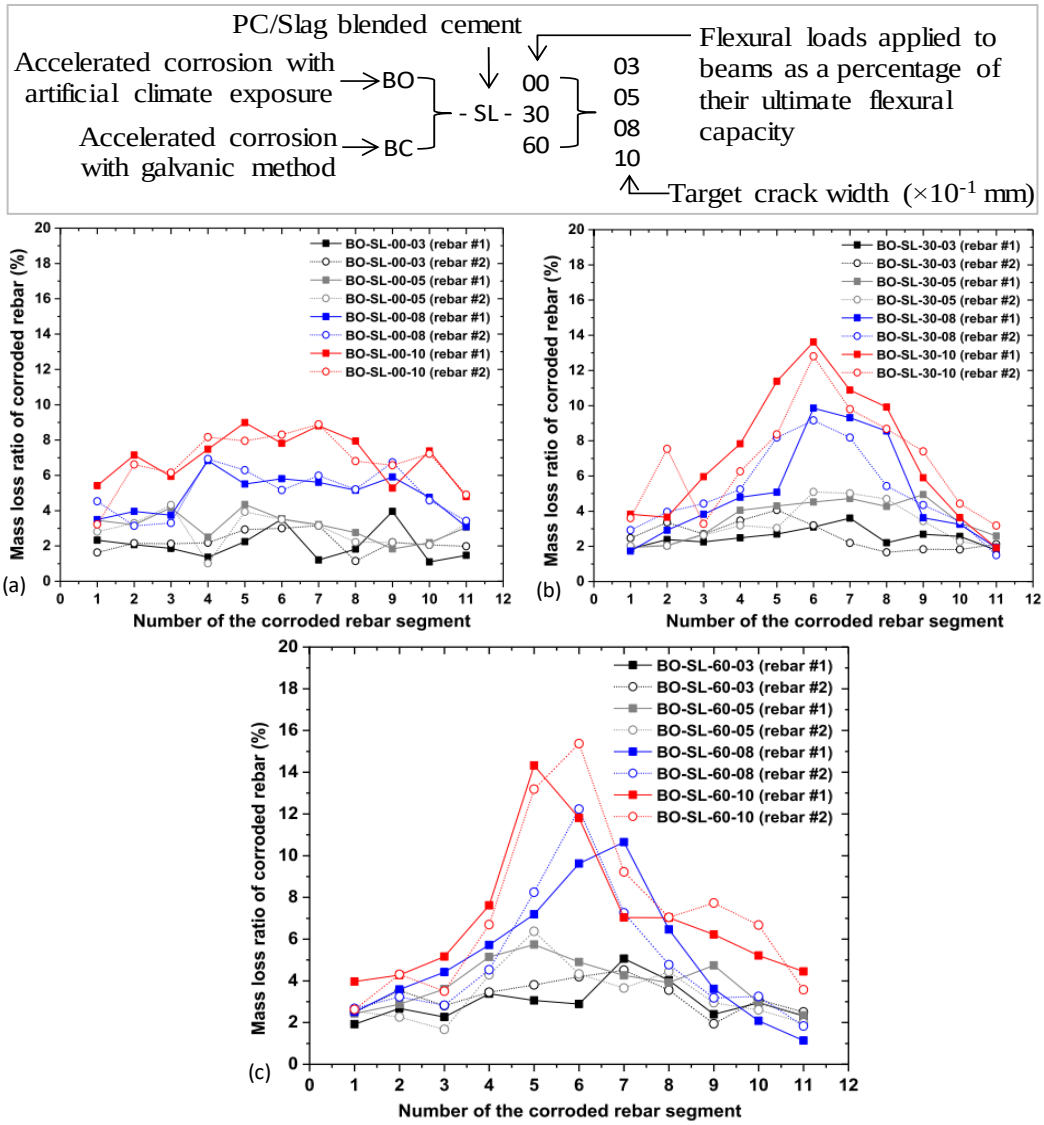


Figure 2.9**:** Mass loss ratio distribution along length of corroded steel in RC beams subjected to artificial climate exposure method (a) specimens without sustained loads (b) specimens with 30% sustained loads (c) specimens with 60% sustained loads (Ye et al., 2018).

Two separate investigations (detailed results not presented) , earlier undertaken by Yoon et al. (2000) and Otieno (2008) showed that the imposition of a constant or varying load on their RC specimens increased the corrosion rate of the steel reinforcement depending on the stress imposed. While Ye et al. (2018a) reported that there was no much difference in mass loss of the specimens subjected to galvanic corrosion, Yoon et al. (2000) used a similar experimental setup (4 point bending technique with both sustained and cyclic flexural stress of 0 – 75% of the

beams ultimate strength imposed on the specimens), their results showed that the corrosion rate increased with varying and increasing flexural stress. It is worth noting that while a sustained load may create stress induced cracks on the concrete surface, these cracks (which are static in nature) are likely to heal with time (Chun-ping, Guang, & Wei, 2015; Jacobsen, Marchand, & Boisvert, 1996; M. Otieno, Beushausen, & Alexander, 2012; Scott & Alexander, 2007; R. Zhang et al., 2010), however, the loading and unloading of the beam hampers the crack healing by reopening them, thereby permitting easy access for the corrosion causing agents into the concrete.

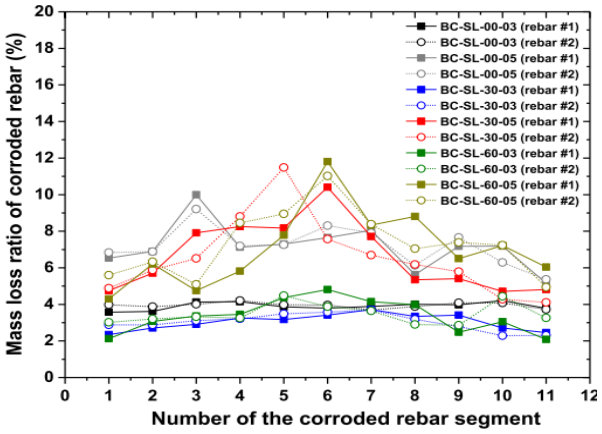


Figure 2.10: Distribution of mass loss ratio of segmented reinforcement bar along the longitudinal direction of corroded reinforcement bar in RC beams accelerated by galvanic method (Ye et al., 2018).

2.8.2.3 Influence of concrete cross sectional dimension on 2D chloride ingress

The effect of dimensional interaction and concrete cross sectional dimension was also studied by Frier and Sørensen (2007) (Figure 2.11).

The study utilized 1D and 2D analytical and numerical solutions to assess the effect of 2D chloride penetration in two concrete elements of square cross-sectional dimensions of 100 mm and 400 mm.

Considering the analysis methods used, the 2D solutions provided a better interpretation of chloride penetration at the concrete corners in comparison to the 1D solution. An assessment of the chloride diffusion profiles of the cross sections shows that the concrete with the smaller cross section is most affected by 2D chloride ingress compared to that with the larger section. This is evident by the

chloride concentration at various depths along the length of the concrete elements. Hence, the close interaction of the diffusion profiles in small concrete cross-sections makes them prone to be easily contaminated with a higher concentration of chlorides at a depth (x) beneath the concrete surface compared to a larger cross-section. This finding is consistent with the provision of BS 8110-1 (1997), section 3.5.2.1 which states that;

> *Concrete is more vulnerable to deterioration due to chemical or climatic attack when it is in thin sections, in sections under hydrostatic pressure from one side only, in partly immersed sections and at corners and edges of elements.*

In order to eliminate the influence of the cross section dimension on the results of the current study where 3 faces of the concrete were left unsealed in this experiment Figure 2.11, this study utilized a concrete of 150 mm square cross-section of which only two adjacent sides at an orthogonal corner were left unsealed (i.e. in the specimens exposed to 2D chloride ingress). This experimental setup is to ensure that only two diffusion profiles interact at a time.

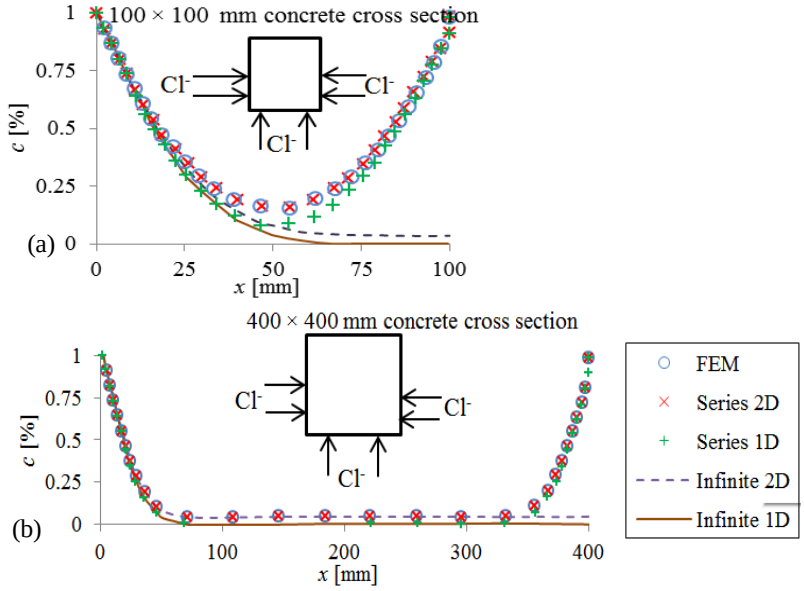


Figure 2.11**:** Chloride ion concentration profile along a concrete edge after 30 years of exposure, 50 mm from the surface with sides of: (a) 100 × 100 mm and (b) 400 × 400 mm cross sections (Frier & Sørensen, 2007).

2.8.2.4 Influence of 2D chloride ingress on time-to-corrosion initiation

In RC, the time-to-corrosion initiation has been widely reported to be dependent on the time it takes for sufficient concentration of chlorides to be deposited on the steel reinforcement bar surface to cause its depassivation. Studies on dimensional interaction suggest that corrosion initiation of steel reinforcement bars placed at orthogonal corners of RC elements will commence earlier when they are exposed to 2D chloride ingress, compared to those exposed to 1D chloride ingress. Other factors which can also influence the time-to-corrosion initiation are the concrete mix composition and the RC elements cross sectional area.

2D analytical solutions to Fick's second law were provided by Crank (1975) and Edwards and Penney (1993) respectively by using;

i. Product solution of two 1D solutions and,
ii. Series solution by separation of variables method.

Numerical methods such as random field, random variable, and finite and boundary element methods (FEM and BEM) have also be used to estimate 2D chloride penetration and time-to-corrosion initiation (Yang, Chen, Gao, & Ju, 2012). In utilizing the random field approach, parameters which affect the diffusion process were taken as varying in time and space thereby capturing possible field variations; this is considered adequate in predicting the chloride penetration as compared to the random variable method which assumes the parameters to be constant. A comparison of the probability of corrosion due to 1D and 2D chloride penetration was assessed by Frier and Sørensen (2007) using the random field, variable and finite element method approaches (Figure 2.12), the results indicated that a higher probability of corrosion initiation exists in concrete specimens exposed to 2D chloride ingress compared to specimens exposed to 1D chloride ingress.

Probabilistic and stochastic methods have also been used to predict 2D chloride penetration; however, various limitations have been cited in adopting this approach as it becomes increasingly complex with the addition of variables which affect the corrosion process (D. V. Val & Trapper, 2006). Inadequate data on 2D chloride penetration studies in literature also serve to limit the use of these methods since a large amount of data is required.

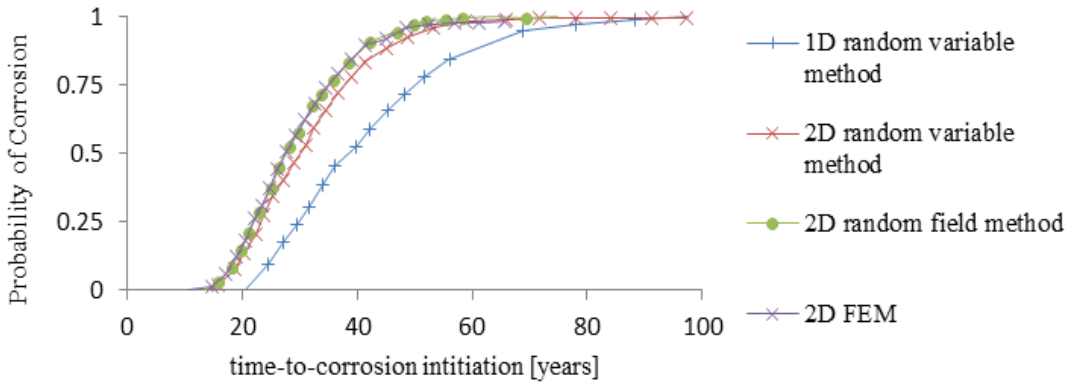


Figure 2.12: Probability distributions for the time-to-corrosion initiation of corner reinforcement bar using random variable, random field and finite element methods (Frier & Sørensen, 2007).

2.8.2.5 Influence of chloride ingress directions on chloride concentration

The influence of chloride ingress directions on chloride concentration was studied by Kang and Shim (2011). They conducted an empirical study of the effect of 2D chloride penetration at the corner of a bridge pier and compared the results with that of a numerical (FEM) prediction model. Comparing 1D and 2D chloride ingress, the chloride concentration at the reinforcement depth was higher at the RC element corners compared to that measured at the middle of the pier up to a depth of about 40 mm from the concrete surface (see Figure 2.13).

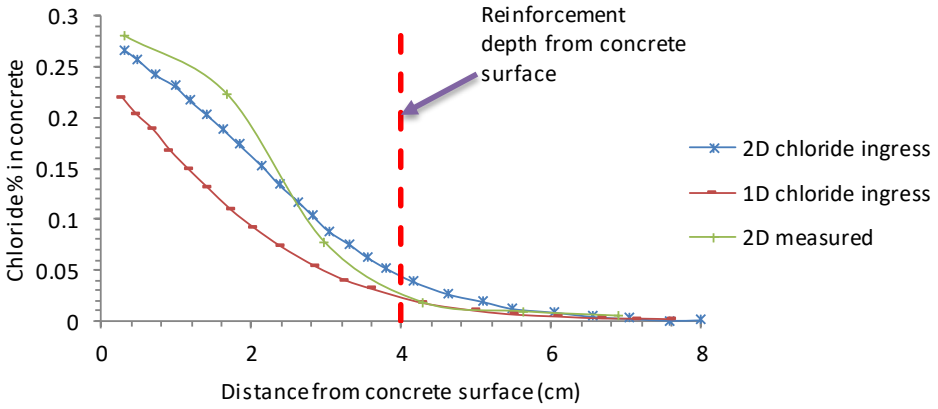


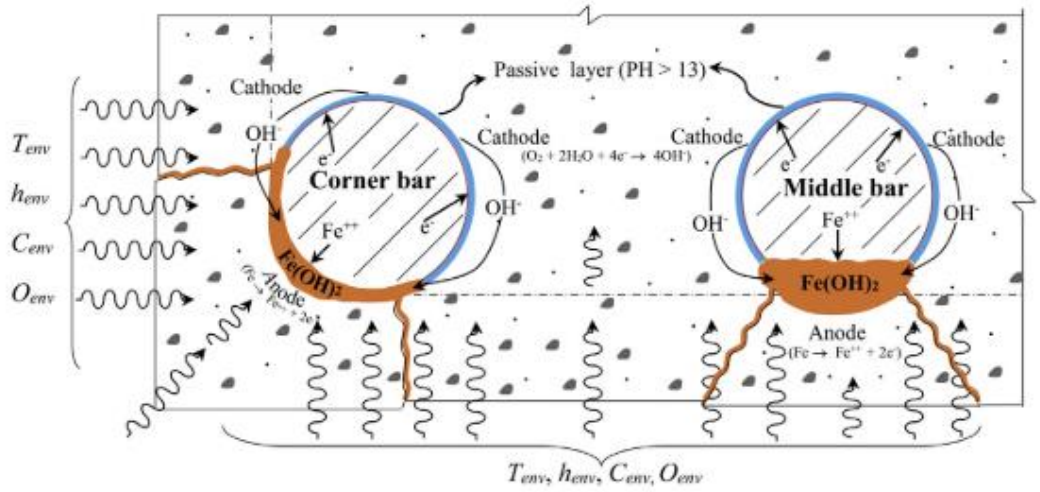
Figure 2.13: Numerically determined and measured chloride profile from concrete bridge pier (Kang & Shim, 2011).

The higher chloride concentration at the corners of the RC element is probably due to 2D chloride ingress. The graph (see Figure 2.13) also reveals that the effect of 2D chloride ingress can be observed up a cover depth of about 35 mm from the

surface of the concrete, beyond this depth, no significant difference in the chloride concentration is observed. However, the chloride concentration at varying cover depths may vary depending on the concrete mix.

2.8.2.6 Corrosion induced damage

The damage resulting from 1D and 2D chloride-induced corrosion differ as the reinforcement bar area exposed to depassivation is greater. Though both the middle and corner reinforcement bars are subjected to non-uniform corrosion, the anode (corroding region) of the corner bars (exposed to 2D chloride ingress) has been observed to be larger than the corroding area of reinforcement bars exposed to only 1D chloride ingress (Figure 2.14) (Muthulingam and Rao, 2015).



T_{env}, h_{env}, C_{env} and O_{env} are temperature, relative humidity, chlorides and oxygen penetrating from the environment

Figure 2.14: Non-uniform corrosion in corner and middle reinforcement bars (Muthulingam and Rao, 2015)

Though the results of the reviewed literature are for uncracked concrete, a preliminary conclusion can be reached that the accumulation of chloride ions from two orthogonal directions, causes a significant reduction in the corrosion-free life of reinforcement bars placed at corners of RC structures (Kang & Shim, 2011).

The extent of the corrosion as a result of 2D chloride ingress in cracked concrete needs to be assessed, since the transport properties of fluids and gases in concrete is affected by cover cracks (Rodríguez & Hooton 2003a; Carmeliet et al. 2004; Otieno 2008; Otieno 2010; Djerbi et al. 2008; Blagojevic et al. 2012; Branko &

Erik 2012). An assessment of the influence of cover cracks may yield an understanding of their influence on time-to-corrosion initiation, corrosion rate and corrosion damage characteristics of steel reinforcement bars placed at orthogonal corners of reinforced concrete elements subjected to 2D chloride ingress.

2.9 Chloride penetration in cracked concrete

The risk of corrosion due to chloride penetration can be reduced by designing crack-free concrete with low penetrability; however, the inherent nature of concrete (especially in-situ cast concrete) is such that cracks are inevitable. Apart from corrosion induced cracks, mechanical loading, thermal effects, plastic and drying shrinkage may also cause concrete to crack (Blagojevic et al. 2012). While some authors posit that RC cover cracks have no influence on corrosion propagation (Ismail et al. 2008; Schießl and Raupach 1997), others have identified that the presence of cover cracks modify concrete transport properties. The near absence of the corrosion initiation phase and higher corrosion rates obtained from cracked RC elements has led to the conclusion by some researchers that cover cracks have an influence on RC corrosion (Adiyastuti, 2005; Audenaert et al. 2009; Branko and Erik, 2012; Otieno et al. 2010). Where cover cracks are induced by stress, damage to the steel-concrete interface (SCI) has also been reported. Hence, Pease (2010) hypothesized that the extent of debonding along the SCI is more important than concrete cover crack width measurements in terms of depassivation and reinforcement corrosion. He reported that measurements from an instrumented reinforcement bar indicated that increased crack width allowed a rapid change in the steel-concrete interface thereby favoring the depassivation of the reinforcement bar. Though a detailed investigation of the SCI condition will not be undertaken in this study, the buildup of corrosion products in this layer will be observed and reported at the end of the experimental program.

While it is generally agreed that diffusion governs chloride penetration in uncracked concrete, a combination of both diffusion and convection has been observed in cracked concrete, thus resulting in greater penetrability (Hunkeler et al., 2005; Schießl & Raupach, 1997). The concrete crack width, shape, density and frequency, depth and degree of connectivity, as well as its origin has been reported to influence the transport mechanism of corrosion causing agents into concrete (Breysse and

Gerard, 1997). The cracks tapper into the concrete as their depth increases (Figure 2.15). A study on influence of crack frequency on concrete penetrability by Arya and Ofori-Darko (1996) showed that concrete penetrability is influenced by crack and pore connectivity. Also multiple cracks located within close proximity in RC has been reported to influence the size of the non-corroding region on reinforcement bars causing an increase in corrosion rate (Pease, 2010). These studies confirm that where many surface cracks (in proximity) exist in concrete, crack frequency (or crack density) dominates crack width.

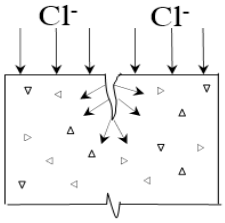


Figure 2.15: Chloride ingress through faces of unsealed cracks

Corrosion-induced cracks are mostly longitudinal; occurring along the length of the reinforcement bar. The coexistence of longitudinal cracks (induced by corrosion) and transverse cracks (due to loads) in a RC element tends to allow more penetration of corrosion-causing agents through the concrete to the steel reinforcement bar thereby resulting in earlier deterioration of the RC element. Unsealed crack faces (see Figure 2.15) also present an increased surface area for chloride ingress.

2.10 Chloride threshold

The chlorides concentration required to breakdown the passive layer on the steel reinforcement surface is referred to as the chloride threshold limit (Sonjoy, 2012). Other terms used in literature are critical chloride concentration or chloride threshold value. The chloride concentration is presented as a mole ratio of $(Cl^-)/(H^+)$ (M), moles/liter (mol/l) or as a percentage weight of binder or concrete (% by weight).

Chloride threshold limits reported in literature have a wide scatter (0.17 – 40) and since various methods have been used to obtain the chloride concentrations, a comparison of the results has not been considered to be appropriate (S. L. Poulsen & Sørensen, 2012). Castel et al. (2003a) suggested that the discrepancy of chloride threshold values reported in literature can be attributed to the failure to take account

of the steel-concrete interface (SCI) quality. Hence a possible correlation between the defects in the SCI and the chloride threshold values may help in solving the disparity in chloride threshold values reported in literature

Apart from this factor, the chloride threshold limit has been identified to depend on a number of other factors such as the chloride binding capacity of the binder, concrete exposure condition (e.g. relative humidity, temperature, moisture level and chloride source), casting direction, concrete defects (e.g. presence of cracks), degree of concrete carbonation, cement alkali content, level of sulfates, steel surface condition and electrochemical potential (U. Angst, Elsener, Larsen, & Vennesland, 2009; U. M. Angst et al., 2017; Ann & Song, 2007; Glass & Buenfeld, 1997; Hussain, Rasheeduzzafar, Al-Musallam, & Al-Gahtani, 1995; Shi et al., 2012).

The chloride limit which causes the destruction of the passive protective oxide layer on the steel surface is widely agreed to be that of the free chlorides.

To minimize corrosion damage due to chloride concentration in RC, the British standards and American concrete institute provided guidelines for maximum free chloride content of percent by weight of binder for various structures (see Table 2.1).

The difference in the adopted chloride threshold limit values shown in Table 2.1 is indicative of the wide range of chloride threshold data values that are available in various studies. The values in Table 2.1 are conservative and may differ widely from what may be obtained in the field.

Table 2.1: British Standard and American Concrete Institute steel reinforced concrete chloride limits.

Type	**Maximum Chloride Content (% weight of binder)**			
	BS 8110	**ACI 201**	**ACI 357**	**ACI 222**
1 Prestressed concrete	0.1	-	0.06	0.08
2 RC exposed to chlorides in service	0.2	0.1	0.1	0.2
3 RC that will dry protected from moisture in service	0.4	-	-	-
4 Other reinforced concretes	-	0.15	-	-

Source: Sonjoy (2012)

2.11 Corrosion assessment techniques

The assessment of RC corrosion can be undertaken by electrochemical and non-electrochemical methods (see Table 2.2); these test methods are mostly non-destructive in nature. The use non-destructive test (NDT) methods to assess RC corrosion has gained wider acceptance to destructive techniques because the NDT methods ensure minimal or no damage is caused to the RC structure being assessed.

Table 2.2: Electrochemical and non-electrochemical methods of corrosion assessment (Bjegovic, Mikulic, & Sekulic, 2007)

Electrochemical Methods	**Non-Electrochemical Methods**
I. Electrostatic Measurements	Visual inspection
Half-cell potential measurements	Seismic method
a. Hand held equipment	Infrared thermography
b. Embedded reference electrodes	Acoustic emission
Corrosion macrocell current measuring	Radiography and radiometry radar
Electrical resistivity of concrete	Electrical resistance method
II. Polarization measurements	Optical fiber sensors
Linear polarization methods (LPR)	Magnetic technique
a. Hand held equipment	Microwave based thermoreflectometry
b. Embedded LPR sensors	
Electrochemical impedance spectroscopy	
Localized electrochemical impedance	
Galvanostatic pulse method	
Scanning reference electrode method	

Some of the corrosion assessment methods that will be used in this study have been widely used by other researchers in both laboratory and field studies. These methods will be discussed under two broad topics of non-electrochemical and electrochemical methods of corrosion assessment.

2.11.1 Visual inspection

This method is a non-electrochemical method of corrosion assessment. Though the easiest means of assessing corrosion activity; the method has the disadvantage that no visible damage to the concrete may be observed in the corrosion initiation phase, hence by the time corrosion defects such as corrosion induced cracks, rust stains, delamination and spalling are noticed, the corrosion process would have advanced to a level wherein costly repair work may be required.

Visual inspections however have the advantage wherein cracks and defects can be characterized e.g. crack lengths, widths, density, identifying locations where rust stains occur and providing information on loss of concrete cover which may occur in the form of spalling or delamination (Poupard et al., 2007).

Most corrosion induced cracks occur along the length of the reinforcement bars. The cracks can be longitudinal (for reinforcement bars that are along the length of the member) or transverse (along the length of shear reinforcement or stirrups) cracks.

Depending on the nature of cracks (longitudinal along reinforcement bar length or transverse across the reinforced concrete element) a relationship between the crack-factor and corrosion rate can be established. This will give an indication of the influence of cracks on the corrosion rate.

Apart from identifying corrosion induced cracks, rust stains can also be observed in RC. However, by the time corrosion induced cracks or rust stains are observed, the steel deterioration may proceed at a rate which may require urgent repair. While rust stains may be easily seen, in some cases, surface cracks may only be identified using magnifying glasses. The need for planned or scheduled maintenance of RC structures means this mode of corrosion assessment is not reliable as it will result in corrective maintenance repair. Hence, electrochemical methods are used to either measure or ascertain the probability of corrosion activity to plan the maintenance of corroding RC structures. Some of the common electrochemical methods used RC corrosion assessment will be briefly discussed in the proceeding sections.

2.11.2 Half-cell potential measurement

This technique is an electrochemical technique. It is used to measure the corrosion potential of steel reinforcement bars embedded in concrete relative to that of a standard reference electrode which in this case could be a copper/copper sulfate ($Cu/CuSO_4$; CSE) or silver/silver chloride (Ag/AgCl; SSE) reference electrode (Park, 2009). In general, the corroding (anode) and passive (cathode) parts of reinforcement bars will show a difference in electric potential due to the formation of macro-cells which generate current flows between these sites. The electric field thus generated can be measured using a suitable high input impedance voltmeter

reference electrode (half-cell) which is placed on the concrete surface. The experimental set-up is shown in Figure 2.16. The voltage reading obtained, can be used to assess the probability of corrosion of the embedded steel reinforcement bar. Increasing negative voltages indicate a high probability of corrosion while more positive voltages indicate a lesser corrosion probability (Table 2.3). It is important to note that the steel reinforcement bar corrosion potential obtained does not provide any information about the kinetics (rate) of the corrosion reaction.

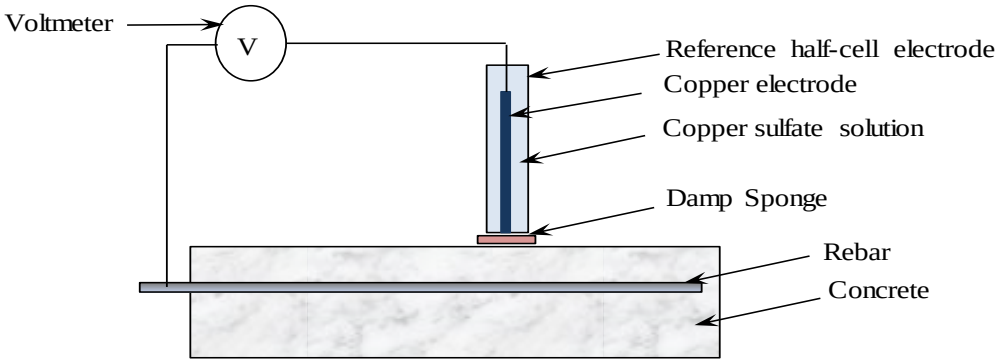


Figure 2.16: Half-cell potential experimental set-up.

Though this non-destructive method of corrosion assessment is easy to use on site, some factors such as concrete moisture content, degree of concrete carbonation, oxygen content at level of steel, quality of concrete, cover cracks, concrete cover thickness and use of stainless steel can influence the electrochemical potentials obtained thereby giving rise to misleading measurements. Various bodies have specified standard test procedures for the HCP test (e.g. ASTM C876, RILEM TC 154).

The $Cu/CuSO_4$ and Ag/AgCl half-cell potential measurements can be interpreted using the ASTM C876 guide provided in Table 2.3;

Table 2.3: Interpretation of corrosion potential results (ASTM C876, 2009)

Measured potential Cu/CuSO4 (mV)	**Measured potential Ag/AgCl (mV)**	**Probability of corrosion activity**
> - 200	> - 119	Less the 10%
- 200 to - 350	- 119 to - 269	Uncertain
- 350 to - 500	- 269 to - 426	More than 90%
< 500	< - 426	Visible evidence of corrosion

Factors which may influence the interpretation of HCP results are discussed in Section 2.12.2.

2.11.3 Concrete resistivity measurement

Resistivity (ρ) is a fundamental property of a material which is used to quantify its ability to transport electrical charge. The measurements are read in either Ω. m or kΩ. cm. The concrete resistivity is the ratio between an applied voltage (V) and resulting current (I) multiplied by a cell constant k (see Eqn. 2.20). Concrete resistivity has been identified as one of the most influential factors that governs the corrosion rate of steel reinforcement in concrete; it determines the corrosion current flow from the anode to the cathode sites. Concrete resistivity depends on the ionic conductivity of the concrete pore solution, its saturation level and the temperature of the concrete; these factors influence the ease with which corrosion current flows in the concrete (Hornbostel, Larsen, & Geiker, 2013). In general, concrete electrical resistivity values have been found to vary widely from as much as 10^6 kΩ-cm to as little as 1 kΩ-cm (Azarsa & Gupta, 2017; Monfore, 1968).

Eqn. 2.20 describes the relationship between concrete resistance and resistivity (Layssi, Ghods, Alizadeh, & Salehi, 2015).

$$\rho = k.R = k.\left(\frac{V}{I}\right) \qquad 2.20$$

where k is the geometric factor which depends on the size and shape of the sample as well as the distance between the probes on the testing device,

V and I are the measured voltage (in *Volts*) and applied current (in *Amperes*) respectively.

The electrical conductivity of concrete (σ_c) can be obtained as the inverse of the concrete resistivity (Eqn. 2.21) (Osterminski, Polder, & Schießl, 2008).

$$\sigma_c = \frac{1}{\rho} \qquad 2.21$$

Hence, a low concrete resistivity will yield a high concrete conductivity and vice versa.

Various methods of measuring concrete resistivity have been developed and used for both laboratory specimens and field structures; they include;

i. Two-point method
ii. Wenner probe (4 point linear or square array) and,
iii. Electrode-disc method.

The two-point method is used to determine the bulk resistivity of hardened concrete (ASTM C1760 - 12). This method is seldom used in the field due to possible difficulty which may be encountered in accessing both sides of concrete elements so as to place the contact electrodes compared to the ease of using other surface resistivity measuring techniques (Wenner probe and electrode- disc method) (Gudimettla & Crawford, 2015). It is important to note that the concrete cover resistivity is most important in assessing risk of RC corrosion, the two-point method reliably measures the bulk resistivity of concrete, however, this method has limitations for use on the field since the concrete needs to the extracted from the structure (Gulikers, 2005; Layssi et al., 2015). The reliability of this method is based on the uniform distribution of current through the specimen being tested, unlike the surface resistivity methods where the current is fed from the surface of the specimen. Other factors which influence the surface resistivity measurements are; non-homogeneity of concrete, size of aggregates and its surface moisture conditions. In general, it has been observed that the surface concrete resistivity methods overestimate the bulk resistivity values by about 10% due to presence of aggregates, this error can however be minimized by taking a multiple readings (U. M. Angst & Elsener, 2013; Spragg, Bu, Snyder, Bentz, & Weiss, 2013).

The use of the Wenner probe and the electrode-disc test method has found wide application in both the laboratory and field. These two methods will be used in this study; therefore, the methods will be briefly discussed. These methods were chosen because they have been widely used in field measurements and it is assumed that the data obtained in this study by using these methods can be correlated with other field and experimental data in which these methods have been used (Spragg et al., 2013). Potential factors which can influence the data obtained and their interpretation are discussed in Section 2.12.1.

2.11.3.1 Wenner (4-point linear array) probe

The method was developed in the 1900's and used for underground exploration of water and minerals and later modified for use in determining concrete resistivity (Broomfield, 2007). For a semi-infinite medium (such as a concrete slab on site), a factor of 2π is used, however a correction factor needs to be used when specimens when small dimension are used else the resistivity value obtained will be overestimated (Morris, Moreno, & Sagüés, 1996).

This device is one of the most adopted for concrete resistivity measurement in both field and laboratory studies due to its ease of use and how rapidly results are obtained (Spragg et al., 2013). The device may consist of two or four probes; however, the four-probe device is most used. The concrete resistivity readings are obtained when the device probes are firmly held down against the concrete surface; the exterior probes apply an alternating current (AC) into the concrete while the potential difference induced by the current is measured from the inner electrodes (see Figure 2.17).

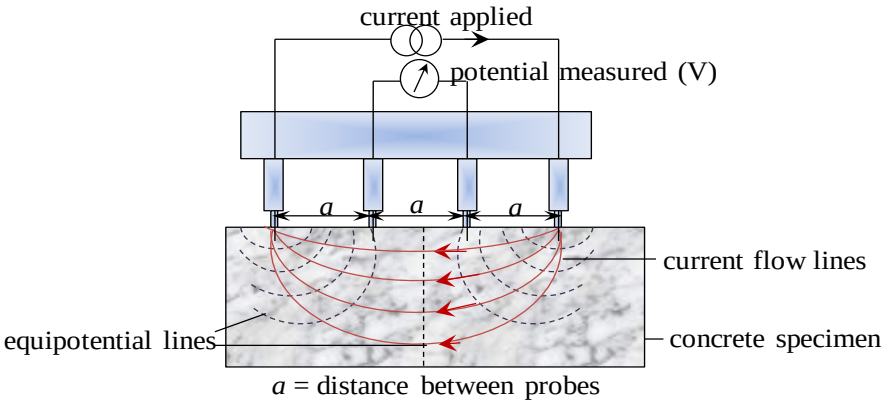


Figure 2.17: 4 point (Wenner probe) concrete resistivity meter (Rob B. Polder, 2001)

To avoid significant errors in the resistivity readings, a number of precautions need to be taken, such as placing a damp conductive material between the probes and concrete surface to reduce contact resistance of the probes, ensuring the probes are at a distance '*a*' (equal to the probe spacing) away from the edges of the specimen and placing the probes transversely across reinforcement bars rather over the embedded steel reinforcement bars. For example, if the Wenner probe is placed over or near an embedded steel reinforcement bar; the steel reinforcement will

conduct current with ease when compared to the concrete which has more resistance to the flow of current because of its heterogeneous nature. More detail about other likely sources of error can be found in the publication by Gowers & Millard (1999).

When the Wenner probe is used for concrete resistivity measurements, Eqn. 2.20 translates to Eqn. 2.22 as shown below (Layssi et al., 2015);

$$\rho = 2\pi a.R \qquad 2.22$$

where $2.\pi$ is dimensionless geometric correction factor,

a is the distance between the probes and

R is the ratio between the applied voltage (V) and the applied current (A) (see Eqn. 2.20).

2.11.3.2 Electrode-disc method

Unlike the Wenner probe method of measuring concrete resistivity which can be affected by the probe closeness to reinforcement bars, the electrode-disc method requires that the device be placed on the concrete surface, directly over a reinforcement bar (Figure 2.18). The concrete resistivity measured is hence that of the cover concrete (i.e. the concrete which lies between the concrete surface and reinforcement). The cover concrete resistivity is important in assessing the risk of corrosion in steel reinforced concrete, hence this method if standardized, can be presumed to provide reliable values which can be used to determine RC durability (Azarsa & Gupta, 2017).

In this method, a current pulse is sent into the concrete via the electrode (placed on the concrete surface, over the reinforcement bar) and the voltage read off from the connection with the reinforcement bar. The resistance (R) is then calculated from the cell constant which varies with cover depth to reinforcement and reinforcement diameter. In general, a cell constant of 0.1 m is normally assumed for cover depth, disc and reinforcement bar diameters between 10 – 50 mm (Rob B. Polder, 2001). The concrete resistivity is computed using Eqn. 2.23;

$$\rho = 0.1 \times R\ (disc - bar) \qquad 2.23$$

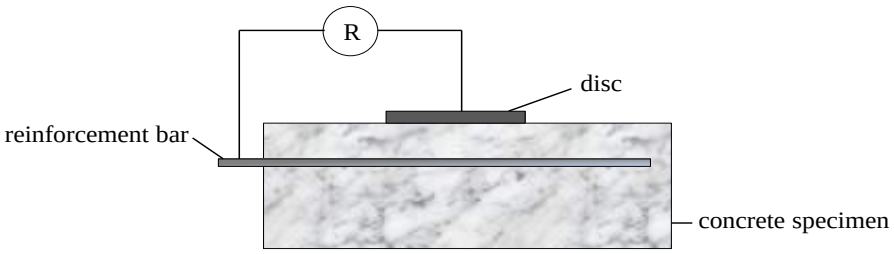


Figure 2.18: One electrode-disc measurement set for concrete resistivity measurement (Azarsa & Gupta, 2017).

The flow of ions between anodic and cathodic sites of a corrosion cell via the concrete pore solution has an impact on the corrosion rate. In general, research results have established a significant correlation between concrete resistivity and corrosion rate of embedded steel reinforcement bars in concrete (Alonso, Andrade, & González, 1988; Azarsa & Gupta, 2017; Gowers & Millard, 1999; Gulikers, 2005; Hornbostel et al., 2013; Morris, Vico, Vazquez, & Sanchez, 2002; M. Otieno, Beushausen, & Alexander, 2015; Yu, Liu, & Chen, 2017). On a general note, the relationship between concrete resistivity and corrosion rate is viewed as complex, however, a simplistic approach suggests that there is an inverse relationship between the concrete resistivity and corrosion rate of steel in concrete (U. M. Angst & Elsener, 2013).

Concrete electrical resistivity measurements can also be used in concrete quality control, predicting chloride permeability and chloride diffusion coefficient, crack detection, setting time of fresh concrete and it can also be used as an indirect means of measuring concrete moisture content (Layssi et al., 2015; Lopez & Gonzalez, 1993; Mutale, 2014; Osterminski et al., 2008; J. Pacheco, Šavija, Schlangen, & Polder, 2012; Ranade, Zhang, Lynch, & Li, 2014; Woelfl & Lauer, 1979).

2.11.4 Corrosion rate measurement techniques

The corrosion rate (I_{corr}) relates to rate of metal dissolution in an environment. This can be measured in terms of mass loss of the material per unit time, unit area, or corrosion current density (Bardal, 2004). In corrosion rate of steel reinforcement in concrete can be measured instantaneously using electrochemical techniques such as linear polarization resistance (LPR), coulostatic method, electrochemical impedance spectroscopy (EIS), and scanning reference electrode method (SRET) (Bjegovic et al., 2007; Suzuki, Kanno, & Sato, 1980).

Though the coulostatic method of measuring corrosion rate will be used in this research, the LPR method will also be discussed. Both methods are based on the same principle and have been commonly used in laboratory and field studies (Suzuki et al., 1980).

Though the coulostatic method of measuring corrosion rate will be used in this research, the LPR method will also be discussed. Both methods are based on the same principle and have been commonly used in laboratory and field studies (Suzuki et al., 1980).

2.11.4.1 Linear polarization resistance technique

The LPR technique setup consists of a reference electrode (*RE*), counter electrode (*CE*) and a working electrode (*WE*). The *CE* is normally a non-reactive metal (e.g. steel) which may (or may not) have a guard ring around it to confine the electric pulse that is discharged into the specimen, while the *WE* is the metal (in this case reinforcement bar) to be tested for corrosion. The setup (see Figure 2.19) could be in the form of a hand held device; in which case, the *CE* is placed on the concrete surface, or fixed; wherein the *CE* is embedded in the concrete (ACI 222R - 01).

The working, reference and counter electrodes may be connected to a digital control system which records the initial corrosion potential (E_{corr}) of the reinforcement bar and the change in its potential (ΔE) after it is perturbed with a polarization current which is discharged from the *CE* unto the test specimen.

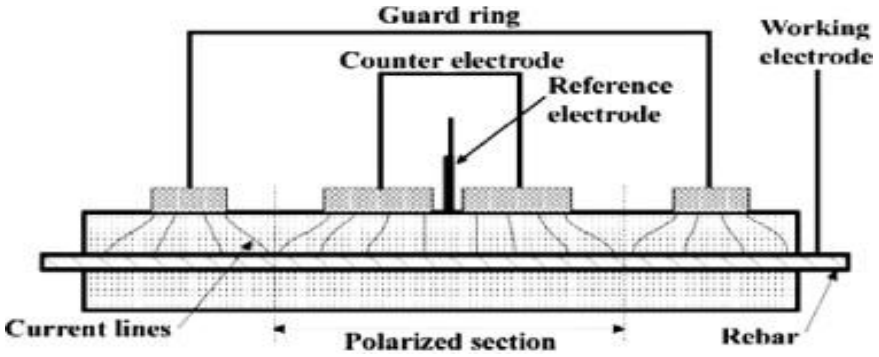


Figure 2.19: Linear Polarization resistance method setup (Gepraegs & Hansson, 2005)

The polarization resistance technique involves the perturbation of the embedded steel bar in concrete by applying a small voltage (ΔE), this voltage raises the metals open circuit potential (E_{corr}). The current flow (Δi) during the perturbation is

measured between two electrodes (reference and working electrode) over some time (Mansfeld, 1976; Ramaniv, Tsirul'nik, Krys'kiv, & Ronchevich, 1989; RILEM TC 154-EMC, 2004).

The polarization resistance (R_p) (Eqn. 2.24) is computed as the ratio between the changes in potential to that of the applied current.

$$R_p = \left(\frac{Change\ in\ potential\ (\Delta E)}{Applied\ current\ (\Delta I)}\right)_{\Delta E \to 0} \qquad 2.24$$

Figure 2.20 depicts how the polarization resistance (R_p) can be empirically obtained from a test specimen. The polarization resistance is also related to the corrosion rate by a constant B, known as the Stern-Geary constant (Eqn. 2.25 and 2.26);

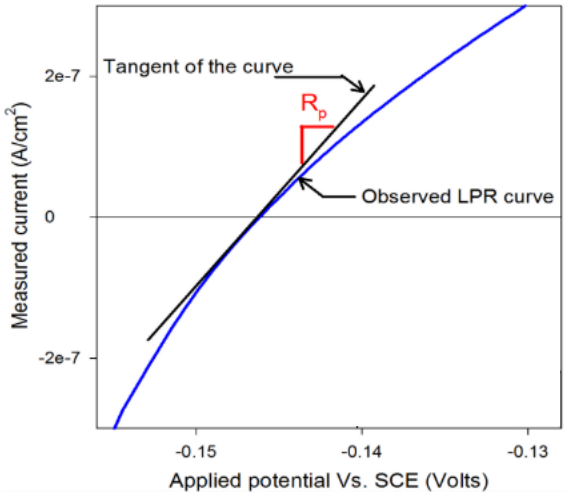


Figure 2.20: Typical LPR curve acquired from a specimen (Pillai, Karuppanasamy, Dhanya, & Nair, 2015)

$$I_{corr} = \frac{B}{R_p} \qquad 2.25$$

$$where\ B = \frac{\beta_a . \beta_c}{2.3(\beta_a + \beta_c)} \qquad 2.26$$

β_a and β_c are the anodic and cathodic Tafel slope values (see Figure 2.21), R_p (kΩ) is the change in potential as given by Eqn. 2.24. The plot of the meeting point of the extrapolated anodic and cathodic Tafel slopes and the corrosion potential (E_{corr}) to the horizontal (log scale) axis gives the corrosion current (see Figure 2.21);

For embedded steel in concrete, the Stern Geary constant (*B*) has been assumed by various researchers to have a value of between 26 mV and 52mV for corroding and passive steel respectively (Bjegovic et al., 2007; Poursaee, 2010).

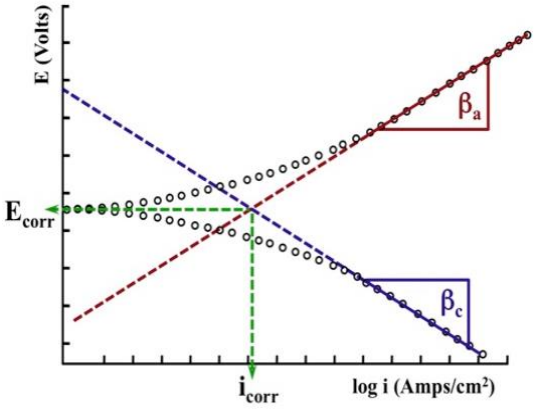


Figure 2.21: A typical Tafel plot showing anodic (β_a) and cathodic (β_c) slopes (Gold standard corrosion science group, 2018)

The corrosion rate (Eqn. 2.27) is also defined as the ratio of the corrosion current to that of the surface area of the steel being polarized (Eqn. 2.28), and can be expressed as;

$$Corrosion\ rate\ (I_{corr}) = \frac{I_{corr}}{A} \qquad 2.27$$

where I_{corr} is corrosion current (μA) and A is the surface area of the polarized steel (cm^2).

$$Surface\ area\ of\ the\ steel, A = \pi\, d\, l \qquad 2.28$$

where d is the metal diameter, l is the estimated length of the reinforcement bar that has been polarized (same as length of counter electrode).

2.11.4.2 Coulostatic technique

The coulostatic method is essentially an LPR technique; however, unlike the LPR method which measures the current flow Δi between the working and reference electrodes after a few minutes, the coulostatic method consists of applying a short current pulse to the metal (also the working electrode) for a very short duration of time (usually some milliseconds) via a counter electrode, computing the overpotential immediately after the charge is supplied and monitoring the potential

decay (relaxation) over a period of time (Glass, 1995). The counter electrode that discharges the charge pulse unto the working electrode can either be embedded in the concrete or placed on the concrete surface. Figure 2.22, shows a typical coulostatic perturbation and response over time.

In order to obtain the corrosion rate, relationships between the overpotential, time transient and perturbation charge need to be established; these relationships are therefore briefly discussed.

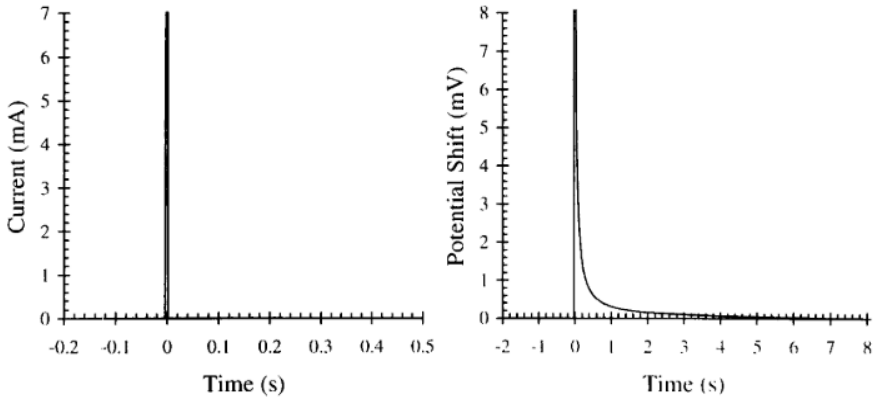


Figure 2.22: A typical coulostatic perturbation and response (Hassanein, Glass, & Buenfeld, 1998).

An empirical relationship which describes the potential transient is given in Eqn. 2.29 (Glass, 1995; Hassanein et al., 1998);

$$\eta_t = \eta_o \, exp\left(\frac{-t}{\tau_c}\right) \qquad 2.29$$

where η_t is defined as the potential shift at a given time t,

η_o is the initial potential shift,

τ_c is the time constant which is computed from Eqn. 2.30;

$$\tau_c = C_{dl} \times R_p \qquad 2.30$$

where C_{dl} is the double layer capacitance and

R_p is the polarization resistance which is obtained using Eqn. 2.24.

The initial potential η_o is obtained by the ratio of the applied charge (ΔQ) to that of the double layer capacitance (C_{dl}) (see Eqn. 2.31);

$$\eta_o = \frac{\Delta Q}{C_{dl}} = \frac{\Delta Q}{C \times S} \qquad 2.31$$

where C is the capacitance of the corroding electrode and S is the surface area of the electrode. Though there may be some resistance to the charge applied, it is ignored since it is small (Hassanein et al., 1998). The capacitance per unit area can also be obtained by making it the dependent variable in Eqn. 2.31.

As in the LPR technique, the corrosion rate is then computed by using the equations proposed by Stern-Geary (Eqn. 2.24 to 2.26). The anodic and cathodic Tafel slopes are also obtained from Figure 2.21 and the constant B computed using Eqn. 2.26.

In general, a high corrosion rate will lead to a rapid decay in the potential transient (Figure 2.23a) due to rapid consumption of the polarization charge by the corroding reinforcement bar, while a low corrosion rate will result in a slower decay in the potential transient after perturbation (Figure 2.23b) since the polarization current is not readily consumed as there is little or no corrosion of the reinforcing steel.

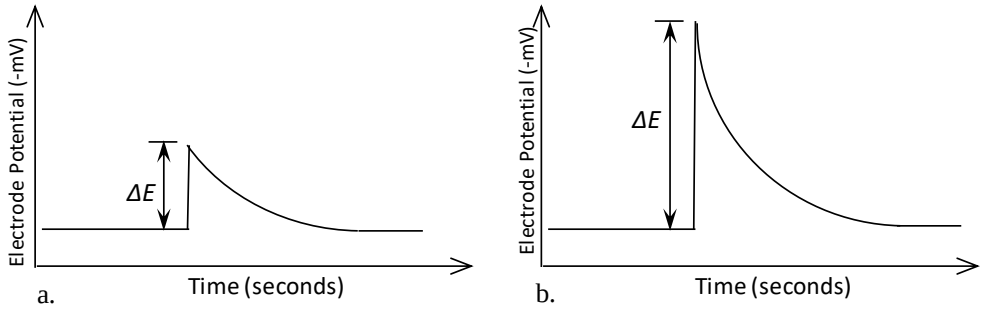


Figure 2.23: Potential transient (a) high corrosion rate and (b) low corrosion rate

The coulostatic method is increasingly used based on these advantages which were highlighted by Glass (1995);

i. Very small perturbation which last for a very short period is required
ii. There is no need to compensate for electrolyte resistance
iii. Determination of the interfacial capacitance as part of the measurements
iv. Insensitivity of the time constant to the steel surface area
v. Its suitability for low frequency measurements when compared to impedance measurements, and
vi. It provides additional information on the corroding interface which may lead to an improved understanding of the corrosion process.

On the other hand, the long transient time required in passive steel as compared to that of direct polarization and limiting of the perturbation of the steel as a result of

the concrete resistance the concrete high resistance may limit the perturbation have been identified as disadvantages of this method.

2.11.5 Gravimetric method

The gravimetric method is a destructive corrosion assessment technique which involves extracting the reinforcing bar from the concrete and measuring its section or mass loss. The results can be presented in various forms e.g. millimeters/year (mm/y). This test method is the most reliable technique of determining the corrosion rate of metals; hence it can be used to verify the results electrochemical corrosion rate measurements. The time required to obtain the mass loss in relation to time and the destructive nature of this test has made the electrochemical techniques more acceptable.

The mass loss or reduction in cross-sectional dimension of the steel rod can be either uniform along the surface area of the reinforcement bar (microcell corrosion) or it can be due to non-uniform loss of diameter due to localized or pitting corrosion which occur at distinct spots along the length of the reinforcement bar (macrocell corrosion) (Figure 2.24). While uniform corrosion is associated with carbonation-induced corrosion, pitting corrosion is mostly associated with chloride-induced corrosion and have been reported to be the main factor which influences cracking in chloride-induced corrosion (R. Zhang et al., 2010). The pits mostly form at chloride rich zones e.g. at positions of transverse and longitudinal cracks (Cao & Cheung, 2014).

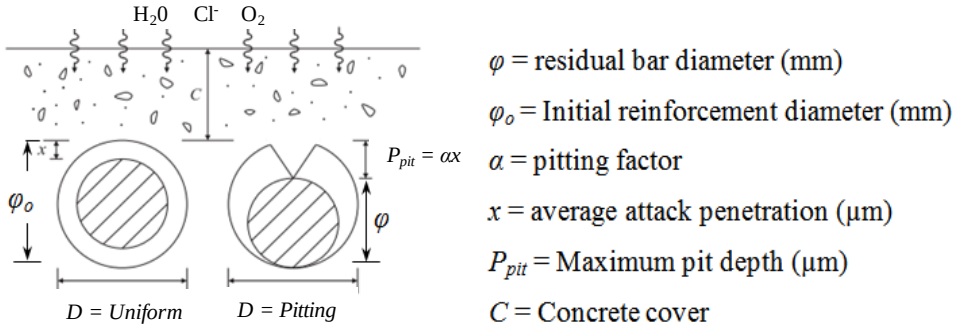


Figure 2.24: Residual reinforcement bar in uniform and pitting corrosion (Cao & Cheung, 2014)

As seen in Figure 2.24 above, the residual diameter of the reinforcement bar is very critical to the load bearing capacity of the RC structure. The residual diameter is

also related to the steel mass loss. The assessment of pitting corrosion can be difficult and time consuming as the concrete needs to be broken to access the corrosion pits (this exposes the steel to greater degradation), the amount of time needed for the formation of the pits via the natural process may be long and the possibility of arriving at reasonable conclusions after the reinforcement bar is accessed have led to the establishment of empirical relationships between the residual diameter and the steel mass loss (Eqns. 2.32 and 2.33). These relationships will be discussed in brief.

The average loss in mass per unit length of the a reinforcement as a result of pitting corrosion was proposed by (R. Zhang et al., 2010) (see Eqn. 2.19).

The attack penetration can be computed from the measured steel mass loss using Eqn. 2.32 (Rodriguez *et al.,* 1996);

$$\varphi = \varphi_o - \alpha x \qquad 2.32$$

where φ is the residual reinforcement bar diameter (mm), φ_o is the initial reinforcement bar diameter (mm), α is the pitting factor (i.e. the pitting factor) and x is the attack penetration (mm).

Lastly, the relationship between the attack penetration and mass loss due to pitting corrosion can be obtained using Eqn. 2.33 (which is the relationship between Eqns. 2.19 and 2.32) (R. Zhang et al., 2010);

$$x = \frac{\varphi_o}{\alpha}\left[1 - \sqrt{1 - \frac{\Delta A_s}{A_s}}\right].10^3 \qquad 2.33$$

where x is the attack penetration (µm),

ΔA_s is the steel cross-sectional loss (mm^2) and

A_s is the initial steel cross-sectional area (mm^2)

In order to determine the mass loss due to pitting corrosion, various authors have suggested the use of pitting factors (i.e. the ratio between the maximum pitting depth, P_{pit} (m) and the uniform attack penetration, x (m)); α = 4 to 10 for natural conditions and α = 5 to 13 in accelerated tests to determine the reinforcement mass loss (Tuutti, 1982; González *et al.*, 1995; Rodriguez *et al.*, 1996; Zhang, Castel and

François, 2009, 2010). In uniform corrosion, the corrosion is assumed to penetrate at an equal rate from all sides of the reinforcement bar, hence, a pitting factor of 2 has been suggested (Rodriguez *et al.*, 1996). Uniform corrosion can occur when chlorides or the carbonation front reaches the rear side of a steel bar.

While there is no agreement in literature with regards to a specific pitting factor to use in the mass loss computation, some researchers have suggested that the average of the maximum and minimum pit depth be used as the pitting factor.

2.12 Factors influencing corrosion assessment measurements

Half-cell potential (HCP) measurements can be influenced by the factors such as the concrete moisture content, surface wetness or dryness, presence of chlorides in the concrete, cover to reinforcement, and concrete carbonation (in this research, it will be reasonable to assume that the HCP measurements will not be significantly influenced by the concrete carbonation since the occurrence of chloride-induced corrosion is likely to outweigh that of carbonation-induced corrosion) (Gulikers, Polder, Raupach, et al., 2003). For instance, more negative potentials are likely to be obtained in concrete that is saturated with moisture compared to concrete that is dry and carbonated (Leelalerkiet, Kyung, Ohtsu, & Yokota, 2004). Despite the influence of the concrete surface condition and its saturation level, it has been reported that the potentials obtained in corroding regions does not vary, however, identifying corroding regions in very dry concrete has proved difficult (Gulikers, Polder, & Raupach, 2003). A summary of different concrete conditions and the likely corrosion potentials to be obtained are listed in Table 2.4.

The HCP can be influenced by the concrete condition e.g. the HCP measurements of steel in carbonated concrete which is contaminated by chlorides may vary from the potentials presented in Table 2.4. The potential values of steel in carbonated concrete that has been contaminated with chlorides may also vary from the values presented in Table 2.4; this is because chlorides influence concrete electrical conductivity. However, since the sustenance of the corrosion process requires the presence of both moisture and oxygen, it can be reasonably assumed that the corrosion process will slow down in dry concrete. Where positive steel potential

values are obtained, the values will need to be crosschecked with the corrosion rate and concrete resistivity results as earlier stated.

Table 2.4: Typical HCP ranges for concrete in certain conditions (Gulikers, Polder, & Raupach, 2003)

Condition	Potential values (mV/CSE)
Humid chloride free concrete	- 200 to + 100
Wet, chloride contaminated concrete	- 600 to - 400
Saturated concrete	- 1000 to - 900
Humid, carbonated concrete	- 400 to + 100
Dry, carbonated concrete	0 to + 200
Dry concrete	0 to + 200

CSE: Copper sulphate electrode

Hence, in view of the above likely sources of misinterpreting potential results, caution must be exercised in interpreting HCP results. It is most appropriate to interpret the HCP results (e.g. see Table 2.3) alongside other corrosion data such as concrete resistivity and corrosion rate measurements.

2.12.1 Factors influencing concrete electrical resistivity measurements

Though the presence of a sufficient concentration of chloride ions at the steel surfaces causes its depassivation, the chloride ions also contribute to the corrosion process by increasing the ionic conductivity of the concrete pore solution which results in a reduction in concrete resistivity. The presence of chlorides in concrete also increases its internal relative humidity (RH) due to its hygroscopic nature; which results in a reduction in concrete resistivity (Yu et al., 2017). Despite lowering the freezing temperature of water, the hygroscopic nature of chlorides in concrete also results in its early deterioration (scaling and detachment of cement paste) in freezing conditions (Bertolini et al., 2004). A reduction in concrete resistivity and increase of internal concrete relative humidity are conditions that also favor the corrosion process (Angst et al. 2010). This effect however varies with regards to the type of binder used in the concrete production. Studies over the years have shown that the use of binders such as fly ash, ground granulated blast furnace slag and silica fume in combination with Portland cement improves concrete durability in chloride environments (Monfore, 1968; Nanukuttan et al., 2015;

Osterminski et al., 2008; Rob B. Polder, 2012; Scott & Alexander, 2007). It has also been established through various studies that concrete resistivity measurements can be influenced by various factors such as presence of cracks, the concrete composition (water/binder ratio, nature of aggregates and its quantity, porosity), environmental factors (temperature, moisture, exposure to chloride salts) and geometric factors (position of reinforcement bars and distance of measurement from the concrete edge) (Soutsos, Breysse, Garnier, Gonçalves, & Monteiro, 2012). Some of the factors influencing concrete resistivity measurements are herein discussed;

2.12.1.1 Influence of concrete porosity on concrete resistivity

Concrete porosity is a measure of the volume of void spaces in the concrete to the volume of the total material. The concrete pore sizes as well as their distribution, connection, and the composition of its pore solution influence its resistivity. Porous concrete will tend to have a lower concrete resistivity compared to densely packed concrete (Hornbostel et al., 2013; Layssi et al., 2015). A major factor which influences concrete porosity is the water/binder (w/b) ratio; when it increases, the internal capillary porosity of the concrete enlarges thereby enhancing the pore connectivity within the concrete (Yu, Yang, Wu, & Li, 2014). Hence the concrete resistivity decreases as the w/b ratio increases (El-Enein, Kotkata, Hanna, Saad, & El Razek, 1995). Gjorv (2013) and Shi et al. (2012) suggested that rather than factor only the w/b ratio in reducing concrete porosity, a careful choice of binders (e.g. replacement of right proportions of Portland cement with fly ash or ground granulated blast furnace slag) will improve the concrete bulk packing and resistance to chloride ingress. Considering the pore solution composition, the presence of chloride ions in the concrete pores will improve its ionic conductivity. Concrete porosity is also influenced by the degree of hydration of the cement paste since the hydration products heal cracks in the concrete and fill its pores (Jacobsen et al., 1996). Hence in taking concrete resistivity measurements, it is important to clearly identify how the concrete porosity influences the results.

2.12.1.2 Influence of concrete pore connectivity and cracks on concrete resistivity

The connectivity of concrete pores lowers its resistivity compared to concrete with discontinuous pores. The presence micro-cracks which connect the concrete pores together can enhance chloride ingress and hence result in lower concrete resistivity (U. M. Angst et al., 2017; Layssi et al., 2015). In general, connected pores enhance the transport properties of a concrete, which also has a bearing on its resistivity; hence, concrete resistivity can be used to give an indication of the connectivity of pores within concrete and by extension the durability of steel reinforced concrete (C. Andrade, Prieto, Tanner, Tavares, & D'Andrea, 2013; Bertolini et al., 2004; J. Pacheco et al., 2012). Conversely, while it has been stated that the connectivity of pores yields a lower concrete resistivity, it (via micro-cracks) may also cause the concrete to dry out easily, thus causing an increase in its concrete resistivity.

2.12.1.3 Influence of moisture content on concrete resistivity

An increase in the concrete internal relative humidity (RH) will result in a decrease in concrete electrical resistivity due to the amount of fluid in the concrete pores. Drier concrete will on the other hand, have higher resistivity compared to moist concrete since the movement of the ions is restricted due to non-availability of fluids in the concrete pores (Layssi et al., 2015). Figure 2.25 shows a plot of the relationship between concrete moisture content and its resistivity.

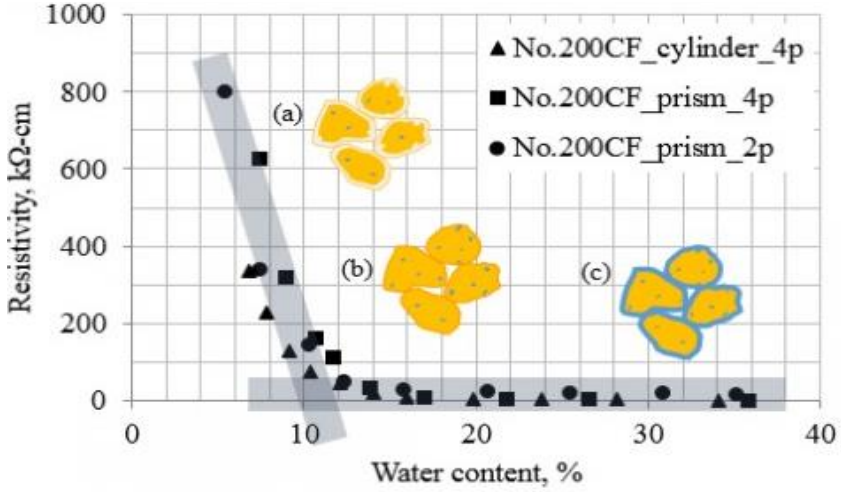


Figure 2.25**:** Concrete resistivity at various moisture contents (a) partially absorbed water; (b) absorbed water (saturated surface-dry); and (c) absorbed + free surface water using different methods (Kim, Zi, & Lange, 2017)

Cylinder and prism specimens made with recycled concrete fine particles (CF) passing through sieve No. 200 were used in the concrete mix while the concrete resistivity was measured using the two-probe (2p) and four-probe (4p) methods. The results of this experiment (Figure 2.25) show that the relationship between resistivity of concrete and its moisture content are identical irrespective of the method used to measure the concrete resistivity.

Concrete resistivity decreases with increasing moisture content and at a moisture content greater than 12%, the concrete resistivity reduces to a value close to zero. This finding is consistent with the findings of other researchers (Azarsa & Gupta, 2017; Saleem, Shameem, Hussain, & Maslehuddin, 1996; Su, Yang, Wu, & Huang, 2002).

Lopez & Gonzalez (1993) tested mortar samples that were contaminated with 0% and 2% chlorides (by mass of binder); they found out that the samples with saturated pores had a low resistivity which increased as the pore saturation reduced due to drying of the mortar (Figure 2.26);

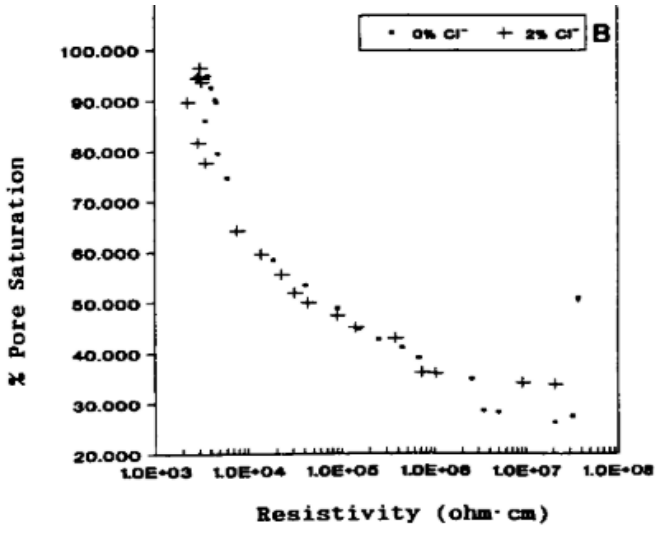


Figure 2.26**:** Effect of pore saturation on mortar resistivity (Lopez & Gonzalez, 1993)

In general, concrete with higher moisture content will have lower resistivity values compared to that with lower moisture content.

2.12.1.4 Influence of temperature on concrete resistivity

An increase in temperature increases ionic movement within the concrete pores which is also related to the concrete resistivity (Layssi et al., 2015; Sengul & Gjørv, 2008; Yuan, Shi, Schutter, & Audenaert, 2009). The relation between a change in temperature and the rate constant (K) is given by Arrhenius (Eqn. 2.34);

$$K_r = A.\exp\left(-\frac{E_a}{RT}\right) \qquad 2.34$$

where K_r = rate of reaction,

A = Constant (frequency factor),

E_a = Activation energy,

R = universal gas constant; 8.314 J / (mol. K) and

T = temperature in Kelvin (K)

The expression on the right side of Eqn. 2.34 represents the number of collisions needed to generate enough energy for a reaction to occur. Hence, an increase in temperature or reduction in the activation energy (E_a) of the system or both will result in an increase in the rate of reaction K_r. The plot of the relationship between concrete resistivity and temperature is shown in Figure 2.27.

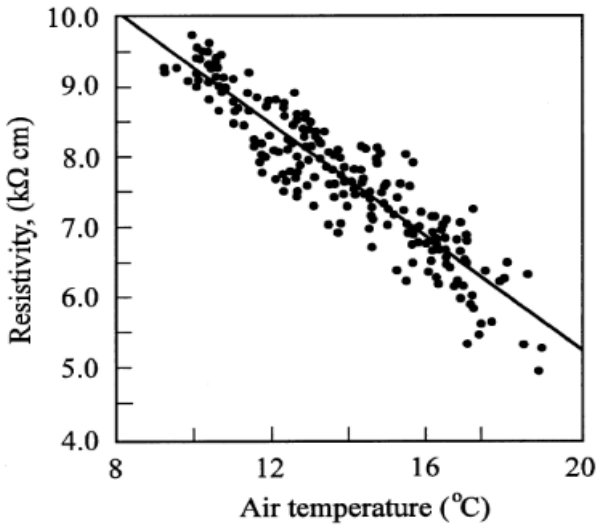


Figure 2.27: Relationship between measured resistivity and temperature (Gowers and Millard, 1999)

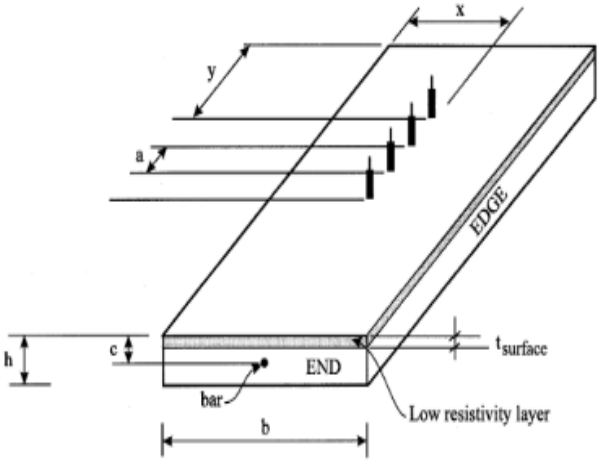
In relation to concrete resistivity, Baboain *et al.*, (2005) and Yuan, Shi, Schutter, *et al.*, (2009) used Eqn. 2.34 to assess the migration and diffusion of chlorides into concrete. Their results showed that higher temperatures resulted in higher chloride

migration and diffusion coefficients, but there was no difference observed in the penetration profile. In a separate research by Andrade, Alonso and Sarŕa (2002), a pure relationship between an increase in temperature and corrosion rate could not be established even though the authors affirmed the relationship between concrete resistivity and corrosion rate.

An increase in the temperature of concrete can cause the moisture in it to dry out faster than normal thus increasing the concrete resistivity. On the other hand, where there is sufficient moisture at the level of the steel, an increase in temperature will cause an increase in the corrosion rate of reinforcement bars.

2.12.1.5 Influence of specimen geometry on concrete resistivity

The current within a mortar or concrete specimen flows along a particular path; hence in using the Wenner probe device (commonly used in the field and laboratory) to assess concrete resistivity, the concrete geometry (which is assumed to be semi-infinite) has been found to affect the concretes resistivity (U. M. Angst & Elsener, 2013). Measurements taken with the Wenner probe have been assessed to be correct only when taken in a semi-infinite volume of material in which case the material thickness must exceed the space between the probes. Significant errors have been observed in specimens with smaller dimensions, this is due to restriction of the current path which is forced to flow in a different path other than that illustrated in Figure 2.17, which results in an overestimation of the concrete resistivity (Gowers & Millard, 1999). A schematic summary of various recommendations which include probe spacing, distance of probes from end and edge of the specimen are presented in Figure 2.28.



a > 40 mm
$\leq \frac{h}{4}$
$\leq \frac{b}{4}$
$\leq \frac{2c}{3}$, if a bar is present
$\geq 8 \times t_{surface}$, if a low resistivity layer is present
$\geq 1.5 \times$ max. aggregate size
x = edge distance $\geq 2a$
y = end distance (no restrictions)

Figure 2.28: Schematic summary of concrete resistivity measurement recommendations (Gowers & Millard, 1999)

2.12.1.6 Influence of type and quality of aggregates in concrete on concrete resistivity

The influence of aggregate size and its volume fraction has been found to influence resistivity measurements. For instance larger aggregates have been reported to increase concrete penetrability (Ahmad, 2003). The interface between the aggregates and binder paste presents a more porous medium where chlorides easily penetrate, with the order of penetration at the interfacial zone between the aggregate and binder paste reported to be as high as 10 times (Delagrave, Bigas, Ollivier, Marchand, & Pigeon, 1997; Hobbs, 1999). Hobbs, (1999) and Caré, (2003) also reported an increase in chloride permeability in concrete mixes with aggregate that is more permeable than the cement paste. Concrete made with aggregates that are more permeable than the cement paste may have a low resistivity than that which is made from impermeable aggregates.

With regards to the volume fraction of aggregates in concrete, Asbridge, Chadboum and Page, (2001) used PC/metakaolin and reported that there was significant increase in the chloride diffusion coefficient when the volume fraction of aggregates (silica glass beads) was increased above 35%. As earlier stated, the increase in chloride diffusivity may have increased at the aggregate boundaries. The bond between the aggregates and cement paste may have also influenced their results. Another research by Wei & Xiao (2011) showed that the concrete resistivity PC concrete increased as the aggregate volume was increased (from 0 – 70%). The authors related the elastic modulus of the concrete to its resistivity property. The property of the aggregate and binders used in these studies may have influenced their conclusions. It is however reasonable to assume that if impermeable concrete is used and rightly proportioned, concrete resistivity will increase as the aggregate volume fraction in the concrete increases. Also, aggregates are generally regarded as insulators while the cement paste allows the flow of ionic current, hence the quantity of aggregates in concrete will influence its resistivity. In order to reduce the influence of aggregates on resistivity measurements, it has been reported that the spacing between the probes needs to exceed the nominal diameter of the

maximum aggregate size (U. M. Angst & Elsener, 2013). In order to reduce the influence of aggregates, it has been suggested that an average of multiple readings be taken from various locations on the specimen; this will allow for a better estimation of the concrete resistivity (Morris et al., 1996). The inhomogeneity in concrete is mostly based on the presence of aggregates, this has been suggested to be the cause of difference between concrete bulk resistivity and results obtained using the Wenner probe (U. M. Angst & Elsener, 2013).

2.12.1.7 Influence of electrode contact resistance on concrete resistivity

This occurs when the probes or disc surface is in direct contact with the concrete surface. In general, high contact resistance increases the total resistance of the circuit, thereby reducing the current flow through the concrete (U. M. Angst & Elsener, 2013). To minimize the occurrence of this error, a good electrolytic contact between the probe electrodes and the concrete surface is required. This can be achieved by ensuring dry concrete surfaces are moistened with a conductive fluid or gel and a damp membrane placed between the resistivity meter probes.

2.12.1.8 Influence of embedded steel reinforcement bars on concrete resistivity

Unlike the one electrode disc method of measuring concrete resistivity which requires that the electrode is placed on the concrete surface directly over the reinforcement bar, the placement of the Wenner probe directly over reinforcement bars affects concrete resistivity readings (Gowers & Millard, 1999). The reinforcement bars present regions of lesser resistance for current flow which is sent into the concrete from the outer probes, thereby resulting in reduced concrete resistivity. To overcome this source of error, the probes need to be aligned at positions that are transverse (Figure 2.29a) or away from the reinforcement mesh or bars (Figure 2.29b).

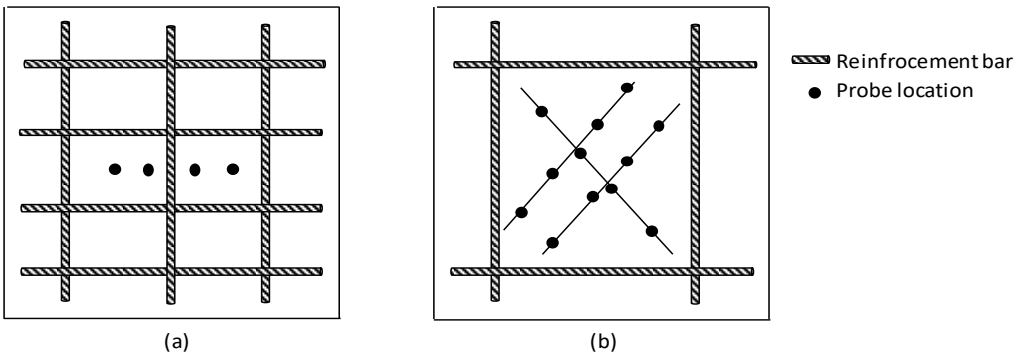


Figure 2.29: Positioning of Wenner probes (a) transverse and (b) away from reinforcement mesh to reduce resistivity measurement error (Lataste, Sirieix, Breysse, & Frappa, 2003; Rob B. Polder, 2001)

The likely of error in the concrete resistivity measurement is also dependent on the reinforcement bar spacing, where closely spaced and multiple layers of reinforcement bars tend to influence the concrete resistivity. The concrete cover as well as the reinforcement bar diameter has been reported not to have an influence on the concrete resistivity measurement as compared to measurements are taken directly over reinforcement bars (Gowers & Millard, 1999).

2.12.2 Factors influencing corrosion rate measurements

Corrosion rate measurements can be affected by a range of factors. These factors can be classified as chloride content at level of the steel reinforcement, concrete quality (type of binder, binder content, admixtures, w/b ratio, aggregates, curing, carbonation), concrete cover and environment conditions such as temperature, humidity and exposure to moisture (Raupach, 1996a).

2.12.2.1 Concrete quality

Concrete quality determines the ease with which corrosion causing agents penetrate from the concrete surface to the depth of the reinforcement. In this section, various factors that influence corrosion rate in relation to concrete penetrability will be discussed.

a. Influence of binder and binder content on corrosion rate

A blend of binders such as fly ash (FA), slag (SL) and silica fume (SF) (also called supplementary cementitious materials, SCMs) with PC have been identified to improve the durability of RC structures (Arya & Xu, 1995;

Ballim & Graham, 2009). Typical binder blends used for concrete in chloride environments consist of PC replacement with FA (15 – 50%) and SL (25 – 70%) (SCA, 2003; Thomas, 2007). SCMs are also known as mineral admixtures.

The reduction in corrosion rate of embedded steel reinforcement in concretes produced from these binder blends (i.e. PC and SCM) has been attributed to an improvement of the concrete pore structure (by ensuring denser packing of the concrete matrix due to their fineness) when compared with PC concretes and their ability to bind chlorides (Harald, 1998; Tuutti, 1982). Some researchers have however reported slightly higher corrosion rates and a reduction in the chloride binding ability of PC/SF concrete compared to PC/FA and PC/SL concretes (Harald, 1998; Page & Havdahl, 1985; Page & Vennesland, 1983). Hence, the PC/FA and PC/SL concrete is more efficient in binding chlorides and reducing the corrosion rate of steel embedded in concrete (E. Güneyisi, Özturan, & Gesolu, 2006).

A comparison of corrosion rates of steel in concrete mixtures of PC concrete and PC with SCMs (i.e. FA, SL and SF) showed that there was a corrosion rate reduction of up to 50% in the PC/SCM concrete mixture compared to the PC only concrete mix. Contrary to PC concrete where the corrosion rate determining factor has been attributed to the supply of oxygen and the concrete cover depth, that of the PC/FA, PC/SL and PC/SF concrete mixtures has been attributed to an improvement in the concrete resistivity (Scott & Alexander, 2007).

Considering the fineness of FA, a study of 45% and 10% fine portion fineness of FA showed that the finer portion had a higher resistance to chloride penetration compared to the less finer portion (Chindaprasirt, Chotithanorm, Cao, & Sirivivatnanon, 2007). The decrease in the corrosion rate in concrete made from a suitable proportion of PC and SCMs has been observed in both cracked and uncracked concrete (M. B. Otieno, 2010; Scott, 2004).

The durability property of concrete also depends on its exposure conditions and durability requirements, hence, various standards have specified a minimum binder content of 350kg/m^3 to be used in concrete that will be severely exposed (EN1992-1, 2004).

b. Influence of concrete admixtures on corrosion rate

This section will consider mainly chemical admixtures. Chemical admixtures containing chlorides (e.g. $CaCl_2$ and some water reducing agents) have been identified as one of the most common cause of corrosion initiation of steel in concrete (ACI 201, 1982). Calcium chloride ($CaCl_2$) is an admixture which is commonly used in concrete to accelerate the hydration of cement in cold weather; however, the chlorides may cause an early corrosion initiation of the steel reinforcement since the chlorides have a direct contact with the steel surface.

Though the concentration of chlorides at the level of the steel is of little significance to the corrosion rate once corrosion has initiated, the presence of chloride admixtures may result in immediate depassivation of the steel reinforcement. For concretes in chloride environments, the steel deterioration may proceed at a higher rate due to further chloride ingress from the environment (Hunkeler et al., 2005). To reduce the influence of $CaCl_2$ admixture in the corrosion process, its use in concrete is limited to concrete that is exposed to non-chloride environments. A guide to the use of this admixture is provided in ACI 201 (1982).

Other admixtures such as chromates, nitrites, benzoates, phosphates, stannous salts and ferrous salts have been used to inhibit corrosion. The admixtures are divided into two main types; anodic and cathodic inhibitors. While the anodic inhibitors cause an anodic shift in corrosion potential, thereby increasing the anodic polarization and passivating the steel, the cathodic inhibitors selectively precipitate on cathodic areas or slow the cathodic reaction by increasing hydrogen evolution which causes the steel concrete interface to become more alkaline due to precipitation of calcium and magnesium oxides (Popov, 2015). An imbalance in the anodic and

cathodic reactions hampers the rapid progress of the corrosion reaction; in some instances, the corrosion rate is significantly reduced.

c. Influence of water/binder ratio on corrosion rate

The water/binder (w/b ratio), type of binder and binder quantity are some of the most important factors which influence the corrosion rate of embedded steel in concrete (Ballim & Graham, 2009). The use of SCMs (FA, SL, SF) generally results in the reduction of the w/b ratio due to the shape (spherical) of their particles as compared to that of PC. The relationship between the w/b ratio and concrete durability can be attributed to the penetrability of concretes; a concrete with a high w/b ratio (> 0.5) will be more penetrable compared to one which has a lower w/b ratio (e.g. w/b ≤ 0. 50) (Adiyastuti, 2005; M. B. Otieno, 2010). Figure 2.30 shows the relationship between various factors (crack width, concrete quality and w/b ratio) which can affect corrosion rate.

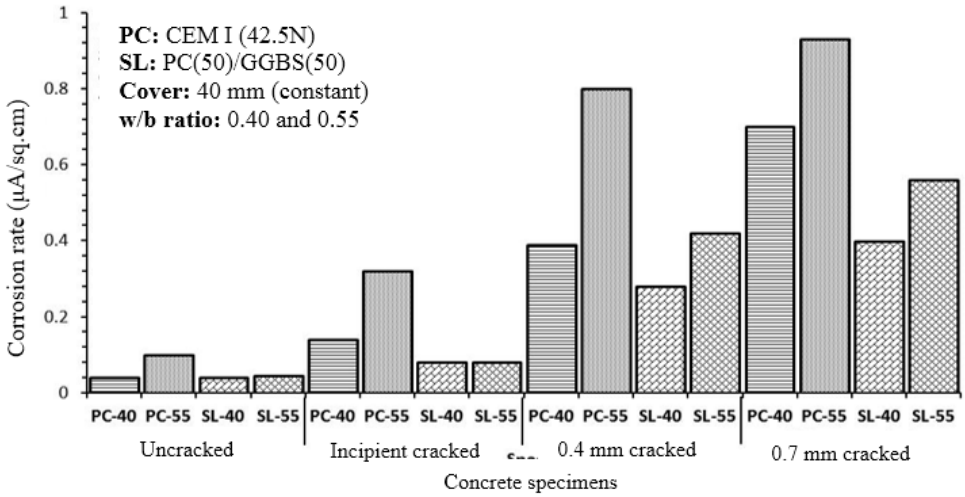


Figure 2.30: Average corrosion rates of 26 – 31 week specimens showing influence of crack width, cover depth and concrete quality on corrosion rate (M. B. Otieno, 2010)

Most of the specimens with a w/b of 0.55 (PC – 55, SL – 55) had higher corrosion rates compared to those with a w/b ratio of 0.40 (PC – 40, SL – 40). Also, much variation was not observed in the corrosion rate of the uncracked and incipient cracked PC/SL specimens, but a notable effect of the w/b ratio on the steel corrosion rate was noticed in the PC specimens.

In general, concretes with low w/b ratios exhibit a more compact pore structure which restricts the easy penetration of chlorides, oxygen and moisture into the concrete thereby reducing the time-to-corrosion initiation and the corrosion rate (Adiyastuti, 2005; Al-Saleh, 2015; Balabanic, Bicanic, & Durekovic, 1996; Golden, 2015).

d. Influence of aggregates on corrosion rate

Apart from the cementitious material, the aggregate type and fraction are an important components which influence concrete penetrability (Hobbs, 1999; Shi et al., 2012). Though a direct link may not be established between aggregates and corrosion rate, its influence on the penetrability of the concrete matrix can be linked to the corrosion rate which to an extent depends on the concrete penetrability. For instance, the permeability of the aggregate (porous or non-porous) used in a concrete mix will influence the concrete penetrability which has a direct link with the concrete durability with porous aggregates presenting a lower resistance to corrosion initiation and propagation (ACI 222R, 2001; Shi et al., 2012). Hence, the choice of an aggregate type will influence the durability performance of any given concrete.

Reactive aggregates (e.g. those prone to cause alkali-aggregate reaction (AAR)) are for instance likely to cause concrete deterioration when they expand; forming cracks which may influence the corrosion of steel reinforcement by allowing easy ingress of corrosion causing agents (ACI 222R, 2001; Bioubakhsh, 2011). Concrete which are made of aggregate sizes which are almost equivalent to the cover depth are also more prone to corrosion. It is advisable that the mean coarse aggregate size is less than the cover depth.

Aggregates which are contaminated with chlorides can also influence the corrosion of steel in concrete (Al-Saleh, 2015; Hussain et al., 1995). It is important to ensure that aggregates used in concrete are free of contaminants (e.g. chlorides and sulfates); uncontaminated aggregates can improve concrete durability.

e. Influence of concrete curing on corrosion rate

The curing of concrete provides a conducive environment for the hydration of cement; the concrete or mortar develops (achieves) desired properties such as compressive strength and durability. Proper hydration of the cement results in a proper development of the concrete pore structure due to the filling and segmentation of capillary voids by hydrated compounds thereby making the concrete more compact; this has been identified as one of the major factors which contributes to concrete durability (Poon, Wong, & Lam, 1997). The pore structure influences the penetrability of concrete to fluids (e.g. moisture, chlorides and air).

The curing period of 28 – 90 days has been advocated by most researchers to allow for PC blends with SCMs to develop superior properties to plain PC concretes, this period is necessary because the blended cements are less reactive compared to plain PC concrete (Erhan Güneyisi, Gesoğlu, Özturan, & Özbay, 2009). In an assessment of the effect of controlled, uncontrolled and wet curing of concrete specimens, Güneyisi et al. (2009) found out that when concrete made from CEM II/A-M, CEM II/B-M, CEM III/A, CEM V/A were subjected to wet curing, they had better resistance to chloride-ion penetration than plain PC concrete while specimens that were not cured in water exhibited unexpected variations in chloride penetrability. The penetration of chloride ions in this concrete generally decreased with prolonged curing of up to 180 days.

High corrosion rates (immediately after curing) of up to 10 times that of PC concrete has been reported in SL blended concretes, this has been attributed to the presence of sulphides which may affect the thin oxide layer covering the steel. However, a decrease in the corrosion rate of the PC/SL concrete over time was later observed. The reduction in the corrosion rate may be attributed to the development of the pore structure, an increase in resistivity of the concrete which in turn directly impacts the corrosion rate (Tromans, 1980; Valentini, Berardo, & Alanis, 1990). The concrete curing condition may be of little importance where the concrete has admixed chlorides, since the steel is likely to be immediately depassivated (as the steel is in direct

contact with the chlorides), however, the corrosion rate may be controlled by the concrete resistivity.

f. Influence of cover cracks on corrosion rate

The presence of both longitudinal and transverse cracks has been shown to ease chloride ingress into concrete which will increase the corrosion rate (Tran & Huang, 2006). Pitting corrosion occurs at points where transverse and longitudinal cracks intersect with the embedded steel reinforcement (Scott & Alexander, 2007).

Figure 2.30 shows the influence of cover crack widths on the corrosion rate of embedded steel reinforcement in PC/SL concrete. The wider cover crack widths result in higher corrosion rates in both the PC and PC/SL concrete, though lower corrosion rates were reported in the 0.40 w/b ratio compared to the concrete with a w/b ratio of 0.50. This indicates that RC concrete made with a low w/b ratio will result in a low corrosion rate.

Though most researchers have focused on the effect of cover cracks on corrosion rate, Schießl and Raupach (1997) and Castel et al. (2003) reported that the corrosion rate in the cracked zone is considerably influenced by the condition of the SCI within the cracked region. In a recent study conducted by Castel and Jenkins (2015), they assessed the condition of the SCI (using tomographic images) within the cracked region of beams which subjected to flexural loads; they observed micro-crack damage in the SCI which resulted in higher corrosion rates. This damage to the SCI has also been reported to be linked with severe corrosion damage which has been observed in tensile steel reinforcement (Papakonstantinou & Shinozuka, 2013). The effect of air voids underneath horizontal and at reinforcement bar lapping can also reduce the compactness of concrete around the reinforcement bar thus weakening the layer of cement hydration products deposited on the SCI; thereby affecting the protective cover of the embedded steel reinforcement bar (Bioubakhsh, 2011).

2.12.2.2 Concrete cover thickness

The cover thickness serves to protect the embedded steel reinforcement since it limits the amount of corrosion agents (oxygen, moisture, carbon-dioxide and chlorides) and gives an indication of how soon they will reach the steel reinforcement. Various cover thicknesses and concrete quality (in terms of minimum cement content and water to cementitious ratio) are specified in various codes of structural use of concrete based on the severity of exposure of concrete elements because it (to an extent) determines the service life of a RC element (SABS 0100-1, 2000; EN1992-1-1, 2004). It is important to mention that though the cover thickness is an important factor which determines the corrosion rate, Balabanic, Bicanic and Durekovic (1996) reported that a change in concrete quality expressed through the reduction in w/c ratio influences much more the corrosion rate than an increase in cover thickness (from 5 to 10 cm) of the concrete cover of the same quality; hence, the efficiency of the cover thickness is to a large extent dependent on the concrete quality.

With concrete of the same quality, the cover thickness gives an indication of the time-to-corrosion initiation (Mangat, Khatib, & Molloy, 1994). This is however valid for uncracked concrete, in cracked concrete where the cover thickness is either partially or wholly breached (depending on whether the crack reaches the depth of the steel reinforcement or not), the cover thickness mostly serves to limit the amount of corrosion agents which are needed to propagate the steel corrosion.

Though the cover thickness provides protection to the steel reinforcement, limits are set to cover thickness (not to exceed 80 – 100 mm) so as to avoid excessive cracks due to flexural bending and shrinkage cracks since an excessive cover thickness will result in a large volume of concrete which is not reinforced (Neville, 1995).

2.12.2.3 Environmental conditions

Environmental conditions present some of the widest variations which affect the corrosion process. In field structures, these conditions may vary depending on season or exposure of a reinforced concrete element. Some of the environmental conditions that have been identified to influence corrosion rate are herein discussed;

a. Influence of temperature on the rate of corrosion

Temperature variations generally influence the kinetics of electrochemical reactions by the loss or gain of kinetic energy (due to decrease or rise in temperature) by the reacting species. Maslehuddin (1996) investigated the effect of temperature on corrosion rate of steel reinforcements embedded in Ordinary PC and sulphate resistant concrete at temperatures between 15^{o}C – 70^{o}C and found out that the corrosion rate progressively increased up to 2 to 6 times from the initial temperature. This trend has however not been verified by other researchers who opine that though an increase in temperature results in an increase in kinetics of chemical reactions, with regard to embedded steel in concrete corrosion, the corrosion rate is not wholly influenced by the mean temperature of the structure alone, but it is also influenced by the relative humidity in the pore system which affects both the electrolyte and oxygen solubility within the concrete pores (Tuutti, 1982). In investigating the influence of ambient temperature as a rate factor of steel reinforcement corrosion, Zivica, (2002) found out that the solubility of oxygen reduced at temperatures higher than 40^{o}C, while the water vapor tension increased by over 300% (see Figure 2.31). This meant that at higher temperatures, less moisture is available to support steel corrosion and the impairment of oxygen dissolution at temperatures higher than 40^{o}C simply means there will be a reduction in the corrosion rate since there is less oxygen and moisture at the steel level. A reduction in oxygen and moisture will hamper the progress of the cathodic reaction thereby leading to an imbalance of the corrosion reactants and subsequently a reduction in the rate of dissolution of the metal at the anode.

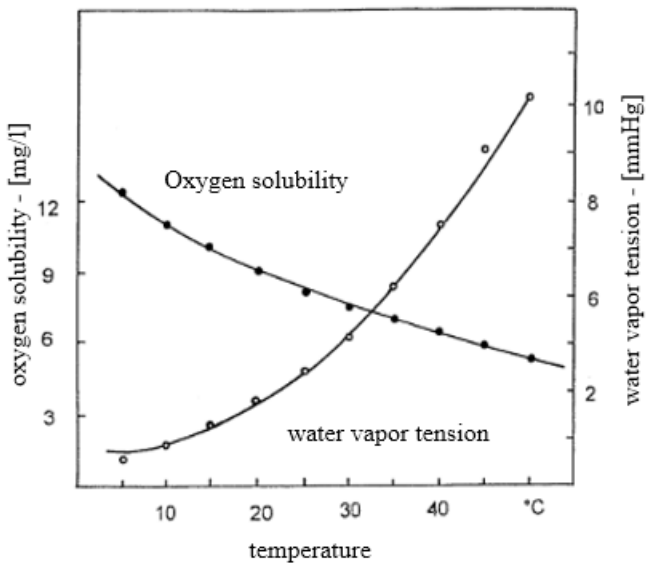


Figure 2.31: Dependence of the solubility of oxygen in water and water vapor tension on the ambient temperature (Zivica, 2002)

Andrade et al. (2002) also identified four weather events which can influence the corrosion rate of reinforced concrete; day–night cycles, seasonal cycles, extreme temperatures and rain periods. In these weather and seasonal changes, higher corrosion rates were recorded during the hot periods of the year compared to colder periods provided temperatures did not rise above 40°C, wherein the solubility of oxygen in the concrete pore solution is impeded.

b. Influence of relative humidity on corrosion rate

Relative humidity of concrete is one of the primary corrosion rate-limiting factors; others are the concrete pH, resistivity, temperature, and oxygen availability at the steel surface (ACI 222R, 2001). As opposed to concrete which is indoors or kept in a non-varying exposure condition, the influence of RH is most pronounced in concrete which is exposed to outdoor conditions wherein there is a daily or seasonal variation in temperature and RH (C. Andrade & Alonso, 1996). Outdoor variations such as contact of concrete with water has been shown to have significant electrochemical effects on the corrosion propagation phase (Sandberg, 1996). RH of concrete has been reported to have an effect on its resistivity (higher RH results in lower concrete resistivity) which in turn governs corrosion rates

based on the saturation of the concrete cover pores with moisture (Glass, Page, & Short, 1991; Lopez & Gonzalez, 1993; Raupach, 1996b).

The influence of RH on high-density and low-density concrete is shown in Figure 2.32;

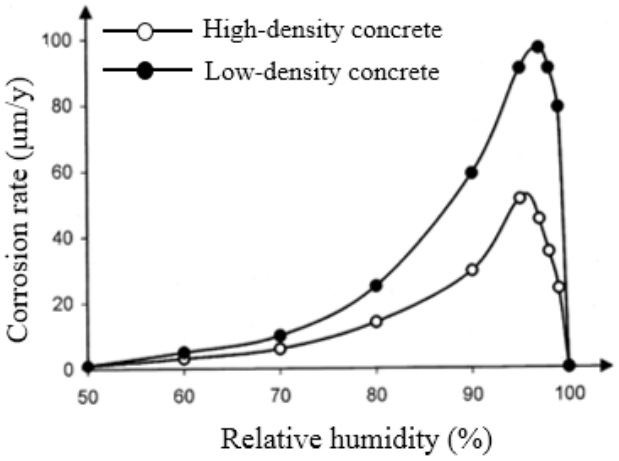


Figure 2.32: Corrosion rate as a function of external RH in case of corrosion initiation due to chlorides for high and low density concretes (Tuutti, 1982)

The corrosion of steel reinforcement is under resistance control when the relative humidity is lower than 55% because the resistivity of dry concrete is very large which causes steel to corrode very slowly (Yu et al., 2014). At higher relative humidity (closer to 100%), the concrete pores are saturated with moisture which affects the supply of oxygen to support the progress of the cathodic reaction, this in turn reduces the rate of the anodic reaction which then lowers that corrosion rate (Raupach, 1996b). Within these range (55 – 98% RH), the corrosion rate increases and reaches an optimal value at a RH of about 95%.

c. *Influence of cyclic wetting and drying*

Unsheltered RC is mostly exposed to wetting and drying conditions which tend to modify its chloride and carbonation penetration behavior and concrete elements exposed to this condition have been proven to be most vulnerable to corrosion damage (Bioubakhsh, 2011). Typical RC elements which are subjected to cyclic wetting and drying cycles are located within tidal and splash zones in marine areas, coastal structures exposed to airborne chlorides, bridge decks and car park slabs exposed to chloride based deicing salts and other non-sheltered and partially sheltered RC elements.

In marine structures, the RC elements are exposed to high chloride concentration since they are in direct contact with sea water. For instance, chloride penetration in the submerged zone is very high but active corrosion is depressed due to low levels of oxygen at the steel level (since oxygen solubility is low in water). In the tidal and splash zones, chloride penetration may be lower, but the steel in these zones is prone to corrode more rapidly due to presence of an ample supply of oxygen at the steel surface (Bardal, 2004; Sandberg, 1996). The removal of corrosion products (in the tidal and splash zones) from the surface of the corroding steel reinforcement (through cracks) by a flowing medium (such as water) may cause an increase in the corrosion rate. When corrosion products are not removed from the surface of the steel reinforcement, they build up and may impair further ingress of corrosion agents (e.g. oxygen and moisture) thereby slowing down the corrosion rate.

In the laboratory, specimens subjected to long drying periods after wetting (spraying or ponding) with a chloride solution have been reported to have higher corrosion rates compared to specimens which have a short drying cycle. The high corrosion rate in specimens which are subjected to longer drying cycle may be attributed to the increase in oxygen supply at the steel surface when the RH reaches its optimum value (see Figure 2.32).

Higher corrosion rates have also been reported immediately after wetting cycles as compared to that at the end of the drying cycle; this however also depends on the drying and wetting cycle duration (Golden, 2015). The high corrosion rates coincide with a low concrete resistivity due to increased moisture content in the concrete. In this case concrete resistivity fails to be corrosion rate-limiting factor; also, an ample supply of chlorides at the steel surface ensures a steady progress of the anodic reaction, leaving the cathodic reaction (via reduction of oxygen supply at the cathode by ensuring short drying cycles) as the corrosion rate controlling factor.

2.13 Literature review summary

In this chapter, the durability performance of steel reinforced concrete has been discussed with specific reference to chloride-induced corrosion. The cause of

corrosion has been identified as the most common detrimental durability problem facing steel reinforced concrete structures in coastal environments and areas where chloride based deicing salts are utilized.

The review of published literature by previous researchers on chloride-induced corrosion due to 2D chloride ingress contrasts most research work that has been conducted based on 1D chloride ingress. The 1D chloride ingress has been seen to dominate in structural elements such as slabs and walls while the 2D chloride ingress dominates at corners of rectangular beams and columns. With a focus on the corrosion free life of steel reinforced concrete structures, it has been understood that chloride ingress at orthogonal edges of beams and columns occurs at a rate that is more than twice that of elements exposed to 1D chloride ingress The higher chloride penetration rate has been attributed to the interaction of penetrating chloride fluxes from the adjacent faces of an orthogonal edge. The chloride penetration rate is further increased when an element is under tensile stress, thus, the time-to-corrosion initiation is shorter. This brings to light the need for further studies in this area since most RC structures in service are stressed due to service loads.

A larger section of reinforcement bars located at orthogonal edges is exposed to corrosion since the corrosion agents penetrate from the two adjacent faces of the concrete element. This larger corroding area gives rise to corrosion products which easily cause the adjacent faces of the concrete edge to crack easily delaminate thereby exposing more of the steel to the corrosion agents.

While it is appreciable that most of the research reviewed in this chapter indicate that the corrosion free life of steel reinforcement located at orthogonal corners of concrete elements can be substantially reduced, the studies have been based on uncracked concrete, however, in RC design, concrete in the tension zone is assumed to be cracked. This research further gives insight into the influence of cracks on the corrosion of steel reinforcement bars that are located at orthogonal edges of concrete elements. In addition to information provided by previous researchers, this research has investigated the rate at which the steel at orthogonal corners degrade with time. Assessing the corrosion rate of the corner located steel reinforcement is

intended to provide information which will assist in ascertaining the deterioration of the reinforcement bars.

3.1 Introduction

This chapter presents the materials and methods used in this laboratory based experimental study. The materials and methods employed are aimed at assessing the influence of 1D and 2D ingress of corrosion-causing agents on corrosion initiation and propagation of steel reinforcement bars which are embedded in cracked and uncracked concrete.

The discussion in this section is focused on the various materials and methods which have been used in this study (e.g. concrete materials, steel reinforcement details, specimen preparation and specimen types, corrosion assessment methods, and depth of chloride penetration and concentration into the concrete after terminating the chloride ponding and drying cycles). A summary of the experimental methods and program is provided in Section 3.15.

3.2 Concrete materials for specimen production

3.2.1 Binders

72 RC beams were cast using two different concrete mixes; a blend of PC/FA and PC/SL (plain PC (CEM I 52.5N, class F fly ash (FA) and slag (SL)). In chloride environments, various binder blends and mix proportions have been suggested in literature, however, in this study the choice of the binder blends (PC(70)/FA(30) and PC(50)/SL(50) herein after referred to as PC/FA and PC/SL) is based on recommendations by other researchers and their subsequent use in field structures which has established that these binder blend proportions provide improved protection against corrosion of embedded steel in concrete (SCA, 2003; Scott & Alexander, 2007; Thomas, 2007), hence, the use of these binder blends will serve as a basis for comparison of results obtained in this study with previous research (Dhir et al. 1996; Otieno 2014; Otieno et al. 2016; Scott 2004). It is worth noting that though the concrete used in this research may have the same binder blend ratio with that used in previous research, its resistance to penetration of oxygen, moisture and chloride ions may vary due to variation in the binder content, w/b ratio and method of exposure to chlorides (1D and 2D chloride ingress).

The chemical composition of the binders used in this research was determined with the X – ray fluorescence method using an S2 ranger X-ray spectrometer analysis machine; the results are presented in Table 3.1;

Table 3.1: Chemical composition of the binders for concrete production

Chemical compound (%)	**Plain Portland cement**	**Fly ash**	**Slag**
CaO	66.26	5.02	38.00
Si_2O	18.92	53.95	30.12
Al_2O_3	4.52	31.08	14.21
Fe_2O_3	3.01	3.33	1.19
MgO	2.30	1.70	10.60
SO_3	3.33	1.46	3.39
Na_2O	0.40	-	0.70
Mn_2O_3	0.21	0.02	0.02
Cl^-	0.06	0.07	0.04
Cr_20_3	0.03	0.05	-
TiO_2	0.24	1.66	0.53
P_2O_5	-	0.59	-
K_2O	0.69	0.80	0.97
ZrO_2	0.01	0.06	0.03
V_2O_5	-	0.03	-
ZnO	0.01	-	0.01
SrO	0.01	0.14	0.18
Total (%) =	100	99.96	99.99

Source of Materials: *PC* - PPCement, *FA* – Dura-Pozz® (Class F Fly Ash), *SL* – PPCement

3.2.2 Coarse and fine aggregates

The crushed aggregates used for concrete production in this study were both obtained from the same parent rock; Andesite rock. The coarse aggregate had a nominal size of 13.2 mm while the fine aggregate used was unwashed. The aggregate physical properties are presented in Table 3.2 while the particle size distribution graph of the fine aggregate is presented in Figure 3.1 (SANS 210:2008).

Table 3.2: Aggregate physical properties

Physical property	Coarse aggregate	Fine aggregate
Relative Density (RD)	2.94	2.94
Water absorption (%)	0.5	0.5
Dry *ACV, %	5.9	—
Particle shape	Angular	Angular

Source: Afrisam South Africa Pty (Ltd) (2017); *ACV = aggregate crushing value

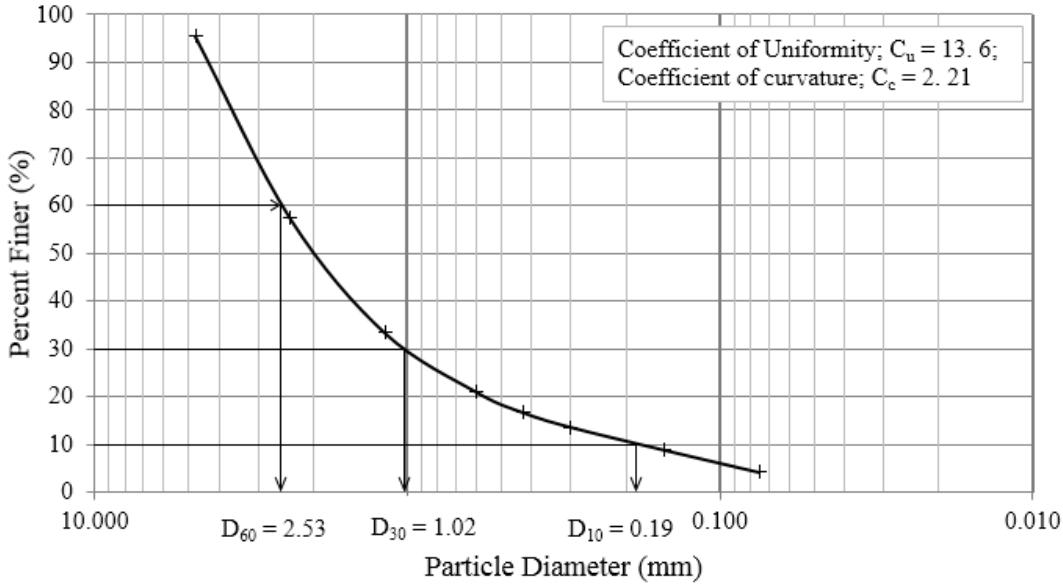


Figure 3.1**:** Particle size distribution curve of fine aggregate

The coefficient of uniformity and curvature (13.6 and 2.21 respectively) obtained from the particle size distribution graph shows that the fine aggregate used in the concrete mix is well graded.

3.3 Concrete mix and compressive strength

The quantity of materials used in the production of the PC/FA and PC/SL concrete are shown in Table 3.4 and Table 3.5.

Table 3.3: Concrete mix materials

Material	Quantity (kg/m^3)					
	PC	FA	SL	Water	Fine aggregate	Coarse aggregate
PC (70)/FA (30)	355	155	-	205	745	1115
PC (50)/SL (50)	255	-	255	205	780	1135

Table 3.4: Mean 28 and 90-day concrete compressive strength

Binder type	PC/FA		PC/SL	
	Compressive strength (N/mm^2)			
	28 day	90 day	28 day	90 day
	59	77	57	71
	59	79	59	72
	60	77	55	73
Average =	59	78	57	72
Standard deviation;	0.21	0.74	0.24	0.57

To determine the concrete compressive strength, 100 mm cubes were cast from the same concrete mix which was used to cast the concrete beams. The mean compressive strength of the concrete was obtained by crushing three (3) cubes at a loading rate of 0.4N/mm^2/sec. While there was no significant difference in the 28-day compressive strength of the specimens, there was a significant difference in their 90-day compressive strength; the PC/FA concrete had a higher compressive strength than the PC/SL concrete. At 90 days, the PC/FA and PC/SL concrete respectively gained an additional 23% and 21% over their 28-day compressive strengths. The strength gain after the 28-day curing period may be attributed to the development of the concrete pore structure due to further hydration of the binder (Bertolini et al., 2004; Portland Cement Association, Portland Cement Asscociation, & Portland Cement Association, 2018).

3.4 Steel reinforcement type and preparation

High yield 10 mm diameter steel reinforcement bars were used in this study. Prior to embedding the reinforcement bars in concrete, they were prepared in accordance to ASTM G1-90 (2003). Millscale was not removed from the surface of the reinforcement bars; however, acetone was used to degrease them. A photo of the section of the steel reinforcement bar used is shown in Figure 3.2.



Figure 3.2: Ribbed steel reinforcement bar

In order to facilitate an effective electrical connection to the reinforcement bars, a small hole was drilled through one end of each bar, after which a multi-strand sheathed copper wire of 1.5 mm diameter was passed through the drilled hole and

securely held in place by winding it round the reinforcement bar. The wires were extended outside the cast concrete after the reinforcement bars were embedded in the concrete. The wires served as the electrical connection between the reinforcement bar (working electrode (WE)) and corrosion monitoring devices that were utilized in this study (see Figure 3.7). The electrical wire and reinforcement rod connection points were first sealed with an electrical tape and then coated with an epoxy paint (abe ®cote 337 epoxy sealant).

After drilling the holes for the electrical wire connection, the mass of each reinforcement bar was obtained by using a balance which could detect an absolute mass change of 0.001g (ASTM G1-90, 2003). The bars were then placed in the concrete. The initial mass (M_i) and final mass (M_f) of each reinforcement were respectively measured before and after the experiment.

3.5 Concrete cover

A concrete cover depth to the steel reinforcement of 20 mm was used in all the specimens to increase the risk of corrosion. Other researchers have also used this concrete cover (Arya & Ofori-Darko, 1996; Scott & Alexander, 2007). To achieve this cover and ensure that the reinforcement bars were kept in their desired position (i.e. at the center or corner of the RC beams) when beam specimens were being cast and vibrated, wooden spacers were fabricated and attached to the mould ends prior to the concrete casting (Figure 3.3).

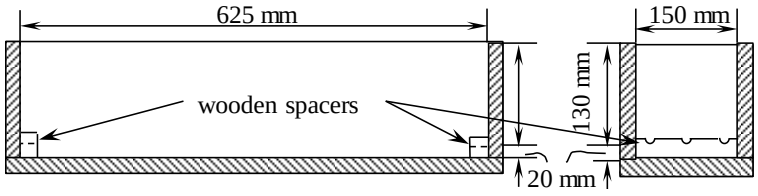


Figure 3.3: Longitudinal and transverse section through concrete mould

3.6 Reinforcement details

In order to assess the influence of the reinforcement position (at the corner and middle of the concrete specimen) and the ingress path of corrosion-causing agents (1D and 2D) on the reinforcement corrosion, 6 (six) different sets of specimens were prepared (Figure 3.4). All the reinforcements were placed at a cover depth of

20 mm from the concrete surface. Below is a description of the various specimen sets;

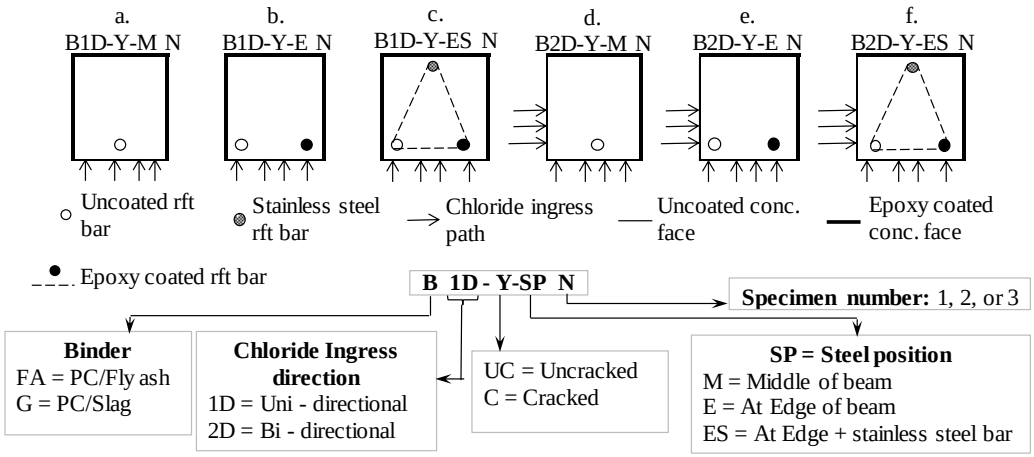


Figure 3.4: Cross section of beam specimens showing chloride exposure, reinforcement details, and specimen labeling key.

a. Specimens a and d (Figure 3.4a & Figure 3.4d**):** In these specimens (B1D-Y-M N and B2D-Y-M N), a single longitudinal reinforcement bar was positioned in the middle of the beam at a cover depth of 20 mm. This reinforcement configuration has been utilized by most RC corrosion researchers where the concrete is exposed to chloride ingress from only one face (1D chloride ingress) (Michel et al. 2013; Otieno, 2008; Richard et al. 2010; Scott, 2004; Suryavanshi and Swamy, 1996).

The specimens (a and d) will be referred to as concrete with reinforcement bars in their middle.

b. Specimens b and e (Figure 3.4b & Figure 3.4e**):** In these specimens (B1D-Y-E N and B2D-Y-E N), the reinforcement bar was positioned at an orthogonal corner with a cover depth of 20 mm from both the vertical and horizontal faces of the beam. In the cracked specimens (see Section 3.7), two reinforcement bars were used in order to prevent shear failure when the RC beam was mechanically loaded to induce cracks while one reinforcement bar was used in the uncracked beam specimens. Only the bar to be monitored for corrosion had an electrical wire connection which was extended to the outer face of the concrete. There was no electrical connection to the second reinforcement bar in this specimen set. The bar

was also isolated from the other reinforcement bars by coating it with epoxy paint.

Subsequently, the specimens b and e will be referred to as concrete beams with reinforcement bars at a corner (i.e. orthogonal corner) or edge.

c. **Specimens c and f (**Figure 3.4c & Figure 3.4f**):** In these specimens, three longitudinal bars (1 - epoxy coated, 1 – uncoated reinforcement bar and, 1 – 8 mm diameter stainless steel bar) were placed in each of these RC beam specimens (B1D-Y-ES N and B2D-Y-ES N). The stainless-steel bar was placed in the compressive face while the other two (epoxy coated and uncoated) bars were placed on either edge of the tensile face of the concrete beam. Three equally spaced triangular shaped stirrups were used to keep the longitudinal bars in their positions within the concrete beam. The stirrups were epoxy coated to prevent them from corroding since corrosion agents will reach them before reaching the longitudinal bars. The bars were also coated to eliminate interference with the monitored corrosion measurements of the reinforcement bar of interest. As mentioned in specimen b and e, one of the reinforcement bars in the concrete face which is exposed to chloride ingress was epoxy sealed while an 8 mm diameter stainless steel bar was placed in the compressive face of the beam. The stainless-steel reinforcement bar was electrically connected to the corroding bar with the aid of an electric cable. The results obtained from these specimens will be used to assess the corrosion characteristics of a single (isolated) reinforcement bar which is at an orthogonal corner (exposed to 1D and 2D ingress of corrosion agents) of concrete with that of a reinforcement bar which is subjected to the same condition but is in connection to passive bar (in this case, a stainless-steel bar).

3.7 Beam specimen production

The concrete was mixed in a pan mixer and compacted in the mold with the aid of a vibrating table (Frequency, 50 Hz). Due to limitation in the mix volume capacity of the mixing pan, three beams were cast per batch of concrete materials. The concrete was placed in three layers in the mould with each layer moderately compacted to avoid segregation of its constituent materials. A total of 72 RC beams

of size 150 × 150 × 625 mm were cast (Figure 3.6). Half of the beams (36 numbers) had a single transverse crack induced at their mid-span while the other beams were uncracked. To facilitate the formation of the single crack, a notch was created (when the concrete was being cast) by inserting a removable thin plastic shim of dimension 8 mm deep × 45µm thick. The RC beam specimen production plan is as shown in Figure 3.5.

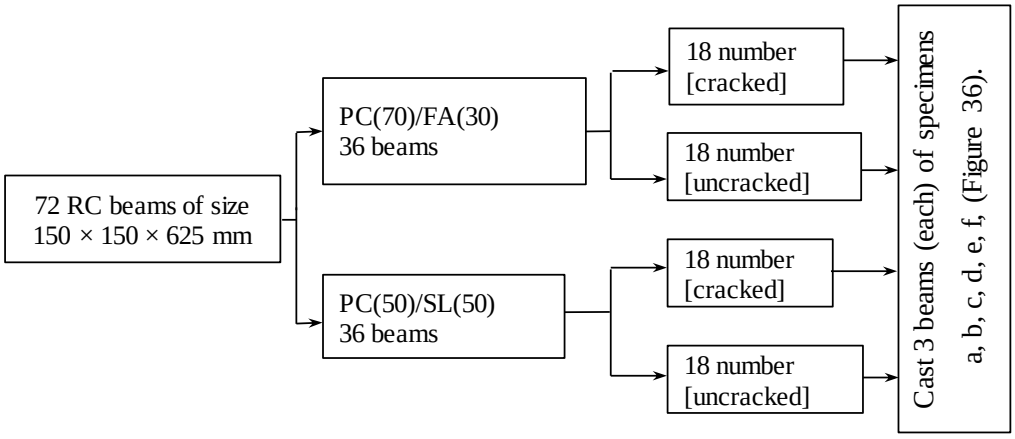


Figure 3.5: RC beam specimen production



Figure 3.6: Cast beam specimens

To test for the 28 and 90-day concrete compressive strength and durability index parameters after moist curing the concrete for 28 days, two 100 mm cubes were cast from each concrete batch which was used to cast the RC beams.

3.8 Specimen curing

The RC beams and cubes were covered with a plastic sheet shortly after they were cast to prevent rapid moisture loss from the concrete to the surrounding

environment. The concrete specimens were demoulded 24 hours after being cast, marked, and immediately placed in a curing tank which was filled with potable water that was maintained at a temperature of 23°C ± 2°C. The RC beams were cured for 28 days while the concrete cubes were cured for 28 and 90 days.

3.9 RC beam epoxy coating

After the 28-day curing period, the beam specimens were air dried (in ambient laboratory environment) for 7 days. After the drying period, a water dispersed, two-part epoxy emulsion sealant (abe ®cote 337 tough epoxy paint) was used to seal the concrete surfaces where penetration by corrosion agents was not desired. This modified the ingress direction of corrosion agents on the beam surfaces to 1D or 2D (see Figure 3.4). Since the beams were epoxy coated before being cracked, ingress of corrosion agents through the cracks was not restricted to the 1D and 2D directions as seen in the concrete surfaces. Application of the epoxy coating after the cracking process ensured that the crack opening and its walls were not sealed.

At least three layers of the epoxy paint were applied to seal off the concrete faces; the last coat was left to cure for at least 72 hours before ponding of the specimens in the chloride solution commenced.

3.10 Cracked and uncracked beam specimens

As earlier mentioned, a total of 72 RC beam specimens were prepared for this study, 36 RC beams (i.e. a half of the specimens) were cracked transversely at the mid-span of the beams using the 3-point loading method. To achieve the single crack, an average load of 7kN was applied at the mid-span of the beams. The other specimens (i.e. 36 RC beams) were left uncracked.

The pre-cracked RC beam specimens were then fitted onto rigs by clamping them back-to-back (using a 3 – point loading (3-PL) arrangement) where the load is applied by a 20 mm galvanized steel rod (see Figure 3.7). This was done to keep the crack mouths from closing after removing the 3-PL and to simulate service condition of structures wherein they are loaded during their service life. The need to keep the cracks open is based on findings from previous researchers that concrete crack openings tend to seal up due to the formation of ettringite, calcite, and brucite around the crack opening, accumulation of corrosion products in the crack

openings, and mineral deposits in in cracks that are exposed to direct contact with sea water (Tarek Uddin Mohammed, Otsuki, & Hamada, 2003; Mike Otieno, 2008; Pease, 2010; Shazali, Rahman, & Baluch, 2010). The quantity of ettringite formed in concrete made with slag and fly ash has been reported to be higher than that of concrete made of plain Portland cement. The intermittent wetting of the concrete throughout the duration of this experimental study also favors the formation of ettringite.

The crack openings were measured using a crack feeler gauge after the beam specimens were clamped onto the rigs (see Figure 3.7).

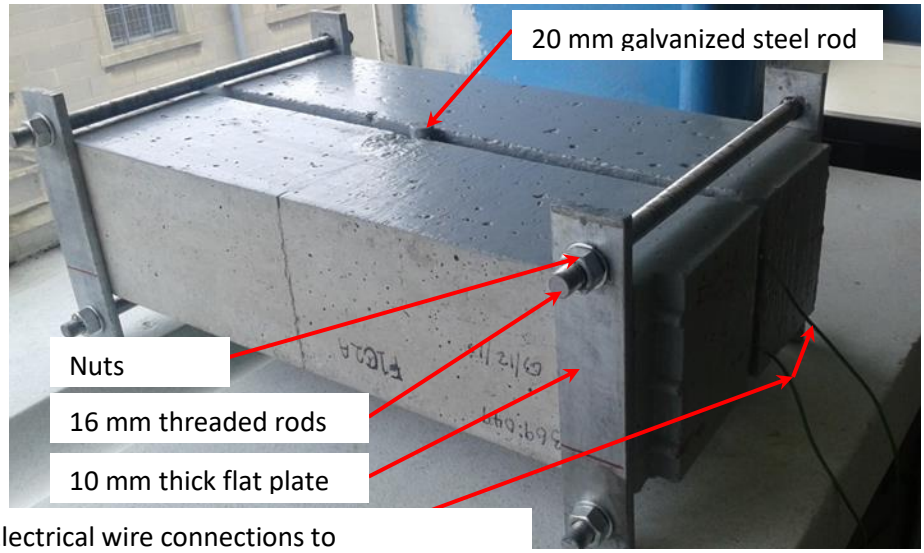


Figure 3.7: Typical cracked RC beam loading rig

The crack openings were in the range of 50% below (i.e. ≈1.6 mm) and 30% (i.e. 0.40 mm) above the 0.30 mm allowable crack width in RC structures (EN1992-1-1 2004; Comité euro-international du béton 1993). This crack width range was adopted to assess its influence on the corrosion of the reinforcement bars as cracks below the allowable crack width have been reported to seal due to ettringite formation (M. Otieno, Beushausen, & Alexander, 2016b; J. F. Pacheco, 2015; Pease, 2010; O. G. Rodríguez et al., 2003).

3.10.1 Crack width measurement

The mechanically-induced and corrosion-induced crack widths (discussed in Section 3.13.4) were measured with the aid of a crack microscope (Figure 3.8). The

microscope had a ×50 magnification and can be used to measure crack widths to an accuracy of 0.02 mm.

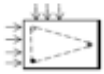


Figure 3.8: Crack microscope

3.10.2 Mechanically induced crack width of specimens

The mechanically induced crack widths in the cracked PC/FA and PC/SL concrete and their standard deviation are presented in Table 3.5.

Table 3.5: Mechanically-induced crack widths for PC/FA and PC/SL specimens

Reinforcement position/chloride ingress direction	PC/FA Specimen	Mechanically induced crack width (mm)	PC/SL Specimen	Mechanically induced crack width (mm)
	F1D-C-M1	0.26	G1D-C-M-A	0.36
	F1D-C-M2	0.20	G1D-C-M-B	0.36
	F1D-C-M3	0.26	G1D-C-M-C	0.28
	F2D-C-M1	0.30	G2D-C-M1	0.22
	F2D-C-M2	0.30	G2D-C-M2	0.20
	F2D-C-M3	0.38	G2D-C-M3	0.20
	F1D-C-E1	0.30	G1D-C-E1	0.28
	F1D-C-E2	0.30	G1D-C-E2	0.26
	F1D-C-E3	0.38	G1D-C-E3	0.26
	F2D-C-E1	0.30	G2D-C-E1	0.26
	F2D-C-E2	0.28	G2D-C-E2	0.28
	F2D-C-E3	0.16	G2D-C-E3	0.40
	F1D-C-ES1	0.28	G1D-C-ES1	0.22
	F1D-C-ES2	0.20	G1D-C-ES2	0.20
	F1D-C-ES3	0.26	G1D-C-ES3	0.26
	F2D-C-ES1	0.30	G2D-C-ES1	0.20
	F2D-C-ES2	0.18	G2D-C-ES2	0.26
	F2D-C-ES3	0.16	G2D-C-ES3	0.28
Mean		0.27		0.27
Standard deviation		0.06		0.06

A test on the variance (not shown in Table 3.5) and standard deviation of these crack widths indicates that the difference in the crack widths of the cracked PC/FA and PC/SL beams was not statistically significant; hence, the corrosion

measurement results can be comparable. The minimum mechanically induced crack width was 0.16 mm while the highest was 0.40 mm wide

3.11 Concrete durability index tests

Concrete durability index tests were conducted after coring the 100 mm concrete cubes at 28 days of curing (SANS 3001-CO3-1, 2015; SANS 3001-CO3-2:, 2015; SANS 3001-CO3-3, 2015). The durability index tests were conducted to characterize the potential durability of the cover concrete by measuring the transport of fluids (gases, ionic diffusion and water absorption) through it. The compressive strength of cured concrete made from a blend of PC with SCMs has been observed to increase significantly until 90-days; this may also influence its transport properties. Since the specimens in this study where not cured in moisture for up to 90 days, only the 28-day DI properties were determined. It is however reasonable to conduct the 90-day DI tests in concrete with SCMs to investigate if the results will vary significantly with respect to the 28-day test results.

The three durability index tests which were conducted to determine these transportation mechanisms through the concrete were; oxygen permeability index (OPI), chloride conductivity index (CCI) and the water sorptivity index (WSI) tests.

The disc specimens that were used for the durability tests were extracted from the concrete cubes in the same manner; by using a water-cooled diamond tipped barrel to core through the center of the cube, perpendicular to the casting direction. The cores were then cut to the required thickness as shown in Figure 3.9. Two (2) discs (labeled 1's in Figure 3.9) with a diameter of 70 ± 2 mm and thickness of 30 ± 2 mm were extracted from each cube. The thickness and diameter of the discs were measured at four equally spaced points around its perimeter. Before conducting the durability tests, all the extracted discs were preconditioned by oven drying them at a temperature of 50 ± 2^{o}C for a period of 7 days after which they were cooled (in a desiccator) to room temperature for 2 hours before being used in the durability index tests. Four (4) discs were used for each of the durability index tests, however, it is specified that a minimum of 3 results from the disc specimens may be used to determine the durability index of the concrete.

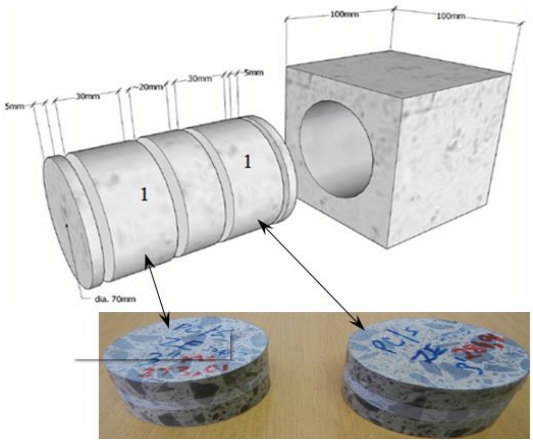


Figure 3.9: Durability index test disc extraction from 100 mm concrete cube (extracted discs shown photo were sourced from SANS 3001-CO3-1: 2015).

3.11.1 Oxygen permeability test

The OPI tests on the samples were conducted according to the specifications in SANS 3001-CO3-2 (2015). The test results will be used to assess the concrete quality via the concrete permeability to oxygen. The specimens used were dry and free of defects (e.g. cracks) which could invalidate the test result. To carry out this test, the specimen thickness and diameter were measured at four different points and the mean measurement recorded. The discs were placed over 5-litre cylindrical oxygen chambers which were kept at an initial pressure of 100 ± 5kPa (see Figure 3.10). A cross-section of the OPI apparatus is shown in Appendix H: (Figure H. 1).

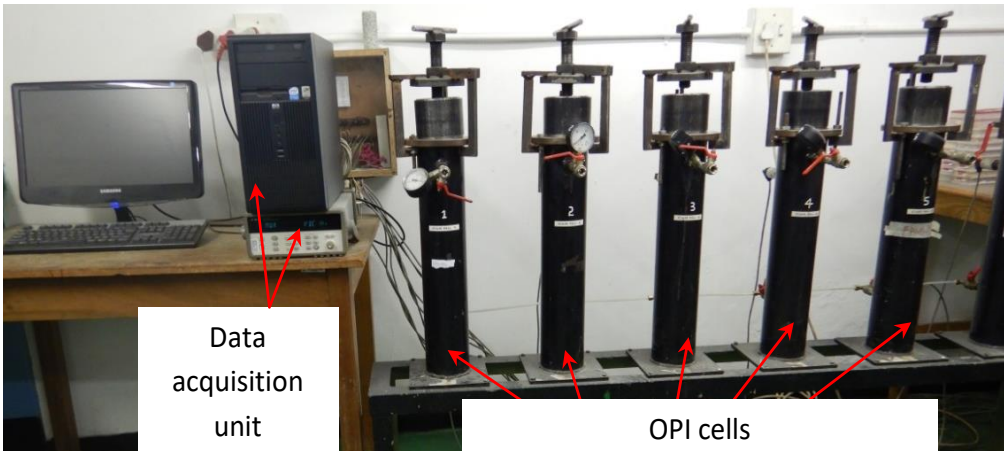


Figure 3.10: OPI test (a) Laboratory equipment

The pressure decay in the chamber was logged at 15 minutes intervals for a period of 6 hours; however, the test was terminated if the pressure in the chamber decreases below 50 kPa before the 6-hour mark.

The data obtained from the OPI test specimens denoted the amount of oxygen which passed through the specimen during the test period. The data collected was processed using the durability index spreadsheet application.

To analyze the data obtained from the pressure decay in the oxygen chamber, a regression plot of the time (*s*) and $ln\frac{P_o}{P_t}$ (the parameters P_o and P_t are defined after Eqn. 3.1) passing through the *0, 0* point is plotted, the slope of the linear regression line (*Z*) was computed using Eqn. 3.1;

$$Z = \frac{\sum\left[ln\left(\frac{P_o}{P_t}\right)\right]^2}{\sum\left[ln\left(\frac{P_o}{P_t}\right).t\right]} \qquad 3.1$$

where P_o is the initial pressure at the start of the test (at time t_o) to the nearest 0.5 kPa,

P_t is the pressure at time *t*, measured from t_o, to the nearest 0.5 kPa and

t is the time (in seconds) at start of the test.

For the OPI results to be valid, the coefficient of correlation (r^2) of the four (4) specimens used in the test, were greater than 0.99 else the specimen was discarded. However, discretion was exercised whether to discard a specimen or not, as it was possible to have very impermeable or alternatively very permeable specimens, where the r^2 value was less than 0.99, but generally achieved 0.98 (SANS 3001-CO3-2:, 2015). In some instances, the test was rerun in order to forestall an unknown error which may have occurred while running the test initially. The correlation coefficient (r^2) was computed from Eqn. 3.2;

$$r^2 = 1 - \frac{\sum\left[t_i - t_{p,i}\right]^2}{\sum t_i^2 - \left[\frac{\left(\sum t_{p,i}\right)^2}{n}\right]} \qquad 3.2$$

where t_i is the time at any given pressure reading, recorded to the nearest minute, in seconds

$t_{p,i}$ is the predicted time at the same pressure reading (based on the linear regression), in seconds (*s*) and;

n is the number of data points observed.

The value of $t_{p,i}$ was computed from Eqn. 3.3;

$$t_{p,i} = \frac{ln\left(\frac{P_o}{P_t}\right)}{z} \qquad 3.3$$

The D'arcy coefficient of permeability (*k*) of the test specimen in meters per second (m/s) was then computed thus from Eqn. 3.4;

$$k = \frac{\omega \times V \times g \times d \times z}{R \times A \times T} \qquad 3.4$$

Where ω is the molecular mass of oxygen (*0. 032 kg/mol*) in kilograms per mole

V is the volume of the permeability cell (5 liters or 0.005m^3) recorded to the nearest 0.01 liter or 0.00001 m^3

g is the acceleration due to gravity (*9.81 m/s*^{2}) in m/s^2.

d is the average specimen thickness to the nearest 0.02 mm,

z is the slope of the linear regression line passing through the 0,0 point, in reciprocal seconds (s^{-1})

R is the universal gas constant (*8.313 Nm/Kmol*), in Newton meters per Kelvin mole

A is the cross-sectional area of the specimen (m^2),

T is the absolute temperature in Kelvin (*K*).

The OPI for each specimen was computed from the coefficient of permeability (*k*) obtained for each test specimen (see Eqn. 3.5);

$$\boldsymbol{OPI = -log_{10}(k)} \qquad 3.5$$

The specimen OPI was computed as the mean of at least 3 OPI values.

3.11.1.1 Interpretation of OPI test results

The OPI values indicate the ease with which fluids permeate through the concrete pore structure; thus, there is a relationship between OPI values and the concrete pore connectivity. A low OPI value is indicative of concrete which has well-connected pores while one with a higher OPI value indicates poor pore connectivity (Alexander et al., 2008; Alexander, Mackechnie, & Ballim, 1999; Kessy, Alexander, & Beushausen, 2015).

3.11.2 Water sorptivity index test

The same specimens which were used in the OPI test were also used in the water sorptivity index test as they had no contact with moisture during the OPI test. This test was used to obtain the effective porosity of into concrete and water sorptivity index (in millimeter per square root hour (mm/√hr)). The experimental setup is shown in Figure 3.11.

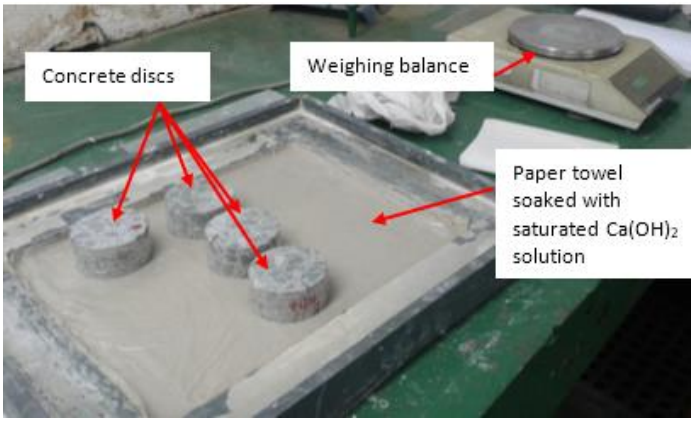


Figure 3.11: Water sorptivity durability index test setup

As with the OPI, the specimen thickness and diameter were measured at four different points and the mean measurement recorded. Before commencing the test, a sealing tape was applied to the vertical face of each concrete disc to impede moisture penetration after which each disc was weighed to obtain its dry mass. A saturated solution of calcium hydroxide was prepared by adding 5g of $Ca(OH)_2$ per liter of water. A paper towel folded into 10 plies was laid in a tray and the saturated solution poured unto it such that the height of the fluid did not exceed 2 mm from the disc base after it was placed over the soaked paper towel. Before placing the

discs on the towel, trapped air was gently expelled from beneath it by smoothing the paper outward towards its edges.

The specimens were gently placed on the soaked paper towel and the mass of each disc was weighed at 3, 5, 7, 9, 12, 16, 20, and 25 minutes intervals. Prior to weighing a disc, any excess moisture was wiped off its surface. The discs were weighed within 10 seconds after being removed from the $Ca(OH)_2$ solution and then immediately placed back onto the solution. After obtaining these results, the vacuum saturated mass of the specimens was obtained by keeping them in a vacuum chamber at a vacuum pressure of – 75 to – 80 kPa for a period of 3hrs ± 15 minutes after which a saturated solution of $Ca(OH)_2$ was allowed into the chamber until it covered the discs. The specimens were further vacuumed (while in the being fully immersed in the saturated $Ca(OH)_2$ solution) for another 1 hr. ± 15 minutes at a pressure not exceeding –75 kPa after which air was allowed into the chamber. The specimens were left in the saturated $Ca(OH)_2$ solution for 18 ± 1 hours before they were removed from the solution, wiped off any excess moisture and then weighed to obtain their saturated mass (M_{sv}).

Eqn. 3.6 was used to obtain the porosity (n_w) of the concrete to water for each of the disc specimens;

$$n_w = \frac{M_{sv} - M_{so}}{Ad\,\rho_w} \times 100 \qquad 3.6$$

Where M_{sv} is the vacuum saturated mass of the specimen to the nearest 0.01 g,

M_{so} is the mass of the specimen at time t_o (start of test) to the nearest 0.01 g,

A is the cross-sectional area of the specimen to the nearest 0.02 mm^2,

d is the average specimen thickness to the nearest 0.02 mm,

ρ_w is the density of water, $10^{-3}g/mm^3$.

The water sorptivity was obtained by finding the slope (F) from the plot of the mass gained (M_{wt}) against the square root of time (see Eqn. 3.7), while the water sorptivity index was computed using Eqn. 3.8;

$$M_{wt} = F\sqrt{t} \qquad 3.7$$

$$S = \frac{Fd}{M_{sv} - M_{so}} \quad 3.8$$

Where S is the specimen sorptivity in mm/√hr and the other parameters are as defined in Eqn. 3.6 and 3.7.

In this test, a coefficient of correlation of the data of not less than 0.98 was required from a set of 5 or more data points.

3.11.2.1 Interpretation of WSI test results

The WSI is most useful in concrete which unsaturated and it is subjected to wetting and drying conditions. Hence, the WSI measures the ease with which the concrete surface absorbs moisture through capillary suction. A high WSI indicates concrete which will easily absorb moisture, while concrete with low WSI value is less prone to absorb moisture. High water absorption by concrete may be indicative of poor concrete curing which has a negative bearing on concrete durability and vice versa (Alexander et al., 2008, 1999; Kessy et al., 2015).

3.11.3 Chloride conductivity index test

The chloride conductivity index (CCI) test result gives an indication of the concrete resistance to the migration of chloride ions and the porosity of the concrete to chloride ions. The specimens (i.e. discs) used in this test were saturated using the same vacuum saturation procedure as that of the water sorptivity index test but the saturation solution in this test was a 5M sodium chloride (NaCl) solution. Before saturating the discs, they were weighed to obtain their dry mass and their saturated mass was also recorded. To determine the CCI of the concrete, each of the discs is put into the test equipment (see Figure 3.12) which has two compartments on either side of the disc. The compartments were each filled with 5M NaCl. A cross-section of the chloride conductivity apparatus is shown in Appendix H: (Figure H. 2). The test equipment had an anode and cathode wherein a DC power supply was used to apply a regulated voltage (of about 10V for a period usually not exceeding 10 seconds) through the specimen, while the current and voltage across the specimen was simultaneously being recorded.

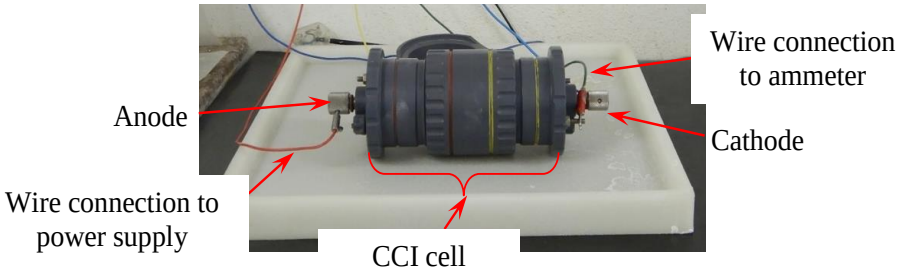


Figure 3.12: Arrangement of CCI test set up (SANS 3001-CO3-3, 2015)

The CCI was computed from Eqn. 3.9;

$$\sigma = \frac{id}{VA} \qquad 3.9$$

Where σ is the specimen conductivity (mS/cm)

i is the electric current measured across the specimen (mA)

d is the average thickness of the specimen (cm)

V is the difference between the applied voltage and the measured voltage across the specimen (V)

A is the cross-sectional area of the specimen (cm^2)

The mean chloride conductivity of the 4 specimens was taken as the concrete CCI.

The porosity of the concrete to chloride ions (n_{cl}) was determined from Eqn. 3.10;

$$n_{cl} = \frac{(M_{sv} - M_d)}{Ad\rho_s} \times 100 \qquad 3.10$$

Where n_{cl} is the porosity as a fraction of the volume of the specimen occupied by the chloride solution, as a percentage (%)

M_{sv} is the vacuum saturated mass of the specimen to the nearest 0.01 g,

M_d is the mass of the dry specimen determined to the nearest 0.01 g,

A is the cross-sectional area of the specimen to the nearest 0.02 mm^2,

d is the average specimen thickness to the nearest 0.02 mm,

ρ_s is the salt solution density (1.19 x 10^{-3} g/mm^3)

3.11.3.1 Interpretation of CCI test results

Concrete which has high chloride conductivity means chloride ions will easily diffuse into it while one with low chloride conductivity will have fewer chloride ions diffusing into it. The effective porosity of the concrete is used to assess the chloride intake of concrete in saturated conditions. The effective porosity is important in determining the potential durability of concrete that will be fully submerged in chloride solution (Alexander et al., 2008, 1999; Kessy et al., 2015).

3.12 Chloride ponding; wetting and drying cycles

A solution containing NaCl salt (i.e. 5% by mass) in potable water was used as the ponding solution. The specimens were placed horizontally and fully submerged in the chloride solution in a chloride bath which was covered with a polythene sheet to minimize moisture evaporation which could result in an increase in chloride concentration during the test.

The uncracked and cracked specimens were fully immersed in the chloride solution for 2 weeks after which they were removed and left to dry in ambient laboratory condition (temperature; 20 ± 5^{o}C and relative humidity; 40 ± 10%) for another 2 weeks. Hence a complete cycle (i.e. 4 weeks) consisted of 2 weeks of chloride ponding and 2 weeks of drying in ambient laboratory condition. This cycle (wetting and drying) was repeated throughout the experimental phase of this study. The possible influence of the adopted ponding method and the specimen epoxy sealing on the corrosion rate results is discussed in Section 4.4.3.

3.13 Steel corrosion measurement and assessment

The steel corrosion was monitored by using monitoring the steel corrosion rate, concrete resistivity and half-cell potential readings. These readings were taken approximately 24 hours after the specimens were removed from the ponding solution, this was to avoid the influence of surface saturation (Hope, Ip, & Manning, 1985; Hussain et al., 1995). Another set of readings (not presented in this report) were also taken a day before the specimens were returned (after air drying for 2 weeks) into the ponding tank (for the next wetting cycle).

Visual inspection of the RC beams for signs of corrosion-induced cracks and rust stains was undertaken along with previously mentioned electrochemical corrosion measurements. Corrosion of the specimens was monitored over a 27-month period.

3.13.1 Steel corrosion potential measurement

The steel corrosion potential was measured using the $Cu/CuSO_4$ half-cell meter (see Figure 3.13).

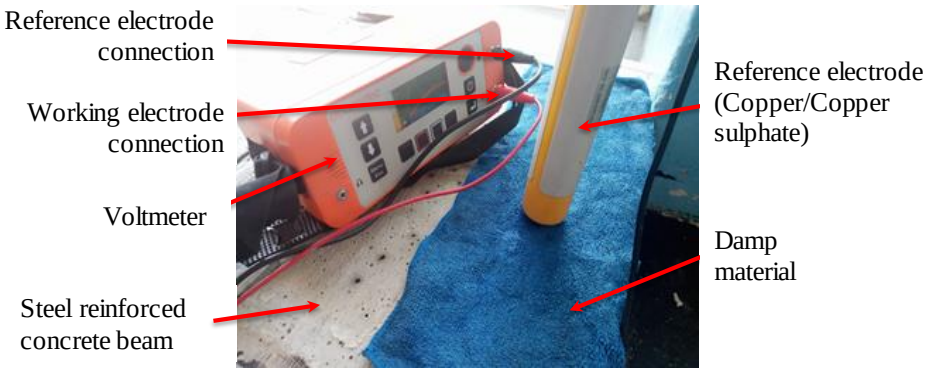


Figure 3.13: $Cu/CuSO_4$ half-cell meter

This method is suited for equipotential mapping of RC structural elements; as it identifies areas that are most liable to corrode (see Table 2.3). Though this method is easy to use, it does not give an indication of the corrosion rate but rather provides the probability of steel corrosion (ASTM C876-09). To conduct this test, an electrical connection to the corroding reinforcement bar is required. In this study, the electrical connection was achieved by means of attaching an electrical wire to the steel reinforcement before it was cast into the concrete. The electrical wire was extended out of the concrete beams as illustrated in Figure 3.7.

Two sets of corrosion potential readings were collated from the RC beam specimens;

i. At the end of the wetting cycle: This data was measured 1-day (≈ 24 hours) after the specimens were removed from the NaCl (ponding) solution. This procedure was adopted in order to mitigate the influence of concrete pore saturation on the measurement being taken.

ii. At end of drying cycle: After air drying the RC beam specimens in ambient laboratory conditions for 2 weeks, this set of readings were taken 1 day (≈24

hours) before the specimens were returned into the NaCl solution for the next wetting cycle.

Though these readings may be used to monitor the effect of wetting and drying on the corrosion potential of the embedded steel reinforcement bar, only measurements taken at the end of the wetting cycle are reported in this study. They were subsequently used in interpreting the corrosion characteristics of the specimens. The data obtained at the end of the drying cycle was not used as it was presumed that since the specimens were not kept in a controlled environment (where temperature and humidity is regulated); they may have dried out at different rates thereby having an influence on the corrosion measurements while using the measurements that were obtained 24 hours after the wetting cycle will limit the influence which may arise due to variation in the drying rate of the specimens. It is worth noting that the measured HCP at the end of the wetting cycle was more negative than that observed at the end of the drying cycle, the difference in these values was due to a variation in the degree of saturation of the concrete pores with time as the specimens were left to air dry (RILEM TC 154-EMC, 2003).

An Elcometer half-cell meter (model 331 HM) was used in this study to monitor the corrosion potential of the steel reinforcement. This hand held device consists of a $Cu/CuSO_4$ probe, a half-cell meter which can measure a voltage range of – 999mV to + 999mV with an accuracy of ± 5mV when operated within a temperature range of 0^oC to 50^oC and two (2) connection wires (one connection each to the half-cell meter from the $Cu/CuSO_4$ electrode and working electrode) (Elcometer Ltd., 2012). The equipment was operated within this temperature range; therefore, its accuracy was assumed to be within the prescribed range. The half-cell measurements were interpreted in line with the provision of ASTM C876 (2009) which was presented in Table 2.3 & Table 2.4.

3.13.2 Concrete resistivity measurement

The concrete resistivity was also monitored after each wetting and drying cycle (see Section 3.13.1). In this study, the single disc electrode–disc method was used to obtain the concrete resistivity (see Section 2.11.3). This method utilized a connection from the device to the reinforcing steel; hence the measured concrete

resistivity is that of the concrete cover. The electrode-disc device used for this test was an integral part of the Coulostat VIII device which was also used to measure the corrosion rate.

Though the Wenner probe has been widely used in corrosion studies, the electrode–disc method was also used in this study since the concrete resistivity will be taken close to the concrete edge. This method mitigates identified errors which are encountered when taking concrete resistivity measurements close to the concrete edge with the Wenner probe (Gowers & Millard 1999; Hornbostel et al. 2013). The method used in processing the measured reading is presented in Appendix A.

3.13.3 Corrosion rate measurement

In this study, the coulostatic method (using a Coulostat VIII device) was used to measure the instantaneous corrosion rate of the embedded steel reinforcement bar in concrete. The method used is essentially a linear polarization resistance method but instead of monitoring the response of the applied potential over a period of time (usually a minute), the coulostat measures the relaxation (potential transient) of the steel potential after the application of a known amount of small current (10 – 20mA) for a few milliseconds (<10 ms). The potential transient was monitored for about 50 seconds; 20 seconds before applying the potential and 30 seconds after it is applied to monitor its decay. The coulostatic device is connected to a computer unit wherein the corrosion data is logged and the corrosion rate (in $\mu A/cm^2$) is computed with the aid of the device software. The Stern Geary constant; $B = 26\,mV$, was used to compute the corrosion rate (this value of B is assumed for depassivated steel) (RILEM TC 154-EMC, 2004).

The used coulostatic device has 3 (Silver/Silver chloride; Ag/AgCl) reference electrodes which are equidistance from each other with the median reference electrode located at the center of the stainless-steel counter electrode (see Figure 3.14). The reference electrodes (of fixed and known potential) measure the potential decay in the working electrode after it is polarized with a small current of known intensity from the counter electrode (diameter = 60 mm) that is placed on the concrete surface which lies directly over the reinforcement bar. Thus, the polarized area of the reinforcement bar (= πdl; where d is the reinforcement diameter, and l is

the diameter of counter electrode) is assumed to be equivalent to the section which lies directly below the counter electrode. The use of the polarized area to compute the corrosion rate assumes that the reinforcement bar is subjected to uniform corrosion, which is not the case in chloride-induced corrosion as pitting corrosion is the dominant type of corrosion. The corrosion rate will vary based on the parameter (polarized area or steel diameter). Since the actual polarized area of reinforcement bar is unknown, its diameter was used as an input parameter for determining its corrosion rate.

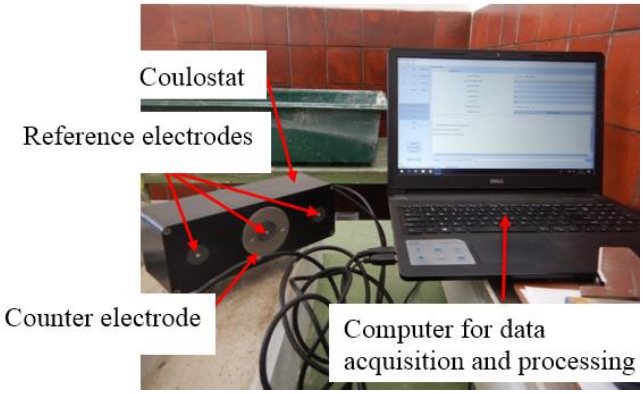


Figure 3.14: Corrosion rate measurement setup – coulostat method

Two corrosion rate measurements (as with the corrosion potential in section 3.13.1) were taken during the course of this study; 24 hours after the end of the wetting period and 24 hours before they are returned into the chloride solution (i.e. at the end of the drying cycle). Only the corrosion measurements taken at the end of the wetting cycle are presented and subsequently used in the analysis. The reading taken at the end of the drying cycle was not utilized due to possible variation in drying rate of the specimens which may influence the corrosion rate measurements since the specimens were left to dry in ambient environment. The corrosion rate measurements were taken about the mid-span of both the cracked and uncracked beam specimens.

3.13.4 Visual observation

Specimens with corrosion stains and corrosion induced cracks were identified and reported and the corrosion-induced crack widths were measured with a crack microscope (see Figure 3.8). The measured crack widths and lengths are both

reported in millimeters (mm). The crack length was measured along its length by using a flexible string and then read off after being stretched along a scaled ruler.

The corrosion-induced crack damage on the specimen sets were characterized by using the crack-factor which was proposed by Poupard et al. (2007) (Eqn. 3.11).

$$crack\ factor = \sum_{i=1}^{N} length(i) \times width\ (i) \qquad 3.11$$

Where N is the number of cracks on the considered beam face.

The crack-factor integrates the product of the crack lengths and their widths thus making it easy for them to be characterized. The crack-factor values were compared to the corrosion rate to determine if it has an influence on the corrosion rate of the steel reinforcement bars. The maximum corrosion-induced crack width was used in the crack-factor computation; this crack width was used because it signified the highest corrosion risk to the steel reinforcement as it will allow easier ingress of corrosion-causing agents.

3.13.5 Reinforcement bar mass and corrosion pit depth measurement

The steel mass loss will be assessed in order to validate the hypothesis that the reinforcement position within the concrete and chloride ingress directions has an influence on its damage characteristics. To access the mass loss, the reinforcement bars were removed from the concrete after terminating the wetting and drying cycles. They were then wire brushed to remove any concrete and rust in accordance with the provisions of ASTM G1-90 (2003), then cleaned with acetone. The reinforcement bars were then weighed to determine their mass loss over the period of the experiment. To assess the corrosion pit depths, the diameter of the reinforcement bars was measured at 5 mm intervals using an outside divider and digital Vernier caliper (Figure 3.15).



Figure 3.15: Outside caliper dividers and Vernier calipers

3.14 Chloride penetration profile measurement

The chloride penetration profile was assessed at the end of the chloride exposure cycles (end of the experiment). The chloride profile was determined by analyzing the percentage of acid soluble chlorides per weight of binder. This method is more reliable and has been widely used and reported compared to the determination of water soluble chlorides (Mackechnie & Alexander, 2001). The concrete dust was obtained using a 14 mm diameter drill bit for specimens exposed to 1D chloride ingress, while an 8 mm drill bit was used to obtain dust at the corners of the specimens exposed to 2D chloride ingress. The concrete dust to be analyzed for chlorides was obtained by collecting drilled dust (from at least 3 positions) at 5 mm depth intervals from the concrete surface to a maximum depth of 25 mm (ASTM-C1543 - 10, 2010; ASTM C1218 / C1218M, 1999). A depth of 25 mm was chosen since it slightly extends beyond the reinforcement cover depth used in this study; i.e. 20 mm.

To determine the percentage weight of chloride in the extracted concrete sample, the drilling was performed perpendicular to the exposed surface for 1D chloride ingress while that of the 2D chloride ingress was drilled at 45^{o} to the concrete corner (Figure 3.16). To collect the concrete dust at the beam corners, 5 mm was chamfered off the edge to ease the drilling. The beam was clamped to a drill press during the dust sample collection. This method of concrete extraction for chloride analysis was suggested and used by Zhang, Sun, Liu, et al. (2011). The chloride profile taken at the angle of the specimen denotes the influence of the chloride penetration from two adjacent directions of the specimen.

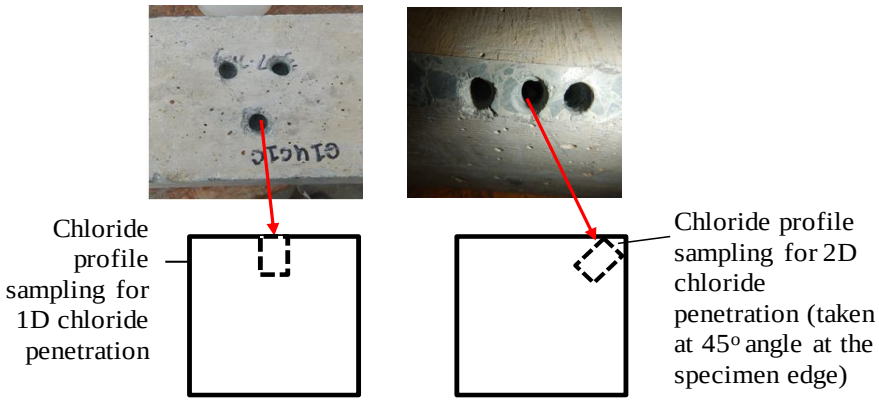


Figure 3.16: Cross section of 1D and 2D chloride profile sampling

3.14.1 Determination of acid-soluble chloride concentration in concrete

The chloride in concrete can be either bound within the concrete paste and aggregates or exist as free chloride in the pore solution. The corrosion of reinforcement bars has been thought to be induced by the presence of free chlorides at the surface of the reinforcement bar. The measurement of free chlorides is not well defined as the value obtained can be influenced by temperature, nature of the sample and duration of the extraction steps. Due to these shortcomings in determining the free chlorides, the use of acid soluble chlorides has been widely adopted as a means to measure the chloride concentration (ACI 222R, 2001; A. Castel et al., 2003a; Hope, Page, et al., 1985). In general, the acid-soluble chloride content per dry concrete (in % by mass) is usually assumed to represent the total chloride content (U. Angst, 2011).

A linear relationship between the concentration of total and free chlorides in a given sample has been reported, hence an increase in free chlorides has been directly related to an increase in total chlorides (T. U. Mohammed & Hamada, 2003). Therefore, the amount of total chlorides can be related to the quantity of free chlorides in a mortar or concrete sample.

The RILEM TC 178 (2002) recommendation was used to determine the chloride concentration in the concrete powder that was drilled from the holes. The chloride content was expressed as a percentage of the relative weight of the binder (% Cl) calculated using Eqn. 3.12;

$$\%Cl = \frac{3.5453\, V_{Ag} M_{Ag} (V_2 - V_1)}{m V_2} \qquad 3.12$$

where V_{Ag} is the volume of $AgNO_3$ added (in cm^3)

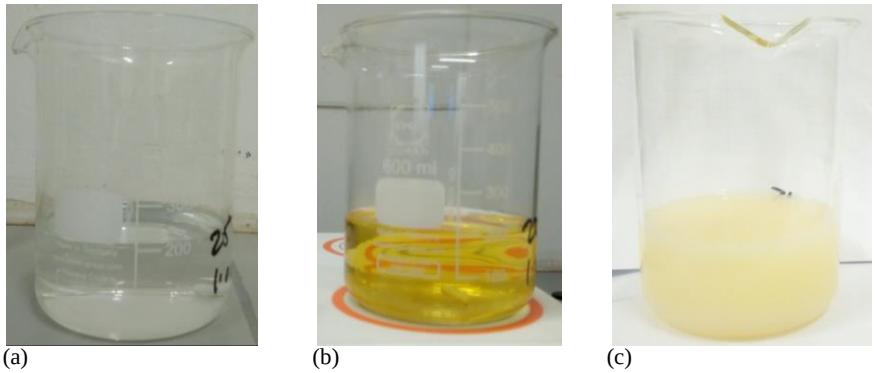
M_{Ag} is the real molarity of the $AgNO_3$ solution (0.05M)

V_1 and V_2 are the volumes of ammonium thiocyanate (NH_4SCN) in cm^3 used in the sample and blank tests respectively and,

m is the mass of binder in 1 *gram* of concrete powder (g)

Figure 3.17a to c shows the change in color of the of the PC/FA and PC/SL concrete samples when testing for the total chloride content in the concrete (before titration

and after titration). Hydrogen peroxide (H_2O_2) was added to the slag concrete sample to prevent sulfide interference with the result (Castellote & Andrade, 2001; RILEM TC 178, 2002).



(a) (b) (c)

Figure 3.17: Change in color during acid-soluble chloride test (a) PC/FA sample after adding indicator (b) PC/SL sample after adding indicator and H_2O_2 (c) after titration

Two titration tests were performed per sample of concrete dust that was collected in each depth interval.

3.15 Summary of experimental methods

A summary of the activities to be undertaken in this study is presented in Figure 3.18.

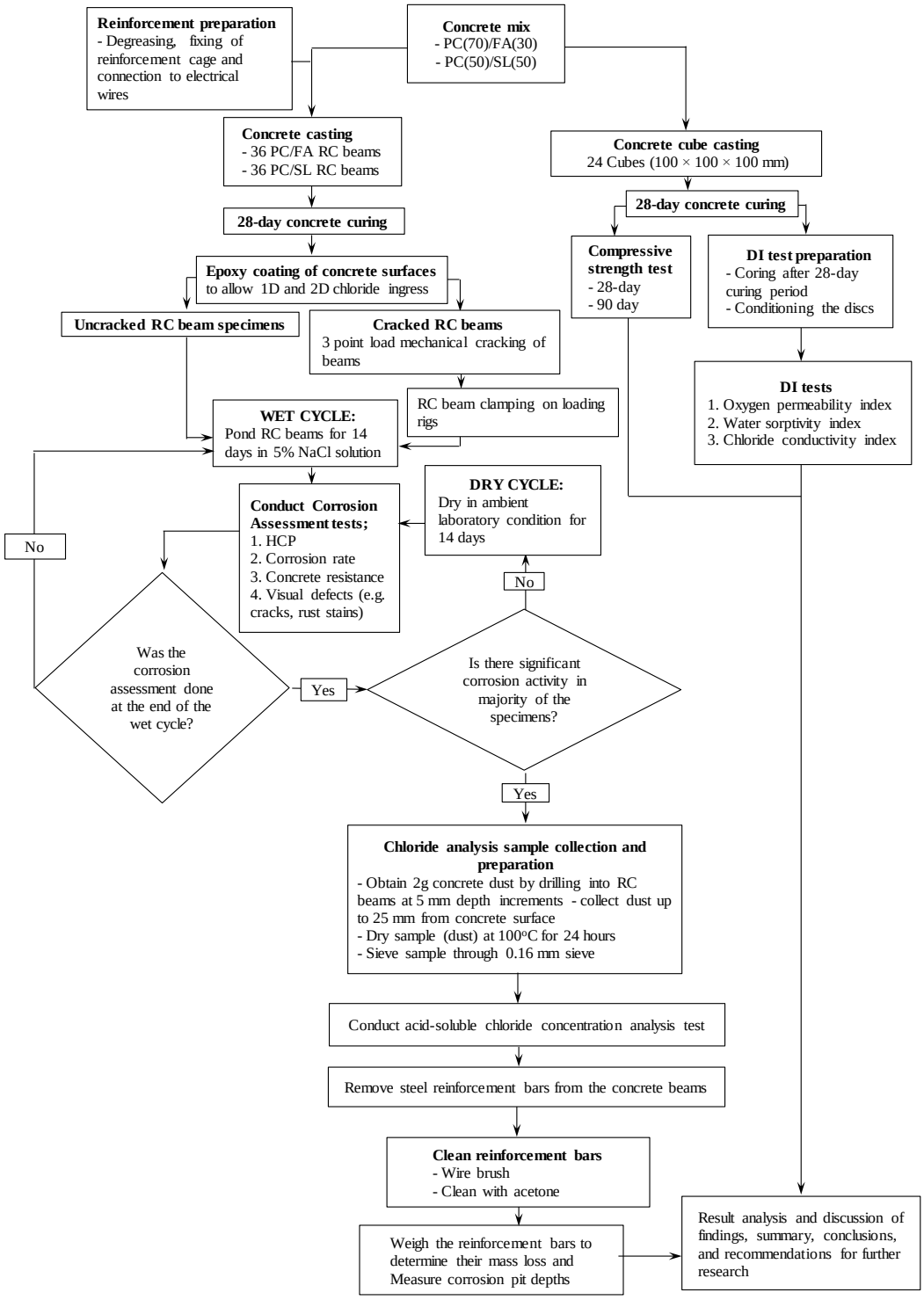


Figure 3.18: Flowchart of experimental program

4.1 Introduction

In this chapter, the durability index test results, corrosion potential, corrosion rate, concrete resistivity, corrosion-induced cracks, steel mass loss due to corrosion, pitting depths, and chloride concentration at various distances from the concrete surface are presented and discussed. In this study, the durability index test results will be most applicable to the uncracked concrete specimens. In the cracked concrete specimens, the penetration of corrosion agents will be influenced by the presence of surface cracks and the imposed flexural stress.

The results in the cracked and uncracked (PC/FA and PC/SL) concretes will also be discussed based on the reinforcement location within the concrete (at middle (-M-), edge (-E-), and at the edge of the concrete beam with a stainless-steel bar (-ES-) and the ingress direction of corrosion agents (1D and 2D) into the concrete (see Figure 3.4). Within this text, the term chloride ingress direction will be used interchangeably with the ingress direction of corrosion agents. The reinforcement nomenclature that will be used to describe the location of the reinforcement bar within the concrete is (see Figure 3.4);

a. Middle (-M-), for reinforcement bar which is placed at the middle of the concrete beam
b. Edge (-E-), for concrete with reinforcement bar that is located at an orthogonal edge/corner, and
c. Edge with stainless steel bar (-ES-) for concrete which has a steel reinforcement bar that is connected to a stainless-steel bar

The commencement of the chloride ponding and drying cycles is denoted as week zero (0) in the corrosion potential, concrete resistivity, and corrosion rate plots; these plots are also 3–point moving average. Appendix A. has further details of the techniques (e.g. outlier identification) which were used to process the results presented in this chapter.

The results are discussed based on observed trends within the first few weeks (week 0 – week 52) after commencing the study while the mean(s) of the results obtained in the last the 52 weeks of the experiment were plotted, and the observed trends

discussed. In some instances, the mean of the last 52-week results provided trends that were not notable when the overall mean of the experimental data was used. This data was assumed to represent the corrosion propagation phase which proceeded at a significantly different rate to the results obtained earlier in the experiment.

The error bars used in some of the plots represent one standard deviation of the data being considered.

4.2 Concrete cover quality

The quality of the concrete cover to the reinforcement bar is its measure of resistance to the ingress of corrosion agents (chlorides, oxygen, and moisture). To assess the potential durability performance of the concretes used in this study, the durability index (DI) parameters were assessed using 28-day moist cured concrete (see Section 3.11) and the results are presented in Table 4.1.

The potential durability performance of concrete is assessed on the basis that the concrete is void of defects such as cracks since the presence of cracks in concrete has been identified to significantly influence the transport mechanism of fluids through it (Audenaert et al., 2009; Mike Otieno, 2008; Pease, 2010; O. G. Rodríguez et al., 2003; Scott & Alexander, 2007; R. Zhang et al., 2010). The DI results will aid in the interpretation of the data obtained from the specimen corrosion measurements.

Table 4.1: Durability Index test results

Test	Durability indices	PC/FA		PC/SL	
		Mean	**S.D.** (σ)	**Mean**	**S.D.** (σ)
OPI	Oxygen permeability	10.55	0.26	10.88	0.33
CCI	Chloride conductivity (mS/cm)	0.56	0.10	0.11	0.01
	Porosity (%)	3.71	0.10	2.07	0.01
WSI	Water sorptivity ($mm/hr^{0.5}$)	7.98	0.48	6.12	0.14
	Porosity (%)	9.85	0.31	7.39	0.01

S.D: standard deviation; **COV:** Coefficient of variation; **OPI:** Oxygen permeability index; **CCI:** Chloride conductivity index; **WSI:** Water sorptivity index

An independent two-tailed t-test with a 95% confidence interval was used to test if there is a significant difference in the values of the durability parameters (OPI, CCI, and WSI) shown in Table 4.1. The t-test details are presented in Appendix F: while a summary of the t-test results is presented in Table 4.2.

Table 4.2: Independent t-test result summary of DI parameters

Durability index parameter	*p-value*	Difference
OPI	0.255	Insignificant
CCI	0.003	Significant
Porosity (Chloride conductivity test)	5.68E-05	Significant
WSI	0.002	Significant
Porosity (Water sorptivity test)	3.87E-04	Significant

The probability values obtained from the t-test indicate that there is a significant difference in the CCI, WSI, and porosity of concrete. Apart from the OPI results which have an insignificant difference, the other DI values indicate that the PC/SL concrete has a higher resistance to chloride penetration and water absorption. This implies that the PC/SL concrete will have higher resistivity values compared to the PC/FA concrete. Its porosity of the PC/SL concrete in the CCI and WSI test is also lower than that of the PC/FA concrete. From these results, it can be concluded that the PC/SL concrete will perform better than the PC/FA concrete when exposed to a chloride environment.

4.3 Corrosion potential of reinforcement bars

The trends of measured corrosion potentials are presented in Figure 4.1 to Figure 4.4, while a plot of the mean corrosion potential of the various concrete specimens is presented in Figure 4.5.

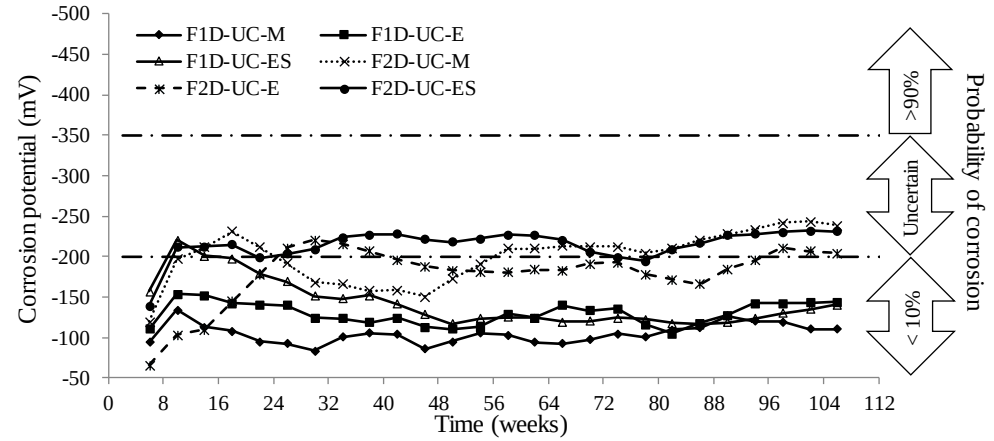


Figure 4.1: 3-point moving average for corrosion potential of uncracked PC/FA specimens exposed to 1D and 2D chloride ingress

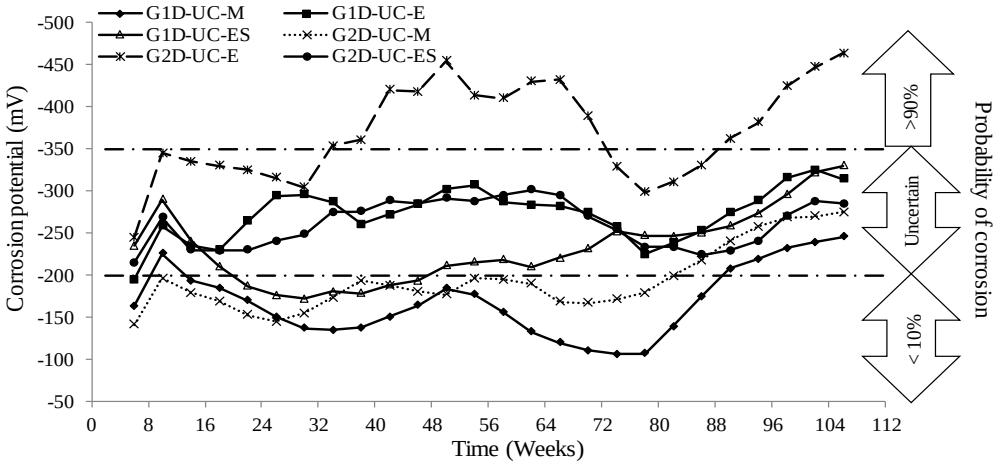


Figure 4.2: 3-point moving average for corrosion potential of uncracked PC/SL specimens exposed to 1D and 2D chloride ingress

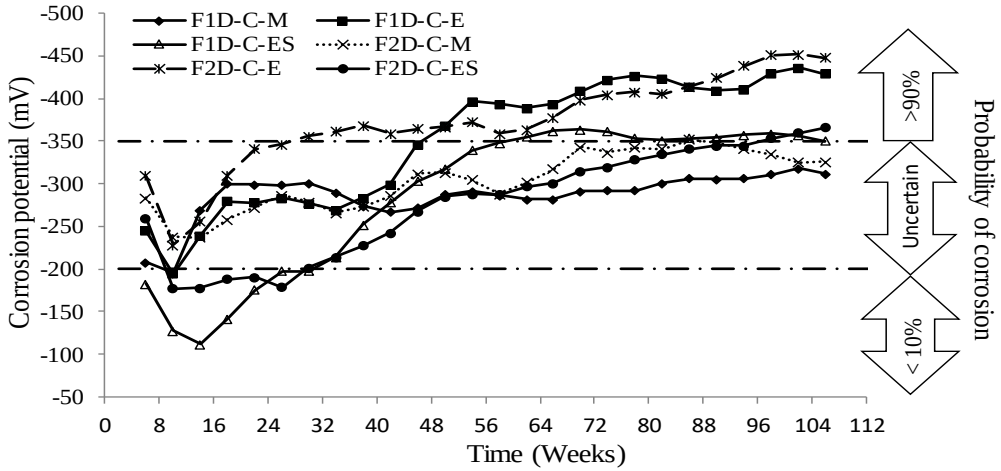


Figure 4.3: 3-point moving average for corrosion potential of cracked PC/FA specimens exposed to 1D and 2D chloride ingress

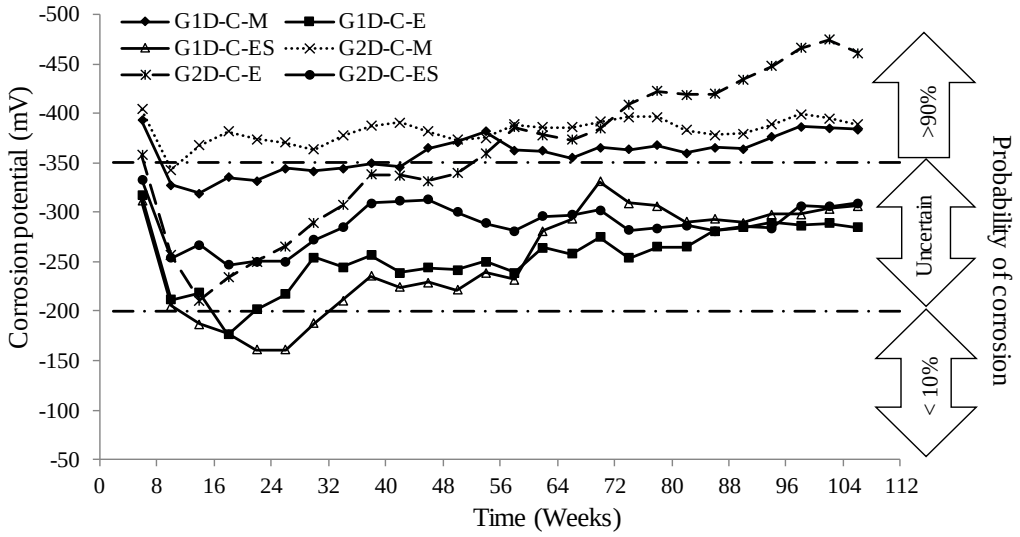


Figure 4.4: 3-point moving average for corrosion potential of cracked PC/SL specimens exposed to 1D and 2D chloride ingress

4.3.1 Corrosion potential in uncracked reinforced concrete

The corrosion potential of the uncracked PC/FA and PC/SL concrete decreased significantly (i.e. they became more negative) within the first 10 weeks after commencing the chloride ponding. The poor development of the concrete pore structure and rapid ingress of chlorides by capillary suction into the concrete within this period may have resulted in this decrease in the corrosion potential. After the 10th week, a different trend in the corrosion potential of the PC/FA and PC/SL concrete was observed. In the PC/FA concrete, the corrosion potentials became more positive after the initial drop and became fairly uniform after the 32nd week (see Figure 4.1). The mean corrosion potential of the PC/FA concrete specimens that were exposed to uni-directional (1D) ingress of corrosion agents had a corrosion potential which was not up to –200mV. On the other hand, all the concrete specimens that were exposed to 2D ingress of corrosion agents had corrosion potentials that were more negative than –200 mV. The increase in negativity of the corrosion potentials of the concrete specimens was of the order; F1D-UC-M < F1D-UC-ES < F1D-UC-E < F2D-UC-E < F2D-UC-ES < F2D-UC-M. The specimens with the most negative corrosion potentials were exposed to 2D ingress of corrosion agents (see Figure 4.5). Although specimen F2D-UC-M had the most negative corrosion potential, its corrosion potential was not significantly different from those of F2D-UC-E and F2D-UC-ES specimens. Since the mean corrosion potentials of

the uncracked PC/FA concrete specimens at the end of the experimental duration was less than -350mV, it was concluded that active corrosion did not commence in these specimens.

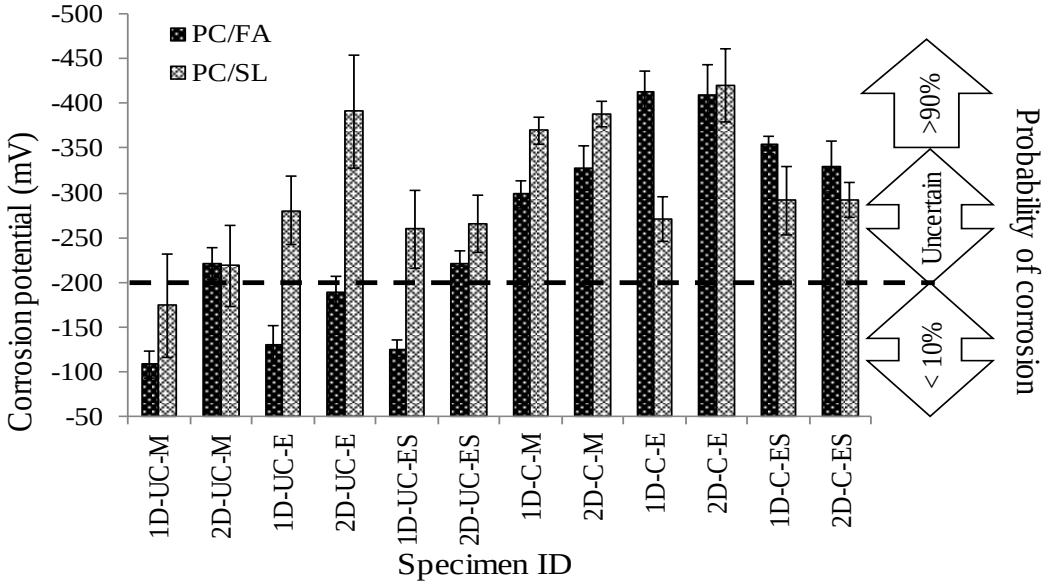


Figure 4.5: Mean corrosion potential of reinforcement bars in concrete (week 54 – week 110)

The corrosion potentials of the PC/SL specimens were more negative than those of the PC/FA specimens. The corrosion potential of these specimens also decreased significantly in the 10th week after commencing the chloride ponding; this trend was also observed in the PC/FA specimens. However, unlike the observed near-constant corrosion potential of the PC/FA concrete (after the 32nd week), the corrosion potential of the reinforcement bars in the PC/SL concrete fluctuated significantly (See Figure 4.2).

The lower corrosion potential and its significant fluctuation during the wetting and drying cycles have been identified to be caused by the presence of sulfides in slag concrete. The sulfides consume oxygen in the concrete which is needed for the development of the passive protective layer at the steel surface (Patterson, Daffner, & Gallo, 2005; Scott, 2004). Hence, the steel does not get passivated; however, as more oxygen becomes available at the steel surface, it becomes passivated, thus resulting in a reduction in the corrosion potential. The PC/SL concrete with reinforcement bars at its middle had the most positive corrosion potential while those with reinforcement bars at the corners had the most negative corrosion

potential. The corrosion potential decreased in the order; G1D-UC-M < G2D-UC-M < G2D-UC-ES < G1D-UC-E < G1D UC-ES < G2D-UC-E. The specimen G2D-UC-E had the least corrosion potential which was more negative than -350mV, this indicates that the risk of commencement of active corrosion is greater than 90% (see Table 2.3).

The concrete with reinforcement bars close to its edge (E) had the most negative corrosion potential than those with reinforcement bars at the middle (M) of the concrete. While all the PC/FA specimens exposed to 2D ingress of corrosion agents had the least corrosion potential, the same trend was not observed in the PC/SL concrete in which specimens with reinforcement bars near the concrete edge (exposed to either 1D and 2D chloride ingress) had the least corrosion potential. The PC/FA and PC/SL specimens, F2-UC-M and G2D-UC-E exposed to 2D ingress of corrosion agents had the least corrosion potential.

The corrosion potential results of the uncracked PC/FA and PC/SL beam specimens exposed to 1D and 2D ingress of corrosion agents with the stainless-steel bar and corroding bar (i.e. specimens with ES notation) will be discussed after the corrosion rate and concrete resistivity results are considered.

4.3.2 Corrosion potential of the cracked concrete

The corrosion potential of steel in the cracked concrete was generally more negative than that of steel in the uncracked concrete, this is likely due to the ease with which the corrosion agents reached the reinforcement bar via the cover cracks (Branko & Erik, 2012; Chun-ping et al., 2015; Tarek Uddin Mohammed, Otsuki, Hisada, & Shibata, 2001; M. Otieno et al., 2016b; Scott, 2004). The first corrosion potential measurements (taken after the first wetting cycle) were below –200mV (see Figure 4.3 and 4.4). The measurement of the corrosion potential shortly after removing the concrete from the chloride solution influenced these results since the concrete pores are saturated with the chloride solution thereby impeding the availability of oxygen at the steel surface; lack of sufficient oxygen at the steel surface has been reported to cause very negative corrosion potential measurements since the steel is not passivated (Broomfield, 2007). As stated earlier in Section 2.12.1, the moisture content of RC affects its corrosion potential (see Table 2.4 for corrosion potential

of concrete with various moisture contents). To avoid the recurrence of these measurements which could lead to error in interpretation of the corrosion potential measurements, the corrosion potentials were measured 24 ± 6 hours after the specimens were removed from the chloride solution.

In both the PC/FA and PC/SL cracked concrete, the most negative corrosion potential was observed in the concrete exposed to 2D ingress of corrosion agents with reinforcement bars at its edge (F2D-C-E and G2D-C-E). In the cracked concrete exposed to 1D ingress by corrosion agents, the specimen F1D-C-E had the most negative corrosion potential while the G1D-C-E specimen had the most positive corrosion potential. The reason for the more positive corrosion potential in the slag concrete is not clear, but it may be related to the stifling of the ingress path of corrosion agents by corrosion product build-up on the steel surface (Tracy Dawn Marcotte, 2001; Mike Otieno, 2008). Although ettringite is widely reported to be formed in the early stages of concrete hardening, its delayed formation has also been reported, thus, it is also possible that the crack openings were sealed by ettringite formation thus reducing access of corrosion agents to the reinforcement bar surface (Cigrovski, 2011; PCA, 2001).

It was observed that the proximity of the reinforcement bar to the concrete edge and the ingress direction of corrosion agents resulted in corrosion potentials that were more negative than -350mV, thus indicating a high probability that active corrosion has commenced in these specimens. Similar corrosion potentials were also observed in both the PC/FA and PC/SL concrete specimens (i.e. 1D-C-M, 2D-C-M and 1D-C-ES, 2D-C-ES), but the corrosion potential of the specimens exposed to 2D chloride ingress was more negative to that exposed to 1D ingress of corrosion agents. In these specimen sets, the 1D-C-ES and 2D-C-ES specimens had the most positive corrosion potential. Their corrosion potential may have been influenced by the stainless-steel bar which is electrically connected to the corroding reinforcement bar. The corrosion characteristics of the specimens with the stainless-steel bars will be discussed alongside their corrosion rate and concrete resistivity results.

Lastly, most specimens that attained a corrosion potential that was more negative than –350 mV were exposed to 2D chloride ingress or they also had reinforcement bars located at the edge of the concrete specimen. This indicates that 2D chloride

ingress influences the corrosion of reinforcement bars as well as the closeness of the reinforcement bar to a concrete edge. This is seen in the cracked concrete where both the PC/FA and PC/SL concretes (i.e. F2D-C-E and G2D-C-E) had a corrosion potential that was more negative than –350 mV (see Figure 4.5). Additional corrosion potential plots are presented in Appendix B. 1:.

4.4 Corrosion rate of PC/FA and PC/SL concrete

The corrosion rates of the cracked and uncracked RC specimens exposed to 1D and 2D chloride ingress are presented in Figure 4.6 to

Figure 4.10. The segment of the plot denoted as missing data refers to a period in which the corrosion measuring device (Coulostat) was dysfunctional. The data points plotted after the missing data were obtained from a centered moving average of 3 wetting–drying cycles.

4.4.1 Corrosion rate of the uncracked concretes

The corrosion rate of the PC/FA specimens rapidly increased within the first 16 weeks after commencing the chloride ponding and then stabilized afterward. This trend is consistent with the corrosion potential measurements of the specimens. At the end of the experiment, there was no significant difference in the corrosion rates of the uncracked PC/FA specimens (Figure 4.6).

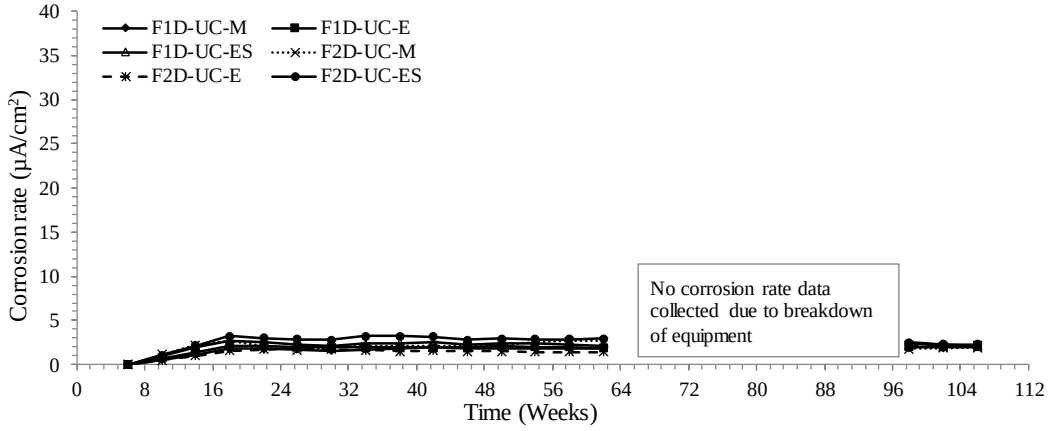


Figure 4.6: 3- point moving average corrosion rates of uncracked PC/FA specimens

The mean corrosion rate of the concrete specimens in the last 52 weeks (1 year) of the experiment increased in the order; F2D-UC-M < F1D-UC-M < F1D-UC-E < F2D-UC-E < F1D-UC-ES < F2D-UC-ES. The concrete exposed to 2D chloride

ingress with reinforcement bars at its edge had the highest corrosion rate (F2D-UC-ES; 2.360 μA/cm^2) while the least corrosion rate was observed in the specimen exposed to 1D chloride ingress with reinforcement bars at the middle of the concrete (i.e. F1D-UC-M; 1.942 μA/cm^2).

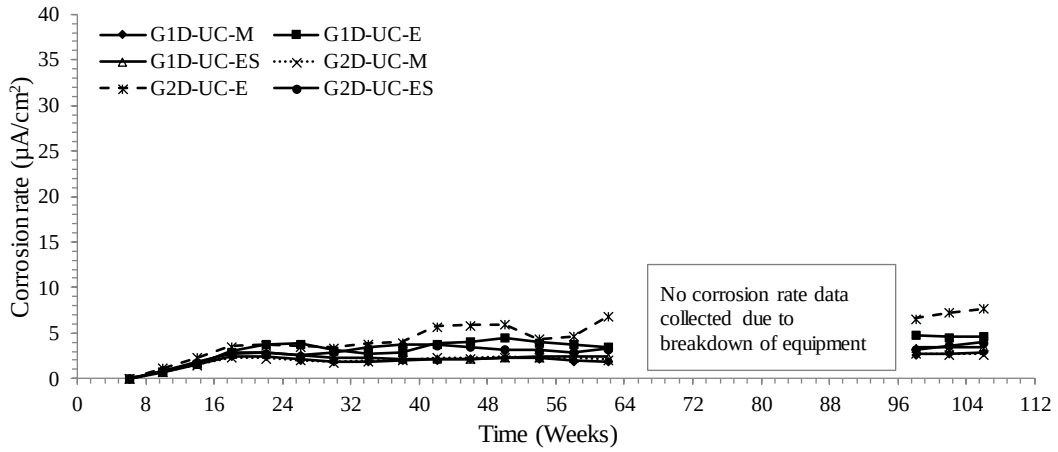


Figure 4.7: 3- point moving average corrosion rates of uncracked PC/SL specimens

The corrosion rate of the reinforcement bars in the PC/SL concrete increased rapidly after the commencement of the chloride ponding and was significantly higher than that of the PC/FA specimens. The highest mean corrosion rate in the uncracked PC/SL specimen (G2D-UC-E) was 5.0 μA/cm^2; the reinforcement bar in this specimen was located at a concrete edge that is exposed to 2D chloride ingress. The lowest mean corrosion rate of 2.2 μA/cm^2 was observed in the specimens G1D-UC-M and G2D-UC-M which had reinforcement bars at the middle of the concrete specimen.

Although corrosion-induced cracks were not noticed on any of the uncracked concrete specimens, rust stains were observed on some of the specimens (Figure 4.8). The specimens with the rust stains also had the highest corrosion rate in their specimen set and their corrosion rates were not used in the computation of the corrosion rate of their specimen sets (Figure 4.3). In general, a significant increase in the corrosion rate of specimens with reinforcement bars near the concrete edge was observed. Hence, the location of the reinforcement within the concrete (near or farther away from an exposed concrete edge), as well as the chloride ingress direction (1D or 2D), influences the corrosion rate of embedded reinforcement bars.

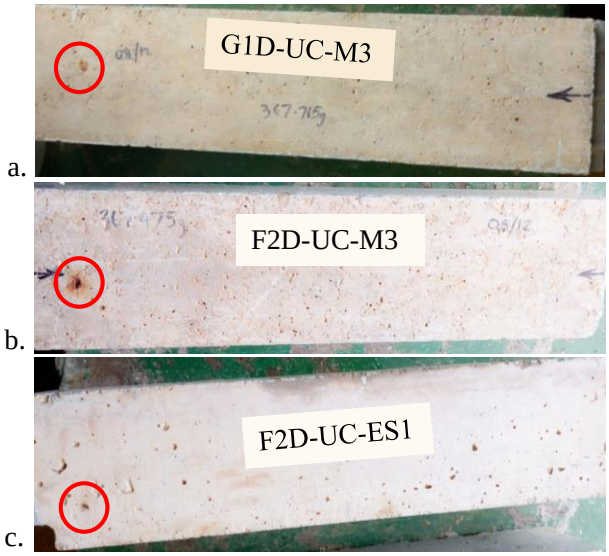


Figure 4.8: Rust stains on uncracked RC beam specimens (a) G1D-UC-M3 (b) F2D-UC-M3, and (c) F2D-UC-ES1 (circles indicate rust stain locations)

4.4.2 Corrosion rate in cracked concrete

The corrosion rate results of the cracked concrete are presented in Figure 4.9 and Figure 4.10). Higher corrosion rates (than that of the uncracked PC/SL specimens) were obtained after the first wetting cycle. This trend was also observed by some researchers who conducted experiments with cracked concrete (Branko & Erik, 2012; Mike Otieno, 2008; O. G. Rodríguez et al., 2003; Scott & Alexander, 2007). The higher corrosion rates were influenced by the ease with which the agents of corrosion easily reach the reinforcement bars via the concrete surface cracks (Chun-ping et al., 2015; Mike Otieno, Beushausen, & Alexander, 2011). The sustained imposed (tensile) load on the cracked beams is another factor that may have influenced the ingress of the corrosion agents into the concrete. The application of stress to concrete leads in the formation of cracks which have been reported to increase the permeability of concrete (Alyousif et al., 2015; Hoseini, Bindiganavile, & Banthia, 2009; M. Otieno et al., 2012; Wu et al., 2014; Yoon et al., 2000; Y. Zhang, Sun, Chen, et al., 2011).

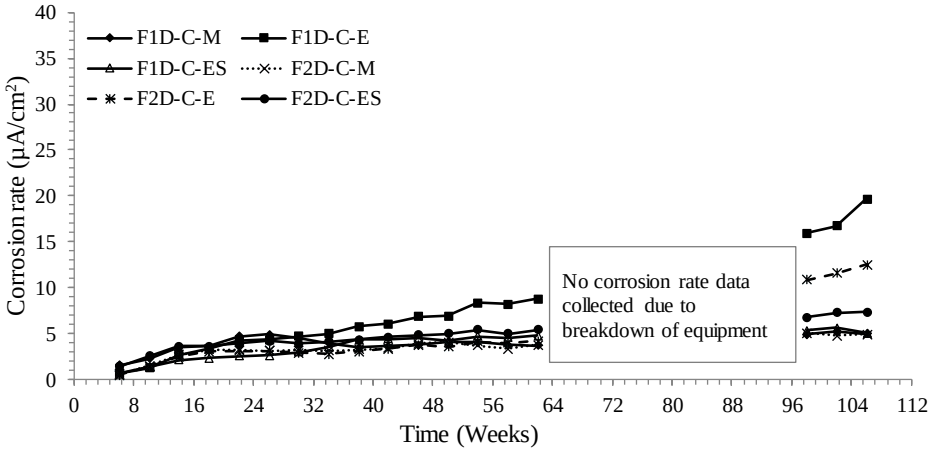


Figure 4.9: 3- point moving average corrosion rates of cracked PC/FA specimens

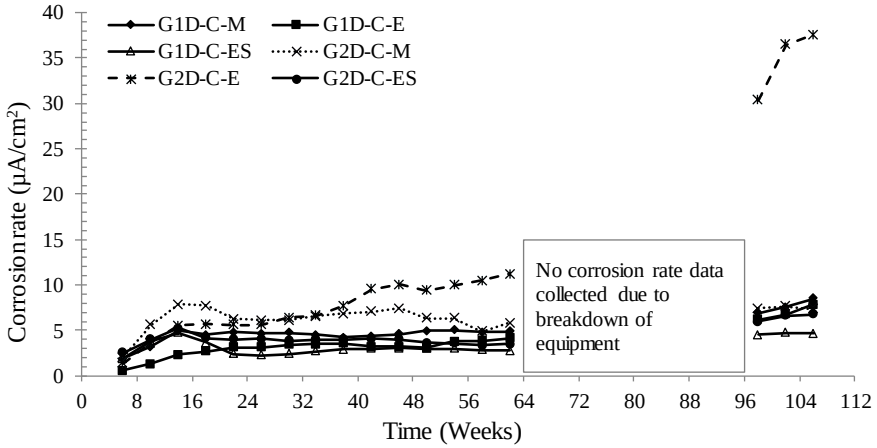


Figure 4.10: 3- point moving average corrosion rates of cracked PC/SL specimens

The corrosion rate of most of the PC/FA specimens increased steadily with time, although the increase was not at the same rate. The corrosion rate of concrete specimens with reinforcement bars located near the concrete edge increased more rapidly (F1D-C-E, F2D-C-E, and F2D-C-ES). There was no significant difference in the corrosion rates of the other PC/FA specimens (i.e. F1D-C-M, F2D-C-M, and F2D-C-ES).

The most significant increase in corrosion rate was observed in the PC/SL concrete specimens G2D-C-E; this may not be unrelated to the formation of corrosion-induced cracks which were noticed in the 30th week after commencing the chloride ponding and drying cycles. The corrosion-induced cracks provided additional paths for the penetration of corrosion agents thereby resulting in the increased corrosion rate. The G2D-C-E concrete had significant corrosion-induced cracks which nearly

caused the delamination of the concrete from the steel reinforcement bar. This result can be seen in the crack-factors presented in Table C. 4 (in Appendix C. 1:) and the corrosion-induced crack patterns in the concrete (Figure C.4 in Appendix C.2). Further discussion on corrosion-induced cracks is presented in Section 4.7.

4.4.3 Summary of corrosion rate results

While most researchers agree that the presence of cover cracks significantly reduces the time-to-corrosion initiation, some have argued that cover cracks do not significantly influence the corrosion propagation phase. The corrosion initiation phase of the concrete specimens will be discussed with the aid of the plots shown in Figure 4.11a-d.

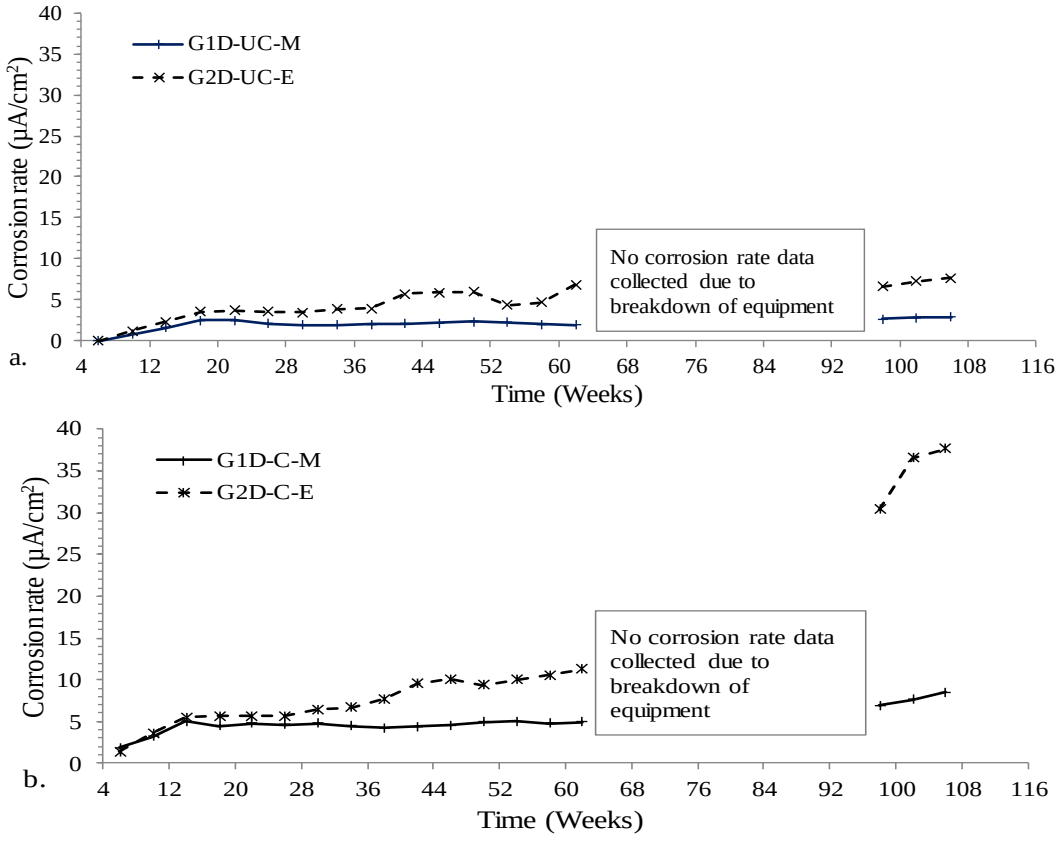
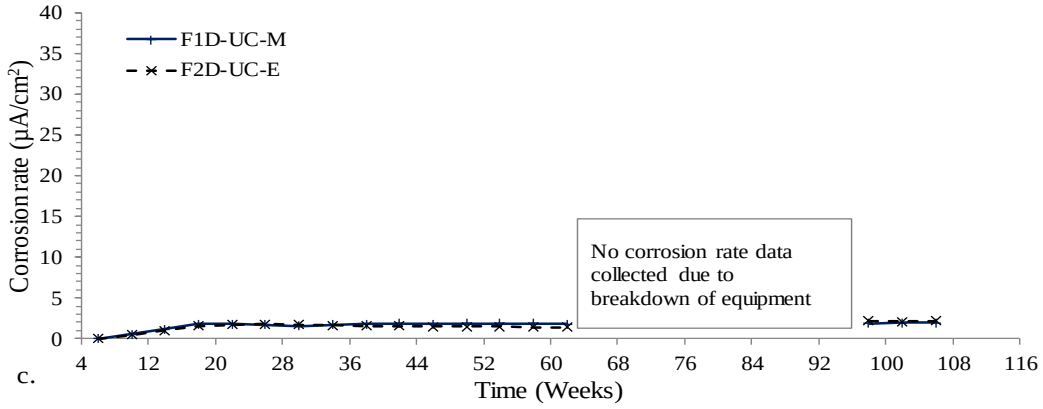
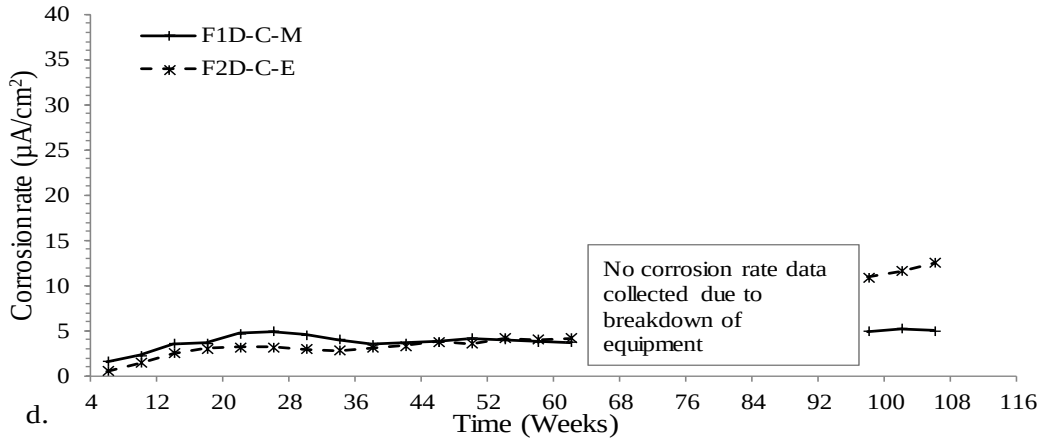


Figure 4.11: Corrosion rate of (a) uncracked and (b) cracked PC/SL concrete exposed to 1D and 2D chloride ingress



c.



d.

Figure 4.11 (contd): Corrosion rate of (c) uncracked and (d) cracked PC/FA concrete exposed to 1D and 2D chloride ingress

There was a significant difference in the time-to-corrosion initiation of the cracked and uncracked PC/SL concrete exposed to both 1D and 2D chloride ingress while there was no significant difference in the time-to-corrosion initiation of the PC/FA concrete. Even though the steel corrosion initiated earlier in the cracked PC/FA concrete exposed to 1D chloride ingress, the presence of cracks was identified to be the influencing factor. The corrosion rate of the specimens exposed to 2D chloride ingress rapidly increased beyond that of the specimens exposed to 1D chloride ingress irrespective of the time-to-corrosion initiation of the specimens. Therefore, with continual chloride exposure, the effect of 2D chloride ingress was more significant in the corrosion propagation phase as observed in the corrosion rate of the specimens. The cracked specimens attained a higher corrosion rate than the uncracked specimens (see Figure 4.12a – d).

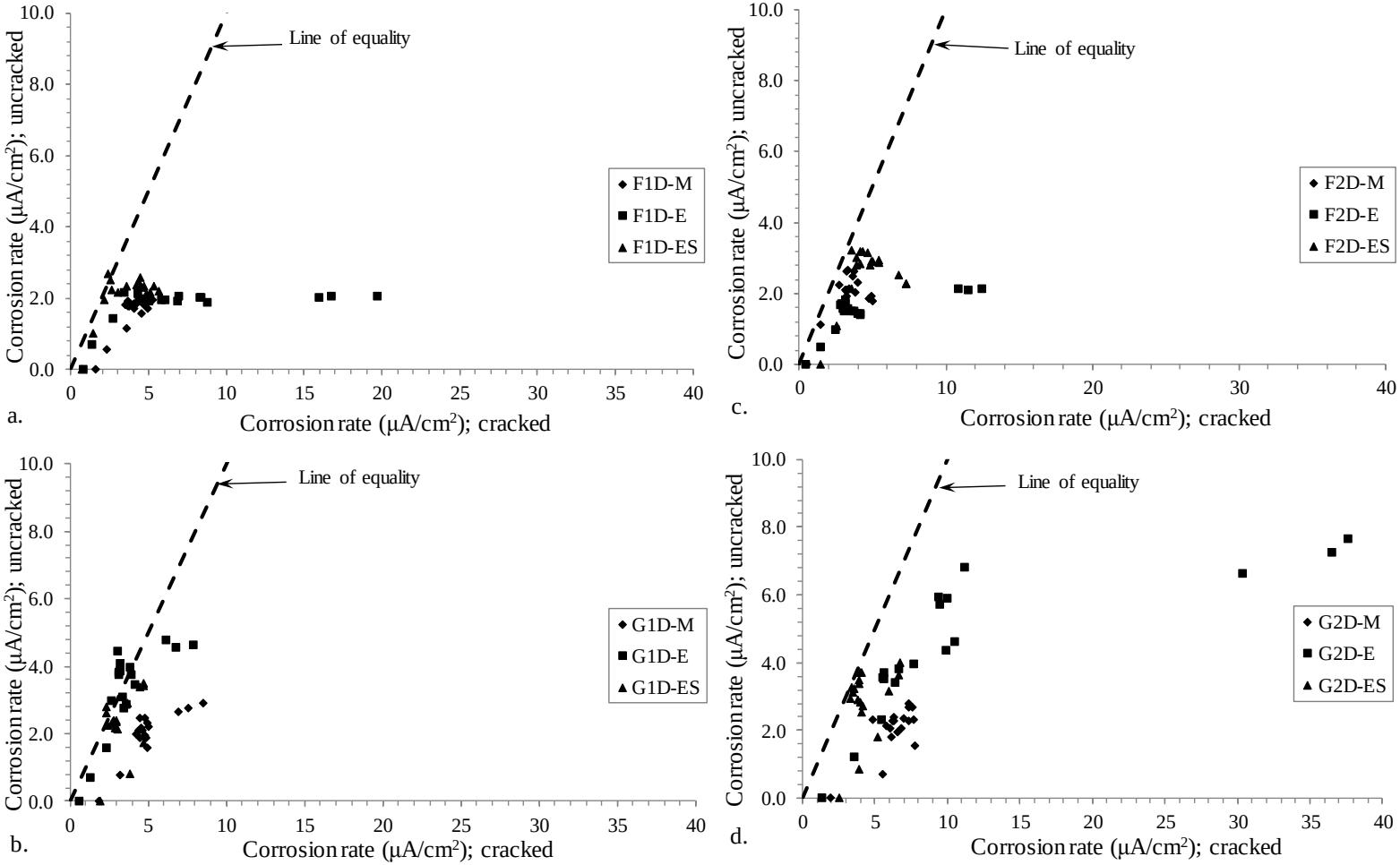


Figure 4.12: Corrosion rate of cracked and uncracked specimens exposed to (a & b) 1D and (c & d) 2D chloride ingress

The results also indicate that the presence of cover cracks influence both the initiation and propagation phases of corrosion (Scott & Alexander, 2007). Given the size of the crack widths used in this study (i.e. 0.16 to 0.40 mm), it can be deduced that steel reinforcement bars in concrete with less than the allowable crack width of 0.30 mm (as stated in some standards; EN1992-1-1 2004; and Comité euro-international du béton 1993) may be subjected to rapid deterioration if the concrete has a reinforcement bar located near the edge of a concrete element that is exposed to 2D ingress of corrosion agents.

The corrosion rate attained by the specimens at termination of the experiment (which was also the highest corrosion rate attained) is shown in

Figure 4.13.

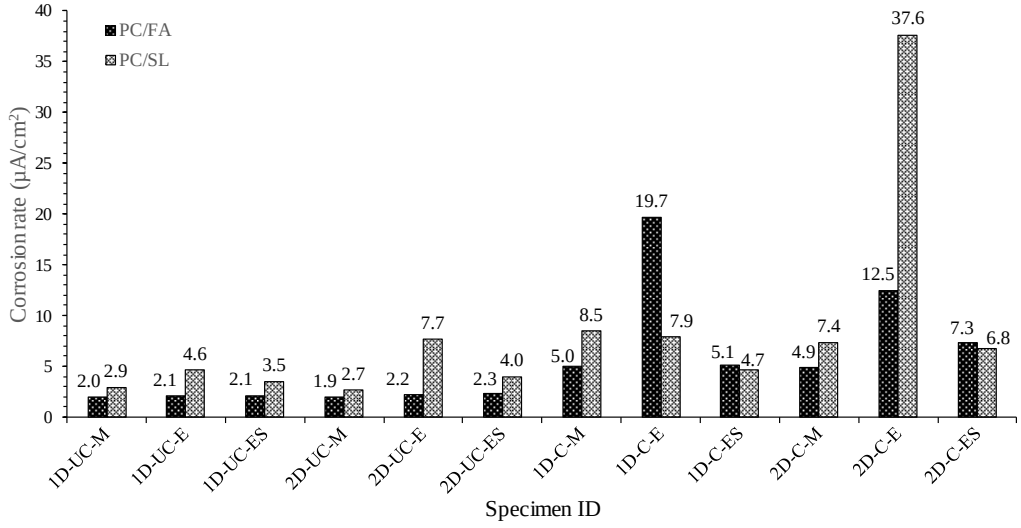


Figure 4.13: Corrosion rate of the concrete specimens (after last wetting cycle - 28)

The corrosion rate of the uncracked PC/FA concrete ranged between 1.9 μA/cm^2 to 2.3 μA/cm^2, there was no significant difference in the corrosion rate of these specimens, however, the specimens with reinforcement near the concrete edge (-E and -ES) had a higher corrosion rate, while specimens with reinforcement in the middle (-M-) of the specimen had the least corrosion rate. The specimens exposed to 2D chloride ingress had the highest corrosion rate.

The corrosion rate of the PC/SL concrete on the other hand had a wider range (between 2.7 μA/cm^2 to 7.7 μA/cm^2) than the PC/FA concrete. The specimens with steel reinforcement bars at the concrete edge (-E- and -ES-) also had a higher

corrosion rate than specimens with reinforcement in the middle (-M-) of the concrete. The specimen G2D-UC-E with reinforcement bar at its edge and exposed to 2D chloride ingress attained the highest corrosion rate in this set of (uncracked) specimens.

The cracked specimen corrosion rate was generally higher than that of the uncracked specimens due to the ease with which chlorides reached the reinforcement bar and the stress induced on the beams. Apart from the specimen F1D-C-E, which had an inexplicably high corrosion rate (19.7 $\mu A/cm^2$), the specimens exposed to 2D chloride ingress with an isolated reinforcement bar at the edge (F2D-C-E; 12.5 $\mu A/cm^2$ and G2D-C-E; 37.6 $\mu A/cm^2$) of the specimen had the highest corrosion rates. In addition to the sustained load and cover cracks on these specimens, the high corrosion rate in these specimens was attributed to the location of the reinforcement bar (i.e. at the concrete edge) and corrosion-induced cracks. Corrosion-induced cracks were more severe in specimens with reinforcement bars at the concrete edge, this allowed additional ingress of corrosion agents into the concrete. The corrosion-induced cracks will be discussed in Section 4.7.1.

An understanding of the relationship between corrosion rates of the specimens was also obtained by observing the mean corrosion rate value taken over the entire period of the experiment. The corrosion rate in the cracked specimens was more than twice that of the uncracked specimens; see Table 4.3.

Table 4.3: Corrosion rate of specimens exposed to 1D and 2D chloride ingress

Binder type	**Corrosion rate (μA/cm.sq)**			
	1D-UC-M	**1D-C-M**	**2D-UC-E**	**2D-C-E**
PC/FA (SD)	1.6 (0.67)	3.9 (1.49)	1.5 (0.67)	4.3 (3.21)
PC/SL (SD)	2.2 (0.91)	4.8 (1.88)	5.0 (2.74)	11.0 (9.87)

Key: UC = Uncracked, C = Cracked, M = Reinforcement bar at middle of beam, E = Reinforcement bar at concrete edge, SD = standard deviation

Considering the SCMs used in the concrete, a lower corrosion was attained by the PC/FA specimens. This result is contrary to the durability index results of the concretes (used in this study; see Section 4.2) which indicate that the PC/SL concrete will be more durable in corrosion-prone environments. Even though the presence of slag in concrete has been reported to affect the corrosion initiation

phase, its composition in the concrete (3.39%; see Table 3.1) and corrosion-induced crack widths (which are higher than that of the cracked PC/FA concrete) were identified as likely factors which influenced the corrosion rate of the steel in the PC/SL concrete. A review of the chloride threshold of fly ash and slag concretes by various researchers does not present an aligned conclusion as other factors (such as pH of the concrete pore solution, oxygen availability and moisture content at the steel surface, carbonation, condition of steel-concrete interface) in addition to those earlier mentioned have been found to influence the corrosion rate of embedded reinforcement bars (S. L. Poulsen & Sørensen, 2012).

The corrosion rates of cracked and uncracked PC/FA and PC/SL specimens (exposed to 1D and 2D chloride ingress) with the stainless-steel bar (i.e. specimens with the mark 'ES') were lower than that of specimens with the single isolated reinforcement bars (i.e. specimens with mark 'E'). This suggests that the inclusion of the stainless-steel bar affected the corrosion rate result (assuming other factors such as imposed stress, chloride ingress directions, crack widths, etc. are constant). The lower corrosion rate in these specimens (compared to specimens with a single isolated reinforcement bar) can be attributed to;

i. High anode-to-cathode ratio; where the stainless-steel bar is assumed to be an anode
ii. Non-availability of dissolved oxygen at the cathodic site, and
iii. High concrete resistivity; the effect of concrete resistivity on the corrosion rate has been reported to decrease as the distance between the anodic and the passive bars reduces (Rodríguez et al. 1999; Andrade & Alonso 1996).

The stainless-steel due to its passivity and lack of dissolved oxygen at its surface may have reduced the corrosion rate (anodic reaction) by limiting the cathodic process. The consideration of concrete resistivity as a corrosion rate-limiting factor in these specimens will be discussed in Section 4.5.

In closing, it was observed that the specimens exposed to 2D chloride ingress had higher corrosion rate than those exposed to 1D chloride ingress. This result may have been influenced by the method used in modifying the chloride ingress

direction. With only one surface left unsealed in the specimens exposed to 1D chloride ingress, the chloride ingress (due to permeation) may have been reduced, while permeation may have been enhanced in the specimens exposed to 2D chloride ingress since two adjacent surfaces of the concrete were left unsealed. However, since diffusion is assumed to be the dominant means of chloride penetration into the concrete, it is possible that leaving only one face unsealed may not have significantly influenced the corrosion rate results.

4.4.4 Relationship between corrosion rate and corrosion potential

The relationship between the corrosion potentials and corrosion rates are presented in Figure 4.14 and Figure 4.15.

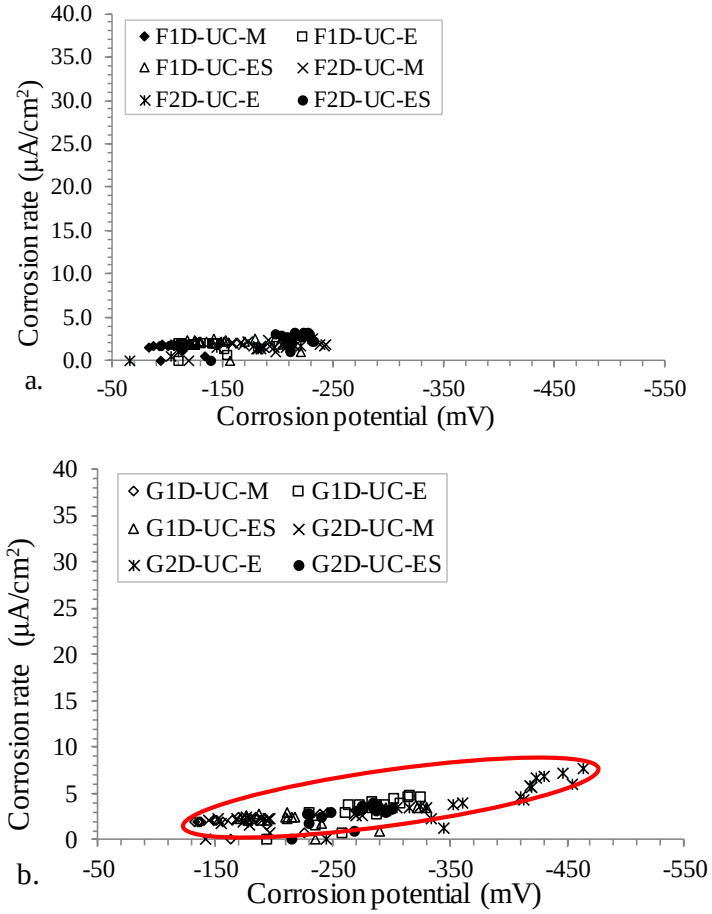


Figure 4.14: Corrosion rate vs corrosion potential in uncracked (a) PC/FA, and (b) PC/SL concrete specimens

Corrosion potentials which are more negative than -350mV (using the $Cu/CuSO_4$ electrode) indicate a 90% probability of commencement of active corrosion (ASTM

C876, 2009). However, the corrosion potentials can be influenced by other factors such as oxygen and moisture availability at the surface of the steel reinforcement bar. Hence, corrosion potential measurements may be misleading as not all specimens which have measurements that are more negative than -350mV are indicative of high corrosion probability (see Section 4.4.2). This means a correlation of the corrosion rate and corrosion potential measurements may not yield reliable conclusions as seen in the plots (Figure 4.14 and Figure 4.15) since a wide range of corrosion rates were obtained with no corresponding change in the corrosion potential of the steel (e.g. F2D-UC-ES plot point in Figure 4.14a). The plotted points clustered in the direction of the vertical or horizontal axis, while other plot points were scattered with an identifiable trend wherein high corrosion rates corresponded to more negative corrosion potentials.

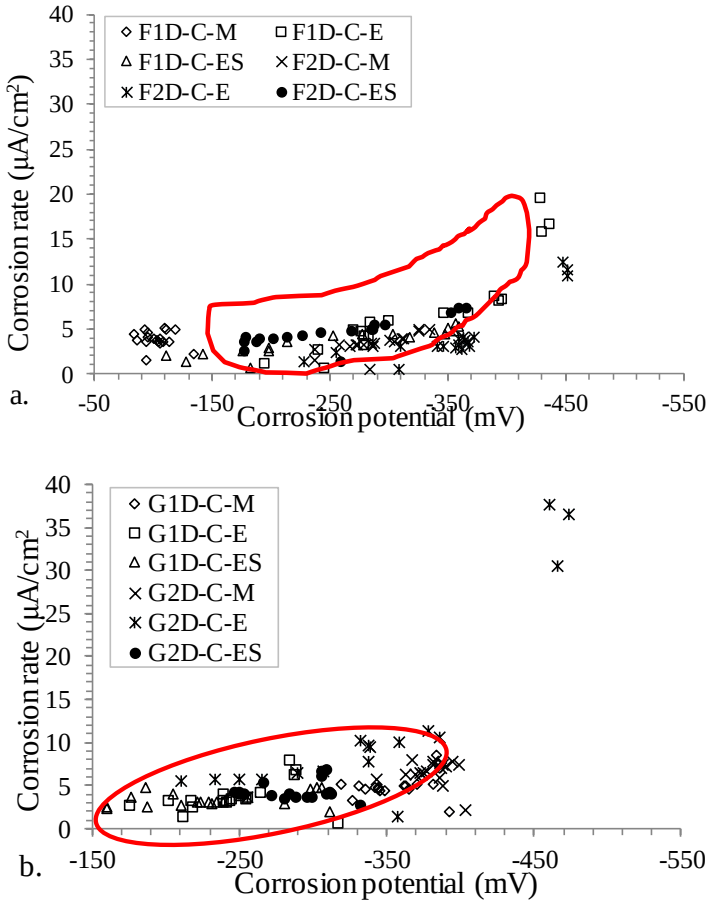


Figure 4.15: Corrosion rate vs corrosion potential in cracked (a) PC/FA, and (b) PC/SL concrete specimens.

The plot (Figure 4.15) shows that the corrosion rate increases as the corrosion potential becomes more negative, but there was the clustering of some of the plots at more corrosion potentials that were below -400mV. Beyond a corrosion potential of -450mV, the corrosion rate increased with no decrease in the corrosion potential.

4.5 Concrete resistivity results

The 3-point moving average plots of the uncracked and cracked concrete resistivities are shown in Figure 4.16 to Figure 4.16. The measurement of the concrete resistivity (using the single electrode-disc method) commenced 24 weeks after commencing the chloride ponding and drying cycles. This was to avoid notable errors that were detected when earlier concrete resistivity measurements were taken near the concrete edge using the Wenner probe.

The concrete resistivity results are discussed regarding the concrete condition (uncracked and cracked), the position of the reinforcement bars (in middle or orthogonal edge) in the concrete, and the ingress direction of the corrosion agents (1D or 2D).

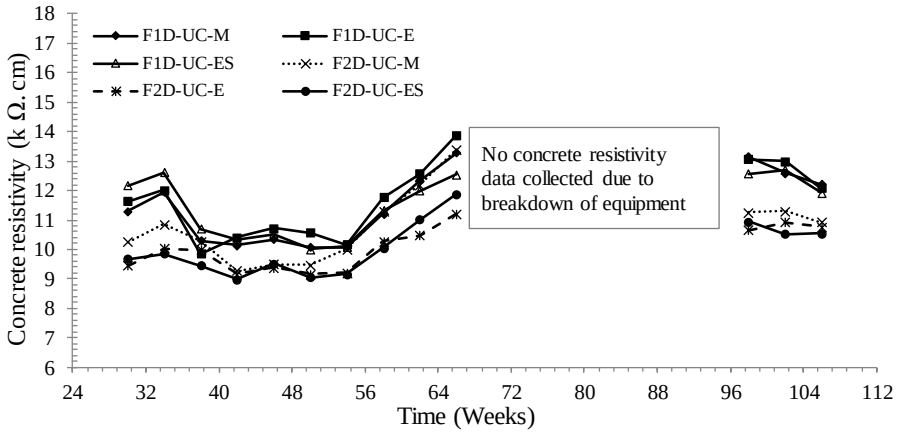


Figure 4.16: 3-point moving average for concrete resistivity of uncracked PC/FA concrete specimens

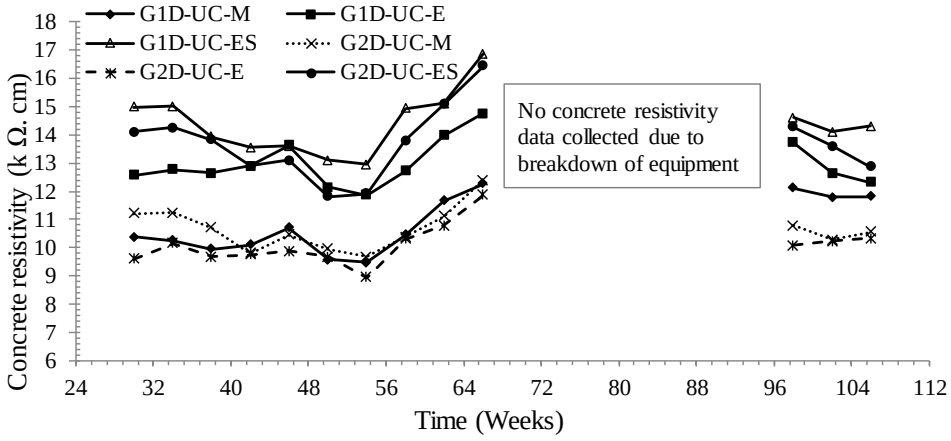


Figure 4.17: 3-point moving average for concrete resistivity of uncracked PC/SL concrete specimens

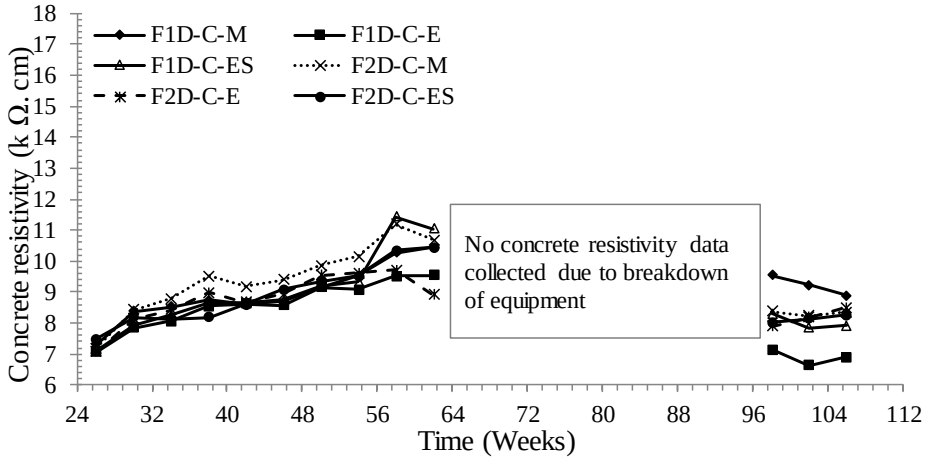


Figure 4.18: 3-point moving average for concrete resistivity of cracked PC/FA concrete specimens

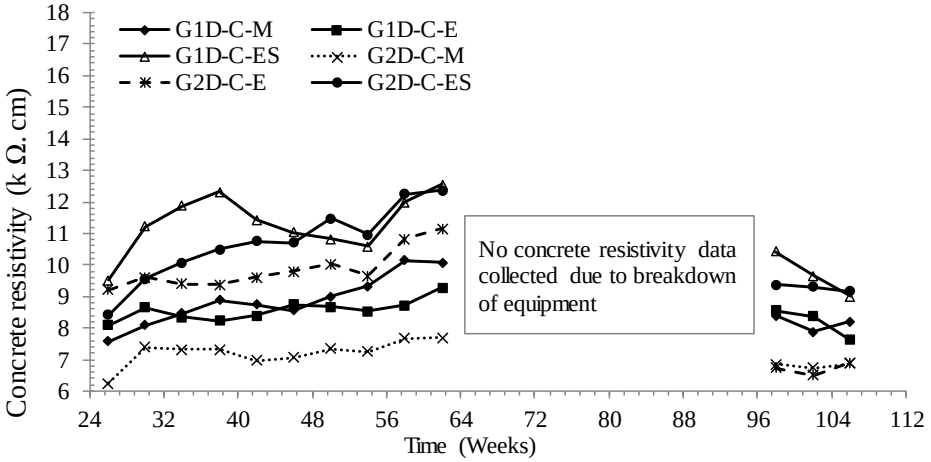


Figure 4.19: 3-point moving average for concrete resistivity of cracked PC/SL concrete specimens

The resistivity of the cracked concrete was lower than that of the uncracked concrete. The presence of cracks which allow easy penetration of chlorides into the concrete was identified as a factor that resulted in the lower resistivity values. Two types of cracks and their influence on concrete resistivity have been identified as conductive cracks (where there is ionic conductivity across the crack) and isolative cracks (where there is no ionic conductivity across the crack). Resistivity measurements taken in concrete with conductive cracks are generally lower than those of concrete with isolative cracks. The cracks in this study may have been conductive since the concrete resistivity measurements were taken about 24 hours after the chloride ponding.

The concrete resistivity of all the uncracked concretes (see Figure 4.16 and Figure 4.17) fluctuated with time. This fluctuation was attributed to temperature variations (see Appendix D:) during the study period. An increase in temperature during the summer months yielded higher concrete resistivity values while lower concrete resistivity values were obtained during the winter months. Thus, the risk of corrosion is higher in warm and humid conditions.

A different trend was observed in the concrete resistivity of the cracked concrete specimens; the resistivity increased, reached a peak 60 weeks after the commencement of the chloride ponding and then began to decline. The increase in the concrete resistivity may be attributed to continuous hydration of the cement paste which mostly corresponds to an improvement in the pore structure of the concrete. The decline in the concrete resistivity on the other hand can be associated with an enhancement of ionic flow in the concrete due to increased chloride concentration in the cover concrete.

The concrete resistivity of uncracked specimens exposed to 1D chloride ingress was higher than that of specimens exposed to 2D chloride ingress (see Figure 4.20a and Figure 4.21a). On the contrary, there was no clear trend in the concrete resistivity in the cracked concrete (see Figure 4.20b and Figure 4.21b). This indicates that the presence of surface cracks influenced chloride ingress and the concrete resistivity. A plot of the mean concrete resistivity over the study period is shown in Figure 4.22.

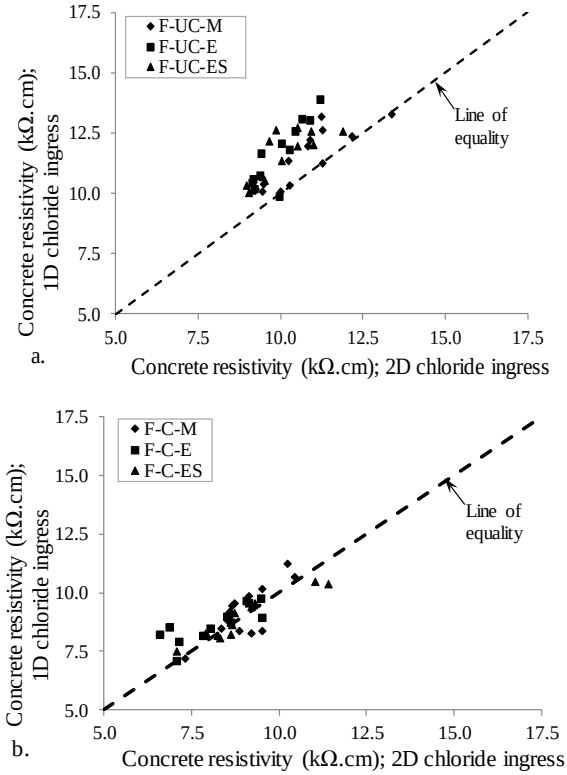


Figure 4.20: Concrete resistivity of (a) uncracked and (b) cracked PC/FA specimens exposed to 1D and 2D chloride ingress

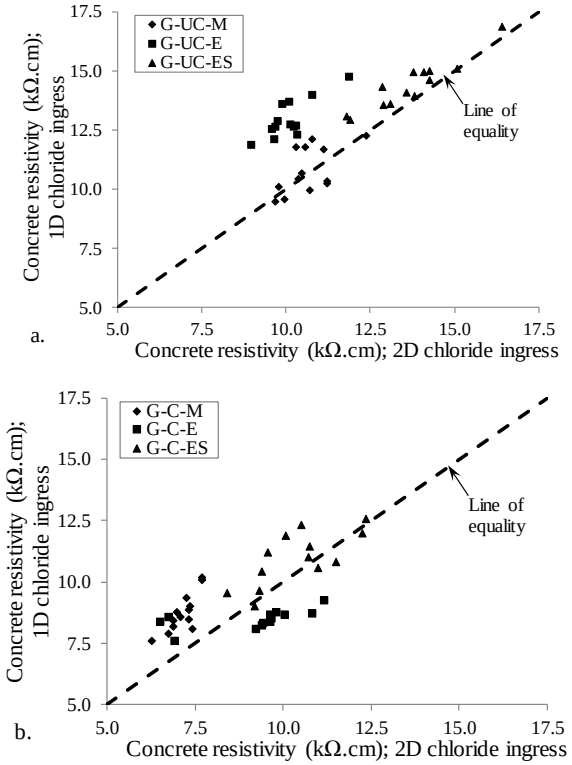


Figure 4.21: Concrete resistivity of (a) uncracked and (b) cracked PC/SL specimens exposed to 1D and 2D chloride ingress

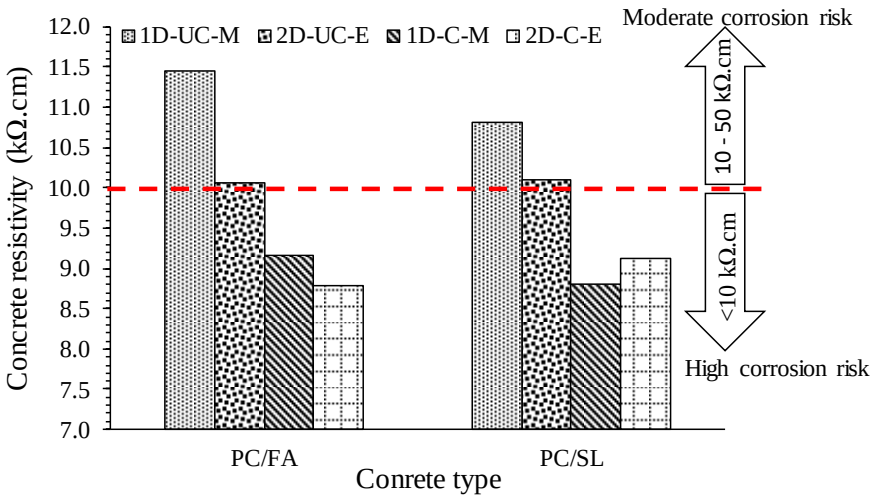


Figure 4.22: Mean concrete resistivity (week 24 - 110) of cracked and uncracked PC/FA and PC/SL RC beams exposed to 1D and 2D chloride ingress

The concrete resistivity results in the uncracked concrete edges exposed to 2D chloride ingress and cracked concrete were lower than 10 kΩ.cm. Corrosion risk has been identified to be high in concrete with resistivity values of less than 10 kΩ.cm (RILEM TC 154-EMC, 2004). The corrosion rate of the PC/FA and PC/SL concrete with the designation 2D-UC-E, 1D-C-M, and 2D-C-E is therefore not limited by the concrete resistivity. The relationship between the concrete resistivity and the corrosion rate will be discussed further in the next section.

4.5.1 Corrosion rate and concrete resistivity

The ionic connectivity between the anodic and cathodic sites on a corroding reinforcement bar is achieved via the concrete pore solution. This is influenced by chloride ion concentration in the concrete pores and the relative humidity of the concrete. In general, a decrease concrete resistivity is indicative of an increased risk of corrosion and vice versa (Gjorv 2013; Liu & Weyers 1998; Balabanic et al. 1996; Angst et al. 2009; Andrade & Buják 2013). Plots of corrosion rate against concrete resistivity are presented in Figure 4.23 and Figure 4.24.

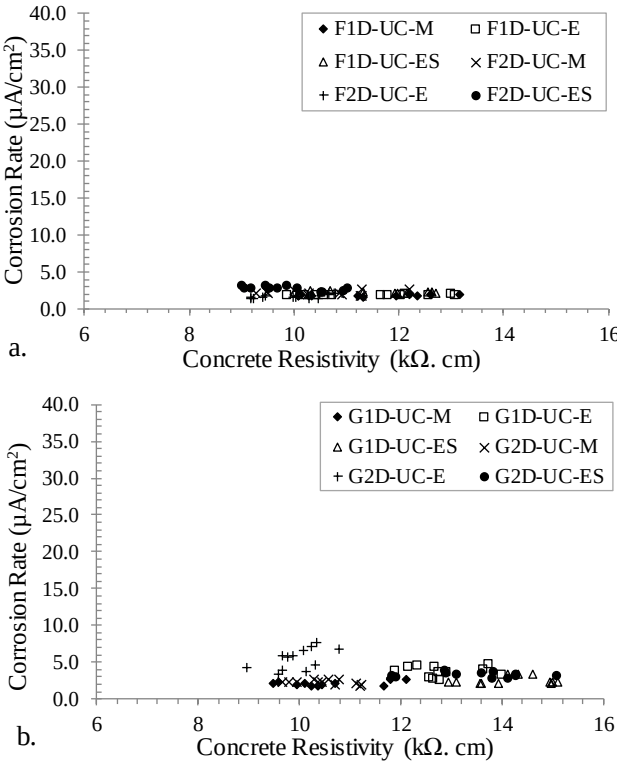


Figure 4.23: Corrosion rate vs concrete resistivity of uncracked (a) PC/FA and (b) PC/SL concrete specimens

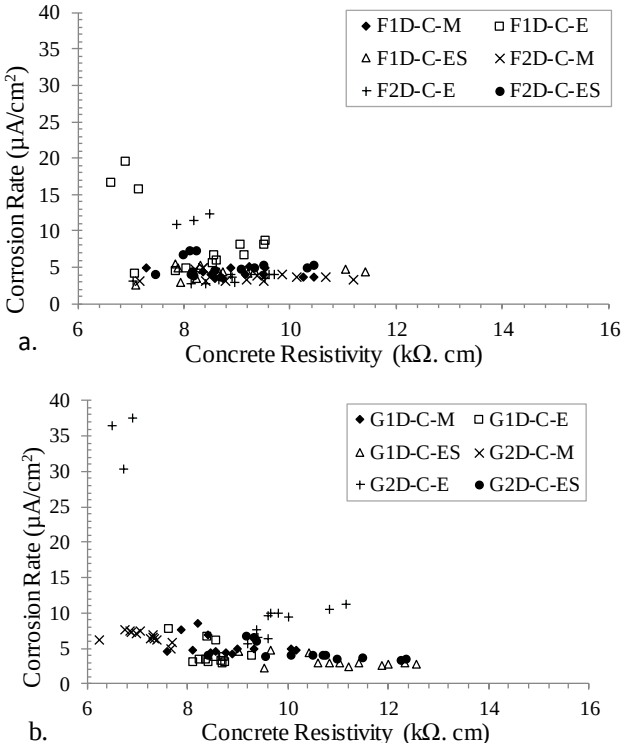


Figure 4.24: Corrosion rate vs concrete resistivity of cracked (a) PC/FA and (b) PC/SL concrete specimens

Andrade & Alonso (1996) identified that at resistivity values >200 kΩ.cm, the corrosion rates may be very low even if the concrete is carbonated or contaminated with chlorides, 10 – 100 kΩ.cm a moderate risk exists, and at a concrete resistivity of less than 10 kΩ.cm, a high corrosion risk exists with resistivity ceasing to be a corrosion rate-limiting factor. At this concrete resistivity (<10 kΩ.cm), high corrosion rates can be attained with no significant change in the concrete resistivity (RILEM TC 154-EMC, 2004).

With the low concrete resistivity obtained, there was no direct relationship between the concrete resistivity and the corrosion rate. However, it is generally observed that an increase in the corrosion rate corresponded with a decrease in the concrete resistivity of some of the specimens. An inexplicable relationship was observed in some specimens (F1D-C-E and G2D-C-E) with reinforcement bars at the concrete edge. These specimens both had the lowest mean concrete resistivity values (8.30 kΩ.cm and 9.13 kΩ.cm respectively) and attained corrosion rates (19.68 μA/cm^2 and 37.62 μA/cm^2 respectively) that were significantly higher than the other specimens.

4.6 Chloride penetration profile in cracked and uncracked concrete

The acid-soluble chloride content (also known as the total chloride content) is presented as a percentage proportion by mass of the binder content in the concrete (Figure 4.25a and Figure 4.25b).

The results show that the cracked PC/FA and PC/SL concrete specimens had significantly higher chloride content at the reinforcement depth than the uncracked specimens. While there was a significant difference in the chloride concentration (at the steel depth) of the cracked PC/FA and PC/SL concretes that were exposed to 1D and 2D chloride ingress, there was no significant difference in the total chloride concentration at the depth of the steel in the uncracked specimens. The significantly high chloride concentration in the cracked specimens subjected to 2D chloride ingress (over those exposed to 1D chloride ingress) was due to the interaction of the chloride profiles from adjacent faces of the concrete (i.e. 2D diffusion) and the effect of the imposed flexural stress on the specimen.

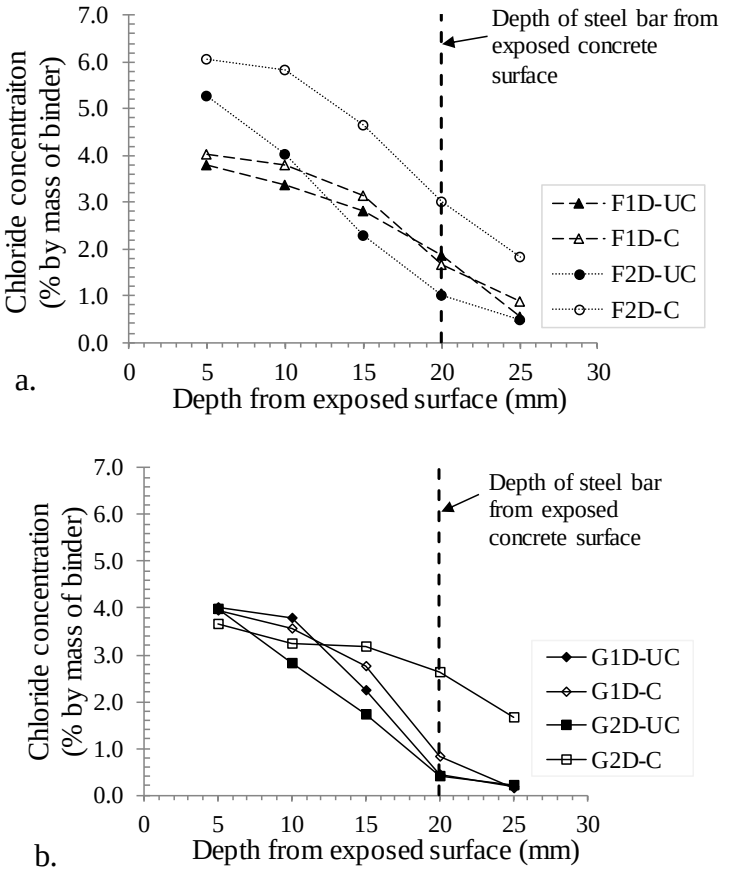


Figure 4.25: Total chloride profiles for (a) PC/FA and, (b) PC/SL concrete

The absence of the imposed load on the uncracked specimens is cited as the reason why there is no significant difference in the chloride concentration at the steel depth.

Although the sustained flexural stress imposed on the concrete specimens was not measured in this experiment, it has been shown by other researchers that the diffusion rate of corrosion agents increases with the imposed flexural stress (Benarbia, Benguediab, & Benguediab, 2013; Francois & Arliguie, 1999; Y. Zhang, Sun, Liu, et al., 2011).

The chloride content at orthogonal edges of the cracked concrete exposed to 2D chloride ingress has been identified to be responsible for the low concrete resistivity and resultant high corrosion rate in reinforcement bars of the F2D-C-E and G2D-C-E concrete specimens (see

Figure 4.13). With low concrete resistivity (<10 kΩ. cm), the supply of oxygen and moisture to the anodic and cathodic sites control the corrosion rate. More oxygen and moisture will reach the anodic in cathodic sites in 2D exposure, on the other

hand, there will be a limited supply of oxygen and moisture to the corrosion sites due to 1D exposure, which in turn reduces their corrosion rate.

4.6.1 Corrosion rate and chloride concentration

A plot of the mean corrosion rate and percentage chloride content by mass of the binder at the depth of the reinforcement bar (i.e. 20 mm from the concrete surface) in both the cracked and uncracked concrete. The results show that the corrosion rate increases as the chloride concentration increases ($R^2 \approx 0.57$ and 0.69 for the PC/SL and PC/FA concrete respectively; see Figure 4.26). The relationship between the mean corrosion rate (from week 71 to 110) and chloride content was assessed by using both the cracked and uncracked (PC/FA and PC/SL) concretes that were exposed to 1D and 2D (i.e. 1D-UC-M, 1D-C-M and 2D-UC-E, 2D-C-E) chloride ingress.

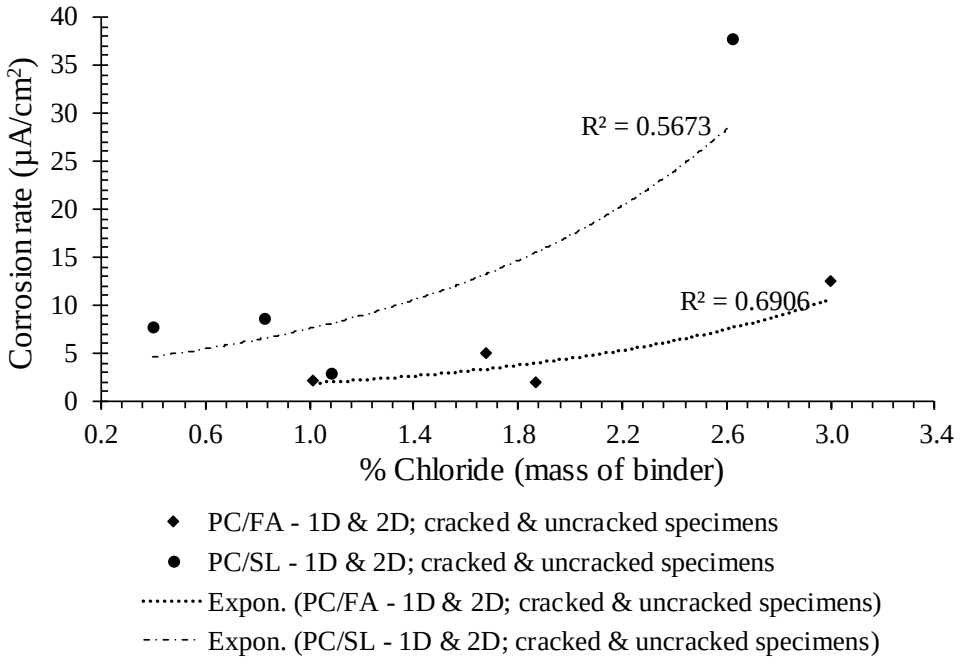


Figure 4.26: Corrosion rate vs chloride concentration at depth of reinforcement bar

The chloride concentration in the binder causes a reduction in the concrete resistivity which increases the risk of the steel reinforcement corrosion. In humid concrete with high chloride concentration in the concrete, the resistivity of the concrete does not limit the corrosion rate; the corrosion rate is therefore controlled reactions at the anodic and cathodic sites which are dependent on the supply of the moisture and oxygen to the sites.

4.7 Corrosion-induced cracks

The corrosion of the reinforcement bar yielded corrosion-induced cracks in the concrete. These cracks were longitudinal cracks formed along the length of the reinforcement bars (Figure 4.27c & d). In concrete with reinforcement bars that are located near its orthogonal edge, the corrosion-induced cracks also propagated towards the concrete edge thus resulting in near delamination at the concrete edge (Figure 4.27a & b). This type of corrosion-induced cracks was identified by other researchers who conducted studies on RC elements that had reinforcement bars located near the edge of concrete elements (Muthulingam & Rao, 2015a; R. Zhang et al., 2010; Zhao, Hu, Yu, & Jin, 2011).



Figure 4.27: Corrosion-induced cracks of concrete with reinforcement at (a & b) edge (-E), and (c & d) middle of beam (-M).

4.7.1 Characterization of corrosion-induced cracks

Corrosion-induced cracks were not noticed on any of the uncracked concrete specimens, while most of the cracked concrete had corrosion-induced cracks. The total area of the corrosion-induced crack per specimen was approximated using the crack-factor (Eqn. 3.11). The crack-factors were subsequently used to characterize the corrosion-induced cracks on the concrete. A plot of the average crack-factor per specimen set is shown in Figure 4.28. The crack-factor computations are presented in Appendix C:.

A high crack-factor value (relative to other obtained values) is indicative of cracks that are longer and wider. Hence, from Figure 4.28, both the PC/FA and PC/SL concrete with reinforcement bars at their edge had the highest crack-factor (2D-C-E and 1D-C-E) values with the concrete exposed to 2D ingress of corrosion agents having the most significant corrosion-induced cracks. The error bars in the plot indicate one standard deviation of the crack-factor values from its mean value. The concrete with single reinforcement bars located near the concrete edge (1D-C-E and 2D-C-E) had the highest crack-factor value spread away from the mean. This indicates that though most of the specimens had corrosion-induced cracks, the crack distribution had a wide variation.

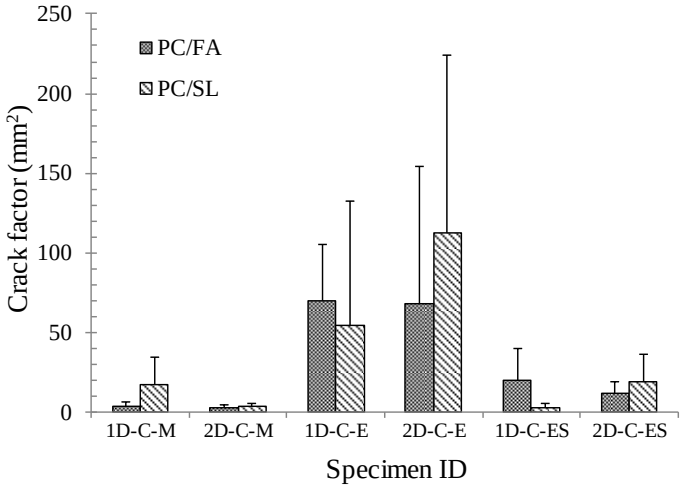


Figure 4.28: Average crack-factor of PC/FA and PC/SL cracked RC beam specimens

Reinforcement bars that are located near the edge of concrete elements have a higher tendency to deteriorate than those that are farther away from the concrete edge (i.e. in the middle of the concrete element). The corrosion-induced cracks in the concrete exposed to 2D ingress of corrosion agents exceeded that of concrete exposed to 1D ingress of corrosion agents.

4.8 Reinforcement mass loss and pitting depths

The mass loss and maximum corrosion pit depths along the length reinforcement bars presented in this section were obtained from the mean of the 3 reinforcement bars used in each RC beam set (refer to Figure 3.4 and Figure 3.5).

A general trend was observed in the mass loss of the reinforcement bars; the mass loss increased as the ingress direction of corrosion agents changed from 1D to 2D (Figure 4.29). The mass loss in reinforcement bars that were close to the edge of the concrete was also higher than that of bars that were placed in the middle of the concrete element. Hence, in the cracked and uncracked concrete, the specimens which were exposed to 2D chloride ingress had the highest mass loss. The error bars shown in Figure 4.29 are standard deviations from the mean mass loss in the reinforcement bars.

The reinforcement bars in specimens with the stainless-steel bar (-ES-) lost lesser mass than those with a single reinforcement bar (-E-). This result can be closely related to the corrosion rate results which were earlier discussed wherein the corrosion rate of the specimens with stainless steel bars was less than that of specimens with a single (isolated) reinforcement bar (see Section 4.4.2).

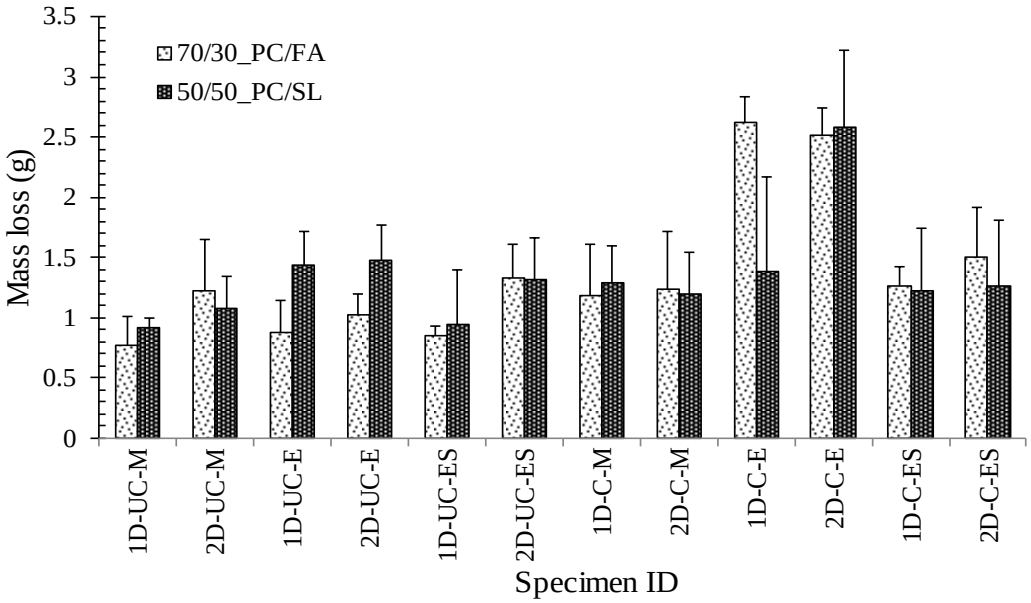


Figure 4.29: Mass loss of reinforcement bars

The steel mass loss in the cracked concrete was generally more than that of the uncracked concrete. Although the specimen F1D-C-E had the highest steel mass loss and its reinforcement was located at the concrete corner. The specimens F2D-C-E and G2D-C-E also had a high reinforcement mass loss. These specimens had reinforcement bars located near the concrete corner and were both exposed to 2D chloride ingress. These results indicate that the mass loss from reinforcement bars

that are located near the corner of concrete elements that are subjected to 2D chloride ingress is higher than that of bars that are farther away from the concrete corner.

4.8.1 Corrosion pits

The steel mass loss in the cracked concrete was generally higher than that of the uncracked concrete. The specimen F1D-C-E had the highest steel mass loss along with specimens F2D-C-E and G2D-C-E. These specimens had reinforcement bars located at the orthogonal edge of the concrete specimen. These results indicate that the mass loss from reinforcement bars that are located near the corner of concrete elements that are subjected to 2D chloride ingress is higher than that of bars that are farther away from the concrete corner.

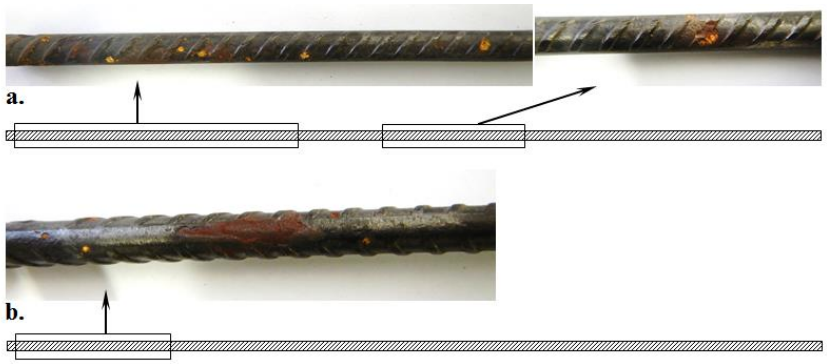


Figure 4.30**:** Corrosion pits on reinforcement bars of uncracked beam specimens (a) F2D-UC-M3, and (b) G2D-UC-M1 (Sketch shows section of rod shown in the picture)

The corrosion pits affected the reinforcement surface that is closer to the concrete surface. The cleaned corroded bars which were extracted from the cracked PC/FA and PC/SL concrete are shown in Figure 4.31 and Figure 4.32. Additional photographs of the reinforcement bars during extraction from the concrete are shown in Appendix E.

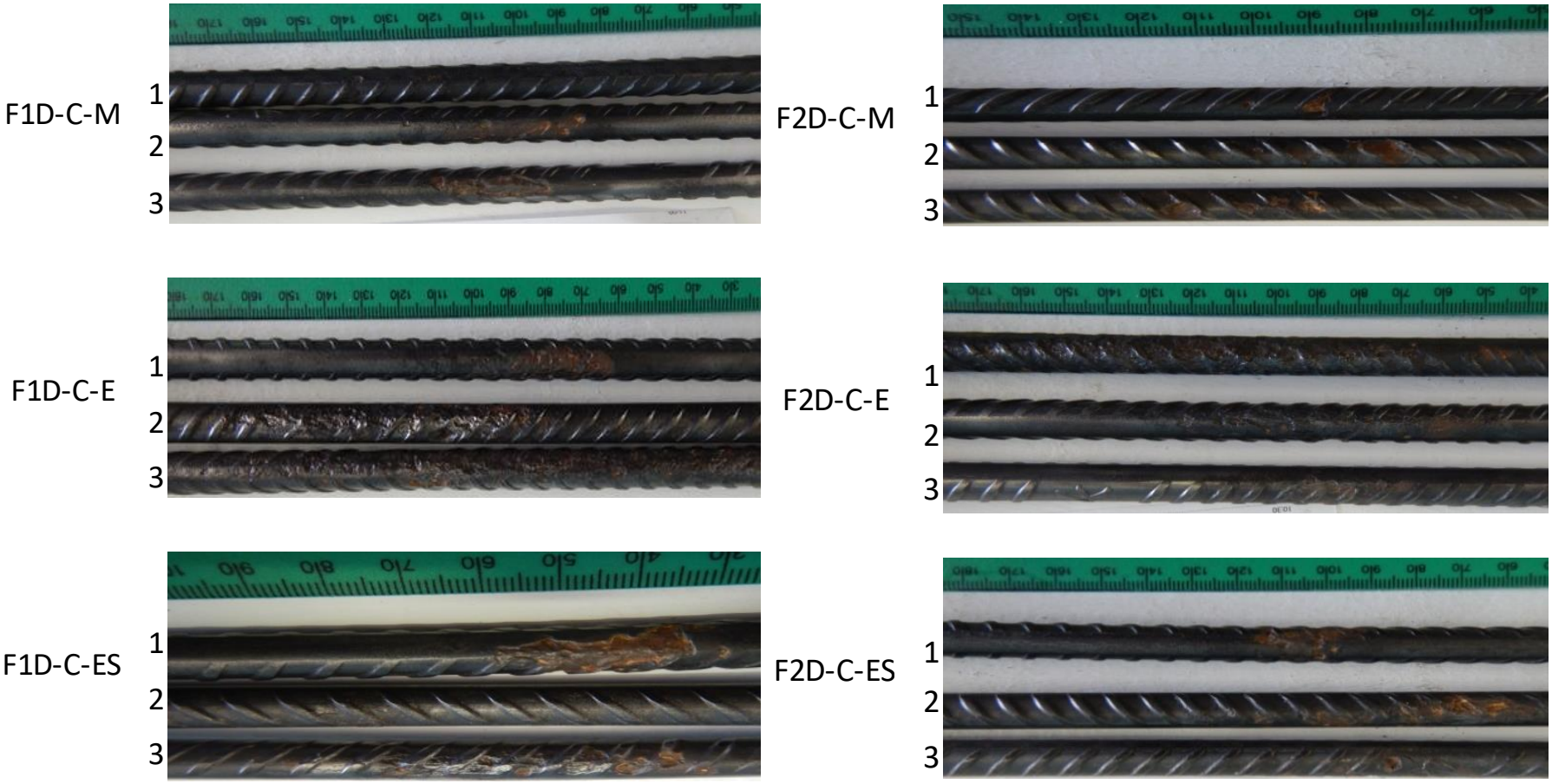


Figure 4.31: Photograph of corroded reinforcement bars from cracked PC/FA concrete specimens

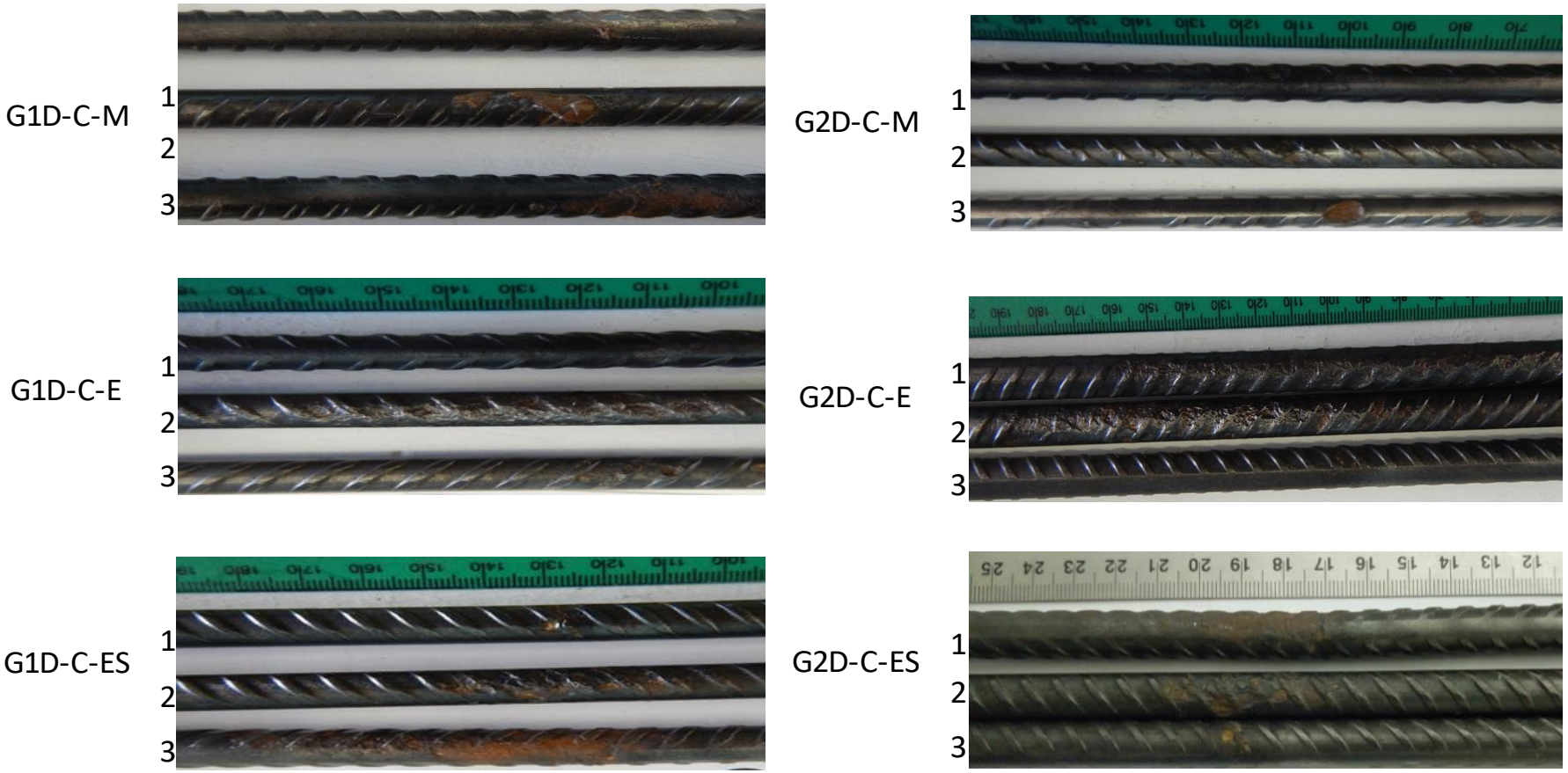


Figure 4.32: Photographs of corroded reinforcement bars from cracked PC/SL concrete specimens

In the cracked concrete, isolated corrosion pits were observed in the concrete that is exposed to 1D chloride ingress with reinforcement bars that were located at the middle (-M-). The corrosion pits in steel bars that were located at orthogonal edges (exposed to 1D and 2D chloride ingress) were spread over a wider area.

The deepest corrosion pits occurred in the cracked concrete and coincided with the crack positions (at the beam midspan). Cracked regions in concrete that are exposed to chlorides have been identified to have an ample supply of corrosion agents (M. Otieno et al., 2016b; J. F. Pacheco, 2015; Pease, 2010; O. G. Rodríguez et al., 2003). The corrosion pits were noticed on the reinforcement bar face that is facing the nearest concrete face and behind the reinforcement bars. The formation of pits at points which were farther away from the concrete surface was caused by the formation of chloride reservoirs in the cracks which easily dry out during when the concrete is undergoing the drying cycle thus allowing an ample supply of oxygen which will result in corrosion at the crack location (Mike Otieno, 2008).

The corrosion pits in the uncracked concrete were located at other points (of the reinforcement bar) which were away from the concrete midspan (see Figure 4.30). Plots of the corrosion pit distribution along the length of the reinforcement bars are shown in Figure 4.33 to Figure 4.36.

The plots show that there is a similarity in the maximum pit depths of the specimens exposed to 1D and 2D chloride ingress. The pit distribution along the reinforcement bar of the cracked RC specimens subjected to 2D chloride ingress spread farther away from the midspan of the reinforcement bar as compared to that of specimens exposed to 1D chloride ingress. The spread of corrosion away from the crack locations was influenced by the formation of microcracks due to the sustained flexural imposed load (Arnaud Castel & Jenkins, 2015).

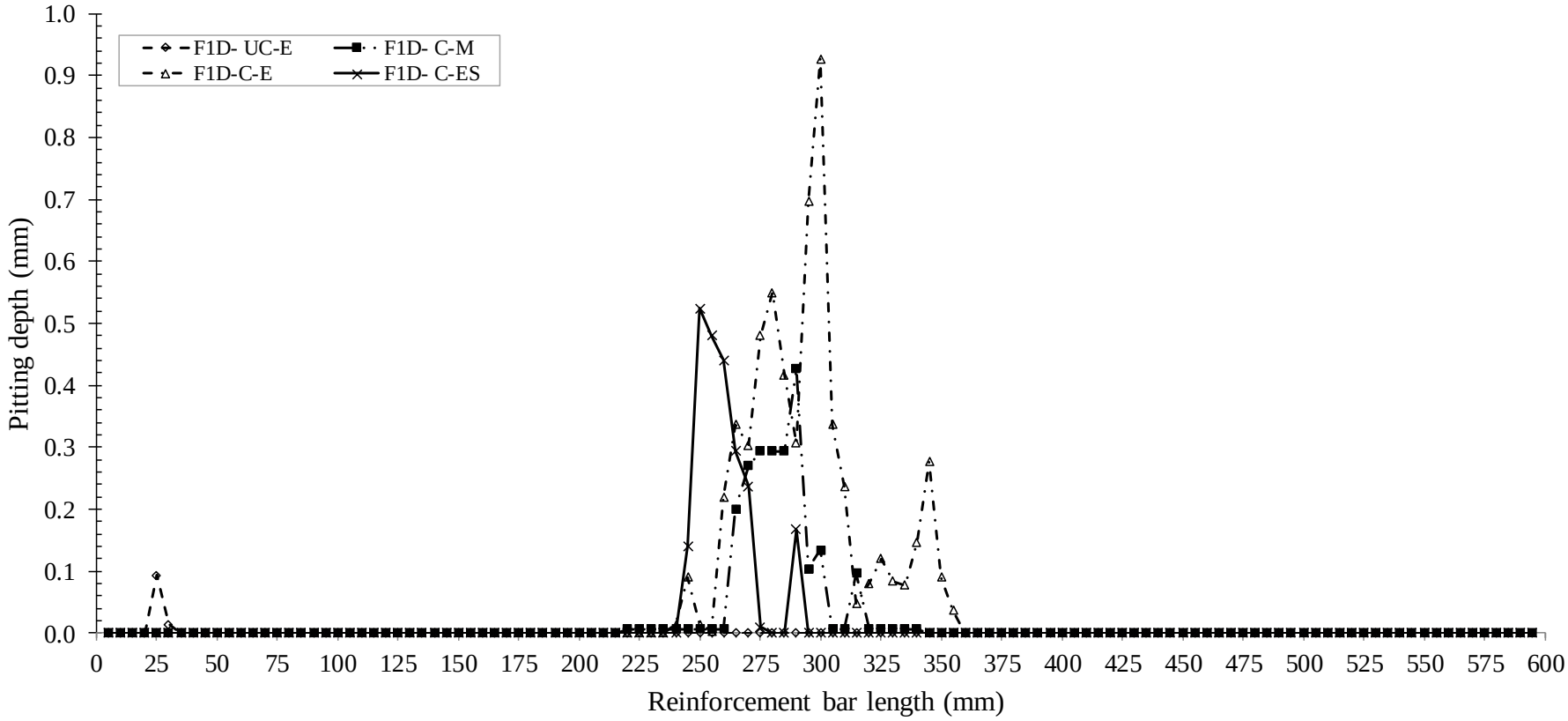


Figure 4.33: Pitting depths along reinforcement bar length PC/FA concrete exposed to 1D ingress of corrosion agents

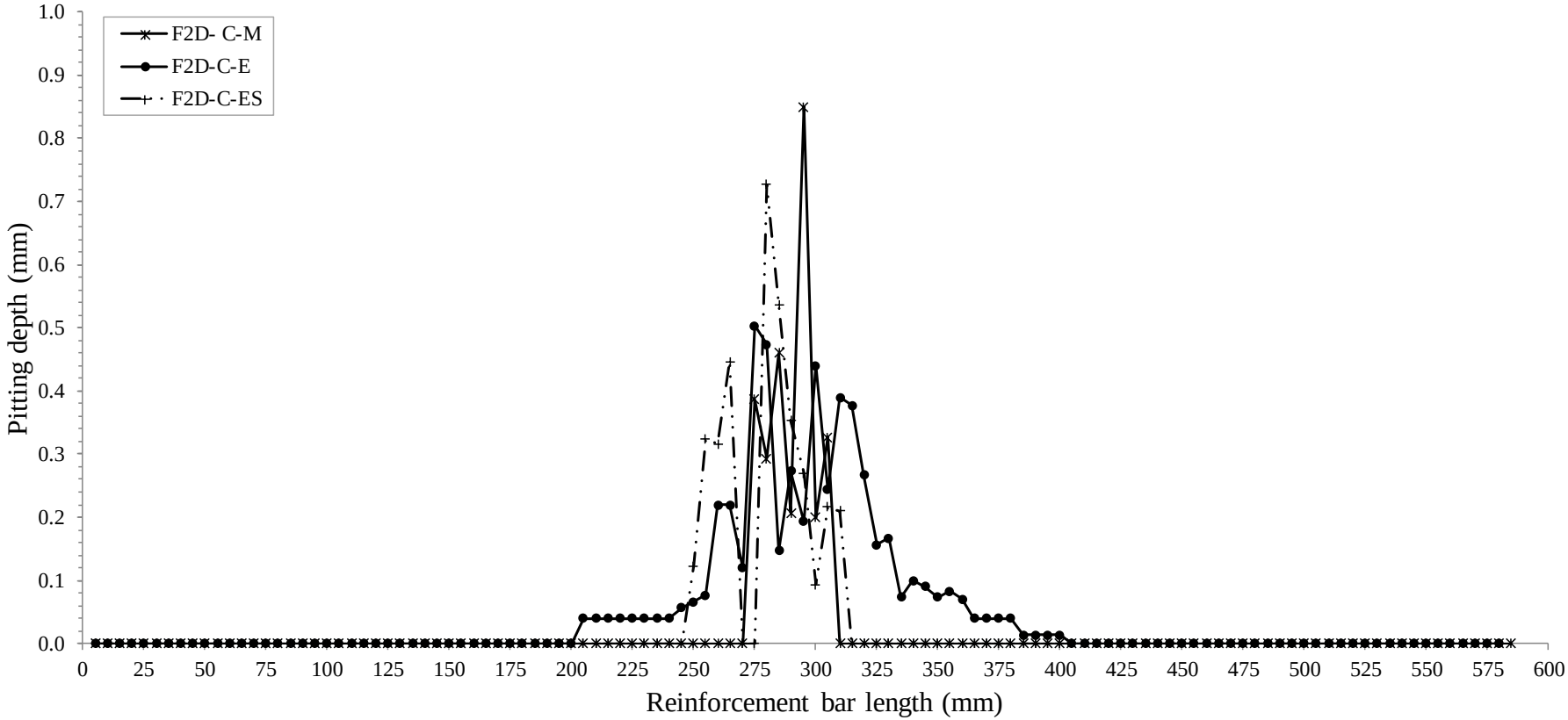


Figure 4.34: Pitting depths along reinforcement bar length of PC/FA concrete exposed to 2D ingress of corrosion agents.

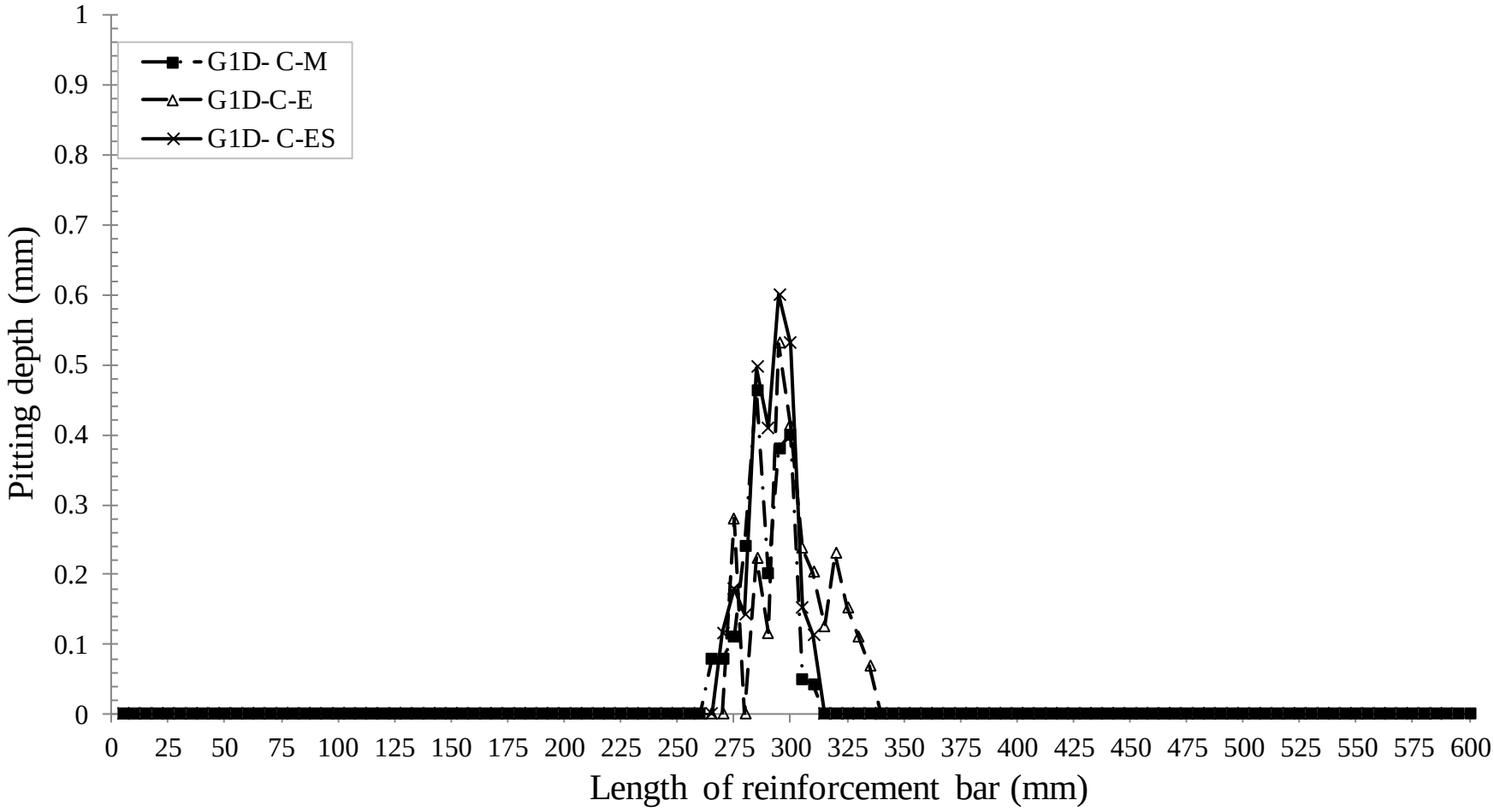


Figure 4.35: Pitting depths along reinforcement bar length PC/SL concrete exposed to 1D ingress of corrosion agents

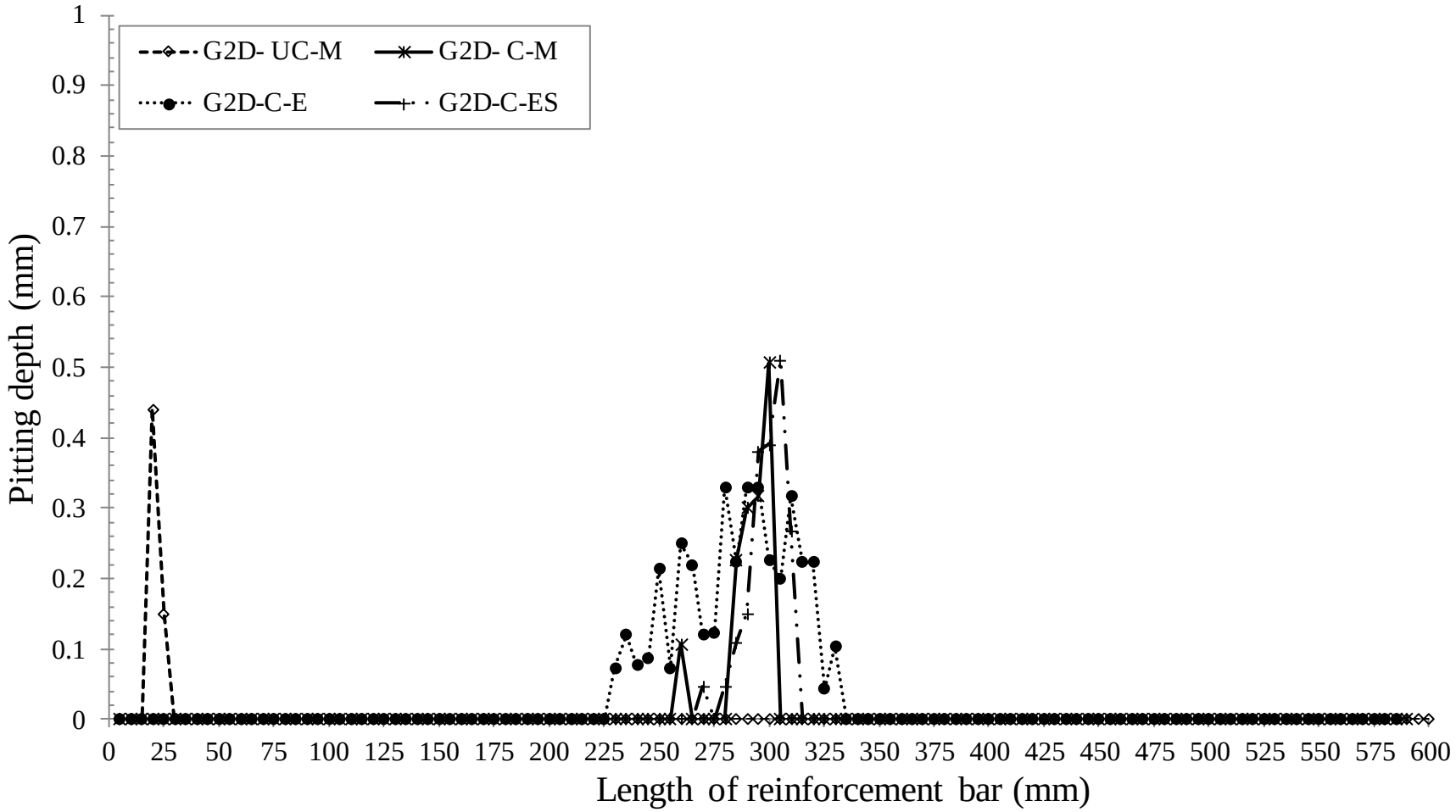


Figure 4.36: Pitting depths along reinforcement bar length PC/SL concrete exposed to 2D ingress of corrosion agent

4.8.2 Corrosion pit factors

The pitting factor (α) is computed by dividing the maximum by the average attack penetration (RILEM TC 154-EMC, 2004);

$$\alpha = \frac{P_{pit}}{x} \qquad 4.1$$

where P_{pit} is the maximum pit depth (mm), and

x is the average corrosion attack penetration (mm)

The computed pitting factors are shown in Table 4.4.

Table 4.4: Reinforcement bar pitting factors

Specimen ID	1D-UC-E	2D-UC-M	1D- C-M	2D- C-M	1D-C-E	2D-C-E	1D- C-ES	2D-C-ES
PC/FA	5	-	3	4	9	6	4	5
PC/SL	-	4	6	4	4	4	3	9

The pitting factors (α = 3 to 9) above, are similar to what other researchers had obtained; (α = 4 to 10) for natural conditions and α = 5 to 13 in accelerated tests (Tuutti, 1982; González *et al.*, 1995; Rodriguez *et al.*, 1996; Zhang, Castel,and François, 2009, 2010).

There was no clear trend in the pitting factor despite a change in ingress direction of corrosion-causing agents from 1D to 2D, however, most of the reinforcement bars with higher pitting factors (i.e. 5 to 9) where located near an orthogonal corner of the concrete element.

4.9 Closing remarks

The results obtained from the concrete durability index tests, steel corrosion potential, concrete resistivity, steel corrosion rate, total chloride concentration at various depths from the surface of the concrete were presented and discussed. The pitting depth at 5 mm intervals along the length of the reinforcement bar and its mass loss were also determined. The ensuing remarks will focus on a few of the findings in this chapter, a comprehensive conclusion will be done in the Chapter 5.

The corrosion potential of the cracked concrete specimens was generally lower (more negative) than that of the uncracked concrete specimens. The low corrosion potential corresponded with a high corrosion rate, however, at corrosion potentials

below – 450 mV, the corrosion rate of specimens with reinforcement bars at their edge increased significantly.

The concrete resistivity of the cracked specimens exposed to 2D chloride was lower than 10 kΩ.cm which signified a high corrosion risk. Thus, despite the binder used, the concrete resistivity was identified not to limit the corrosion rate of reinforcement bars that were located near the concrete edge. The percentage total chloride in the binder steadily reduced in concentration at sampled depths (of 5 mm up to 25 mm) away from the concrete surface. The sustained load on the specimens influenced the total chloride concentration in the cracked specimens with specimens exposed to 2D chloride ingress having significantly higher chloride concentration at the depth of the reinforcement bar than the cracked concrete specimens exposed to 1D chloride ingress. In the uncracked concrete, there was no significant difference in the chloride concentration at the steel depth of specimens exposed to both 1D and 2D chloride ingress. The results indicate that reinforcement bars at the edge of cracked concrete structures (which are in service) exposed to 2D chloride ingress will have a shorter corrosion initiation period and their corrosion rate may increase rapidly during the corrosion propagation phase as observed in some of the cracked specimens.

CHAPTER 5: CONCLUSIONS AND RECOMMENDATIONS

5.1 Introduction

This study aimed to provide an understanding of the influence of uni-directional (1D) and bi-directional (2D) ingress of corrosion agents (chlorides, oxygen, and moisture) into cracked and uncracked concrete. In all, 72 beams of size 150 × 150 × 625 mm were cast using a blended cement of plain Portland cement (PC), fly ash (FA) and slag (SL) (PC(70)/FA(30) and PC(50)/SL(50)). After the beams were cast, they were cured for 28 days in water and epoxy sealed to modify the ingress direction of corrosion agents. This was achieved by epoxy sealing the surfaces where ingress was not desired while only the surfaces where corrosion ingress was desired were left unsealed.

The beam specimens were grouped in 3's based on the position of the 10 mm high yield steel reinforcement bar position in the concrete; all the steel bars were placed longitudinally along the length of the beam at a uniform cover of 20 mm from the exposed concrete surface(s);

i. Along the middle of the beam
ii. Along an orthogonal edge of the beam
iii. Along an orthogonal edge of the beam with a stainless-steel rod in the compression face

While the first two groups (i and ii above) consist of isolated reinforcement bars in the concrete, the third specimen (iii above) with the stainless-steel bar was electrically connected to the reinforcement bar to ascertain the corrosion characteristics of the reinforcement bar when it is connected to a passive steel rod.

The cracked concrete specimens each had a single crack of width 0.16 – 0.40 mm which was mechanically-induced using the 3-point loading technique. The cracked specimens were clamped (back-to-back) in a 3-point loading system. The sustained load (via the clamps) maintained the crack width opening during the experiment.

The beams were subjected to 2-week cycles of wetting (by ponding in 5% NaCl solution) and drying in ambient laboratory conditions, for a period of 110 weeks.

The ensuing sections provide conclusions of the findings of this study, and recommendations.

5.2 Conclusions

5.2.1 Corrosion initiation and propagation phases

Corrosion initiation occurred earlier in both the cracked and uncracked PC/SL concrete exposed to 2D chloride ingress. In the PC/FA concrete, corrosion initiated earlier in the specimens exposed to 1D chloride ingress, however, in the corrosion propagation phase, 75% of the PC/SL and PC/FA concretes exposed to 2D chloride had a corrosion rate that was significantly higher than that of specimens exposed to 1D chloride ingress. The corrosion rate in specimens exposed to 2D ingress of corrosion agents was higher than that of specimens exposed to 1D ingress of corrosion agents (Figure 4.13).

Higher corrosion rates were attained by the cracked concrete specimens (over the same time period), hence, the time-to-corrosion initiation was generally shorter in the cracked concrete specimens, this was due to the ease in which the corrosion agents easily reached the reinforcement bar. This result confirms the findings of some researchers who have studied corrosion initiation and propagation in cracked concrete. Thus, the presence of cover cracks significantly reduces the time-to-corrosion initiation of embedded reinforcement bars in concrete.

In the corrosion propagation phase, the corrosion rate of specimens exposed to 2D chloride exposure was significantly higher than that of specimens exposed to 1D ingress of corrosion agents. The only exception being the uncracked PC/FA specimens were the difference in the corrosion rate of specimens exposed to 1D and 2D chloride ingress was not significant.

5.2.2 Factors influencing the corrosion rate

5.2.2.1 Cover cracks

The corrosion rate of reinforcement bars in the cracked concrete was higher than that of the uncracked concrete. This is due to the ease with which the corrosion agents reach the reinforcement bars via the mechanically-induced cover cracks. Concrete with mechanically-induced cover cracks as small as 0.16 mm also had a

high corrosion rate; this crack width is about one half of the allowable crack width specification in some reinforced concrete design codes (i.e. 0.30 mm).

Concrete with cover cracks smaller than that prescribed in the codes can be subjected to high ingress of corrosion agents if the cracks do not "heal" (e.g. due to ettringite formation). Although the level of the sustained flexural stress on the cracked beams was not measured as it was meant to keep the crack mouths open during the wetting-drying cycles, it may have influenced the ingress of corrosion agents into the concrete.

5.2.2.2 Ingress direction of corrosion agents

Concrete subjected to 2D ingress of corrosion agents had a higher corrosion rate than those exposed to 1D chloride ingress. The corrosion rate was significantly higher in concretes with an isolated reinforcement bar at its edge which is exposed to 2D ingress of corrosion agents.

The chloride ingress direction influenced the following:

a. Chloride concentration: The chloride concentration at the depth of the reinforcement in the concrete exposed to 2D chloride ingress was about twice as much as that of concrete specimens exposed to 1D chloride ingress. For example, the percentage of chlorides per unit weight of the cementitious binder at the depth of the steel bar in the cracked concrete were 3.0 and 2.6 for the fly ash and slag concrete respectively. The percentage chloride concentration of the cracked concrete specimens exposed to 1D chloride ingress were 1.7 and 0.8 for the fly ash and slag concretes respectively. The difference in chloride concentration at various depths into the concrete was not very significant in the uncracked concretes that were exposed to both 1D and 2D chloride ingress. A high chloride concentration at the concrete edge (due to bi-directional chloride ingress) results in higher ionic conductivity in moist concrete which ensures connectivity between the anodic and cathodic sites.
b. Concrete resistivity: The chloride concentration in the concrete is linked to its resistivity. The cracked concrete (exposed to 1D and 2D chloride ingress) and uncracked concrete exposed to 2D chloride ingress had a concrete

resistivity (≈10 kΩ.cm) that suggests that the concrete resistivity is not a corrosion rate-limiting factor. Only the uncracked concrete exposed to 1D chloride ingress had a resistivity value that was greater than 10 kΩ.cm.

5.2.3 Corrosion-induced cracks

Concretes with embedded reinforcement bars near the edge had the longest and widest corrosion-induced cracks while those with reinforcement bars placed in the middle of the concrete beam had the least corrosion-induced cracks. Corroding bars that are near a concrete edge readily cause the concrete to crack and provide additional paths for corrosion agent ingress into the concrete. This also gives rise to an exponential increase in the corrosion rate as observed in some of the specimens.

5.2.4 Pitting corrosion depths and reinforcement mass loss

Isolated corrosion pits were observed on the reinforcement bars that were positioned in the middle of the concrete beam exposed to 1D ingress of corrosion agents. The corrosion pits in the reinforcement bars that were near the edge of the concrete were not isolated but covered a wider surface of the reinforcement bars. The corrosion pits affected the reinforcement face that is closer to the exposed concrete surface. The corrosion pits reduced as the distance from the location of the mechanically induced cracks increased.

5.3 Limitations of the research

This study is laboratory-based and will only focus on chloride-induced corrosion of steel embedded in concrete. The concrete will be exposed to chloride ions by ponding in a 5% sodium chloride (NaCl) solution; hence, depassivation of the steel reinforcement bar is caused by the buildup of a critical concentration of chlorides on the steel surface.

A 2-week repeated cycle of wetting (by ponding) in the chloride solution and then air-drying in ambient laboratory condition for the same period (2-weeks) will be utilized throughout the period of this study. No impressed current will be used throughout this test regime.

While a varying number of concrete edges (e.g. chamfered, rounded, square etc.), cover depths to reinforcement, reinforcement diameter sizes, water/binder ratios, and binder blends exist, this study will utilize concrete with orthogonal edges (i.e.

90^{o} corners), 20 mm cover to reinforcement, 10 mm high yield reinforcement diameter bars, water/binder = 0.40 and concrete with binder blends of [1]PC (70)/[2]FA (30) and PC (50)/[3]SL (50).

The faces of the RC specimens will be sealed (with an epoxy sealant) to allow only 1D and 2D chloride ingress through the concrete surface during the chloride ponding. However, at crack positions, ingress of corrosion agents is not restricted to the 1D and 2D ingress directions (it is multi-directional) since the concrete surfaces were epoxy sealed before the beams were cracked.

The cracks in the RC specimens were mechanically-induced by using the 3-point load technique, after which the specimens were clamped onto rigs to prevent the closing of the crack mouth openings (which ranged from 0.16 – 0.40 mm). The flexural loads imposed on the cracked specimens were static, hence it is possible that the crack mouths may 'seal' due to ettringite formation. Sealing of the cracks can reduce the ingress of corrosion agents, thereby reducing the corrosion rate of reinforcement bars. The creep characteristics due to the flexural loads on the concrete will also not be assessed as it was deemed not needful in the interpretation of the corrosion measurement results of this study.

Though it is assumed that the partial replacement of plain PC with supplementary cementitious materials (SCMs) such as FA will result in chloride binding, this phenomenon was not assessed; rather the total chloride content (i.e. acid soluble chlorides) was assessed at the termination of the chloride ponding and drying cycles.

Corrosion rate, concrete resistivity, and half-cell potential measurements will be monitored 24 hours after termination of each wetting cycle and before each drying cycle. Since the drying cycle was undertaken in ambient laboratory condition, only the monitored results after the wetting cycle were used. This was to overcome inconsistencies which may be encountered due to uneven drying of the concrete

[1] PC = plain Portland cement

[2] FA = Fly ash

[3] SL = Ground granulated blast furnace slag

beams since they were not kept in a controlled (temperature and relative humidity) environment.

It is expected that the corrosion data will continue to vary with time during this study, hence, the experimental program will be terminated when a noticeable trend is obtained in the corrosion measurements, however, the termination period will not be less than 12 months. Other considerations for the termination of this experiment are the appearance of visual defects such as corrosion-induced cracks, spalling, and delamination, and excessive rust stains on the concrete surface.

5.4 Practical implications of the research findings

Since a wide variety of concrete edges exist, the practical implications of the findings of this study refer to orthogonal concrete edges.

a. The corrosion-free life of reinforcement bars that are located near concrete edges of cracked (which are stressed with a sustained load flexural load) and uncracked concrete elements is shorter than that of reinforcement bars that are farther away from the concrete edge. Although beams used in this study had orthogonal angled edges, it is logical to assume that acute-angled edges will be more susceptible to higher ingress of corrosion agents due to the closeness of the penetrating profile fronts as compared to obtuse-angled edges. Despite the risk posed by 2D chloride ingress of corrosion agents, increasing the existing cover depth specified in RC construction codes will subject the concrete to wider cover cracks. Hence, rather than increase the cover depth, where the risk outweighs the cost, galvanized or stainless steel reinforcement bars can be used at the orthogonal edges. Alternatively, the concrete edges should be treated with sealants that prevent moisture ingress into the concrete.
b. Smaller concrete surface cracks of about one half that recommended in design codes; 0.30 mm which are located at concrete edges exposed to more than 1D ingress of corrosion agents have been identified to be detrimental to concrete durability.

c. The corrosion rate of reinforcement bars at edges of cracked concrete proceeds at a rate that is higher than that of reinforcement bars that are farther away from the concrete edge.
d. Corrosion initiation models that are based on uni-directional ingress of corrosion agents will not sufficiently predict the corrosion state of reinforcement bars that are positioned near the edge of concrete elements.
e. The resistivity of concrete at concrete edges exposed to 2D chloride ingress was observed to be low, thus it did not limit the corrosion rate of the reinforcement bars located near the concrete edge. The cover depth of reinforcement bars at edges of severely exposed concrete elements should be closely monitored during construction to achieve the prescribed cover. A means of protecting the concrete edges from the ingress of corrosion agents, delaying the corrosion of reinforcement bars by using cathodic protection, or more passive reinforcement bars at the orthogonal edges should be adopted to prevent early corrosion initiation and rapid corrosion propagation.

5.5 Recommendations for further work

Based on this study, the following recommendations are made:

1. The cracked and uncracked concrete specimens should be subjected to various quantifiable levels of the sustained flexural load to determine the effect of the load on chloride penetration into the concrete. Knowledge of the sustained load may yield a relationship with the chloride concentration at various depths within the concrete.
2. The effect of the sustained load on the steel-concrete interface should be determined. Only the cover cracks were considered in this study, however, a study of the steel-concrete interface may provide additional information on microcrack formation at the interface which could be related to the steel corrosion.
3. The sustained flexural load was kept constant throughout the study while in field structures, the imposed load is not constant but varies with time. The sustained load can thus be reduced and then reintroduced to its initial intensity to ascertain the effect of varying load on the steel corrosion.

4. Although a single crack was used in this research, the effect of multiple cover cracks of various widths in concrete which is exposed to 1D and 2D chloride ingress may present a different corrosion characteristic than that which was observed in this study.
5. As observed in this study, there was a significant reduction in the corrosion rate of specimens that had embedded steel reinforcement bars connected to a stainless-steel bar. The possible generation of a galvanic current may have caused the reduction in the corrosion rate. The galvanic current can be measured to ascertain its influence of the corrosion of the reinforcement bar.
6. In the 1D exposure in this study, only the surface exposed to chloride ingress was left unsealed (all other surfaces were sealed). This may have influenced the sorption of chlorides into the concrete. Although it is assumed that diffusion is the dominant means of chloride ingress into the concrete, it is suggested that only the vertical faces of the concrete be epoxy sealed in the specimens exposed to 1D chloride ingress. This will ascertain if poor sorption due to exposure of only one surface influenced the results.
7. An assessment of different cover depths and its influence on the corrosion rate of reinforcement bars should be investigated.
8. Development of a model that accounts for the corrosion rate of reinforcement bars that are positioned at the edge of concrete elements exposed to 2D ingress of corrosion agents. A reliable model could not be developed with the data obtained in this study due to limited variables as the same cover depth to reinforcement, similar crack width, and concrete quality was used in the experimental design.

REFERENCES

ACI 201. (1982). *Chloride content limits recommended by ACI Committee 201*. *Concrete*.

ACI 222R. (2001). Protection of Metals in Concrete Against Corrosion. *American Concrete Institute*, 1–41.

Adiyastuti, S. M. (2005). *Influence of Cracks on Chloride Induced Corrosion in Reinforced Concrete Flexural Members*. The University of New South Wales, Sydney, Australia.

Afrisam South Africa Pty (Ltd). (2017). *AfrisamTechnical Reference Guide* (8th Editio). Weltevredenpark, South Africa: Promise.

Ahmad, S. (2003). Reinforcement corrosion in concrete structures, its monitoring and service life prediction—a review. *Cement and Concrete Composites*, *25*(4–5), 459–471.

Al-Saleh, S. A. (2015). Analysis of total chloride content in concrete. *Case Studies in Construction Materials*, *3*, 78–82.

Alexander, M. G., Ballim, Y., & Stanish, K. (2008). A framework for use of durability indexes in performance-based design and specifications for reinforced concrete structures. *Materials and Structures*, *41*, 921–936.

Alexander, M. G., Mackechnie, J. R., & Ballim, Y. (1999). *Guide to the use of durability indexes for achieving durability in concrete structures*. *Research monograph No. 2*. Cape Town and Johannesburg.

Allen, R. T. L. (1998). *Concrete in Coastal Structures*. Thomas Telford.

Alonso, C., Andrade, C., & González, J. A. (1988). Relation between resistivity and corrosion rate of reinforcements in carbonated mortar made with several cement types. *Cement and Concrete Research*, *18*, 687–698.

Alonso, C., Castellote, M., & Andrade, C. (2001). Dependence of Chloride Threshold with the Electrical Potentials of Reinforcements. In C. Andrade & J. Kropp (Eds.), *PRO 19: 2nd International RILEM Workshop on Testing and Modelling the Chloride Ingress into Concrete (11-12 september, 2000)* (pp. 415–425). Paris, France: RILEM Publications.

Alyousif, A., Lachemi, M., Yildirim, G., Şahmaran, M., Alyousif, A., Lachemi, M., Mustafa, Ş. (2015). Effect of Self-Healing on the Different Transport Properties of Cementitious Composites. *Journal of Advanced Concrete Technology; Materials, Structures and Environment*, *13*, 112–123.

Andrade, C. (1993). Calculation of chloride diffusion coefficients in concrete from ionic migration measurements. *Cement and Concrete Research*, *23*(3), 724–742.

Andrade, C., & Alonso, C. (1996). Corrosion rate monitoring in the laboratory and

on-site. *Construction and Building Materials*, *10*(5), 315–328.

Andrade, C., Alonso, C., & Sarŕa, J. (2002). Corrosion rate evolution in concrete structures exposed to the atmosphere. *Cement and Concrete Composites*, *24*(1), 55–64.

Andrade, C., Prieto, M., Tanner, P., Tavares, F., & D'Andrea, R. (2013). Testing and modelling chloride penetration into concrete. *Construction and Building Materials*, *39*, 9–18.

Andrade, Carmen, & Buják, R. (2013). Effects of some mineral additions to Portland cement on reinforcement corrosion. *Cement and Concrete Research*, *53*, 59–67.

Angst, U. (2011). *Chloride induced reinforcement corrosion in concrete - Concept of critical chloride content – methods and mechanisms*. *Concept of Critical Chloride Content—Methods and …*. Norwegian Universtiy of Science and Technology. 2

Angst, U., Elsener, B., Larsen, C. K., & Vennesland, Ø. (2009). Critical chloride content in reinforced concrete — A review. *Cement and Concrete Research*, *39*(12), 1122–1138.

Angst, U., Larsen, C. K., Vennesland, Ø., & Elsener, B. (2010). Influence of casting direction on chloride-induced rebar corrosion. In C. Pedro, E. I. Moreno, K. Sakai, O. E. Gjorv, & N. Banthai (Eds.), *Proceedings of the 6th International Concrete Under Severe Conditions (CONSEC '10)* (Volume 1, p. 410). Mexico: Taylor & Francis Group.

Angst, U. M., & Elsener, B. (2013). On the Applicability of the Wenner Method for Resistivity Measurements of Concrete. *ACI Materials Journal*, *MS*(M-2013–024), 661–671.

Angst, U. M., Geiker, M. R., Michel, A., Gehlen, C., Wong, H., Isgor, O. B., … Buenfeld, N. (2017). The steel–concrete interface. *Materials and Structures*, *50*(2), 143.

Ann, K. Y., & Song, H.-W. (2007). Chloride Threshold Level for Corrosion of Steel in Concrete. *Corrosion Science*, *49*(11), 4113–4133.

Arya, C., & Ofori-Darko, F. K. (1996). Influence of crack frequency on reinforcement corrosion in concrete. *Cement and Concrete Research*, *26*(3), 345–353.

Arya, C., & Xu, Y. (1995). Effect of cement type on chloride binding and corrosion of steel in concrete. *Cement and Concrete Research*, *25*(4), 893–902.

Asbridge, A. H., Chadbourn, G. A., & Page, C. L. (2001). Effects of metakaolin and the interfacial transition zone on the diffusion of chloride ions through cement mortars. *Cement and Concrete Research*, *31*(11), 1567–1572.

ASTM-C1543 - 10. (2010). Standard Test Method for Determining the Penetration

of Chloride Ion into Concrete by Ponding | Document Center, Inc. In *American Standard ofr Testing Materials* (pp. 764–767). ASTM International.

ASTM C1218 / C1218M. (1999). ASTM C1218 / C1218M - 17 Standard Test Method for Water-Soluble Chloride in Mortar and Concrete. In *American Standard for Testing Materials* (pp. 665–667).

ASTM C1760 - 12. (2012). Standard Test Method for Bulk Electrical Conductivity of Hardened Concrete. *ASTM*. America: ASTM.

ASTM C876. (2009). *Standard Test Method for Corrosion Potentials of Uncoated Reinforcing Steel in Concrete*.

ASTM G1-90. (2003). ASTM G1 Standard Practice for Preparing, Cleaning, and Evaluation Corrosion Test Specimens. *ASTM*, 8.

Audenaert, K., Schutter, D. G., & Marsavina, L. (2009). Influence of cracks on chloride penetration and corrosion intiation time.pdf. In *2nd International RILEM Workshop on Concrete Durability and Service Life Planning.* (pp. 80–84). Haifa, Israel: Rilem Publ.

Azarsa, P., & Gupta, R. (2017). Electrical Resistivity of Concrete for Durability Evaluation : A Review. *Advances in Materials Science and Engineering*, *2017*, 30.

Baboain, R., Dean, S. W. J., Hack, H. P., Hibner, E. L., & Scully, J. R. (2005). *Corrosion Tests and Standards : Application and Interpretation*. (B. Robert, Ed.) (2nd Editio). Balltimore, MD, USA: ASTM International.

Balabanic, G., Bicanic, N., & Durekovic, A. (1996). The influence of w/c ratio, concrete cover thickness and degree of water saturation on the corrosion rate of reinforcing steel in concrete. *Cement and Concrete Research*, *26*(5), 761–769.

Ballim, Y., & Graham, P. (2009). *Fulton's Concrete Technology*. *Fulton's Concrete Technology*.

Bardal, E. (2004). *Corrosion and protection*. *Mechanics of Composite Materials*. Springer - Verlag London Limited.

Bastidas-Arteaga, E., Chateauneuf, A., Sánchez-Silva, M., Bressolette, P., & Schoefs, F. (2010). Influence of weather and global warming in chloride ingress into concrete: A stochastic approach. *Structural Safety*, *32*(4), 238–249.

Benarbia, D., Benguediab, M., & Benguediab, S. (2013). Two-dimensional Analysis of Cracks Propagation in Structures of Concrete. *Engineering, Technology & Applied Science Research*, *3*(3), 429–432.

Bentz, D. P., Garboczi, E. J., Lu, Y., Martys, N., Sakulich, A. R., & Weiss, W. J. (2013). Modeling of the influence of transverse cracking on chloride penetration into concrete. *Cement and Concrete Composites*, *38*, 65–74.

Bertolini, L., Elsener, B., Pedeferri, P., & Polder, R. P. (2004). *Corrosion of Steel in Concrete: Prevention, Diagnosis, Repair*.

Bioubakhsh, S. (2011). The penetration of chloride in concrete subject to wetting and drying: measurement and modelling. *Cement and Concrete Composites*, *1*, 355.

Bjegovic, D., Mikulic, D., & Sekulic, D. (2007). Non-destructive corrosion rate monitoring for reinforced concrete structures.

Blagojevic, A., Fennis, S., & Walraven, J. C. (2012). Impact of cracks on chloride-induced corrosion and durability of reinforced concrete structures - A literature review, 80–91.

Branko, Š. (2014). *Experimental and numerical investigation of chloride ingress in cracked concrete*. Delft University of Technology, Netherlands.

Branko, Š., & Erik, S. (2012). Chloride Ingress in Cracked Concrete- A Literature Review. In C. Andrade & J. Gulikers (Eds.), *4th International RILEM PhD Workshop.* (pp. 85–93). Madrid, Spain. Rilem Publ.

Breysse, D., & Gerard, B. (1997). Modeling of Permeability in Cement-Based Materials: Part 1- Uncracked Medium. *Cement and Concrete Composites*, *27*(5), 761–775.

Broomfield, J. P. (2007). *Corrosion of Steel in Concrete Understanding, Investigation and Repair*. (P. J. Broomfield, Ed.) (2nd Ed.). London and New York: Taylor & Francis Group.

BS 8007:1987. (1987). *Design of concrete structures for retaining aqoeus liquids.*

BS 8110-1. (1997). *Structural Use of Concrete* (2nd Editio). British Standards Institute.

Cabrera, J. G. (1996). Deterioration of concrete due to reinforcement steel corrosion. *Cement and Concrete Composites*, *18*(1), 47–59.

Cairns, J. (1996). Concrete in the Service of Mankind: Appropriate Concrete Technology. In K. D. Ravindra & J. M. Michael (Eds.), *International Conference held at the University of dundee, 24-26 JUne 1996* (pp. 232–242). Scotland, UK: Taylor & Francis Group.

Cao, C., & Cheung, M. M. S. (2014). Non-uniform rust expansion for chloride-induced pitting corrosion in RC structures. *Construction and Building Materials*, *51*, 75–81.

Caré, S. (2003). Influence of aggregates on chloride diffusion coefficient into mortar. *Cement and Concrete Research*, *33*(7), 1021–1028.

Caré, S., & Raharinaivo, A. (2007). Influence of impressed current on the initiation of damage in reinforced mortar due to corrosion of embedded steel. *Cement and Concrete Research*, *37*(12), 1598–1612.

Carmeliet, J., Delerue, J.-F., Vandersteen, K., & Roels, S. (2004). Three-dimensional liquid transport in concrete cracks. *International Journal for Numerical and Analytical Methods in Geomechanics*, *28*(78), 671–687.

Castel, A., Vidal, T., François, R., & Arliguie, G. (2003a). Influence of steel–concrete interface quality on reinforcement corrosion induced by chlorides. *Magazine of Concrete Research*, *55*(2), 151–159.

Castel, A., Vidal, T., François, R., & Arliguie, G. (2003b, April). Magazine of Concrete Research. *Influence of Steel–Concrete Interface Quality on Reinforcement Corrosion Induced by Chlorides*, *55*(2), 151–159.

Castel, Arnaud, & Jenkins, D. (2015). Concrete In Australia. *Concrete Institute of Australia*, *41*(3), 36–64.

Castellote, M., & Andrade, C. (2001). TC 178-TMC : Round-Robin test on chloride analysis in concrete Part 1: Analysis of total chloride content. *Materials and Structures*, *34*(November), 532–556.

Castellote, M., Andrade, C., & Alonso, C. (1999). Chloride-binding isotherms in concrete submitted to non-steady-state migration experiments. *Cement and Concrete Research*, *29*, 1799–1806.

Chindaprasirt, P., Chotithanorm, C., Cao, H. T., & Sirivivatnanon, V. (2007). Influence of fly ash fineness on the chloride penetration of concrete. *Construction and Building Materials*, *21*(2), 356–361.

Christian, U. (2013). *Acoustic Emission: Testing Basics - for research applications in civil engineering*. (U. G. Christian & O. Masayasu, Eds.), *Journal of Chemical Information and Modeling* (Vol. 53). Springer.

Chun-ping, G., Guang, Y., & Wei, S. (2015). A review of the chloride transport properties of cracked concrete: experiments and simulations. *Journal of Zhejiang University Science A*, *16*(2), 81–92.

Cigrovski, I. (2011). Some aspects of the delayed ettringite formation in concrete - A review. In *Workshop on performance-based specifications for concrete. 14 - 15 June, 2011* (pp. 1–9). Leipzig.

Comité euro-international du béton. (1993). *CEB-FIP Model code 1990: Design code*. London: T. Telford.

Crank, J. (1975). *The Mathematics of Diffusion* (2nd Editio). Oxford: Clarendon

Delagrave, A., Bigas, J. P., Ollivier, J. P., Marchand, J., & Pigeon, M. (1997). Influence of the interfacial zone on the chloride diffusivity of mortars. *Advanced Cement Based Materials*, *5*(3–4), 86–92.

Dhir, R. K., El-Mohr, M. A. K., & Dyer, T. D. (1996). Chloride Binding in GGBS Concrete. *Cement and Concrete Research*, *26*(12), 1767–1773.

Djerbi, A., Bonnet, S., Khelidj, A., & Baroghel-bouny, V. (2008). Influence of traversing crack on chloride diffusion into concrete. *Cement and Concrete*

Research, *38*(6), 877–883.

Edvardsenl, C., & Mohr, L. DURACRETE - A guideline for durability based design of concrete structures. (2000).

Edwards, C., & Penney, D. (1993). Elementary differential equations with boundary value problems.

El-Enein, S. A. A., Kotkata, M. F., Hanna, G. B., Saad, M., & El Razek, M. M. A. (1995). Electrical conductivity of concrete containing silica fume. *Cement and Concrete Research*, *25*(8), 1615–1620.

Elcometer Ltd. (2012). *Half-Cell Meter Model H Operating Instructions*. England.

EN1992-1-1. (2004). *BS EN 1992-1-1:2004 - Eurocode 2: Design of concrete structures - Part 1-1: General rules and rules for buildings*. *Eurocode 2* (Vol. 1).

Fang, C., Gylltoft, K., Lundgren, K., & Plos, M. (2006). Effect of corrosion on bond in reinforced concrete under cyclic loading. *Cement and Concrete Research*, *36*(3), 548–555.

Florea, M. V. A., & Brouwers, H. J. H. (2012). Chloride binding related to hydration products part I: Ordinary Portland cement. *Cement and Concrete Research*, *42*, 282–290.

Francois, R., & Arliguie, G. (1999). Effect of microcracking and cracking on the development of corrosion in reinforced concrete members. *Magazine of Concrete Research*, *51*(2), 143–150.

Frier, C., & Sørensen, J. D. (2007). Stochastic analysis of the multi-dimensional effect of chloride ingress into reinforced concrete. In J. Kanda, T. Takada, & H. Furuta (Eds.), *Proceedings of the 10th International Conference, 31 July - 3 August 2007*. (pp. 191–200). Tokyo, Japan: Marcel Dekker Incorporated.

Gepraegs, O., & Hansson, C. (2005). A Comparative Evaluation of Three Commercial Instruments for Field Measurements of Reinforcing Steel Corrosion Rates. *Journal of ASTM International*, *2*(8), 11789.

Gjorv, O. E. (2013). Durability design and quality assurance of major infrastructure. *Advances in Concrete Construction*, *1*(1), 45–63.

Glass, G. K. (1995). An assessment of the coulostatic method applied to the corrosion of steel in concrete. *Corrosion Science*, *37*(4), 597–605.

Glass, G. K., & Buenfeld, N. R. (1997). The presentation of the chloride threshold level for corrosion of steel in concrete. *Corrosion Science*, *39*(5), 1001–1013.

Glass, G. K., & Buenfeld, N. R. (2000). The influence of chloride binding on the chloride induced corrosion risk in reinforced concrete. *Corrosion Science*, *42*(2), 329–344.

Glass, G. K., Page, C. L., & Short, N. R. (1991). Factors affecting the corrosion rate

of steel in carbonated mortars. *Corrosion Science*, *32*(12), 1283–1294.

Gold standard corrosion science group, L. (2018). Electrochemical Tests _ Tafel Extrapolation _ GSCSG _ Boston MA.

Golden, G. (2015). *The Effect of Cyclic Wetting and Drying on the Corrosion Rate of Steel in Reinforced Concrete*. University of Cape Town, South Africa.

González, J. A., Andrade, C., Alonso, C., & Feliu, S. (1995). Comparison of rates of general corrosion and maximum pitting penetration on concrete embedded steel reinforcement. *Cement and Concrete Research*, *25*(2), 257–264.

Gowers, K. R., & Millard, S. G. (1999). Measurement of concrete resistivity for assessment of corrosion severity of steel using wenner technique. *ACI Materials Journal*, *96*(5), 536–541.

Gudimettla, J. M., & Crawford, G. L. (2015). Field experience in using Resistivity Tests for Concrete. In *94th Annual Meeting of the Transport Research Board* (p. 16). New Jersey: Transport Research Board, Federal Highway Administration.

Gulikers, J. (2005). Theoretical considerations on the supposed linear relationship between concrete resistivity and corrosion rate of steel reinforcement. *Materials and Corrosion*, *56*(6), 393–403.

Gulikers, J., Polder, R., & Raupach, M. (2003). Half-cell potential measurements – Potential mapping on reinforced concrete structures. *Materials and Structures*, *36*(September), 1–11.

Gulikers, J., Polder, R., Raupach, M., RILEM TC 154-EMC: Electrochemical techniques for Measuring Mettalic Corosion, Gulikers, J., Polder, R., & Raupach, M. (2003). Half-cell potential measurements – Potential mapping on reinforced concrete structures. *Materials and Structures*, *36*(September), 1–11.

Güneyisi, E., Özturan, T., & Gesolu, M. (2006). Performance of plain and belended cement concretes against corrosion cracking. In *Measuring, Monitoring and Modeling Concrete Properties* (pp. 189–198). Dordrecht: Springer

Güneyisi, Erhan, Gesoğlu, M., Özturan, T., & Özbay, E. (2009). Estimation of chloride permeability of concretes by empirical modeling: Considering effects of cement type, curing condition and age. *Construction and Building Materials*, *23*(1), 469–481.

Harald, J. (1998). A review of chloride binding in cementitious systems. *Nordic Concrete Research Publications*, *21*, 48-63.

Hassanein, A. M., Glass, G. K., & Buenfeld, N. R. (1998). The use of small electrochemical perturbations to assess the corrosion of steel in concrete. *NDT & E International*, *31*(4), 265–272.

Hobbs, D. W. (1999). Aggregate influence on chloride ion diffusion into concrete.

Cement and Concrete Research, *29*(12), 1995–1998.

Hope, B. B., Ip, A. K., & Manning, D. G. (1985). Corrosion and electrical impedance in concrete. *Cement and Concrete Research*, *15*(3), 525–534.

Hope, B. B., Page, J. A., & Poland, J. S. (1985). The determination of the chloride content of concrete. *Cement and Concrete Research*, *15*(5), 863–870.

Hornbostel, K., Larsen, C. K., & Geiker, M. R. (2013). Relationship between concrete resistivity and corrosion rate – A literature review. *Cement and Concrete Composites*, *39*, 32.

Hoseini, M., Bindiganavile, V., & Banthia, N. (2009). The effect of mechanical stress on permeability of concrete : A review. *Cement and Concrete Composites*, *31*(4), 213–220.

Hunkeler, F., Schiegg, Y., Gulikers, J., Schiessl, P., Raupach, M., Buchler, M., & Polder, R. B. (2005). *Corrosion in reinforced concrete structures*. (H. Bohni, Ed.). Cambridge, England.: Woodhead Publishing Limited.

Hussain, S. E., Rasheeduzzafar, Al-Musallam, A., & Al-Gahtani, A. S. (1995). Factors affecting threshold chloride for reinforcement corrosion in concrete. *Cement and Concrete Research*, *25*(7), 1543–1555.

Isgor, O. B., & Razaqpur, a G. (2006). Modeling steel corrosion in concrete structures. *Materials and Structures*, *53*(12), 291–302.

Ismail, M., Toumi, A., François, R., & Gagné, R. (2008). Effect of crack opening on the local diffusion of chloride in cracked mortar samples. *Cement and Concrete Research*, *38*(8–9), 1106–1111.

Jacobsen, S., Marchand, J., & Boisvert, L. (1996). Effect of cracking and healing on chloride transport in OPC concrete. *Cement and Concrete Research*, *26*(6), 869–881.

Jang, S. Y., Kim, B. S., & Oh, B. H. (2011). Effect of crack width on chloride diffusion coefficients of concrete by steady-state migration tests. *Cement and Concrete Research*, *41*(1), 9–19.

Ji, Y., Hu, Y., Zhang, L., & Bao, Z. (2016). Laboratory studies on influence of transverse cracking on chloride-induced corrosion rate in concrete. *Cement and Concrete Composites*, *69*, 28–37.

Jin, L., Zhang, R., Du, X., & Li, Y. (2015). Investigation on the cracking behavior of concrete cover induced by corner located rebar corrosion. *Engineering Failure Analysis*, *52*, 129–143.

Kang, B., & Shim, H. (2011). Two Dimensional Chloride Ion Diffusion in Reinforced Concrete Structures for Railway. *International Journal of Railway*, *4*(4), 86–92.

Kessy, J. G., Alexander, M. G., & Beushausen, H. (2015). Concrete durability standards: International trends and the South African context. *Journal of the*

South African Institution of Civil Engineering, *57*(1), 47–58.

Kim, J., Zi, G., & Lange, D. A. (2017). Measurement of water absorption of very fine particles using electrical resistivity. *ACI Materials Journal*.

Kong, J. S., Ababneh, A. N., Frangopol, D. M., & Xi, Y. (2002). Reliability analysis of chloride penetration in saturated concrete. *Probabilistic Engineering Mechanics*, *17*(3), 305–315.

Lataste, J. F., Sirieix, C., Breysse, D., & Frappa, M. (2003). Electrical resistivity measurement applied to cracking assessment on reinforced concrete structures in civil engineering. *NDT and E International*, *36*(6), 383–394.

Layssi, H., Ghods, P., Alizadeh, A. R., & Salehi, M. (2015). Electrical Resistivity of Concrete. *Concrete International*, (MAY), 1–33.

Leelalerkiet, V., Kyung, J. W., Ohtsu, M., & Yokota, M. (2004). Analysis of half-cell potential measurement for corrosion of reinforced concrete. *Construction and Building Materials*, *18*(3), 155–162.

Litzner, H.-U., & Becker, A. (1998). Design of Concrete Structures for Durability and strength to Eurocode 2. *Materials and Structures*, *32*, 323–330.

Liu, T., & Weyers, R. . (1998). Modeling the Dynamic Corrosion Process in Chloride Contaminated Concrete Structures. *Cement and Concrete Research*, *28*(3), 365–379.

Lopez, W., & Gonzalez, J. A. (1993). Influence of the degree of pore saturation on the resistivity of concrete and the corrosion rate of steel reinforcement. *Cement and Concrete Research*, *23*(2), 368–376.

Lu, C. H., Gao, Y., & Liu, R. G. (2014). Effect of Transverse Crack on Chloride Penetration into Concrete Subjected to Drying – Wetting Cycles. In *4th International conference on the Durability of Concrete Structures* (pp. 169–175). Indiana, USA.

Lu, Y., Garboczi, E., Bentz, D. P., & Davis, J. (2012). Modeling chloride transport in cracked concrete: a 3-D image–based microstructure simulation. *COMSOL Conference 2012, Boston, MA, USA*, 1–15.

Mackechnie, J. R., & Alexander, M. G. (2001). *Repair principles for corrosion-damaged reinforced concrete structures*. *Research Monograph*. Cape Town.

Mangat, P. S., Khatib, J. M., & Molloy, B. T. (1994). Microstructure, chloride diffusion and reinforcement corrosion in blended cement paste and concrete. *Cement and Concrete Composites*, *16*(2), 73–81.

Mansfeld, F. (1976). The Polarization Resistance Technique for Measuring Corrosion Currents. In M. G. Fontana & R. W. Staehle (Eds.), *Advances in Corrosion Science and Technology: Volume 6* (pp. 163–262). Boston, MA: Springer US.

Marcotte, T. D., & Hansson, C. M. (2007). Corrosion products that form on steel

within cement paste. *Materials and Structures*, *40*, 325–340.

Marcotte, Tracy Dawn. (2001). *Characterization of Chloride-Induced Corrosion Products that form in Steel-Reinforced Cementitious Materials*. University of Waterloo.

Martin-Perez, B., Zibara, H., Hooton, R. D., & Thomas, M. D. A. (2000). A study of the effect of chloride binding on service life predictions. *Cement and Concrete Research*, *30*, 1215–1223.

Martín-Pérez, B., Pantazopoulou, S. J., & Thomas, M. D. a. (2001). Numerical solution of mass transport equations in concrete structures. *Computers & Structures*, *79*(13), 1251–1264.

Maslehuddin, M. (1996). Effect of temperature on pore solution chemistry and reinforcement corrosion in contaminated concrete. *Royal Society of Chemistry, Thomas Graham House, Science Park, Cambridge CB4 4WF*, 68–75.

Michel, A., Solgaard, A. O. S., Pease, B. J., Geiker, M. R., Stang, H., & Olesen, J. F. (2013). Experimental investigation of the relation between damage at the concrete-steel interface and initiation of reinforcement corrosion in plain and fibre reinforced concrete. In *Corrosion Science* (Vol. 77, pp. 308–321). Elsevier Ltd.

Mohammed, T. U., & Hamada, H. (2003). Relationship between free chloride and total chloride contents in concrete. *Cement and Concrete Research*, *33*(9), 1487–1490.

Mohammed, Tarek Uddin, Otsuki, N., & Hamada, H. (2003). Corrosion of Steel Bars in Cracked Concrete under Marine Environment. *Journal of Materials in Civil Engineering*, *15*(10), 460–469.

Mohammed, Tarek Uddin, Otsuki, N., Hamada, H., & Yamaji, T. (2002). Chloride-Induced Corrosion of Steel Bars in Concrete with Presence of Gap at Steel-Concrete Interface. *ACI Materials Journal*, *99*(2), 149–156.

Mohammed, Tarek Uddin, Otsuki, N., Hisada, M., & Shibata, T. (2001). Effect of Crack Width and Bar Types on Corrosion of Steel in Concrete. *Journal of Materials in Civil Engineering*, *13*(3), 194–201.

Monfore, G. (1968). The electrical resistivity of concrete. *Journal of The PCA Research and Development Laboratories*, *10*(2), 35–48.

Morga, M., & Marano, G. C. (2015). Chloride Penetration in Circular Concrete Columns. *International Journal of Concrete Structures and Materials*, *9*(2), 173–183.

Morris, W., Moreno, E. I., & Sagüés, A. (1996). Practical Evaluation of Resistivity of Concrete in Test Cylinders Using A Wenner Array Probe. *Cement and Concrete Research*, *26*(12), 1779–1787.

Morris, W., Vico, A., Vazquez, M., & Sanchez, S. R. De. (2002). Corrosion of

reinforcing steel evaluated by means of concrete resistivity measurements. *Corrosion Science*, *44*, 81–99.

Mutale, L. (2014). *An investigation into the relationship between surface concrete resistivity and chloride conductivity tests*. University of Cape Town, South Africa.

Muthulingam, S., & Rao, B. N. (2015a). Non-uniform corrosion states of rebar in concrete under chloride environment. *Corrosion Science*, *93*, 267–282.

Muthulingam, S., & Rao, B. N. (2015b). Numerical assessment of non-uniform corrosion scenarios of rebar in concrete exposed to natural chloride environment. *Indian Academy of Sciences*, *40;* (June), 1313–1341.

Nanukuttan, S. V, Basheer, P. A. M., Mccarter, W. J., Tang, L., Holmes, N., Chrisp, T. M., … Magee, B. (2015). The performance of concrete exposed to marine environments : Predictive modelling and use of laboratory / on site test methods. *Construction and Building Materials*, *93*, 831–840.

Němeček, J., Kruis, J., Koudelka, T., & Krejčí, T. (2018). Simulation of chloride migration in reinforced concrete. *Applied Mathematics and Computation*, *319*, 575–585.

Neville, A. (1995). Chloride Attack of Reinforcement Concrete: An Overview. *Materials and Structures*, *28*, 63–70.

Oh, B. H., & Jang, S. Y. (2007). Effects of material and environmental parameters on chloride penetration profiles in concrete structures. *Cement and Concrete Research*, *37*(1), 47–53.

Osterminski, K., Polder, R., & Schießl, P. (2008). Long term behaviour of the resistivity of concrete. *Heron*, *53*(1), 59–78.

Otieno, M. B. (2010). *Transport mechanisms in concrete. Corrosion of steel in concrete (initiation, propagation & factors affecting). University of Cape Town*. University of Cape Town.

Otieno, M. B. (2012). *The Development of Empirical Chloride-induced Corrosion Rate Prediction Models for Cracked and Uncracked Steel Reinforced Concrete Structures in the Marine Tidal Zone University*. University of Cape Town.

Otieno, M., Beushausen, H., & Alexander, M. (2012). Prediction of corrosion rate in reinforced concrete structures - A critical review and preliminary results. *Materials and Corrosion*, *63*(9), 777–790.

Otieno, M., Beushausen, H., & Alexander, M. (2015). Resistivity-based chloride-induced corrosion rate prediction models and hypothetical framework for interpretation of resistivity measurements in cracked RC structures. *Materials and Structures*, *49*(6), 1–18.

Otieno, M., Beushausen, H., & Alexander, M. (2016a). Chloride-induced corrosion

of steel in cracked concrete—Part II: Corrosion rate prediction models. *Cement and Concrete Research*, *79*, 386–394.

Otieno, M., Beushausen, H., & Alexander, M. (2016b). Chloride-induced corrosion of steel in cracked concrete - Part I: Experimental studies under accelerated and natural marine environments. *Cement and Concrete Research*, *79*, 373–385.

Otieno, Mike. (2008). *Corrosion Propagation in Cracked and Un-cracked Concrete*. Univeristy of Cape Town.

Otieno, Mike, Beushausen, H., & Alexander, M. (2011). Prediction of corrosion rate in RC structures - A critical review. *RILEM Bookseries*, *5*(9), 15–37.

Pacheco, J. F. (2015). *Corrosion of steel in cracked concrete- Chloride microanalysis and service life predictions*. Delft University of Technology.

Pacheco, J., Šavija, B., Schlangen, E., & Polder, R. B. (2012). Relationship Between Cracking and Electrical Resistance in Reinforced and Unreinforced Concrete . In G. Ye, K. van Breugel, S. Wei, & C. Miao (Eds.), *2nd International Conference on Microstructural-related Durability of Cementitious Composites* (pp. 458–466). Amsterdam, The Netherlands: Rilem Publ.

Page, C. L., & Havdahl, J. (1985). *Electrochemical monitoring of corrosion of steel in microsilica cement paste*. *Materials and Structures* (Vol. 18).

Page, C. L., & Vennesland, Ø. (1983). *Pore Solution Composition and Chloride Binding Capacity of Silica Fume Cement Pastes*. *Materiaux et Construction* (Vol. 16).

Papakonstantinou, K. G., & Shinozuka, M. (2013). Probabilistic model for steel corrosion in reinforced concrete structures of large dimensions considering crack effects. *Engineering Structures*, *57*, 306–326.

Park, R. M. (2009). A Guide to A Understanding Reference Electrode Readings. *Materials Performance*, 32–36.

Patterson, S. P., Daffner, R. H., & Gallo, R. a. (2005). *Fundamentals of Electrochemical Corrosion*.

PCA. (2001, January). Ettringite Formation and the Performance of Concrete. *Concrete Information*, (IS147), 1–7.

PCA. (2002). *Types and Causes of Concrete Deterioration*. *Concrete Information*.

Pease, B. J. (2010). *Influence of concrete cracking on ingress and reinforcement corrosion*. Technical University of Denmark.

Peng, L., & Stewart, M. G. (2015). Concrete In Australia. *Concrete Institute of Australia*, *41*(3), 36–47.

Pillai, R. G., Karuppanasamy, J., Dhanya, B. S., & Nair, S. A. O. (2015). Enhancing

the corrosion resistance of reinforced concrete structures – Indian scenario and challenges ahead. In S. Degan, M. Lau, A. Kulkarni, V. K. Saraswat, R. Chalker, J. Feather, U. K. Mudali (Eds.), *CORCON*. Chennai, India: Corrosionpedia.

Polder, R. B., Peelen, W. H. a., Stoop, B. T. J., & Neeft, E. a. C. (2011). Early stage beneficial effects of cathodic protection in concrete structures. *Materials and Corrosion*, *62*(2), 105–110.

Polder, Rob B. (2001). Test methods for on site measurement of resistivity of concrete - a RILEM TC-154 technical recommendation. *Construction and Building Materials*, *15*(2–3), 125–131.

Polder, Rob B. (2012). Effects of slag and fly ash on reinforcement corrosion in concrete in chloride environment - Research from the Netherlands. *HERON*, *57*(3), 197–210.

Poon, C. S., Wong, Y. L., & Lam, L. (1997). The influence of different curing conditions onthe pore structure and related properties of fly-ash cement pastes and mortars. *Construction and Building Materials*, *11*(7–8), 383–393.

Popov, B. N. (2015). *Corrosion Engineering: Principles and Solved Problems*. *Corrosion Engineering: Principles and Solved Problems*. Oxford, OX5 1GB, UK: Elsevier Science & Technology Books. Portland Cement Association, Portland Cement Asscociation, & Portland Cement Association. (2018). Supplementary Cementing Materials.

Poulsen, E., & Mejlbro, L. (2006). *Diffusion of Chloride in Concrete: Theory and Application*. (A. Bentur & S. Mindness, Eds.). London and New York: Taylor & Francis Group.

Poulsen, S. L., & Sørensen, H. E. (2012). Chloride Threshold Values - State of the art. *Danish Expert Centre for Infrastructure Constructions*, 0–33.

Poupard, O., L'Hostis, V., Bouteiller, V., Capra, B., Catinaud, S., Francois, D., … Tache, G. (2007). Corrosion diagnosis of reinforced concrete beams after 40 years exposure in marine environment by non destructive tools. *Revue Européenne de Génie Civil*, *11*(1–2), 35–54.

Poursaee, A. (2010). Potentiostatic transient technique, a simple approach to estimate the corrosion current density and Stern-Geary constant of reinforcing steel in concrete. *Cement and Concrete Research*, *40*(9), 1451–1458.

Ramaniv, O. N., Tsirul'nik, A. T., Krys'kiv, A. S., & Ronchevich, I. C. (1989). Electrochemical Methods In Corrosion Monitoring of Metals (Review). *Soviet Materials Science*, *25*(1), 1–12.

Ranade, R., Zhang, J., Lynch, J. P., & Li, V. C. (2014). Influence of micro-cracking on the composite resistivity of Engineered Cementitious Composites. *Cement and Concrete Research*, *58*, 1–12.

Raupach, M. (1996a). Chloride-induced macrocell corrosion of steel in concrete -

Theoretical background and practical consequences. *Construction and Building Materials*, *10*(5), 329–338.

Raupach, M. (1996b). Investigations on the influence of oxygen on corrosion of steel in concrete—Part 1. *Materials and Structures*, *29*(3), 174–184.

Raupach, M. (2006). Patch repairs on reinforced concrete structures - Model investigations on the required size and practical consequences. *Cement and Concrete Composites*, *28*(8), 679–684.

Richard, B., Ragueneau, F., Cremona, C., Adelaide, L., & Tailhan, J. L. (2010). A three-dimensional steel/concrete interface model including corrosion effects. *Engineering Fracture Mechanics*, *77*(6), 951–973.

RILEM TC 154-EMC. (2004). "Electrochemical Techniques for measuring metallic corrosion": Test methods for on-site corrosion rate measurement of steel reinforcement in concrete by means of the polarization resistance method. *Materials and Structures*, *37*(9), 623–643.

RILEM TC 178. (2002). RILEM Technical Committees RILEM Tc 178-Tmc : ' Testing and modelling chloride penetration in concrete''.' *Materials and Structures*, *35*(November 2002), 586–588.

Rodriguez, J., Ortega, L. M., Casal, J., & Diez, J. M. (1996). Assessing structural conditions of concrete structures with corroded reinforcement. In R. K. Dhir & M. R. Jones (Eds.), *Conference, Concrete repair, rehabilitation and protection* (p. 434). Dundee, UK: fib Fédération internationale du béton.

Rodríguez, O. G., & Hooton, R. D. (2003). Influence of cracks on chloride ingress into concrete. *American Concrete Institute*, *100*(2), 120–126.

Rodríguez, O. G., Hooton, R. D., Rodriguez, O. G., Hooton, R. D., Rodríguez, O. G., & Hooton, R. D. (2003). Influence of cracks on chloride ingress into concrete. *American Concrete Institute*, *100*(2), 120–126.

Rodríguez, P., Ramirez, E., Feliu, S., Gonzalez, J. A., & Lopez, W. (1999). Significance of coplanar macrocells to corrosion in concrete-embedded steel. *Corrosion*, *55*(3), 319–325.

SABS 0100-1. (2000). *South African Standard The structural use of concrete Part 1: Design (Edition 2.2, 2000)*.

Saleem, M., Shameem, M., Hussain, S. E., & Maslehuddin, M. (1996). Effect of moisture, chloride and sulphate contamination on the electrical resistivity of Portland cement concrete. *Construction and Building Materials*, *10*(3), 209–214.

Sandberg, P. (1996). *Durability of concrete in saline environment*. Lund, Sweden: Cementa.

SANS 210: (2008). *SOUTH AFRICAN NATIONAL STANDARD Sieve analysis fines , content and dust content of aggregates*.

SANS 3001-CO3-1. (2015). *Part CO3-1: Concrete durability inde testing - Preparation of test specimens*.

SANS 3001-CO3-2: Part CO3-2: Concrete durability index testing - Oxygen permeability test (2015).

SANS 3001-CO3-3. Concrete durability index testing - Chloride conductivity test (2015).

SANS 50197-1. (2013). *SANS 50197-1 : 2013 EN 197-1 : 2011 Part 1 : Composition , specifications and conformity criteria for common cements*. Pretoria.

SCA. (2003). *Slag Cement Association: Suggested Specifications for Slag Cement in Concrete*. Georgia, USA.

Schießl, P., & Raupach, M. (1997). Laboratory studies and calculations on the influence of crack width on chloride-induced corrosion of steel in concrete. *ACI Materials Journal*, *94*(1), 56–61.

Scott, A. N. (2004). *The Influence of Binder Type and Cracking on Reinforcing Steel Corrosion in Concrete*. University of Cape Town.

Scott, A. N., & Alexander, M. G. (2007). The influence of binder type, cracking and cover on corrosion rates of steel in chloride-contaminated concrete. *Magazine of Concrete Research*, *59*(7), 495–505.

Sengul, O., & Gjørv, O. E. (2008). Electrical Resistivity Measurements for Quality Control During Concrete Construction. *ACI Materials Journal*, *105*(6), 541–547.

Shazali, M. A., Rahman, M. K., & Baluch, M. H. (2010). Modeling University of Cape Town chloride conduction test for concrete. In A. Zingoni (Ed.), *SEMC 2010 : The 4th International Conference on Structural Engineering Mechanics and Computation* (pp. 909–912). London: Taylor & Francis Group.

Shen, Q., & Yang, R. (2015). Thompson-Tau outlier detection method for Detecting Abnormal Data of Listed Pharmaceutical companies in China. In *2015 8th International Symposium on Computational Intelligence and Design (ISCID)* (Vol. 1, pp. 379–382). Hangzhou, China,12-13 December, 2015: IEEE.

Shi, X., Xie, N., Fortune, K., & Gong, J. (2012). Durability of steel reinforced concrete in chloride environments: An overview. *Construction and Building Materials*, *30*, 125–138.

Sonjoy, D. (2012). Critical Chloride Content in Reinforced Concrete. *The Masterbuilder*, (August 2012), 58–66.

Sørensen, J. D., & Frier, C. (2004). Stochastic Modeling of Reinforced Concrete Structures Exposed to Chloride Attack. In *Life-Cycle Performance of Deteriorating Structures: Assessment, Design, and Management* (pp. 175–182).

Soutsos, M., Breysse, D., Garnier, V., Gonçalves, A. F., & Monteiro, A. V. (2012). *Non-Destructive Assessment of Concrete Structures: Reliability and Limits of Single and Combined Techniques*. *State-of-the-Art Report of the RILEM Technical Committee 207-INR, Non-Destructive Assessment of Concrete Structures: Reliability and Limits of Single and Combined Techniques*.

Söylev, T. A., & François, R. (2005). Corrosion of Reinforcement in Relation to Presence of Defects at the Interface between Steel and Concrete. *Journal of Materials in Civil Engineering*, *17*(August), 447–455.

Spragg, R., Bu, Y., Snyder, K., Bentz, D., & Weiss, J. (2013). *Electrical Testing of Cement-Based Materials: Role of Testing Techniques, Sample Conditioning*. *FHWA/IN/JTRP-2013/28. Joint Transportation Research Program, Indian Department of Transportation and Purdue University, West Lafayette, Indiana*.

Su, J. K., Yang, C. C., Wu, W. B., & Huang, R. (2002). Effect of moisture content on concrete resistivity measurement. *Journal of the Chinese Institute of Engineers, Transactions of the Chinese Institute of Engineers,Series A/Chung-Kuo Kung Ch'eng Hsuch K'an*, *25*(1), 117–122.

Suryavanshi, A. K., & Swamy, R. N. (1996). Stability of Fridel's Salt in Carbonated Concrete Structural Elements. *Cement and Concrete Research*, *26*(5), 729–741.

Suzuki, M., Kanno, K.-I., & Sato, Y. (1980). An application of the coulostatic method to corrosion rate measurements. *Wertstoffe Und Korrosion*, *31*, 364–370.

Thomas, M. (2007). Optimizing the Use of Fly Ash in Concrete. *Portland Cement Association*, 24.

Torres-Luque, M., Bastidas-Arteaga, E., Schoefs, F., Sánchez-Silva, M., & Osma, J. F. (2014). Non-destructive methods for measuring chloride ingress into concrete: State-of-the-art and future challenges. *Construction and Building Materials*, *68*, 68–81.

Tran, N. T., & Huang, Q. (2006). *Influence of Cracks on Chloride-Induced Corrosion in Reinforced Concrete Structures*. Chalmers University of Technology, Gothenburg, Sweden.

Tromans, D. (1980). Anodic Polarization Behavior of Mild Steel in Hot Alkaline Sulfide Solutions. *Journal of The Electrochemical Society*, *127*(6), 1253–1253.

Tuutti, K. (1982). *Corrosion of steel in concrete*. *Swedish Cement and Concrete Research Institute*. Royal Institute of Technology, Stockholm, Stockholm.

Val, D. V., & Trapper, P. A. (2006). Probabilistic evaluation of time to corrosion initiation in RC elements exposed to chlorides: 2-D modelling. In *3rd International Conference on Bridge Maintenance, Safety and Management - Bridge Maintenance, Safety, Management, Life-Cycle Performance and Cost*

(pp. 527–528).

Val, Dimitri V., & Trapper, P. A. (2008). Probabilistic evaluation of initiation time of chloride-induced corrosion. *Reliability Engineering and System Safety*, *93*(3), 364–372.

Valentini, C., Berardo, L., & Alanis, I. (1990). Influence of Blast Furnace Slags on the Corrosion Rate of Steel in Concrete. In *Corrosion Rates of Steel in Concrete* (pp. 17–28). Philedelphia: American Society for Testing and Materials (ASTM) International.

Verma, S. K., Bhadauria, S. S., & Akhtar, S. (2014). Probabilistic Evaluation of Service Life for Reinforced Concrete Structures, *2014*.

Wei, X., & Xiao, L. (2011). Influence of the aggregate volume on the electrical resistivity and properties of portland cement concretes. *Journal Wuhan University of Technology, Materials Science Edition*, *26*(5), 965–971.

Woelfl, G., & Lauer, K. (1979). The Electrical Resistivity of Concrete with Emphasis on the Use of Electrical Resistance for Measuring Moisture Content BT - The Electrical Resistivity of Concrete with Emphasis on the Use of Electrical Resistance for Measuring Moisture Content.

Wu, Z., Wong, H. S., Buenfeld, N. R., Wu, Z., Wong, H. S., & Buenfeld, N. R. (2014). Effect of confining pressure and microcracks on mass transport properties of concrete. *Advances in Applied Ceramics*, *113*(8), 485–495.

Yang, L. F., Chen, Z., Gao, Q., & Ju, J. W. (2012). Compensation length of two-dimensional chloride diffusion in concrete using a boundary element model. *Acta Mechanica*, *224*(1), 123–137.

Ye, H., Fu, C., Jin, N., & Jin, X. (2018). Performance of reinforced concrete beams corroded under sustained service loads : A comparative study of two accelerated corrosion techniques. *Construction and Building Materials*, *162*, 286–297.

Yoon, S., Wang, K., Weiss, W. J., & Shah, S. P. (2000). Interaction between Loading, Corrosion, and Serviceability of Reinforced Concrete. *ACI Materials Journal*, *97*(6), 637–644.

Yu, B., Liu, J., & Chen, Z. (2017). Probabilistic evaluation method for corrosion risk of steel reinforcement based on concrete resistivity. *Construction and Building Materials*, *138*, 101–113.

Yu, B., Yang, L., Wu, M., & Li, B. (2014). Practical model for predicting corrosion rate of steel reinforcement in concrete structures. *Construction and Building Materials*, *54*, 385–401.

Yuan, Q., Shi, C., De Schutter, G., Audenaert, K., & Deng, D. (2009). Chloride binding of cement-based materials subjected to external chloride environment – A review. *Construction and Building Materials*, *23*(1), 1–13.

Yuan, Q., Shi, C., Schutter, G. De, & Audenaert, K. (2009). Effect of temperature on transport of chloride ions in concrete. *Concrete Repair, Rehabilitation and Retrofitting II*, *1*(1), 345–352.

Zhang, R., Castel, A., & François, R. (2009). The corrosion pattern of reinforcement and its influence on serviceability of reinforced concrete members in chloride environment. *Cement and Concrete Research*, *39*(11), 1077–1086.

Zhang, R., Castel, A., & François, R. (2010). Concrete cover cracking with reinforcement corrosion of RC beam during chloride-induced corrosion process. *Cement and Concrete Research*, *40*(3), 415–425.

Zhang, Y., Sun, W., Chen, S., & Guo, F. (2011). Two- and three-dimensional chloride ingress into fly ash concrete. *Journal of Wuhan University of Technology-Mater. Sci. Ed.*, *26*(5), 978–982.

Zhang, Y., Sun, W., Liu, Z., & Chen, S. (2011). One and two dimensional chloride ion diffusion of fly ash concrete under flexural stress. *Journal of Zhejiang University - SCIENCE A (Applied Physics & Engineering)*, *12*(9), 692–701.

Zhao, Y., Hu, B., Yu, J., & Jin, W. (2011). Non-uniform distribution of rust layer around steel bar in concrete. *Corrosion Science*, *53*(12), 4300–4308.

Zivica, V. (2002). Significance and influence of the ambient temperature as a rate factor of steel reinforcement corrosion. *Bulletin of Materials Science*, *25*(5), 375–379.

Appendix A: Data analysis

Appendix A. 1: Introduction

This chapter discusses the methods used in analyzing the data collected from the corrosion monitoring techniques mentioned in Chapter 3. These techniques include;

a. Outlier identification, and
b. Moving average computation.

Appendix A. 2: Outlier identification

An outlier is an observation that is substantially different from the population; hence it tends not to be representative of the population. In this study, the modified Thompson Tau's test was used to identify potential outliers in the collated data. The method essentially tests one potential outlier at a time using the T-test. The procedure is repeated until all the identified outliers are deleted from the data set. This outlier identification technique is suitable for use in data that range from 3 to over 5000. The method identifies potential outliers by comparing the deviation of the data from the data set mean and their standard deviation. The parameter which is used in identifying the data in the rejection region (Tau (τ)) is computed from T critical values of the student's T-distribution (Shen & Yang, 2015). The modified Thompson Tau's table can be used, or Eqn. A.1 can be used to compute and subsequently identify data which is in the rejection region.

$$\tau = \frac{t\,.(n-1)}{\sqrt{n}\sqrt{n-2+t^2}} \qquad \text{A.1}$$

Where *n* is the number of data points or sample size,

t is the student's *T* critical value

Despite the use of this method to identify potential outliers in the measured corrosion parameters, the result of the outlier identification was interpreted with caution to avoid deleting data which may be classified as unusual (an outlier) due to clustering of the outliers. It must be mentioned that in some instances, discretion was used in retaining data which may have been detected to be an outlier, since removing such may distort the trend of earlier collected data. Except otherwise

mentioned, Appendix A. 2:, gives specific details of how the Thompson Tau's outlier identification technique was used to analyze the data collected.

Appendix A. 3: Data collation and analysis

Appendix A. 3. 1: Half-cell potential data analysis

In each cycle, a single HCP reading was recorded per specimen after which an average of the data collated per specimen set (say F1D-C-M1, F1D-C-M2, and F1D-C-M3) is computed (see Eqn. A.2).

The HCP data were not subjected to the outlier test since the corrosion potential of the specimens (per set) did not differ significantly. In a few instances, specimens which had readings that differed from the mean data in their specimen set were easily identified and such data eliminated. The corrosion potential per specimen set was computed from the mean of at least 2 or 3 specimens (see Eqn. A.2).

$$\text{Average monitored data per specimen set} = \left(\frac{A_1 + A_2 + A_3}{n}\right) \qquad \text{A.2}$$

A_1, A_2, and A_3 are the data recorded per specimen (e.g. F1D-C-M1, F1D-C-M2, and F1D-C-M3) in a set, while n is the number of valid readings obtained from the specimens in a test set.

Appendix A. 3. 2: Resistivity data analysis

The resistivity of the concrete was monitored using both the Wenner probe and the electrode-disc method.

In the electrode-disc method, the concrete resistivity was obtained after conducting a single test while with the Wenner probe; an average of three measurements taken about the center of the specimen was computed and recorded as the specimen concrete resistivity. In the cracked specimens, the resistivity was measured transversely across the crack which is located at the middle of the specimen. Taking measurements over reinforcement bars and close to the specimen edge was avoided (Gowers & Millard, 1999). The mean concrete resistivity per specimen set was computed as shown in Eqn. A.2.

Unlike the HCP measurements, the outlier test was separately conducted for the data obtained from specimens exposed to 1D and 2D chloride ingress. This outlier

detection grouping was adopted based on the assumption that for concrete of the same mix and chloride exposure (1D and 2D), the concrete resistivity will not vary significantly.

Appendix A. 3. 3: Corrosion rate data analysis

Three corrosion rate readings were obtained from each specimen; one each for the three reference electrodes on the Coulostat device (see Figure 3.14). Hence, the outlier detection data per specimen set consisted of nine (9) measurements (e.g. C_{11} – C_{33} shown in Table A. 1);

Table A. 1: Number of corrosion rate data recorded per specimen set

Reference electrode	Specimens		
	F1C1A	F1C1B	F1C1C
$*R_1$	C_{11}	C_{21}	C_{31}
$*R_2$	C_{12}	C_{22}	C_{32}
$*R_3$	C_{13}	C_{23}	C_{33}

Where $*R_{1-3}$, are reference electrodes and C_{11} – C_{33} are the corrosion rate measurements obtained from the reference electrodes

An average of the data which passed the outlier test was computed and utilized as the corrosion rate of the specimen set being considered.

Appendix A. 4: Data smoothing

After removal of outliers from the measured data, the moving average of the data is computed and plotted. The moving average method is a data smoothing technique which involves the removal of random variations in the data thereby revealing trends and cyclic components within a given data set. Though the simple moving average or exponential methods may be used, the simple moving average method was used in this study since the data did not appear to increase exponentially; the exponential method is used when the data increases exponentially while the simple averaging method is used to smooth data plots which appear to increase linearly. The moving average plots can also be used to forecast trends in the measured data. This method has been used by various authors in presenting monitored corrosion

data (Christian, 2013; M. Otieno et al., 2016b; Mike Otieno, 2008; Scott & Alexander, 2007).

Appendix A. 4. 1: Moving average

In general, the moving average gives an enhanced view of the data distribution. The moving average can be computed from two or more data points. In this study, a 3-point moving average of the data was computed and subsequently used in the data plots. The moving average is normally taken from an equal number of data on either side and plotted at the central value (see Eqn. A.3)

$$\mu_{i+1} = \frac{x_i + x_{i+1} + x_{i+2}}{3} \qquad \text{A.3}$$

Where μ_{i+1} is the moving average of the data, x_i, x_{i+1}, and x_{i+2}

Each data is multiplied by a uniform weight (i.e. 1/3).

All the plots that will be presented in Chapter 4 are moving averages plotted at the point i+1 with successive data points plotted at increments of i. Hence, the first and last data points are not plotted.

There are potential pitfalls which may arise when the moving average is used to process data. They include letting go off a significant amount of signal and the risk of inversion (e.g. the data may have a peak while the smoothed data appears to have a trough). The plot can also be devoid of being smooth when data with higher values are not identified and removed from the data set.

Appendix A. 5: Error bars

The error bars used are obtained from standard deviation of the data that is considered. A long error bar indicates a wide spread of the data about its mean while a short error bar indicates that most of the data lies close to its mean. The short error bars also indicate that the results are more reliable since it does not deviate significantly from the mean.

Appendix B: Corrosion measurement results

Appendix B. 1: Half-cell potential measurement plots

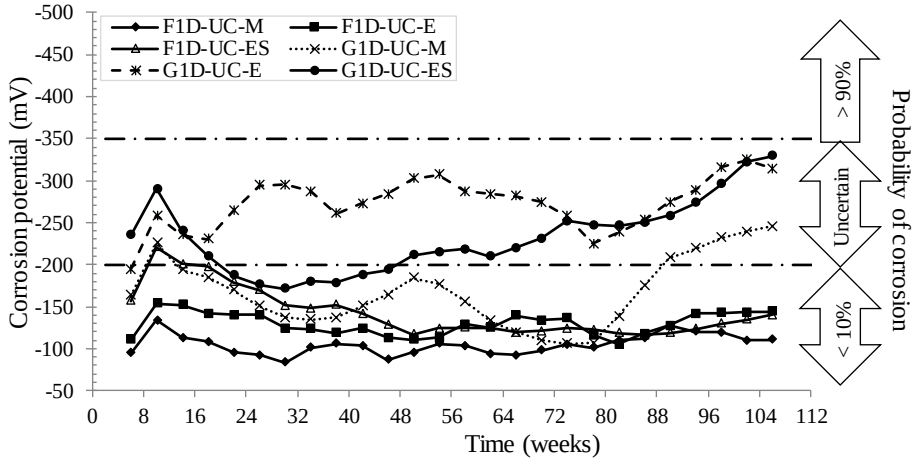


Figure B. 1**:** Half-cell potentials of uncracked PC/FA and PC/SL RC beam specimens exposed to 1D chloride ingress**.**

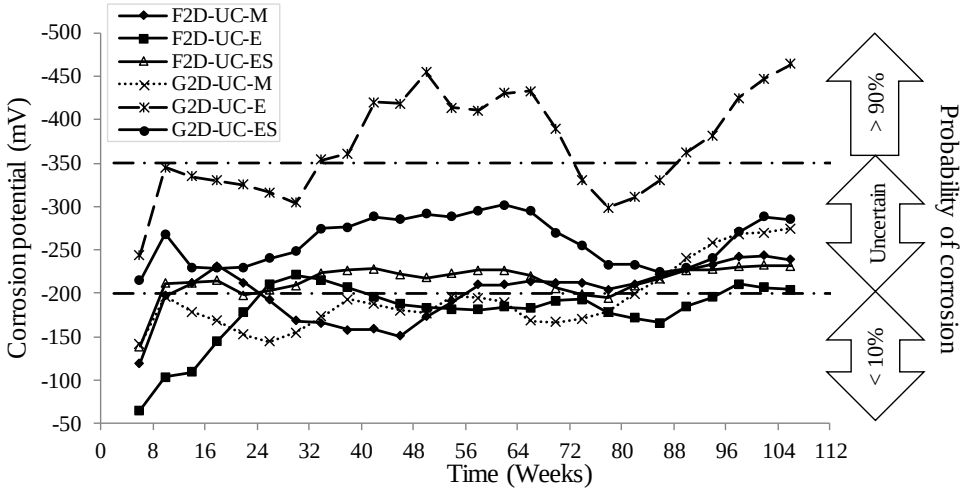


Figure B. 2: Half-cell potentials of uncracked PC/FA and PC/SL RC beam specimens exposed to 2D chloride ingress.

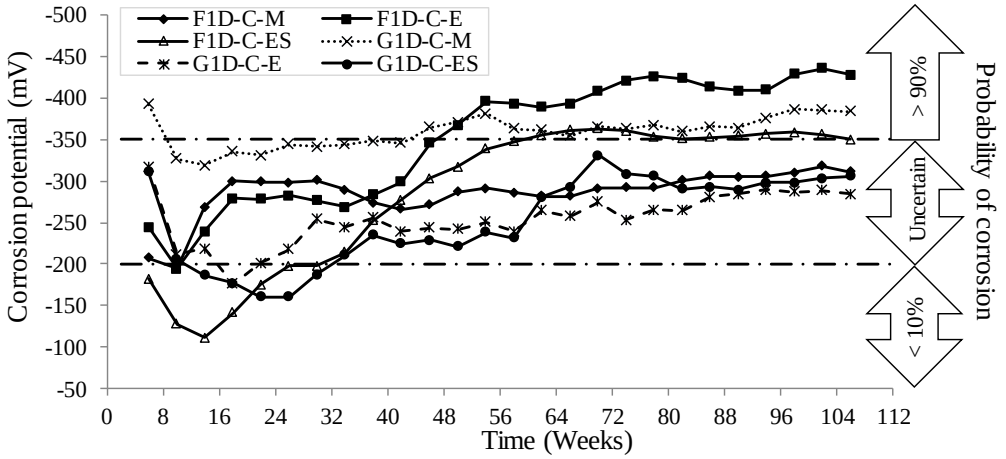


Figure B. 3: Half-cell potentials of cracked PC/FA and PC/SL RC beam specimens exposed to 1D chloride ingress.

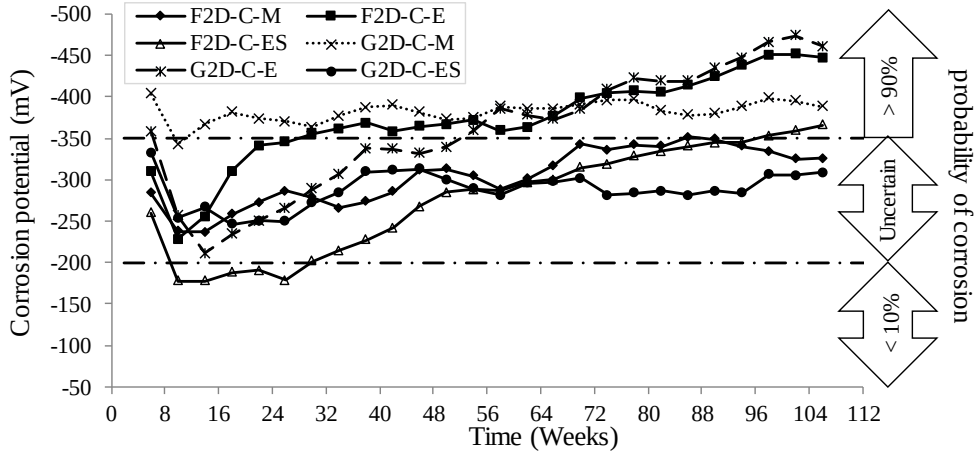


Figure B. 4: Half-cell potentials of cracked PC/FA and PC/SL RC beam specimens exposed to 2D chloride ingress.

Appendix B. 2: Corrosion rate measurement plots

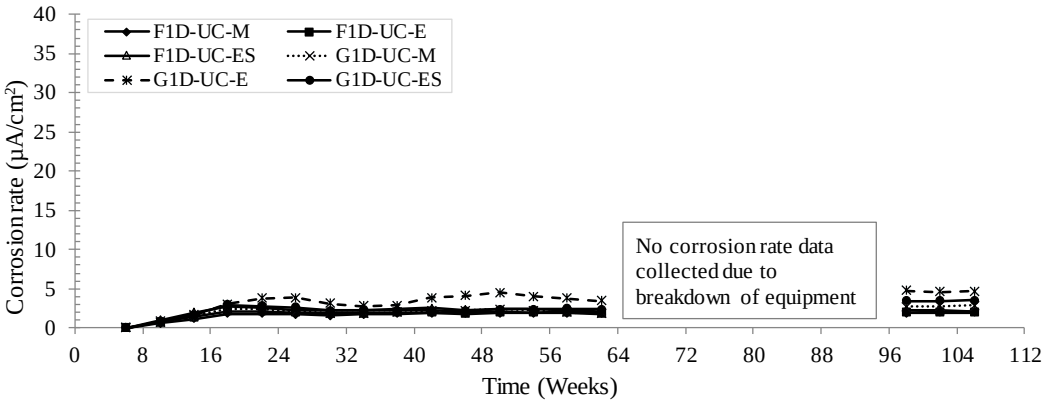


Figure B. 5**:** Corrosion rate of uncracked PC/FA and PC/SL RC beam specimens exposed to 1D chloride ingress.

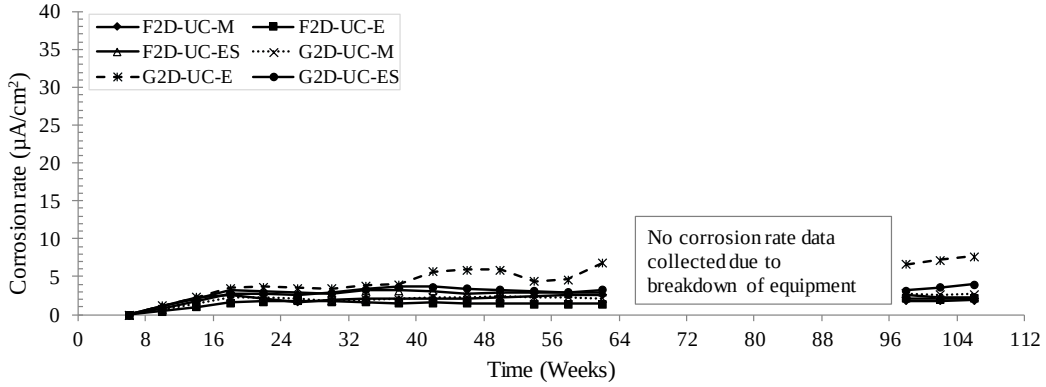


Figure B. 6**:** Corrosion rate of uncracked PC/FA and PC/SL RC beam specimens exposed to 2D chloride ingress.

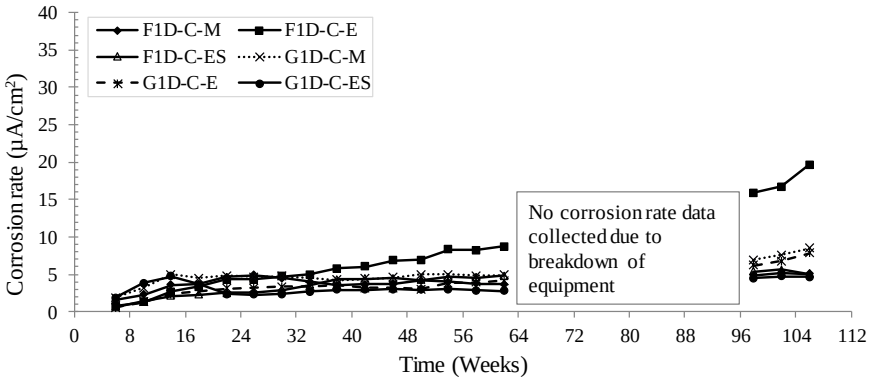


Figure B. 7: Corrosion rate of cracked PC/FA and PC/SL RC beam specimens exposed to 1D chloride ingress.

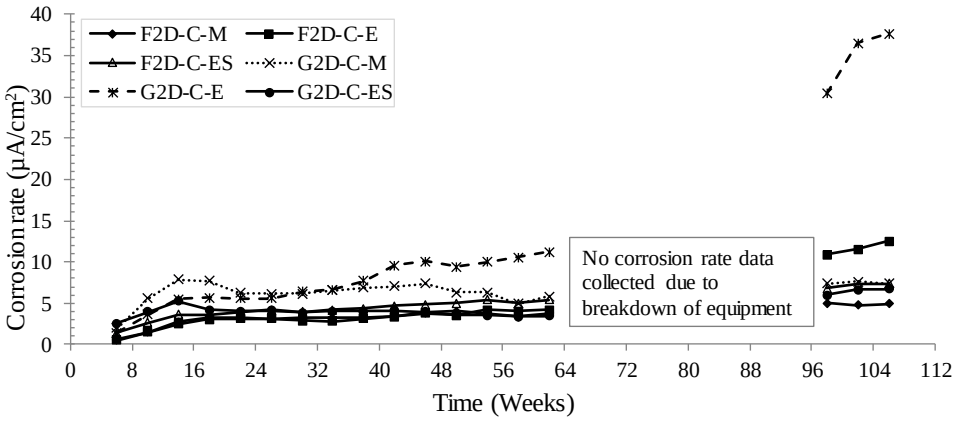


Figure B. 8: Corrosion rate of cracked PC/FA and PC/SL RC beam specimens exposed to 2D chloride ingress.

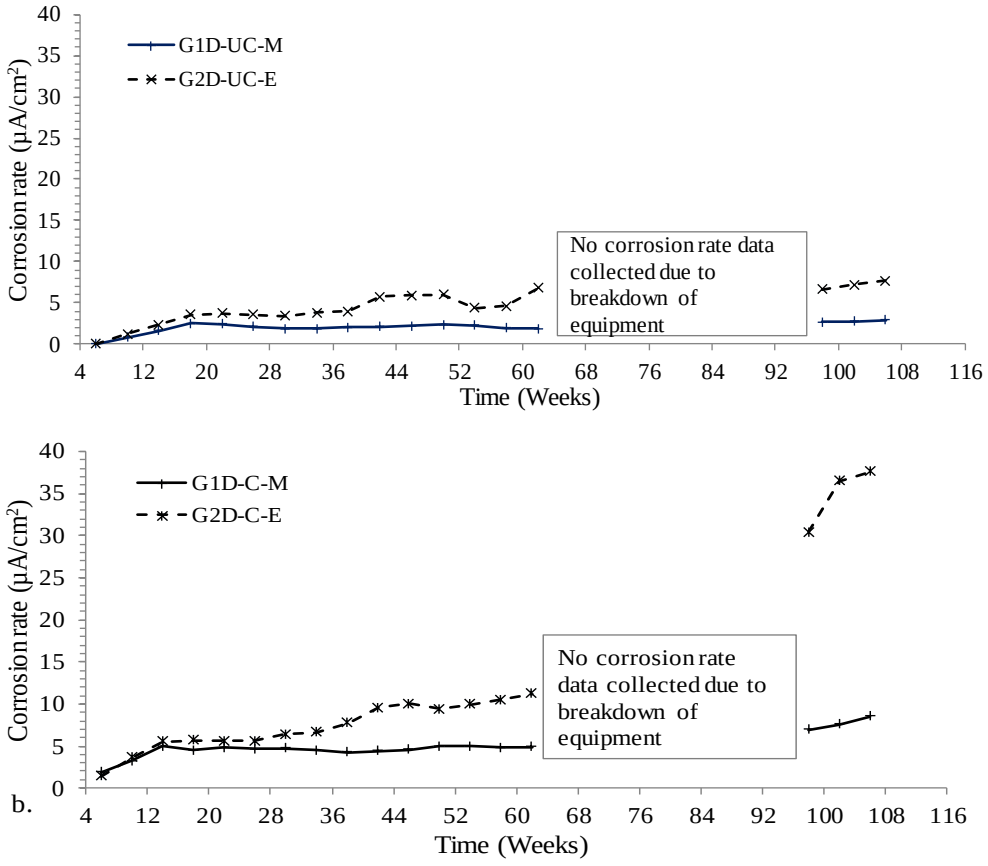


Figure B. 9: Corrosion rate of (a) uncracked and cracked (b) PC/SL concrete exposed to 1D and 2D chloride ingress

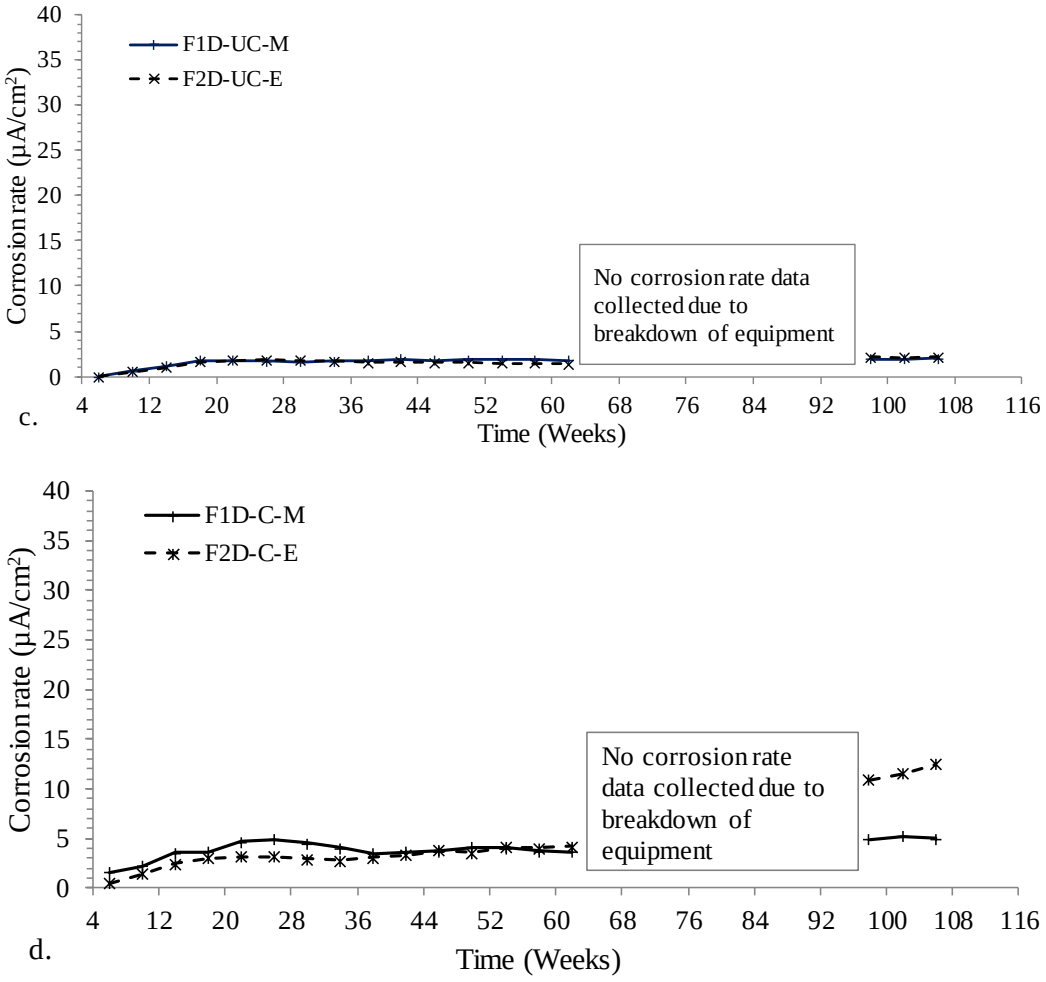
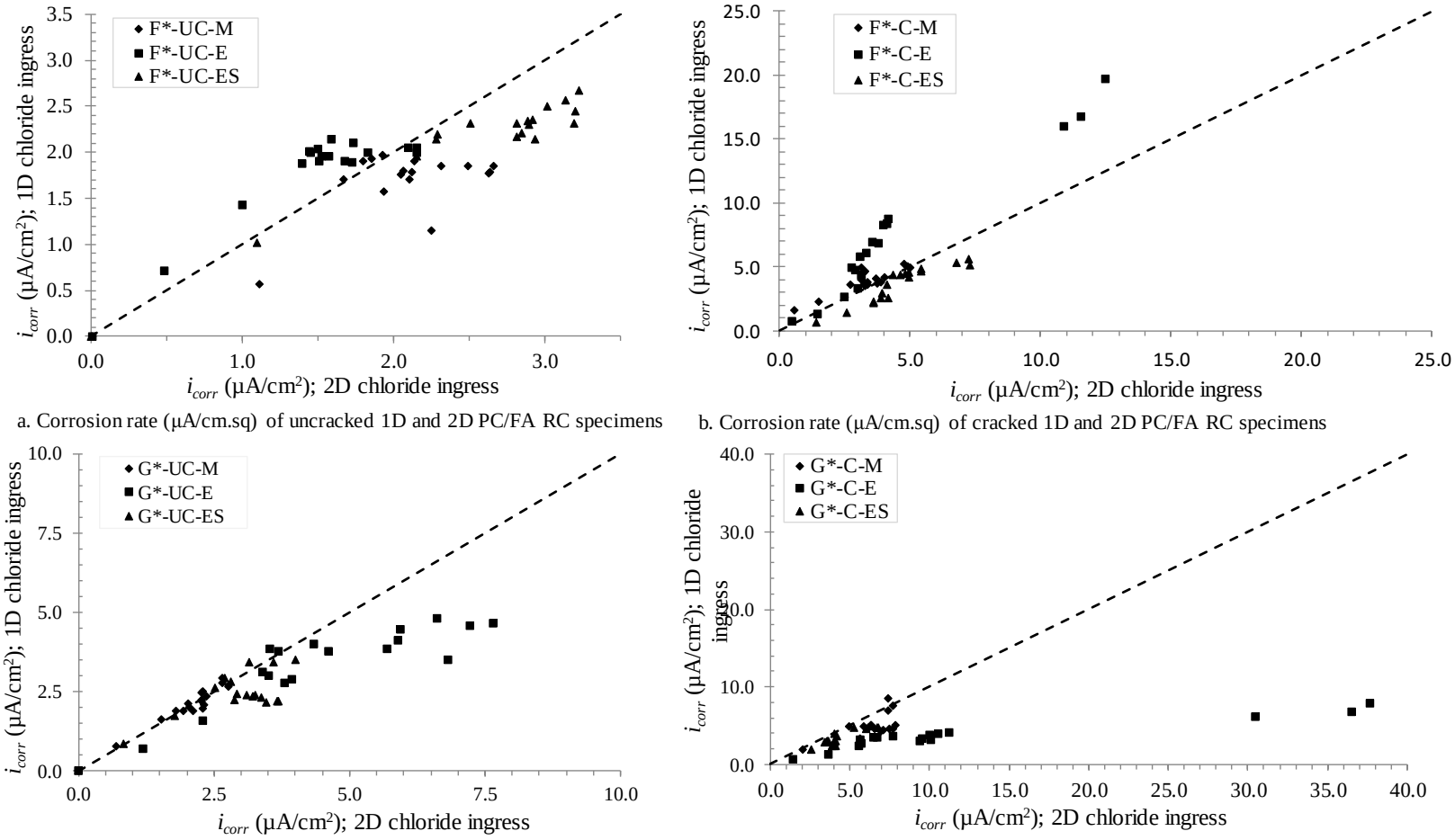


Figure B. 10: Corrosion rate of (a) uncracked and (b) cracked PC/FA concrete exposed to 1D and 2D chloride ingress



a. Corrosion rate (µA/cm.sq) of uncracked 1D and 2D PC/FA RC specimens

b. Corrosion rate (µA/cm.sq) of cracked 1D and 2D PC/FA RC specimens

c. Corrosion rate (µA/cm.sq) of uncracked 1D and 2D PC/SL RC specimens

c. Corrosion rate (µA/cm.sq) of cracked 1D and 2D PC/SL RC specimens

Figure B. 11: Corrosion rate of RC beam specimens exposed to 1D and 2D chloride ingress

Appendix B. 3: Concrete resistivity plots

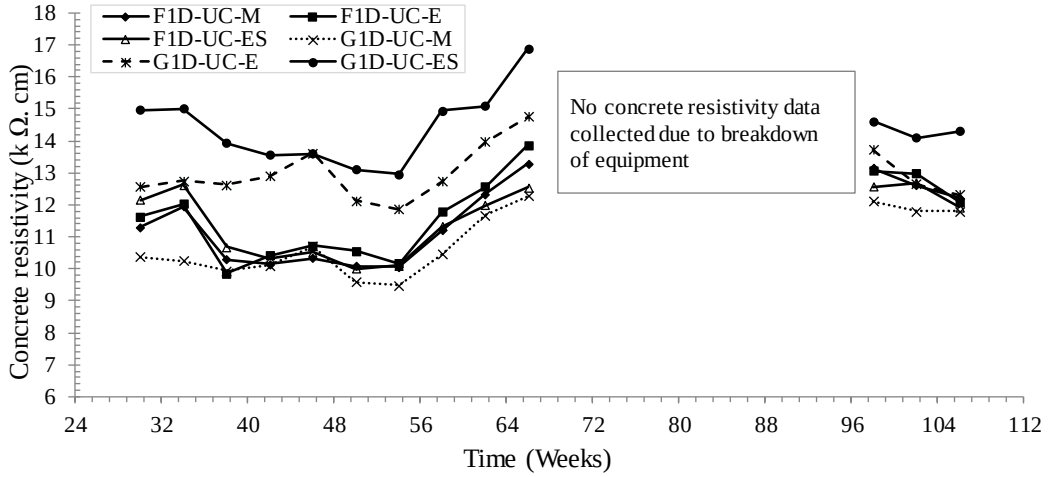


Figure B. 12: Concrete resistivity of uncracked PC/FA and PC/SL RC beam specimens exposed to 1D chloride ingress.

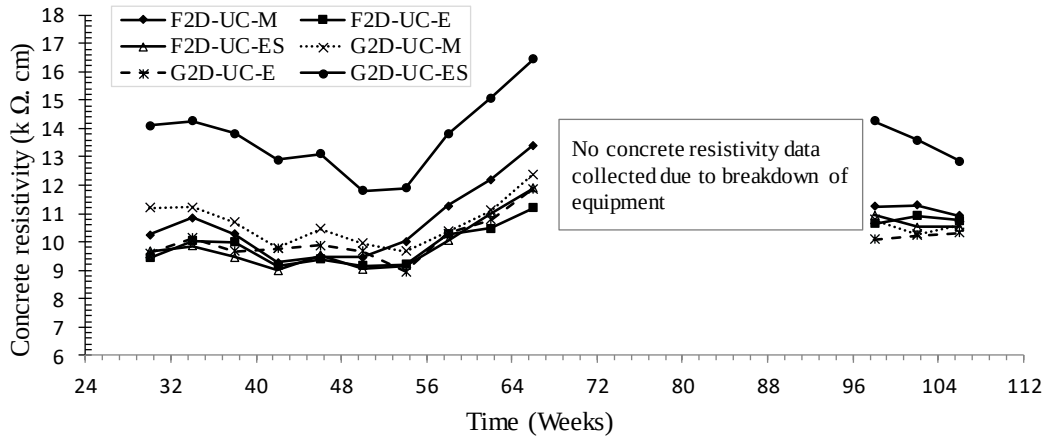


Figure B. 13: Concrete resistivity of uncracked PC/FA and PC/SL RC beam specimens exposed to 2D chloride ingress.

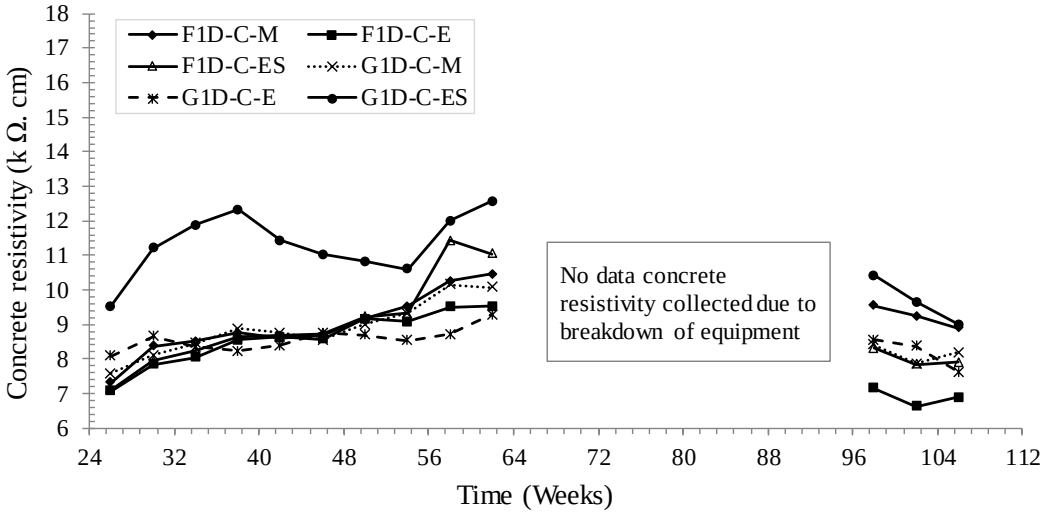


Figure B. 14**:** Concrete resistivity of cracked PC/FA and PC/SL RC beam specimens exposed to 1D chloride ingress.

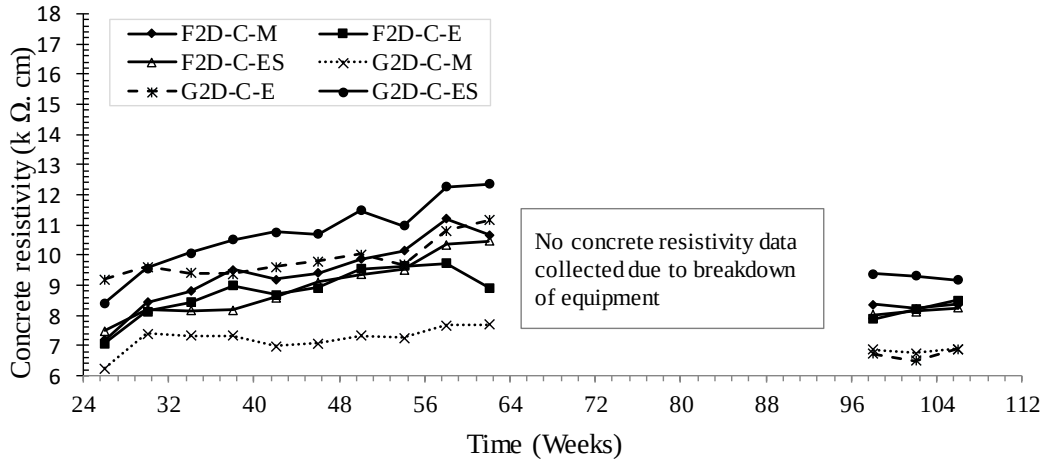


Figure B. 15: Concrete resistivity of cracked PC/FA and PC/SL RC beam specimens exposed to 2D chloride ingress.

Appendix C: Visual assessment – Corrosion-induced cracks

Appendix C. 1: Visual assessment - Crack-factors

Table C. 1: Crack width and length of PC/FA specimens exposed to 1D chloride ingress

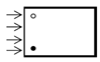
Specimens		Measured Parameters			Crack factor (mm.sq)
		Initial Crack width (mm)	Total length of corrosion induced crack (mm)	Corrosion-induced crack width (mm)	
	F1D-C-M1	0.26	118	0.04	4.72
	F1D-C-M2	0.20	64	0.08	5.12
	F1D-C-M3	0.26	24	0.02	0.48
	F1D-C-E1	0.30	226	0.40	90.40
	F1D-C-E2	0.30	180	0.50	90.00
	F1D-C-E3	0.38	136	0.22	29.92
	F1D-C-ES1	0.28	177	0.24	42.48
	F1D-C-ES2	0.20	51	0.10	5.10
	F1D-C-ES3	0.26	81	0.16	12.96

Table C. 2: Crack width and length of PC/SL specimens exposed to 1D chloride ingress

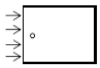
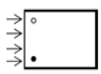
Specimens		Measured Parameters			Crack factor (mm.sq)
		Initial Crack width (mm)	Total length of corrosion induced crack (mm)	Corrosion-induced crack width (mm)	
	G1D-C-M1	0.36	44	0.08	3.52
	G1D-C-M2	0.36	154	0.24	36.96
	G1D-C-M3	0.28	106	0.10	10.60
	G1D-C-E1	0.28	72	0.22	15.84
	G1D-C-E2	0.26	240	0.60	144.00
	G1D-C-E3	0.26	47	0.06	2.82
	G1D-C-ES1	0.22	45	0.01	0.45
	G1D-C-ES2	0.20	81	0.06	4.86
	G1D-C-ES3	0.26	32	0.12	3.84

Table C. 3: Crack width and length of PC/FA specimens exposed to 2D chloride ingress

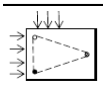
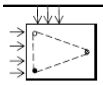
Specimens		Measured Parameters			Crack factor (mm.sq)
		Initial Crack width (mm)	Total length of corrosion induced crack (mm)	Corrosion-induced crack width (mm)	
	F2D-C-M1	0.30	85	0.06	5.10
	F2D-C-M2	0.30	43	0.04	1.72
	F2D-C-M3	0.38	31	0.04	1.24
	F2D-C-E1	0.30	87	0.1	8.70
	F2D-C-E2	0.28	288	0.1	28.80
	F2D-C-E3	0.16	232	0.72	167.04
	F2D-C-ES1	0.30	97	0.1	9.70
	F2D-C-ES2	0.18	198	0.1	19.80
	F2D-C-ES3	0.16	113	0.06	6.78

Table C. 4: Crack width and length of PC/SL specimens exposed to 2D chloride ingress

Specimens		Measured Parameters			Crack factor (mm.sq)
		Initial Crack width (mm)	Total length of corrosion induced crack (mm)	Corrosion-induced crack width (mm)	
	G2D-C-M1	0.22	67	0.08	5.36
	G2D-C-M2	0.20	31	0.04	1.24
	G2D-C-M3	0.20	80	0.04	3.20
	G2D-C-E1	0.26	16	0.1	1.60
	G2D-C-E2	0.28	312	0.72	224.64
	G2D-C-E3	0.40	263	0.42	110.46
	G2D-C-ES1	0.20	56	0.08	4.48
	G2D-C-ES2	0.26	150	0.22	33.00
	G2D-C-ES3	0.28	0	0	0.00

Appendix C. 2: Corrosion-induced crack patterns

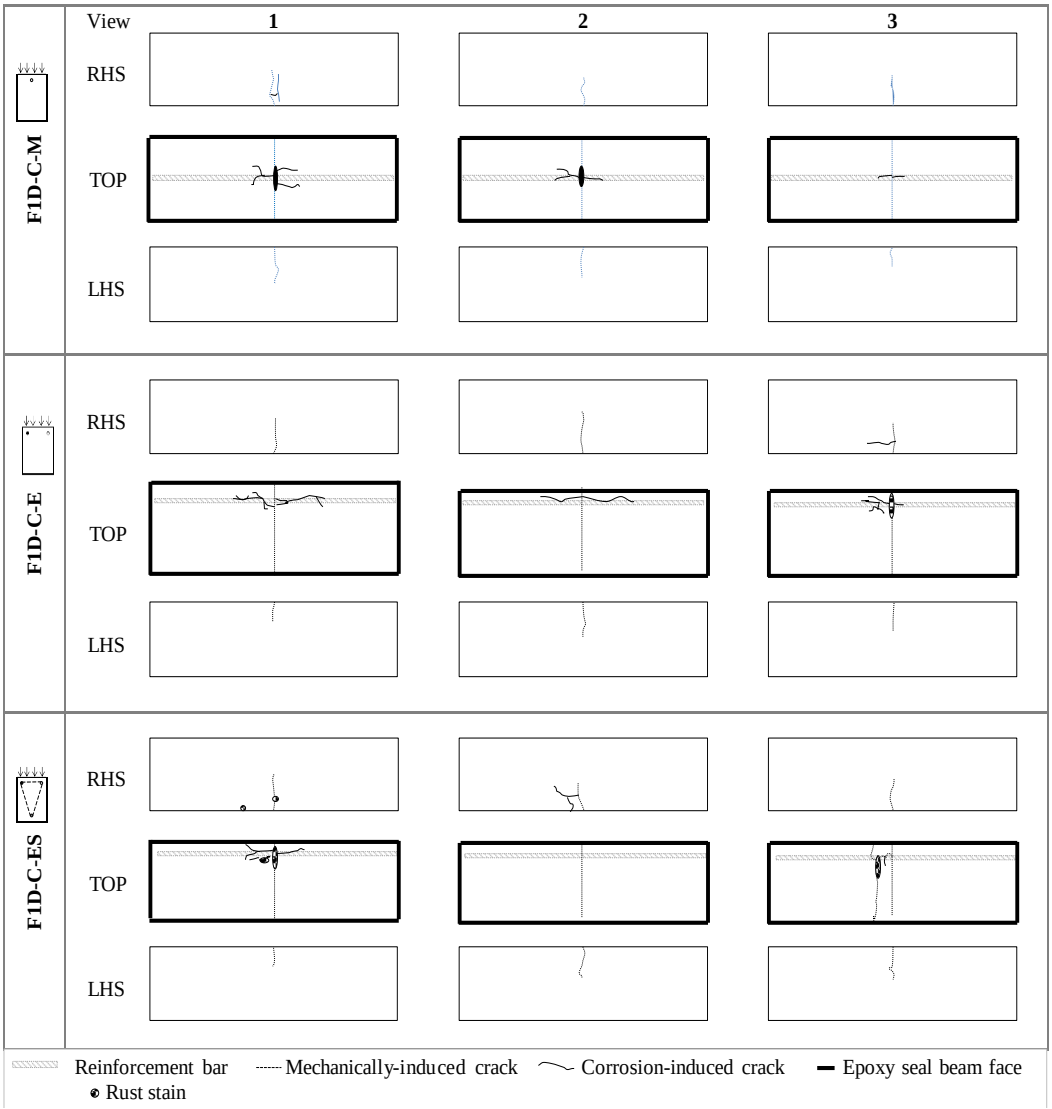


Figure C. 1: Visual defects in cracked (PC/FA) RC beams exposed to 1D chloride ingress.

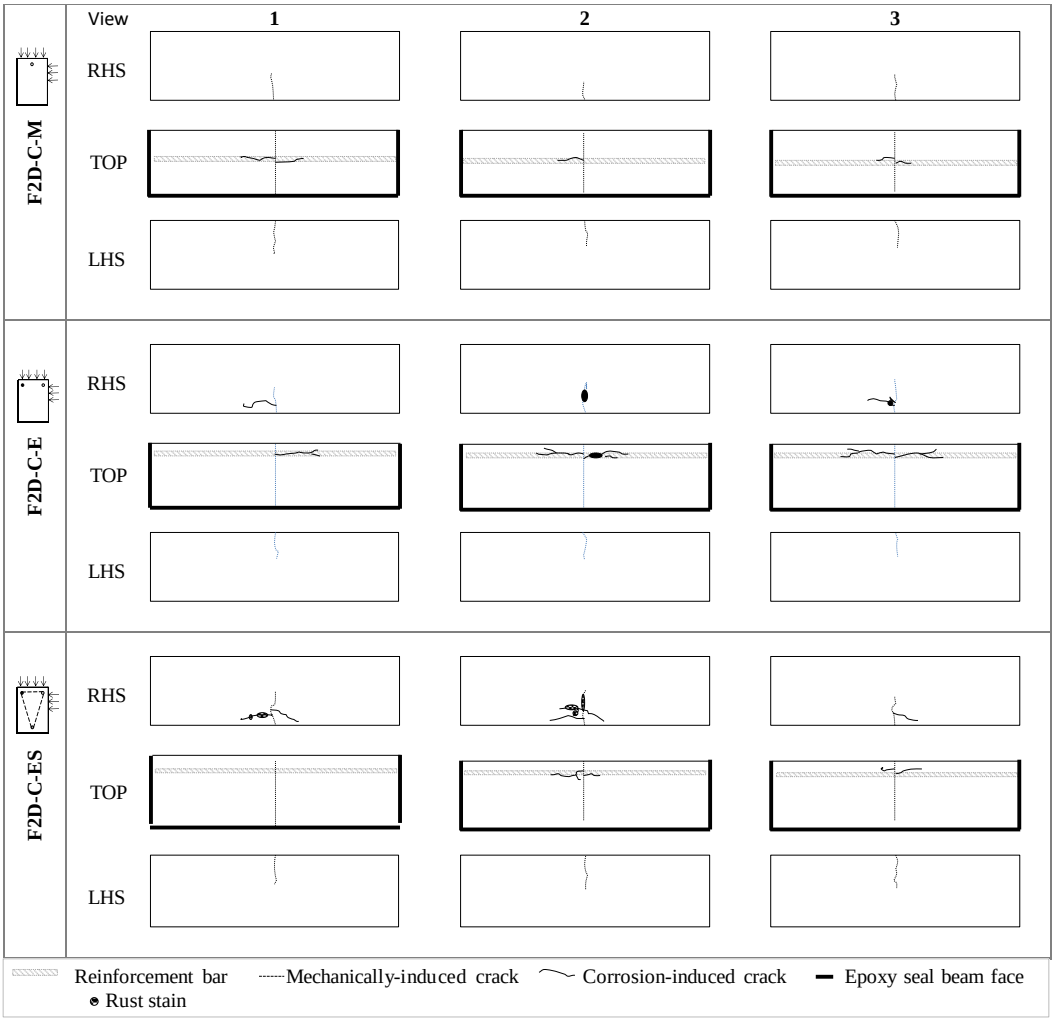


Figure C. 2**:** Visual defects in cracked (PC/FA) RC beams exposed to 2D chloride ingress.

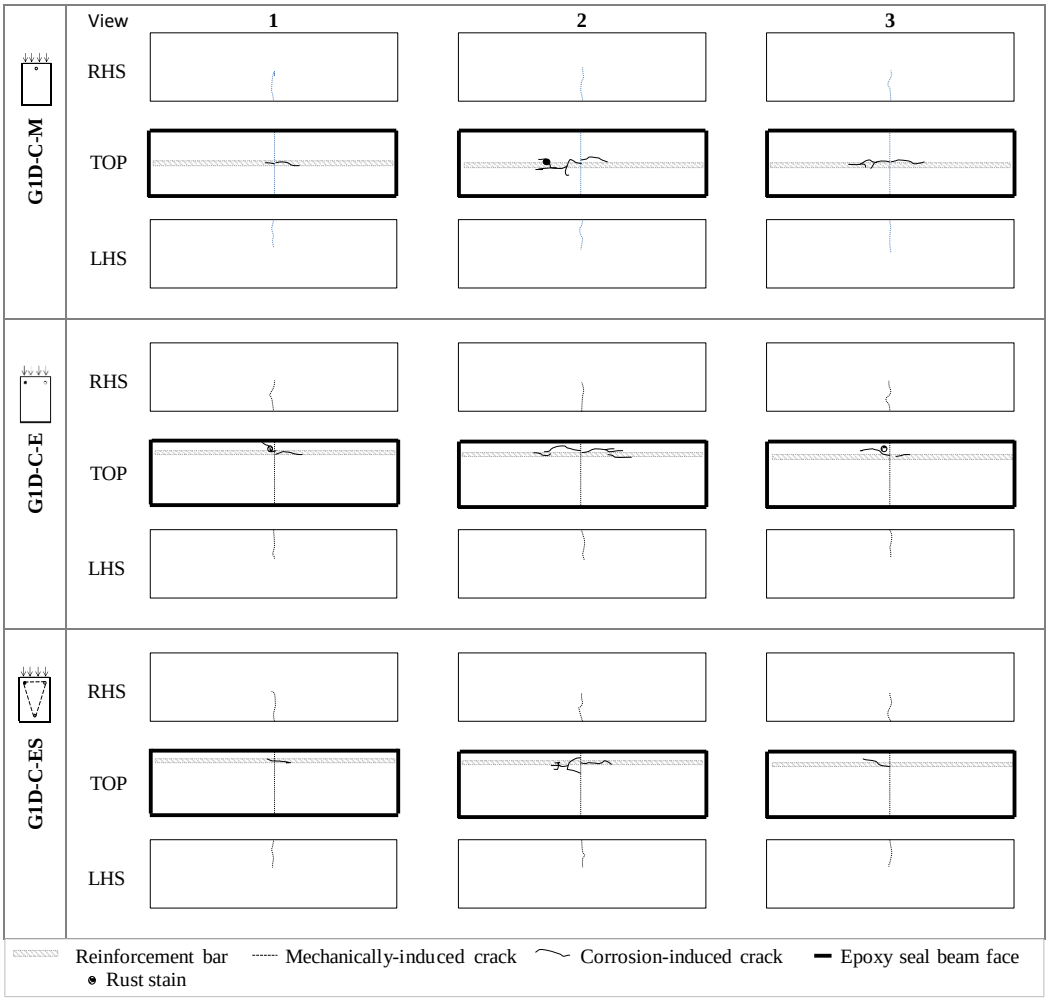


Figure C. 3: Visual defects in cracked (PC/SL) RC beams exposed to 1D chloride ingress.

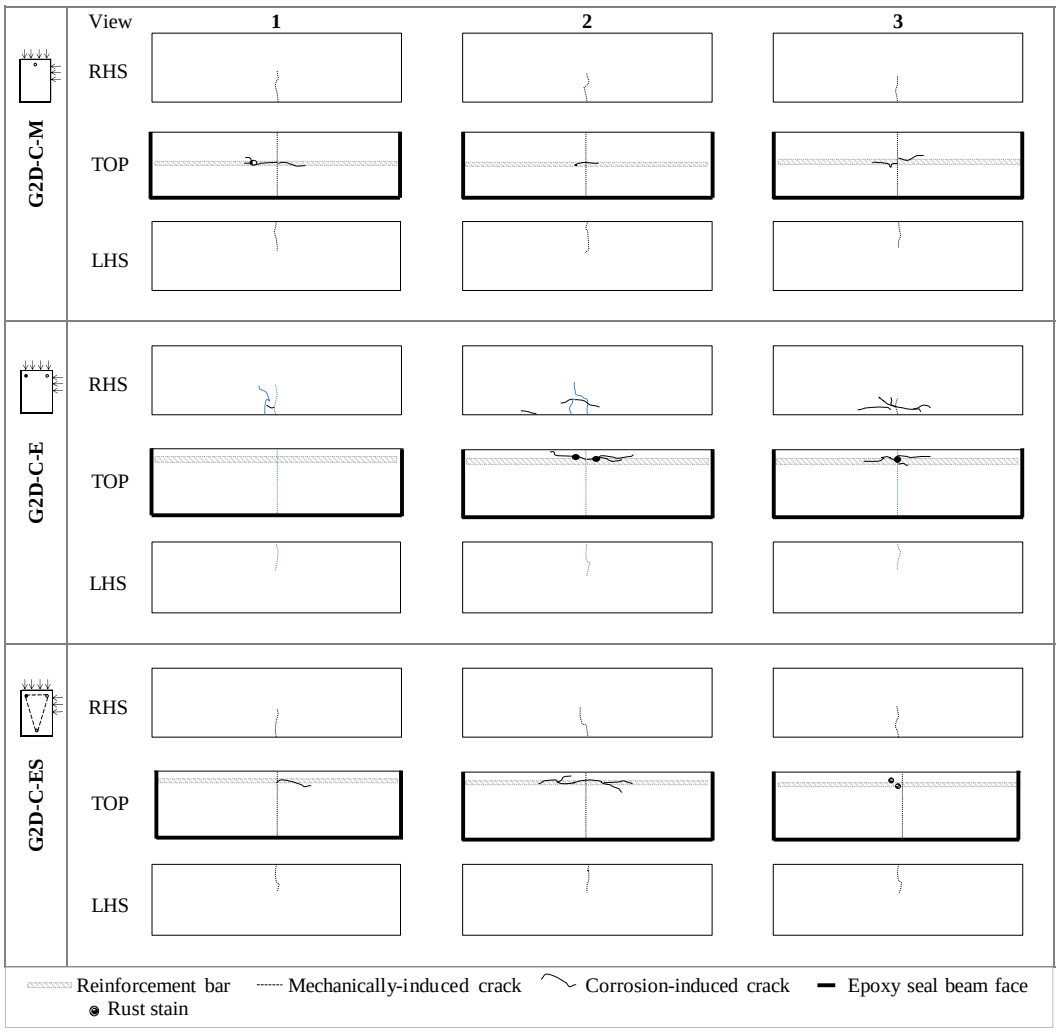


Figure C. 4**:** Visual defects in cracked (PC/SL) RC beams exposed to 2D chloride ingress.

Appendix C. 3: Summary of visual defects in the RC beam specimens

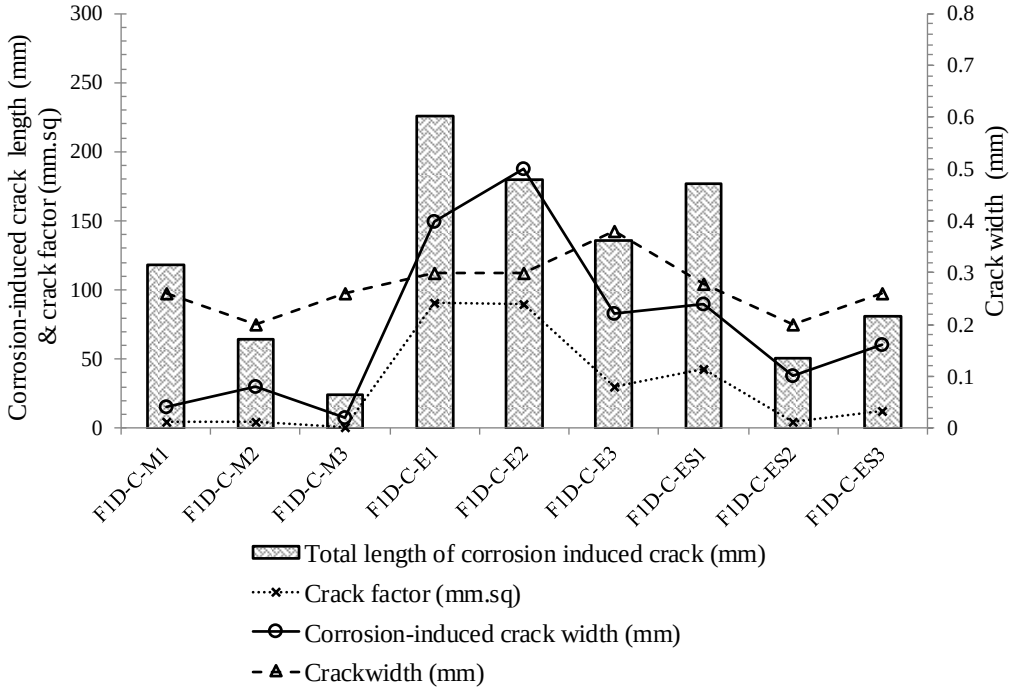


Figure C. 5: Summary of visual defects on PC/FA specimens exposed to 1D chloride ingress

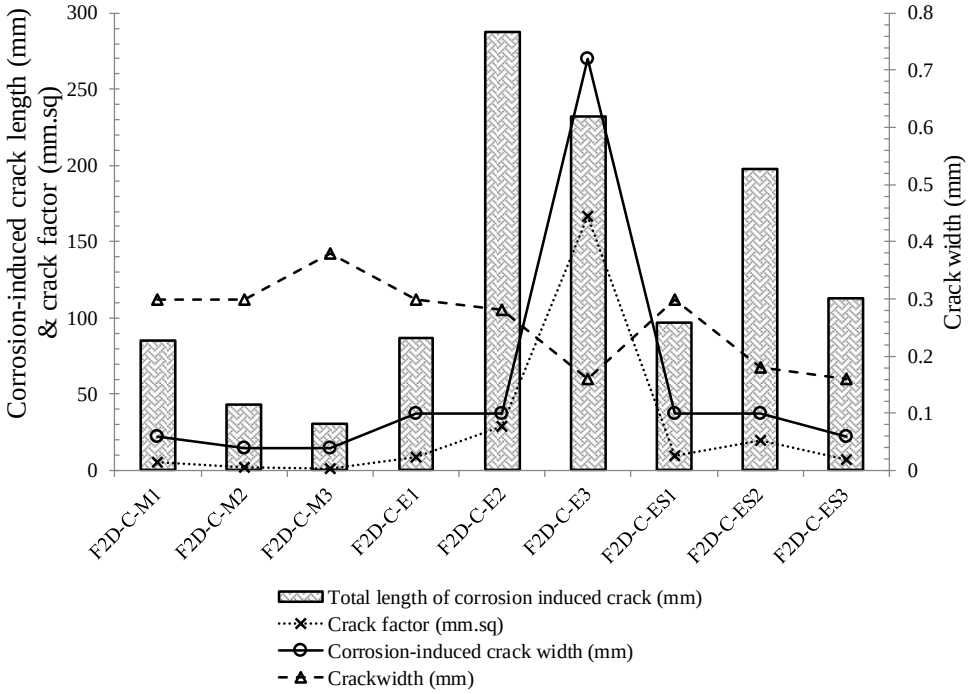


Figure C. 6: Summary of visual defects on PC/SL specimens exposed to 1D chloride ingress

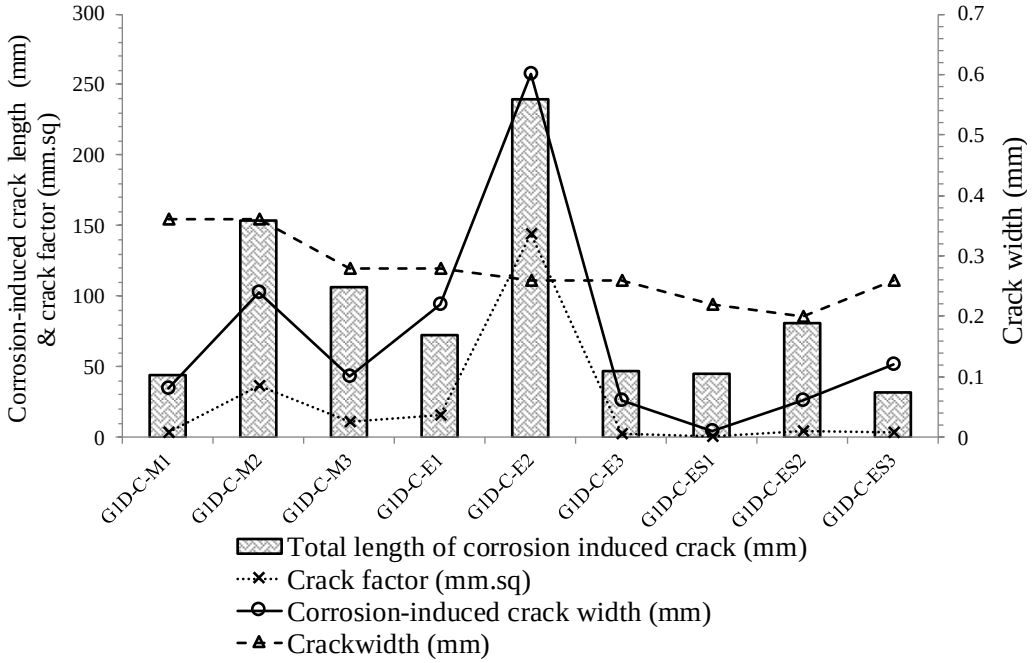


Figure C. 7**:** Summary of corrosion-induced defects on PC/FA specimens exposed to 2D chloride ingress

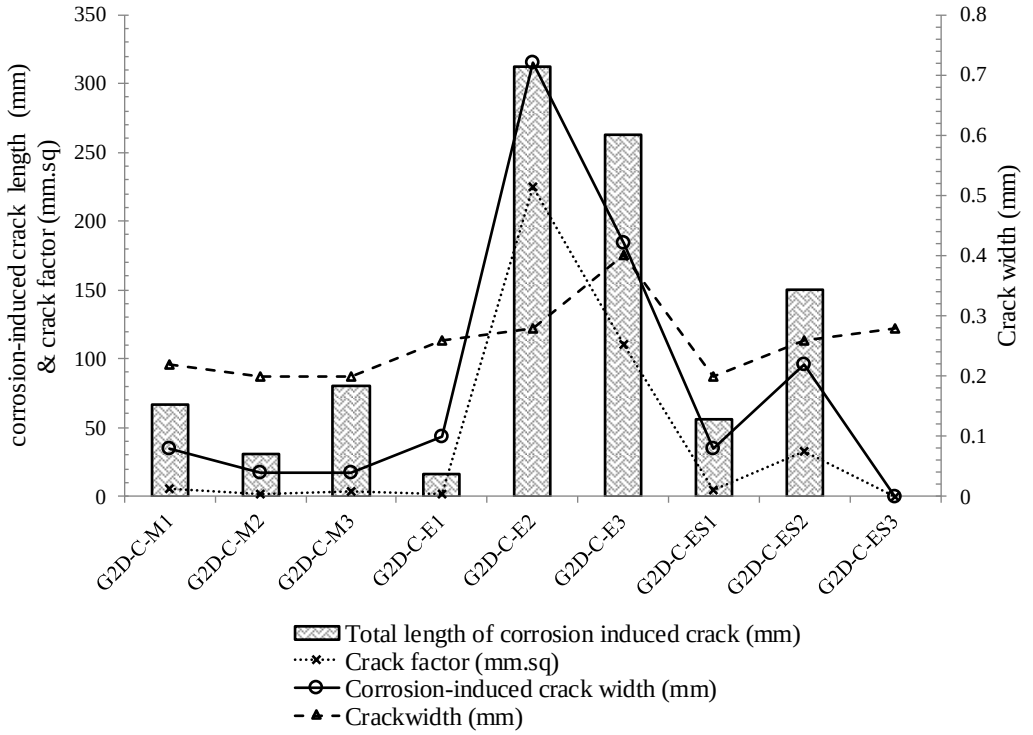


Figure C. 8: Summary of corrosion-induced defects on PC/SL specimens exposed to 2D chloride ingress

Appendix D: Atmospheric temperature variation during test period

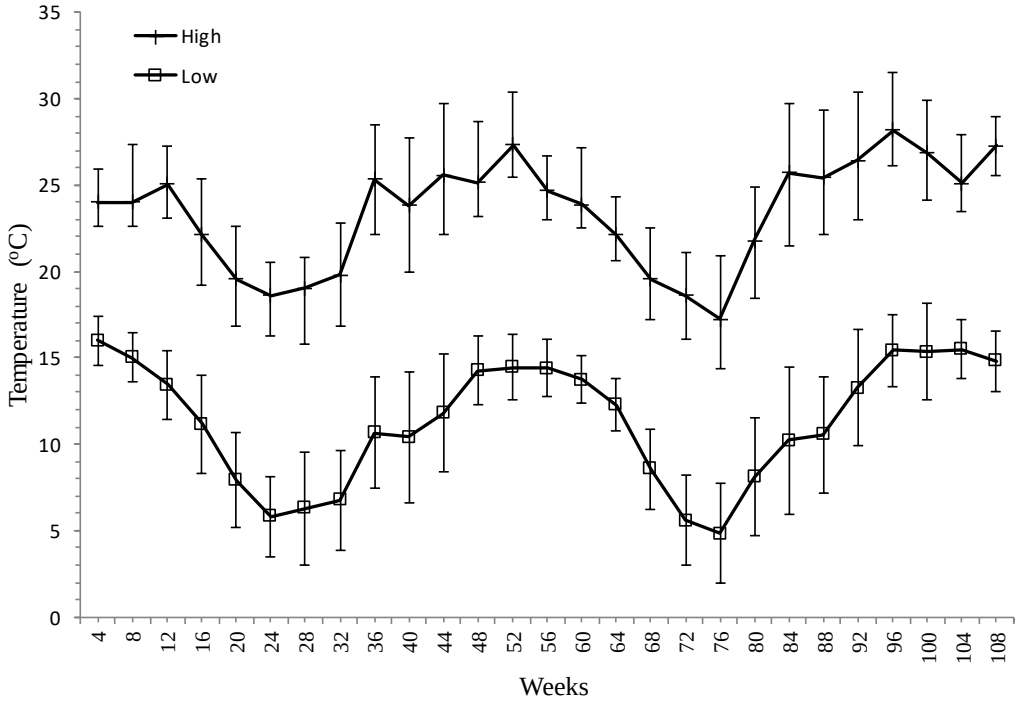


Figure D. 1: Mean temperature variation during the test period

Source: https://www.accuweather.com/en/za/johannesburg/305448/may-weather/305448?monyr=5/1/2019

Appendix E: Photographs of corroded bars in concrete

Reinforcement extraction from concrete (**Note:** the crack widths may appear larger than the prevailing cracks during the experiment)

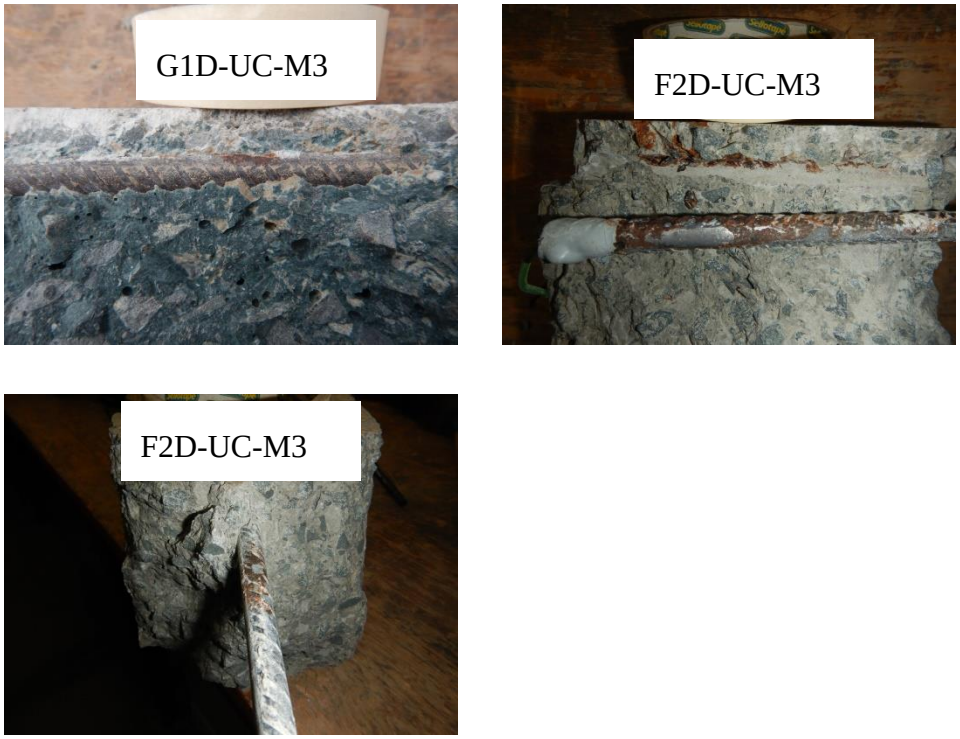


Figure E. 1**:** Photographs of corroded reinforcement bars in uncracked concrete

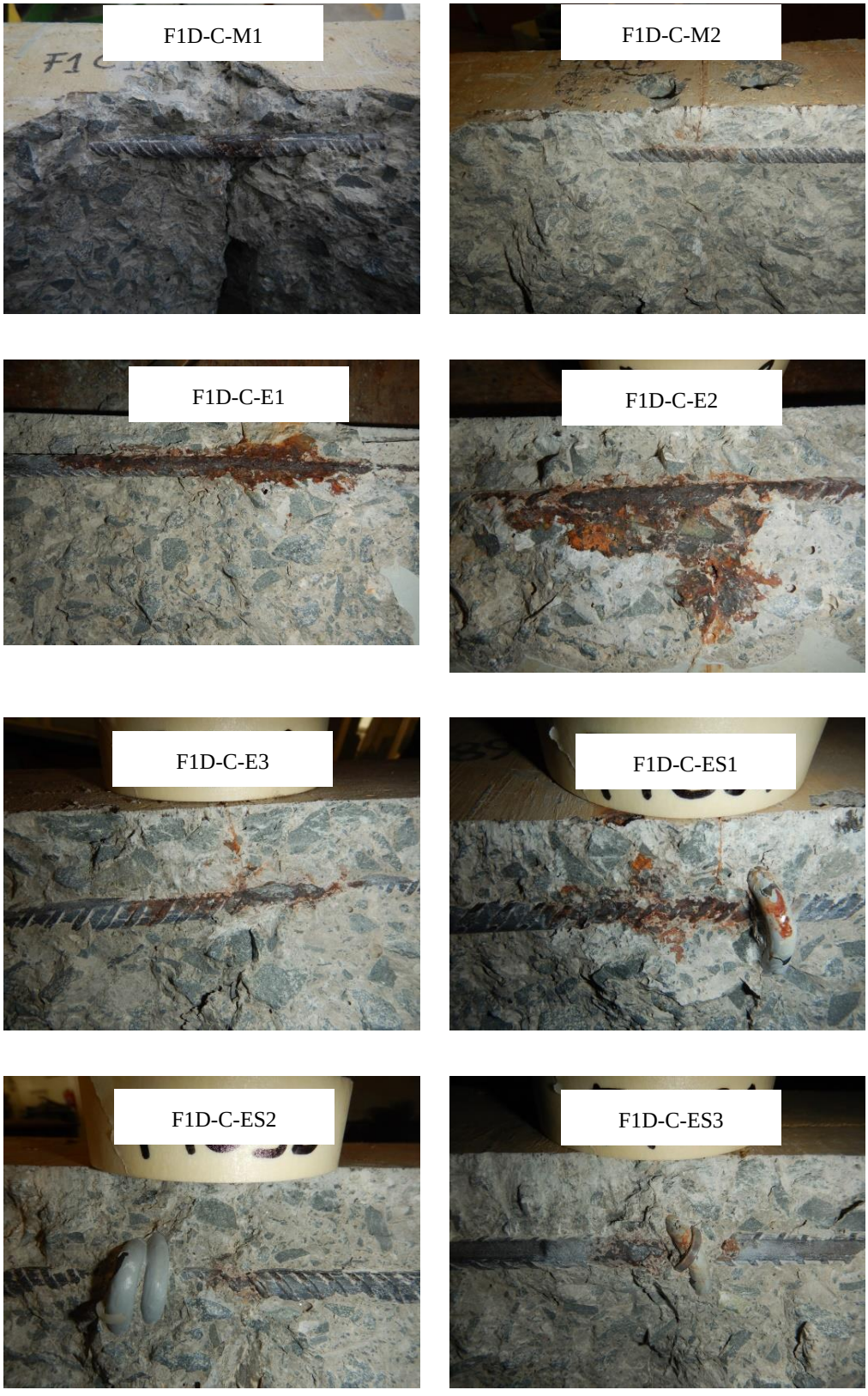


Figure E. 2**:** Photographs of corroded reinforcement bars in cracked PC/FA concrete



Figure E. 3**:** Photographs of corroded reinforcement bars in cracked PC/FA concrete (contd.)



Figure E. 4**:** Photographs of corroded reinforcement bars in cracked PC/SL concrete (contd.)

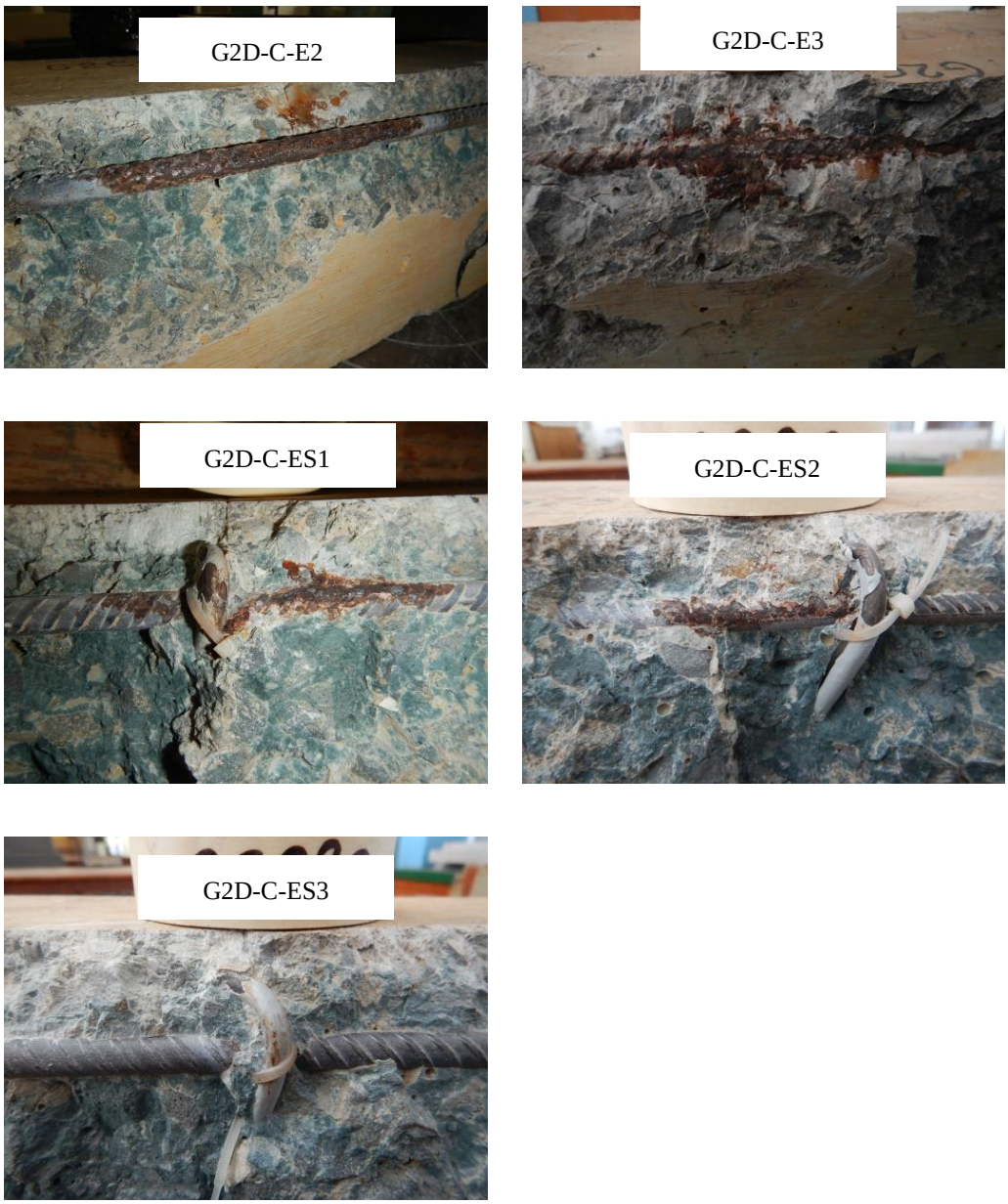


Figure E. 5**:** Photographs of corroded reinforcement bars in cracked PC/SL concrete.

Appendix F: t-test results of durability parameters

OPI

t-Test: Two-Sample Assuming Unequal Variances

	Variable 1	*Variable 2*
Mean	10.8825	10.6075
Variance	0.107425	0.0832917
Observations	4	4
Hypothesized Mean Difference	0	
df	6	
t Stat	1.259413562	
P(T<=t) one-tail	0.127327911	
t Critical one-tail	1.943180281	
P(T<=t) two-tail	0.254655822	
t Critical two-tail	2.446911851	

CCI

t-Test: Two-Sample Assuming Unequal Variances

	Variable 1	*Variable 2*
Mean	0.5625	0.1125
Variance	0.010291667	0.000025
Observations	4	4
Hypothesized Mean Difference	0	
df	3	
t Stat	8.860797471	
P(T<=t) one-tail	0.001515162	
t Critical one-tail	2.353363435	
P(T<=t) two-tail	0.003030325	
t Critical two-tail	3.182446305	

Porosity to Chlorides

t-Test: Two-Sample Assuming Unequal Variances

	Variable 1	*Variable 2*
Mean	3.715	2.07
Variance	0.0051	0.0285333
Observations	4	4
Hypothesized Mean Difference	0	
df	4	
t Stat	17.9395251	
P(T<=t) one-tail	2.83749E-05	
t Critical one-tail	2.131846786	
P(T<=t) two-tail	5.67498E-05	
t Critical two-tail	2.776445105	

WSI

t-Test: Two-Sample Assuming Unequal Variances

	Variable 1	*Variable 2*
Mean	7.98	6.125
Variance	0.234066667	0.0211667
Observations	4	4
Hypothesized Mean Difference	0	
df	4	
t Stat	7.34353575	
P(T<=t) one-tail	0.000915445	
t Critical one-tail	2.131846786	
P(T<=t) two-tail	0.00183089	
t Critical two-tail	2.776445105	

Porosity to water

t-Test: Two-Sample Assuming Unequal Variances

	Variable 1	*Variable 2*
Mean	9.933333333	7.385
Variance	0.096033333	0.0861667
Observations	3	4
Hypothesized Mean Difference	0	
df	4	
t Stat	11.01197543	
P(T<=t) one-tail	0.000193265	
t Critical one-tail	2.131846786	
P(T<=t) two-tail	0.00038653	
t Critical two-tail	2.776445105	

Appendix G: t-test results of concrete resistivity

F1D-UC-M & F2D-UC-E

t-Test: Two-Sample Assuming Unequal Variances

	Variable 1	*Variable 2*
Mean	11.45893162	10.05440171
Variance	1.446333717	0.522375178
Observations	13	13
Hypothesized Mean Difference	0	
df	20	
t Stat	3.609208054	
P(T<=t) one-tail	0.000875247	
t Critical one-tail	1.724718243	
P(T<=t) two-tail	0.001750493	
t Critical two-tail	2.085963447	

F1D-C-M & F2D-C-E

t-Test: Two-Sample Assuming Unequal Variances

	Variable 1	*Variable 2*
Mean	9.021381766	8.656680912
Variance	0.67659039	0.562628689
Observations	13	13
Hypothesized Mean Difference	0	
df	24	
t Stat	1.181229846	
P(T<=t) one-tail	0.12454248	
t Critical one-tail	1.71088208	
P(T<=t) two-tail	0.249084961	
t Critical two-tail	2.063898562	

G1D-UC-M & G2D-UC-E

t-Test: Two-Sample Assuming Unequal Variances

	Variable 1	*Variable 2*
Mean	10.80777778	10.09641026
Variance	0.97786034	0.485221842
Observations	13	13
Hypothesized Mean Difference	0	
df	22	
t Stat	2.120466171	
P(T<=t) one-tail	0.022739639	
t Critical one-tail	1.717144374	
P(T<=t) two-tail	0.045479278	
t Critical two-tail	2.073873068	

G1D-C-M & G2D-C-E

t-Test: Two-Sample Assuming Unequal Variances

	Variable 1	*Variable 2*
Mean	9.134230769	8.717008547
Variance	2.234464174	0.602580943
Observations	13	13
Hypothesized Mean Difference	0	
df	18	
t Stat	0.893112128	
P(T<=t) one-tail	0.191791298	
t Critical one-tail	1.734063607	
P(T<=t) two-tail	0.383582596	
t Critical two-tail	2.10092204	

The difference in the concrete resistivity of the uncracked concrete exposed to 1D and 2D chloride ingress is significant – concrete exposed to 2D chloride ingress has lower resistivity while the difference in concrete resistivity in the cracked concrete is not significant.

Appendix H: Cross section of OPI and CCI apparatus

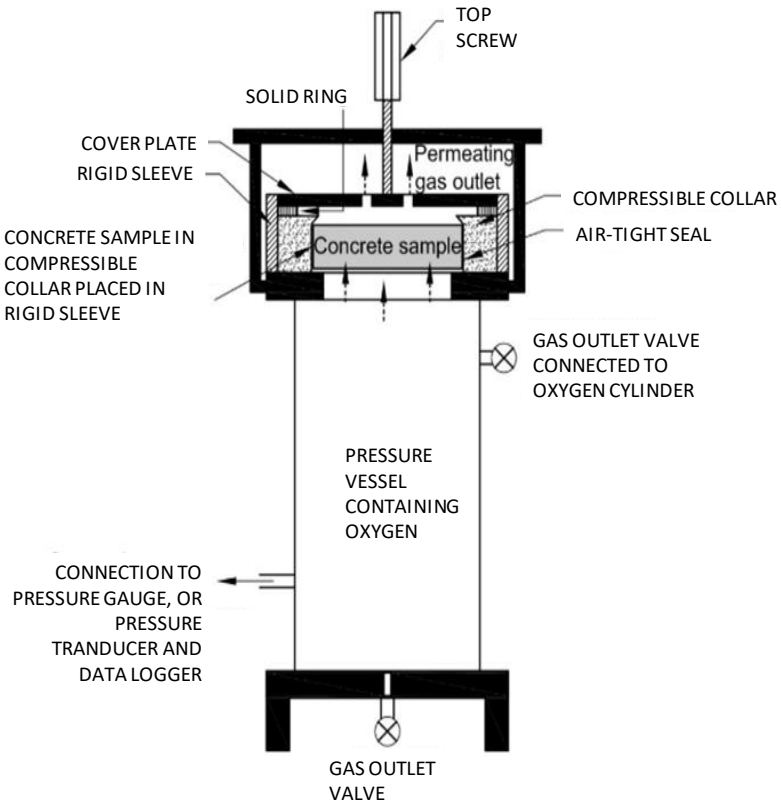


Figure H. 1: Cross section of oxygen permeability apparatus

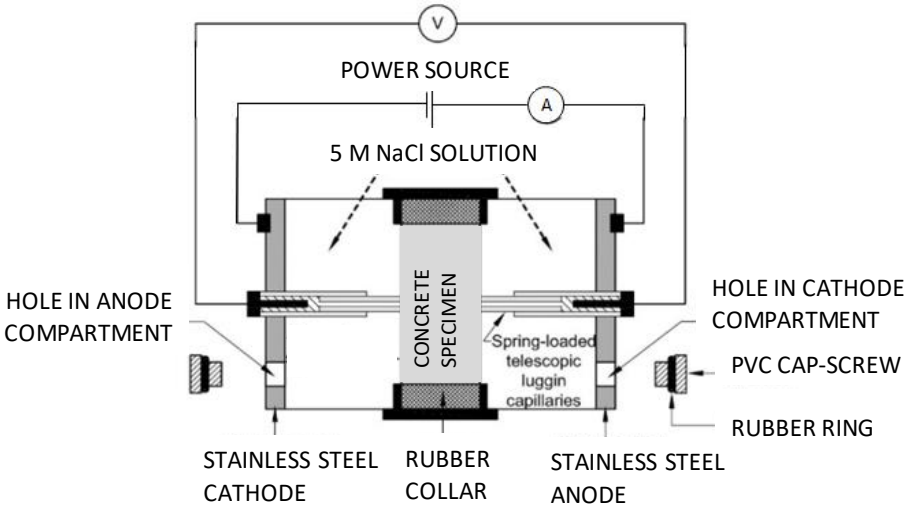


Figure H. 2: Cross section of chloride conductivity apparatus